EXPLOITING ORGANOCATALYSIS IN PHOTOCHEMICAL PROCESSES

Sara Cuadros Huertas

Sara Cuadros Huertas

Exploiting Organocatalysis in Photochemical Processes

Doctoral Thesis

Supervised by Prof. Paolo Melchiorre

ICIQ – Institut Català d'Investigació Química

UNIVERSITAT ROVIRA i VIRGILI

Tarragona, 2019

Prof. Paolo Melchiorre, ICREA Research Professor & ICIQ Group Leader

I STATE that the present study, entitled "Exploiting Organocatalysis in Photochemical Processes", presented by SARA CUADROS HUERTAS for the award of the degree of Doctor, has been carried out under my supervision at the Institut Català d'Investigació Química (ICIQ).

Tarragona, September the 2nd, 2019

Doctoral Thesis Supervisor

Prof. Paolo Melchiorre

Acknowledgements

I would like to express my deep gratitude to *Prof. Paolo Melchiorre*, my PhD supervisor, for giving me the opportunity to be part of his research group, and for providing me guidance and support along these five years.

A very special word of acknowledgement deserves *Prof. Takashi Ooi*, who kindly received me in his research group at Nagoya University, during my research experience in Japan. I would also like to thank *Prof. Daisuke Uraguchi*, *Tsuyoshi Ohtani*, and all the members of the Ooi group for enriching my stay with their chemistry knowledge and showing me the beauties of their country.

I would like to acknowledge all the former and current members of the Melchiorre group. I feel very privileged to have had the opportunity of learning from all of them. In particular, I am grateful to *Luca Dell'Amico*, for helping me during the MSc and at the beginning of my doctoral studies, as well as for all the unforgettable nights that we have enjoyed in Tarragona. To *Alberto Vega, "*mi carnalito", for being the best partner to go for a "PEDA*"*, and a terrible salsa teacher. To *Cao*, for all the hilarious moments in Lab 1.7. To *G. Filippini*, for introducing me to Lucio Dalla. To the "chemistry couple" *Hamish-Yannick*, for their help in the lab and their continuous advices. To *Bertie*, the "most respectable" senior postdoc of ICIQ, for suggesting me to "calm down", when needed. To *L. Buzzetti*, for his ability to diligently repair all the damage he can cause (the sake bottle…). To *Pablito*, for making more enjoyable the practice of doing columns. To *L. Perego*, for his admirable patience in discussing chemistry (or whatever topic). To *G. E. Crisenza* and *G. Goti* for the revision of some parts of this doctoral thesis, as well as for the "most venerable" party-nights. To *Giando*, for the "vermouth e andiamo a scrivere". To *Daniele* and *Eugenio*, for making me feel "elegant" every day. To *Nurty*, for being brave enough to come to the sin city, Benidorm. Overall, all of the members of the Melchiorre group should deserve a special mention, thank you very much.

I am also grateful to *Dr. Lorna Piazzi*, *Maria Checa* and *Núria Planella* for administrative support.

I would also like to extend my gratitude to the Research Support Units of ICIQ for their invaluable help. Especially, thanks to the NMR Unit, the CELLEX-HTE Lab and the Photophysics Unit.

I wish to acknowledge *Fran Mercader*, for giving me the photo of the *Puig Campana*, the cover picture of this thesis; and *Miguelito*, for helping me editing the original photo (tienes un arte que "no se puede aguantar").

I would also like to express my gratitude to the friends that I met in Tarragona. A *Sergio*, por "llevarme" a tantos lugares/bares/restaurantes nuevos. A *Jesús*, por tu arroz "con cosas" del

domingo y por hacerme reír tanto; pero no me toques... A *Javi*, mi eterno “punching-ball”, por tu valioso apoyo al inicio de esta etapa. A *la Juana* y *José*, por vuestra ayuda, las paellas, y por regalarme el momento más extravagante de mis vivencias aquí. A *Serena*, mi drama-queen favorita, ojalá hubieses llegado antes...A la estupendísima de *Irene*, por TODO lo que haces por mí; ¡te debo tanto!.

Finally, I wish to thank my parents, *Fernando* y *Mercedes*, and my brother, *Fernando*, for their love and unconditional support.

Pelocho…grazie per le correzioni, e sopratutto per *essere arrivato*. Ti stavo aspettando qui e non lo sapevo nemmeno, sai?.

Support from the fellowship programme *Formacion de Personal Universitario (FPU)*, granted by the Ministry of Science, Innovation and Universities of the Spanish Government is gratefully acknowledged.

Fellowship Reference: FPU14/06541.

List of Publications

Some of the results presented in this thesis have been published:

- Dell'Amico, L.; Vega-Peñaloza, A.; **Cuadros, S.**; Melchiorre, P. Enantioselective Organocatalytic Diels-Alder Trapping of Photochemically Generated Hydroxy-*o*-Quinodimethanes. *Angew. Chem. Int. Ed.* **2016**, *55*, 3313-3317.

- **Cuadros, S.**; Dell'Amico, L.; Melchiorre, P. Forging Fluorine-Containing Quaternary Stereocenters by a Light-driven Organocatalytic Aldol Desymmetrization Process. *Angew. Chem. Int. Ed.* **2017**, *56*, 11875-11879.

- **Cuadros, S.**; Melchiorre, P. Organocatalytic Strategies to Stereoselectively Trap Photochemically Generated Hydroxy-*o*-Quinodimethanes. *Eur. J. Org. Chem.* **2018**, 2884-2891.

- **Cuadros, S.**; Horwitz, M. A.; Schweitzer-Chaput, B.; Melchiorre, P. A Visible-Light Mediated Three-Component Radical Process using Dithiocarbamate Anion Catalysis. *Chem. Sci.* **2019**, *10*, 5484-5488.

To my family

Table of Contents

Chapter I

General Overview

The work described in this dissertation focuses on the combination of two powerful strategies for the activation of organic molecules: photochemistry and organocatalysis. Specifically, the potential of organocatalytic approaches has been exploited to overcome some of the limitations of established photochemical processes. Aim of this chapter is to provide a brief overview of the research background and the state-of-the-art regarding the merger of these two consolidated fields of research.

1.1. Organocatalysis for Enantioselective Photochemistry

Channeling light-driven processes toward a stereocontrolled pattern is one of the major challenges in modern synthetic photochemistry.[1] One of the fascinating aspects of photochemistry lies in the construction of scaffolds and bonds that are unique or difficult to access by classical thermal mechanisms.[2] The engagement of photochemically generated intermediates in enantioselective C-C bond forming processes can provide an exclusive access to chiral molecules. However, controlling the stereochemical outcome of photochemical processes is difficult, particularly when using substoichiometric amounts of chiral catalysts.

Organocatalysis is a mature area of research with broad applications in contemporary asymmetric synthesis.[3] This approach uses small organic molecules as chiral catalysts. Generally, organocatalysts are inexpensive, non-toxic and tolerant to air and moisture, therefore their manipulation does not normally require special precautions, such as working under inert atmosphere or using dry solvents. One of the powers of organocatalysis is that it has offered novel *generic modes of activation*, which are characterized by a chiral reactive species that can participate in mechanistically-related but different types of reactions with consistently high enantioselectivity. Such reactive species arise from the interaction of a chiral organocatalyst with a key functional group of the substrate in a highly organized and

[1] Brimioulle, R.; Lenhart, D.; Maturi, M. M.; Bach, T. Enantioselective Catalysis of Photochemical Reactions. *Angew. Chem Int. Ed.* **2015**, *54*, 3872–3890.

[2] (a) Hoffman, N. Photochemical Reactions as Key Steps in Organic Synthesis. *Chem. Rev*. **2008**, *108*, 1052–1103. (b) Bach, T.; Hehn, J. P. Photochemical Reactions as Key Steps in Natural Product Synthesis. *Angew. Chem. Int. Ed.* **2011**, *50*, 1000–1045. (c) Kärkäs, M. D.; Porco, J. A., Jr.; Stephenson, C. R. J. Photochemical Approaches to Complex Chemotypes: Applications in Natural Product Synthesis. *Chem Rev*. **2016**, *116*, 9683–9747.

[3] Dalko, P. I. (ed.) Comprehensive Enantioselective Organocatalysis: Catalysts, Reactions, and Applications. Wiley-VCH, **2013**.

predictable manner.[4] Based on the nature of the interaction between the catalyst and the substrate, organocatalytic reactions can be classified in two main generic modes of activation. The *covalent activation* methods involve the formation of covalent adducts within the catalytic cycle, while *non-covalent activation* methods rely on hydrogen bonding interactions or the formation of ion-pairs. Within these two generic modes of activation, some characteristic structures of both catalysts and reactive intermediates can be listed (see Figures 1.1 and 1.2).[5]

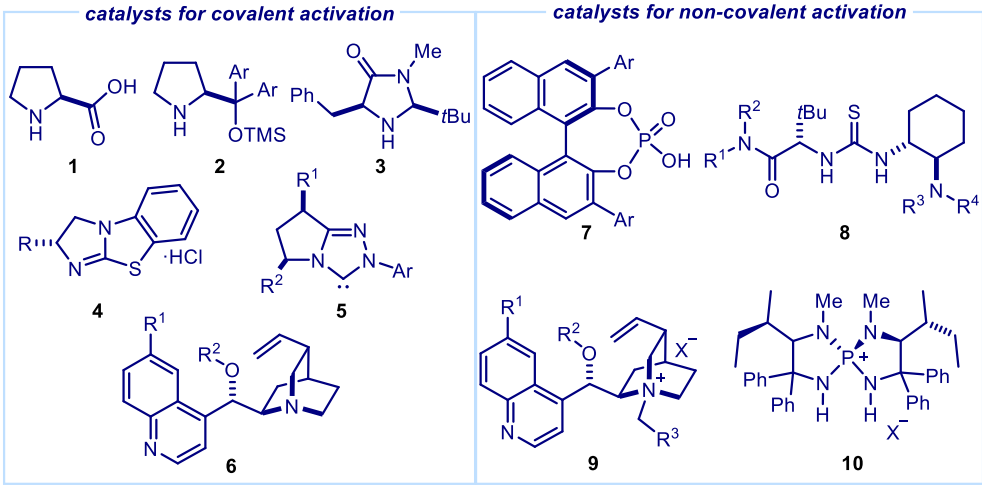

Figure 1.1. Selection of representative chiral organic catalysts that operate via covalent or non-covalent modes of substrate activation.

[4] MacMillan, D. W. C. The Advent and Development of Organocatalysis. *Nature* **2008**, *455*, 304–308.
[5] (a) Melchiorre, P., Marigo, M., Carlone, A., Bartoli, G. Asymmetric Aminocatalysis-Gold Rush in Organic Chemistry. *Angew. Chem. Int. Ed.* **2008**, *47*, 6138–6171. (b) Beeson, T. D., Mastracchio, A., Hong, J.-B., Ashton, K., MacMillan, D. W. C. Enantioselective Organocatalysis Using SOMO Activation. *Science*, **2007**, *316*, 582–585. (c) Gaunt, M. J., Johansson, C. C. C. Recent Developments in the Use of Catalytic Asymmetric Ammonium Enolates in Chemical Synthesis. *Chem. Rev*. **2007**, *107*, 5596–5605. (d) Morrill, L. C., Smith, A. D. Organocatalytic Lewis Based Functionalization of Carboxylic Acids, Esters and Anhydrides via C1-Ammonium or Azolium Enolates. *Chem. Soc. Rev.* **2014**, *43*, 6214–6226.(e) Bugaut, X., Glorius, F. Organocatalytic Umpolung: *N*-heterocyclic Carbenes and Beyond. *Chem. Soc. Rev.* **2012**, *41*, 3511–3522. (f) Doyle, A. G., Jacobsen, E. N. Small-molecule H-bond Donors in Asymmetric Catalysis. *Chem. Rev.* **2007**, *107*, 5713–5743. (g) Brak, K., Jacobsen, E. N. Asymmetric Ion-Pairing Catalysis. *Angew. Chem. Int. Ed.* **2013**, *52*, 534–561.

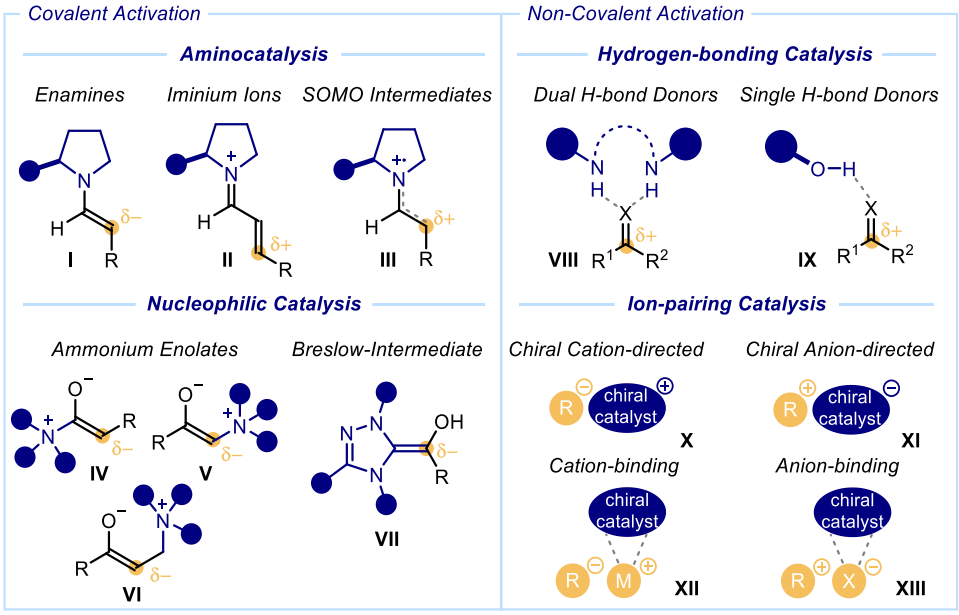

Figure 1.2. Generic modes of activation in organocatalysis. Here are represented the generic reactive intermediates involved in organocatalytic cycles. Blue circles represent fragments on the chiral catalyst scaffold. SOMO: singly occupied molecular orbital. For intermediates **VIII** and **IX:** X= O, NR.

Some of these generic reactive intermediates (listed in Figure 1.2) have proven useful also in asymmetric photochemistry, and they have been successfully used to infer stereocontrol over different types of light-driven reactions. When it comes to enantioselective photochemistry, it is important to distinguish between two general types of processes. There are photochemical reactions where the key bond-forming or bond-fragmenting event occurs in the *electronically excited state*, and transformations where *photochemically generated reactive intermediates* undergo a subsequent *ground-state reaction*. The following sections 1.1.1 and 1.1.2 will highlight the pioneering examples demonstrating how chiral organocatalytic intermediates can be used in enantioselective photochemical transformations.

1.1.1. Stereoselective Control in Reactions of Electronically Excited Species

Organocatalysis has allowed the stereocontrol over the reactivity of *electronically excited intermediates*. One of the main difficulties here is controlling unselective *racemic background photoreactions*,[6] which implies the direct transformation of the substrates without the assistance of a chiral catalyst. This can be better understood if we compare the reaction pathways of a ground-state catalyzed reaction with a photochemical one (Figure 1.3). In the

[6] Yoon, T. P. Photochemical Stereocontrol Using Tandem Photoredox-Chiral Lewis Acid Catalysis. *Acc. Chem. Res.* **2016**, *49*, 2307–2315.

ground-state reactivity, the use of a catalyst decreases the activation barrier of a chemical reaction, securing a lower energy pathway (Figure 1.3a). If the catalyst is chiral, it is then possible to direct the reaction through an enantioselective pattern. This conventional strategy for stereocontrol is difficult to implement in the case of a photochemical transformation (Figure 1.3b) because, after excitation, the molecule gains sufficient energy to undergo a fast subsequent process that generally does not need any catalyst to proceed. Additionally, it must be considered that the short lifetime of the excited intermediates (**R***) limits the ability of a chiral catalyst to control the stereoselectivity of the process.

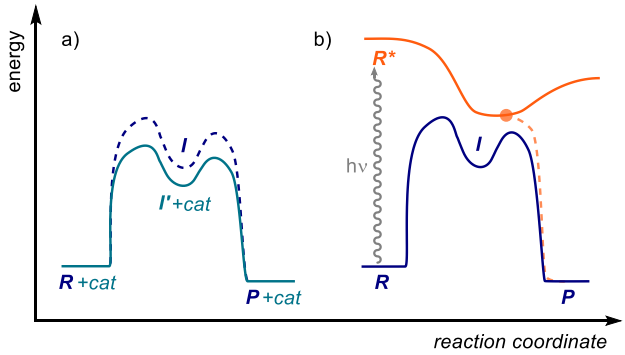

Figure 1.3. Reaction pathways in: (a) a ground-state-catalyzed reaction, and (b) a photochemical reaction. **R:** reagent; **P:** product; **cat**: catalyst; **I** and **I'**: intermediates; **R***: excited reagent. The conical intersection in the photochemical process (b) is represented with a filled orange dot.

Considering this, the main objective of a chiral catalyst in an enantioselective photochemical reaction is not to lower the activation barrier, but instead to ensure that the substrate molecule already resides in a chiral environment during the excitation event. The first effective methodology to achieve this goal was reported by the research group of Thorsten Bach.[7] They used the chiral ketone **12**, appropriately adorned with a hydrogen bonding motif, to catalyze the light-triggered stereoselective cyclization of lactams **11** (Figure 1.4). The ketone-based organic catalyst effectively binds the substrate through a double hydrogen-bond interaction, enabling the selective photoexcitation of a chiral catalyst-substrate complex. Upon excitation by UV-light absorption of the complex, a photoinduced electron transfer (PET) occurs from the amine moiety within substrate **11** to the photoexcited catalyst, affording intermediate **XIV**. Subsequent proton loss from the amine radical cation leads to the formation of an α-aminoradical (see intermediate **XV**), which undergoes a radical cyclization within the tethered 2-quinolone moiety of **11**. After the radical cyclization reaction, back electron transfer (ET) from the catalyst generates an enolate (not shown in Figure 1.4), which is protonated to yield the products **13**. In this strategy, catalyst **12** serves not only as a PET catalyst, but also as a

[7] Bauer, A.; Westkämper, F.; Grimme, S.; Bach, T. Catalytic Enantioselective Reactions Driven by Photoinduced Electron Transfer. *Nature* **2005**, *436*, 1139–1140.

rigid stereocontrolling element that induces enantiofacial differentiation during the radical cyclization step.

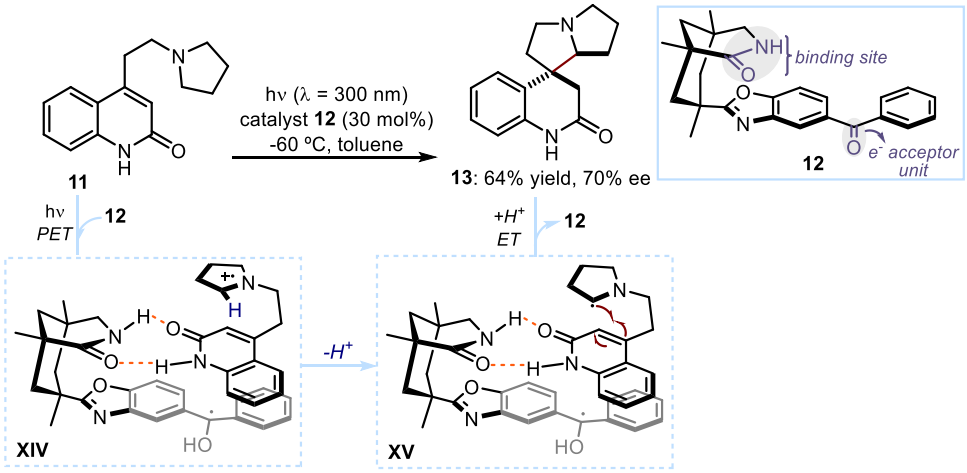

Figure 1.4. Early use of H-bonding catalysis in an asymmetric photochemical reaction occurring in the excited state. PET: photoinduced electron transfer. ET: electron transfer

This strategy has been also used in *energy-transfer*-induced photochemical reactions.[8] UV-vis-light absorbing xanthone or thioxanthone moieties were incorporated within the chiral catalyst **15** (Figure 1.5).

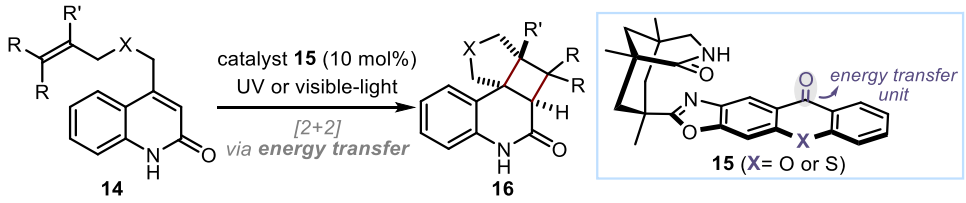

Figure 1.5. Chiral xanthone and thioxanthone-based catalysts (**15**) have enabled the enantioselective [2+2]-photocycloaddition of quinolones **14** *via* an energy-transfer mechanism.

The thioxanthone catalyst (**15**, X=S) exhibits a significant absorption in the visible region in comparison to the xanthone (**15**, X=O), therefore it can be selectively activated by low energy, visible-light irradiation. Upon selective excitation of the substrate-catalyst complex (**14**+**15**), catalyst **15** can activate the quinolones **14** *via* a proximity-driven Dexter energy transfer

[8] (a) Müller, C.; Bauer, A.; Bach, T. Light-Driven Enantioselective Organocatalysis. *Angew. Chem. Int. Ed.* **2009**, *48*, 6640–6642. (b) Alonso, R.; Bach, T. A Chiral Thioxanthone as an Organocatalyst for Enantioselective [2+2] Photocycloadditions Reactions Induced by Visible-Light. *Angew. Chem. Int. Ed.* **2014**, *53*, 4368–4371.

mechanism[9] and direct an intramolecular [2+2]-cycloaddition of **14** in the triplet energy hypersurface. The corresponding products **16** are obtained with high yield and enantioselectivity (up to 97% yield, 94% ee).

Chiral thioureas also proved as competent organocatalysts in stereocontrolled photoreactions. Sibi, Sivaguru and coworkers[10] showed that the atropoisomeric thiourea **18** could induce stereoselectivity in excited-state processes of coumarins **17** (Figure 1.6).

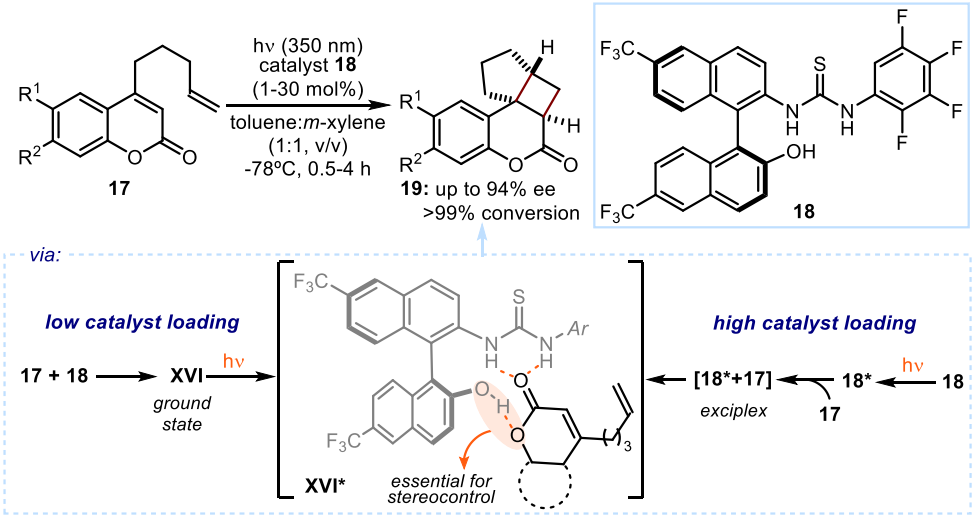

Figure 1.6. Enantioselective [2+2]-cycloaddition of coumarins **17** mediated by the atropoisomeric thiourea **18**.

Based on photophysical studies, the authors proposed two different mechanisms depending on the concentration of the catalyst. At low catalyst loadings (Figure 1.6 below, left pathway) a ground-state association complex[11] (**XVI**) between substrate **17** and the catalyst was formed, which displayed a bathochromic shift in its absorption spectrum. Direct excitation of **XVI** triggered a stereocontrolled [2+2]-cycloaddition of the coumarine **17**, leading to the formation

---

[9] This photochemical mechanism involves a double electron exchange between an excited-state donor molecule (D*) and a ground-state acceptor molecule (A). One electron in the LUMO of D* is transferred to the LUMO of A, while another electron from the HOMO of A is transferred to the HOMO of D*. This mechanism occurs only at short distances, requiring an orbital overlap between the donor and the acceptor molecules. For an extensive discussion, see: Balzani, V.; Ceroni, P.; Juris, A.; Photochemistry and Photophysics: Concepts, Research, Applications. Chapter 6. Quenching and Sensitization Processes in Molecular and Supramolecular Species. **2014**; John Wiley & Sons.

[10] Vallavoju, N.; Selvakumar, S.; Jockusch, S.; Sibi, M. P.; Sivaguru, J. Enantioselective Organo-Photocatalysis Mediated by Atropisomeric Thiourea Derivatives. *Angew. Chem. Int. Ed.* **2014**, *53*, 5604–5608.

[11] (a) Mulliken, R. S. Molecular Compounds and Their Spectra. II. *J. Am. Chem. Soc.* **1952**, *74*, 811–824. (b) Rathore, R.; Kochi, J. K. Donor/Acceptor Organizations and the Electron-Transfer Paradigm for Organic Reactivity. *Adv. Phys. Org. Chem.* **2000**, *35*, 193–318.

of the enantio-enriched product **19**. When the catalyst loading was increased (Figure 1.6 below, right pathway), the main responsible for the light-absorption was the free catalyst **18**, because it possessed higher absorbance than the complex **XVI** at 350 nm. After light-absorption, the excited catalyst **18*** binds the substrate **17** to form an exciplex ([**18***+**17**])[12] that afforded the cyclized product **19**. In both cases, the hydroxyl group within the binaphthyl framework of **18** was found to be essential for achieving high enantioselectivity, as hydrogen bond is formed to the lactone oxygen atom of the coumarin substrate.

The use of Lewis acid catalysis has also allowed the development of enantioselective [2+2]-photocycloadditions. In 2013, Bach and collaborators[13] showed that the chiral $AlBr_3$-activated oxazaborolidine **21** could enable the [2+2]-photocycloaddition of dihydropyridones **20** (Figure 1.7). This class of substrates (**20**) exhibits both a prominent batochromic shift ($\Delta\lambda$ = 50-60 nm) and a very strong absorption coefficient ($\varepsilon > 10000\ M^{-1}cm^{-1}$), in the presence of Lewis acids. Consequently, upon activation, the main responsible for the light-absorption was the substrate-catalyst complex **XVII**, and not the unbounded substrate **20**. This strategy secured that the reaction to give products **22** proceeded only from the chiral complex **XVII**, thus achieving high levels of stereoselectivity. The origin of stereocontrol was explained based on an established model for face differentiation applied to the thermal reactions of enones catalyzed by oxazaborolidine-based Lewis acids.[14]

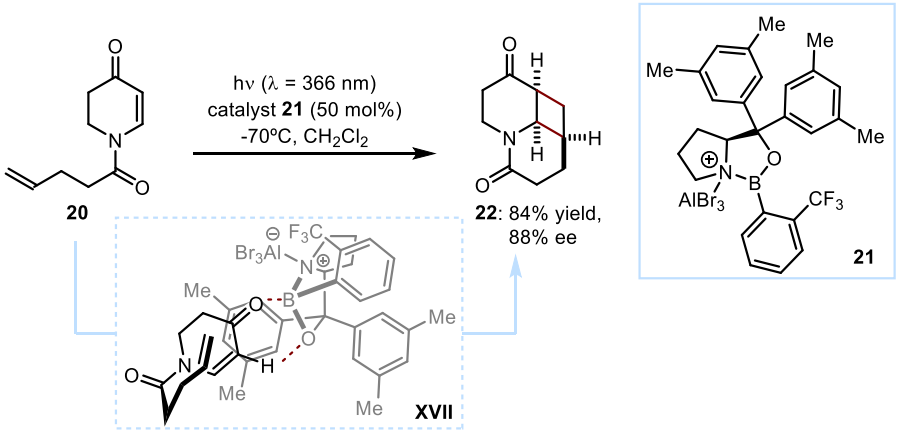

Figure 1.7. Enantioselective [2+2]-photocycloaddition of enones **20** enabled by the chiral oxazaborolidine **21.**

[12] An exciplex is a non-covalent electronically excited complex formed between a molecule in an excited-state with a different molecule in the ground-state. In this case, the exciplex formation triggers a photochemical process in the excited-state.

[13] Brimioulle, R.; Bach, T. Enantioselective Lewis Acid Catalysis of Intramolecular Enone [2+2] Photocycloaddition Reactions. *Science* **2013**, *342*, 840–843.

[14] Corey, E. J. Enantioselective Catalysis Based on Cationic Oxazaborolidines. *Angew. Chem. Int. Ed.* **2009**, *48*, 2100–2117.

1.1.2. Stereoselective Control over Photochemically Generated Intermediates

Dual-catalysis has offered an alternative strategy to perform enantioselective light-driven processes.[15] This approach is based on the separation of the photochemical step and the enantioselective bond-forming event. To this end, an achiral metal-based or organic photocatalyst is commonly used to trigger the formation of a radical or radical-ion intermediate, and a second, independent chiral catalyst is used to channel the reactivity of the photogenerated species toward a stereocontrolled pathway. During the last decade, the activity of photoredox catalysts[16] has been successfully combined with the generic mechanisms of activation that define the ground-state reactivity of chiral organocatalytic intermediates (shown in Figure 1.2). In 2008, the MacMillan's group reported the first example[17] of such successful combination (Figure 1.8). They showed how catalytically generated chiral enamines **XVIII** (formed upon condensation of aldehyde **23** with the chiral secondary amine catalyst **25**) could be used to trap electro-deficient radicals **XIX**, produced upon single-electron transfer (SET) reduction of α-bromo carbonyl compounds **24** by the photocatalyst $[Ru(bpy)_3]^{+}$.[18]

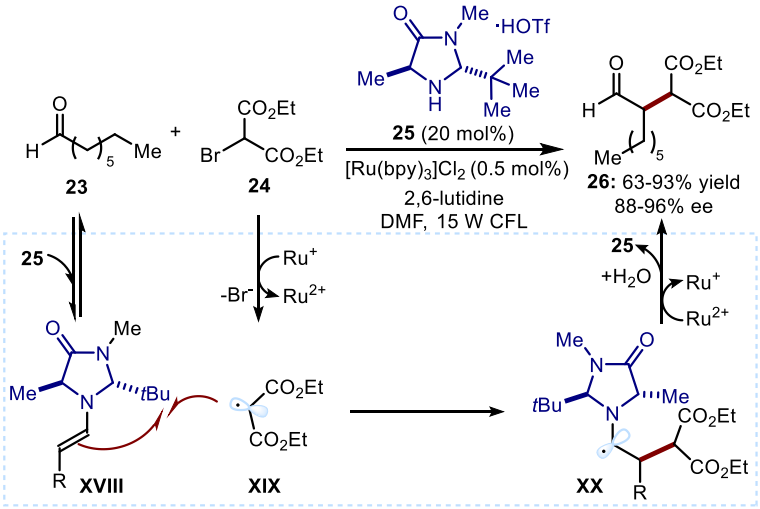

Figure 1.8. The first example on the combination of photoredox catalysis with enantioselective organocatalysis (enamine-catalysis).

[15] Skubi, K. L.; Blum, T. R.; Yoon, T. P. Dual Catalysis Strategies in Photochemical Synthesis. *Chem. Rev.* **2016**, *116*, 10035–10074.

[16] Shaw, M. H.; Twilton, J.; MacMillan, D. W. C. Photoredox Catalysis in Organic Chemistry. *J. Org. Chem.* **2016**, *81*, 6898–6926.

[17] Nicewicz, D. A.; MacMillan, D. W. C. Merging Photoredox Catalysis with Organocatalysis: the Direct Asymmetric Alkylation of Aldehydes. *Science* **2008**, *322*, 77–80.

[18] For a detailed discussion on the mechanism, see: Cismesia, M. A.; Yoon, T. P. Characterizing Chain Processes in Visible Light Photoredox Catalysis. *Chem. Sci.* **2015**, *6*, 5426-5434.

This transformation led to the formation of α-alkylated aldehydes **26** with high levels of enantiocontrol. Such study was very influential for the synthetic community due to two main reasons: (*i*) it demonstrated that radical intermediates could be generated under mild conditions by using a photocatalyst activated by visible light; and (*ii*) it proved that enantioselective organocatalytic strategies, originally conceived for ionic processes, could be successfully translated within radical reactivity patterns. Following this seminal example, many efforts have been devoted to identify suitable conditions for merging organocatalytic cycles, which afford chiral organic intermediates, with photoredox catalytic cycles, which provide reactive open-shell intermediates.[19]

The Melchiorre group[20] has demonstrated that iminium ion activation can facilitate the enantioselective conjugate addition of nucleophilic radicals, generated by an external light-activated photocatalyst, to the β-carbon atom of β-substituted cyclic enones **27** (Figure 1.9).

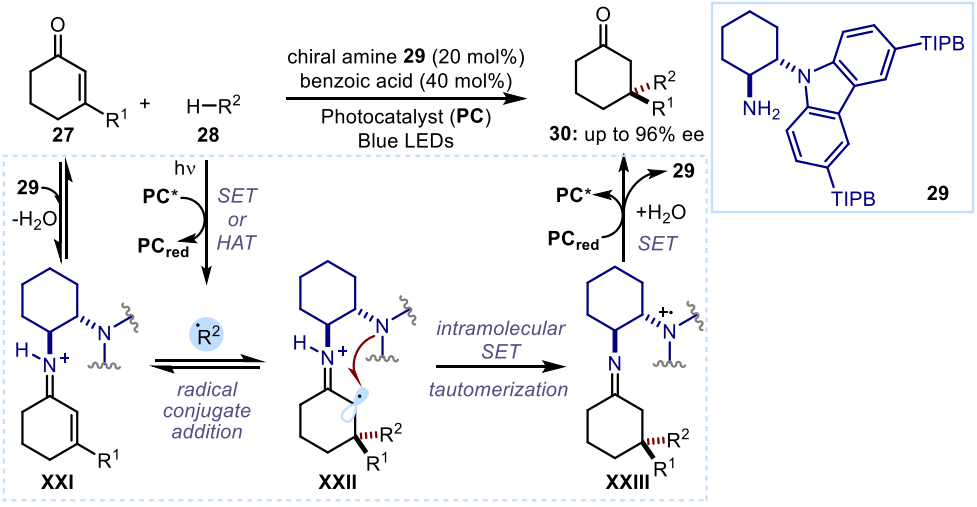

Figure 1.9. First example on the use of iminium ion-activation in the enantioselective conjugate addition of nucleophilic radicals to β-substituted cyclic enones **27**. SET: single-electron reduction. HAT: hydrogen atom abstraction. TIPB: triisopropylbenzene.

[19] For other examples involving the use of enamines, see: (a) Nagib, D. A.; Scott, M. E.; MacMillan, D. W. C. Enantioselective α -Trifluoromethylation of Aldehydes via Photoredox Organocatalysis. *J. Am. Chem. Soc.* **2009**, *131*, 10875–10877. (b) Shih, H.-W.; Vander Wal, M. N.; Grange, R. L.; MacMillan, D. W. C. Enantioselective α -Benzylation of Aldehydes via Photoredox Organocatalysis. *J. Am. Chem. Soc.* **2010**, *132*, 13600–13603. (c) Welin, E. R.; Warkentin, A. A.; Conrad, J. C.; MacMillan, D. W. C. Enantioselective α-Alkylation of Aldehydes by Photoredox Organocatalysis: Rapid Access to Pharmacophore Fragments from β-Cyanoaldehydes. *Angew. Chem. Int. Ed.* **2015**, *54*, 9668–9672. (d) Zhu, Y.; Zhang, L.; Luo, S. Asymmetric α-Photoalkylation of β-Ketocarbonyls by Primary Amine Catalysis: Facile Access to Acyclic all-Carbon Quaternary Stereocenters. *J. Am. Chem. Soc.* **2014**, *136*, 14642–14645.

[20] Murphy, J. J.; Bastida, D.; Paria, S.; Fagnoni, M.; Melchiorre, P. Asymmetric Catalytic Formation of Quaternary Carbons by Iminium Ion Trapping of Radicals. *Nature* **2016**, *532*, 218–222.

Developing this reaction was not trivial since the radical addition to cationic iminium ions **XXI** creates an unstable α-iminyl radical cation **XXII**, which tends to undergo a β-scission to regenerate the more stable iminium ion **XXI**. Key to success was the design of the primary amine catalyst **29**, bearing an electron-rich carbazole moiety. This catalyst could undergo a rapid intermolecular SET reduction of the unstable **XXII**, preventing it from breaking down. A fast tautomerization of the transient enamine intermediate (not shown) leads to the imine **XXIII**, thus avoiding a possible competitive back electron transfer (BET). Finally, intermediate **XXIII** undergoes SET reduction from the reduced photoredox catalyst (PC_{red}), restoring the catalyst **29** and yielding the quaternary product **30**.

The above-mentioned strategies deal with covalent organocatalysis. Non-covalent modes of activation have been also used to enable the enantioselective trapping of photogenerated species. This organocatalytic strategy, in polar domains, has demonstrated to be sufficiently activating and directional to be useful in asymmetric synthesis.[5f-g] However, only a few studies have shown that H-bond donor catalysts can also provide an adequate chiral environment to undergo enantioselective radical-based C-C bond forming reactions. In 2013, the group of Knowles[21] reported the first such example, developing a highly enantioselective intramolecular reductive coupling of ketones and hydrazones (Figure 1.10). By kinetically coupling a SET to a H-bonding event between substrate **31** and the chiral acid **32**, a proton-coupled electron transfer (PCET)[22] activation enabled the generation of radical intermediates as catalyst-bound adducts (see intermediate **XXIV**). Such H-bonding complexes are long-lived enough to serve as a basis for asymmetric induction in the subsequent cyclization step that affords the α-aminoalcohols **33**.

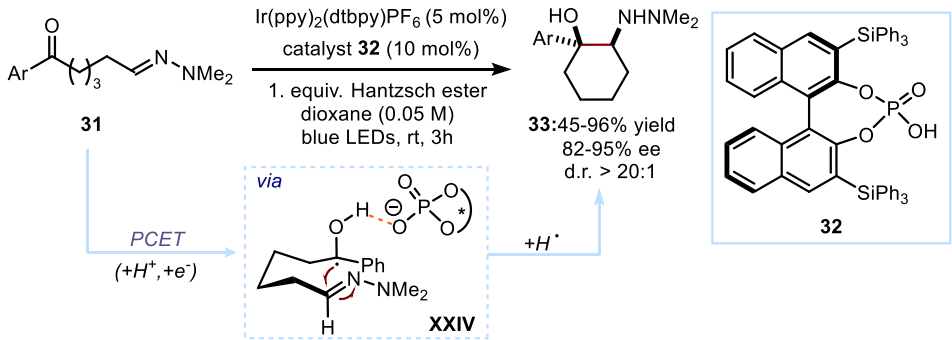

Figure 1.10. Seminal example using a chiral Brønsted acid in a proton-coupled electron transfer (PCET) process.

[21] Rono, L. J.; Yayla, H. G.; Wang, D. Y.; Armstrong, M. F.; Knowles, R. R. Enantioselective Photoredox Catalysis Enabled by Proton-Coupled Electron Transfer: Development of an Asymmetric Aza-pinacol Cyclization. *J. Am. Chem. Soc.* **2013**, *135*, 17735–17738.

[22] Huynh, M. H. V.; Meyer, T. J. Proton-Coupled Electron Transfer. *Chem. Rev.* **2007**, *107*, 5004–5064.

On the other hand, the Ooi's research group[23] reported a highly enantioselective coupling of aldimines **34** with *N*-arylaminomethanes **35**, mediated by the action of a chiral *P*-spiro arylaminophosphonium ion **36** (Figure 1.11). This study exploited the use of an iridium photoredox catalyst that reduced *N*-sulfonyl aldimines **34** to form **XXV**, and oxidized diarylaminomethanes **35** to afford **XXVI**. The chiral cation **36** could selectively bind the anion radical **XXV** through ion-pairing interactions, which secured an appropriate chiral environment to engage **XXV** in a stereocontrolled radical coupling with **XXVI**. This strategy enabled access to 1,2-diamine products **37** in good yields and high levels of enantioselectivity.

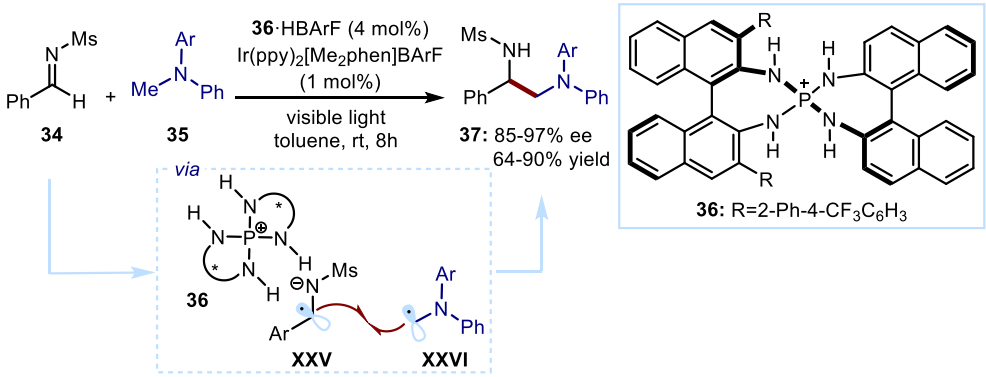

Figure 1.11. Seminal example of a chiral cation (**36**) dictating the selectivity of an ion-radical (**XXV**) during a radical coupling event.

More recently, the group of Phipps[24] has shown how chiral phosphoric acids could efficiently catalyze the asymmetric Minisci-type reaction between prochiral α-amino radicals, generated upon SET reduction of the redox active esters **39**, and pyridines or quinolines **38** (Figure 1.12). The authors proposed that a reversible radical addition event occurs through intermediate **XXVII**, wherein the chiral phosphate catalyst (**40** or **41**) engage in hydrogen-bonding interactions with both the α-amino radical and the pyridium counterion. Due to the reversibility of the radical addition event, diastereoisomeric intermediates of **XXVIII** could presumably be formed. The relative energies of the two diastereoisomeric forms of **XXVIII** and their barrier to deprotonation, would explain the excellent enantioselectivities observed.

[23] Uraguchi, D.; Kinoshita, N.; Kizu, T.; Ooi, T. Synergistic Catalysis of Ionic Brønsted Acid and Photosensitizer for a Redox Neutral Asymmetric α-Coupling of *N*-Arylaminomethanes with Aldimines. *J. Am. Chem. Soc.* **2015**, *137*, 13768–13771.

[24] Proctor, R. S. J.; Davis, H. J.; Phipps, R. J. Catalytic Enantioselective Minisci-Type Addition to Heteroarenes. *Science* **2018**, *360*, 419–422.

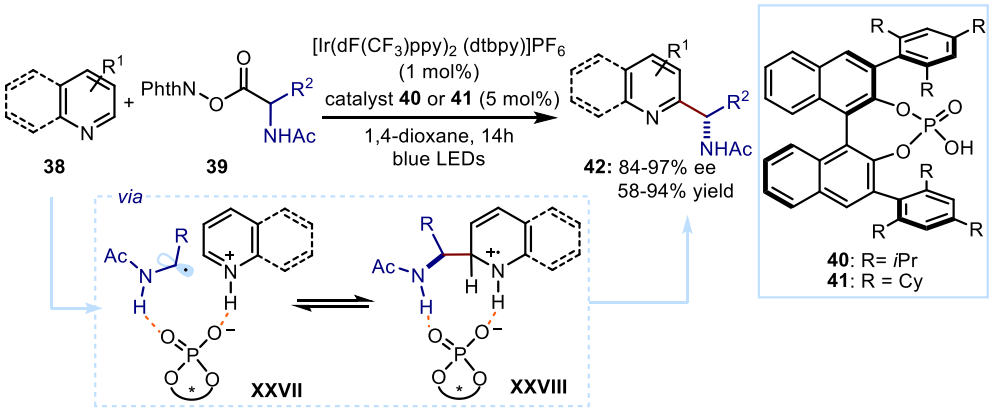

Figure 1.12. Pioneering example using a chiral Brønsted acid to control the enantio- and regioselectivity of the Minisci-type addition of prochiral α-aminoradicals to pyridines or quinolines **38**. NPhth: phthalimide.

Overall, these examples have demonstrated that organocatalytic tools can be successfully used to enforce high levels of stereocontrol in different types of light-driven transformations.

1.2. Organocatalysis in the Excited State for the Mild Generation of Radicals

The functions of organocatalysis within photochemical transformations are not only limited to provide chiral environments suitable for enantioselective bond-forming events. Organocatalysis in the *excited state* has recently emerged as a new methodology to enable radical-type reactivity without the need of using external photoredox catalysts.[25] This approach exploits the ability of colored organocatalytic intermediates to reach an electronically excited state directly upon absorption of visible light, triggering the formation of open-shell intermediates. At the same time, if the organocatalyst is chiral, an effective stereochemical control over the ensuing radical reactions can be achieved. In recent years, our research group has been investigating different types of *radical generation mechanisms* in which well-established organocatalytic intermediates can participate upon *direct excitation*.[26]

[25] Silvi, M.; Melchiorre, P. Enhancing the Potential of Enantioselective Organocatalysis with Light. *Nature* **2018**, *554*, 41–49.

[26] For selected studies, see: (a) Arceo, E.; Jurberg, I. D.; Alvarez-Fernández, A.; Melchiorre, P. Photochemical Activity of a Key Donor-Acceptor Complex can Drive Stereoselective Catalytic α-Alkylation of Aldehydes. *Nat. Chem.* **2013**, *5*, 750–756. (b) Wozniak, Ł.; Murphy, J. J.; Melchiorre, P. Photo-Organocatalytic Enantioselective Perfluoroalkylation of β-Ketoesters. *J. Am. Chem. Soc.* **2015**, *137*, 5678–5681. (c) Silvi, M.; Arceo, E.; Jurberg, I. D.; Cassani, C; Melchiorre, P. Enantioselective Organocatalytic Alkylation of Aldehydes and Enals Driven by the Direct Photoexcitation of Enamines. *J. Am. Chem. Soc.* **2015**, *137*, 6120–6123. (d) Bahamonde, A.; Melchiorre, P. Mechanism of the Stereoselective α -Alkylation of Aldehydes Driven by the Photochemical Activity of Enamines. *J. Am. Chem. Soc.* **2016**, *138*, 8019–8030. (e) Silvi, M.; Verrier, C.; Rey, Y. P.; Buzzetti, L.; Melchiorre, P.

In 2013,[26a] we established that enamines **Ia** (Figure 1.13), formed upon condensation of aldehydes **43** with the secondary amine **45**,[27] could trigger the photochemical generation of radicals through the formation of ground-state, photoactive electron donor-acceptor (EDA) complexes with electron-deficient benzyl bromides **44**.

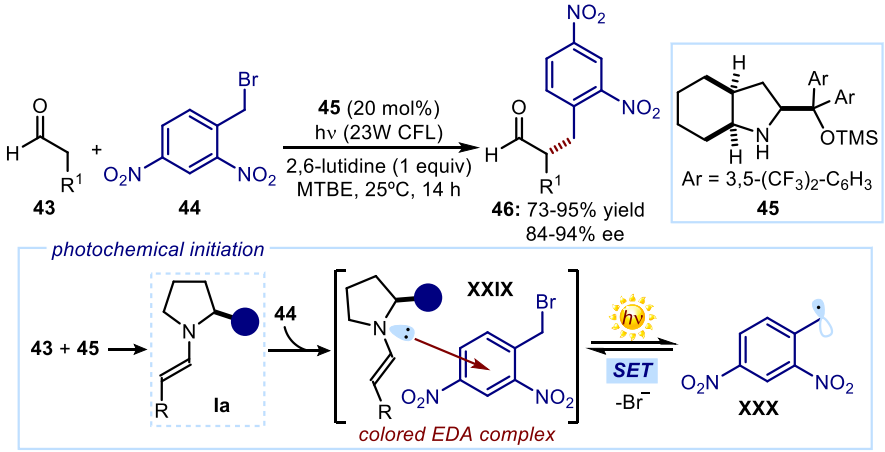

Figure 1.13. Seminal example using catalytically generated enamines **Ia** in the formation of EDA complexes with electron-deficient benzyl bromides **44**. Visible-light irradiation of the EDA-complex **XXIX** triggered the formation of electrophilic radicals of type **XXX**.

Irradiation of the colored EDA-complex **XXIX** with visible light[11] induced a SET event that led to the formation of the open-shell intermediate **XXX**. This radical species could subsequently engage in a self-propagating radical chain mechanism,[26d] affording the chiral α-alkylated products **46** in good yields and enantiomeric excess.

Following this study, our group found[26b] that chiral enolates of type **XXXI** (Figure 1.14), generated upon deprotonation of β-ketoesters **47** under phase-transfer catalysis conditions,[28] could also participate in the formation of colored EDA-complexes with electron-deficient perfluoroalkyl iodides **48**.

Visible-Light Excitation of Iminium Ions Enables the Enantioselective Catalytic β-Alkylation of Enals. *Nat. Chem.* **2017**, 9, 868–873.

[27] Donslund, B. S.; Johansen, T. K.; Poulsen, P. H.; Halskov, K. S.; Jørgensen, K. A. The Diarylprolinol Silyl Ethers: Ten Years After. *Angew. Chem. Int. Ed.* **2015**, 54, 13860–13874.

[28] Shirakawa, S.; Maruoka, K. Recent Developments in Asymmetric Phase-Transfer Reactions. *Angew. Chem. Int. Ed.* **2013**, 52, 4312–4348.

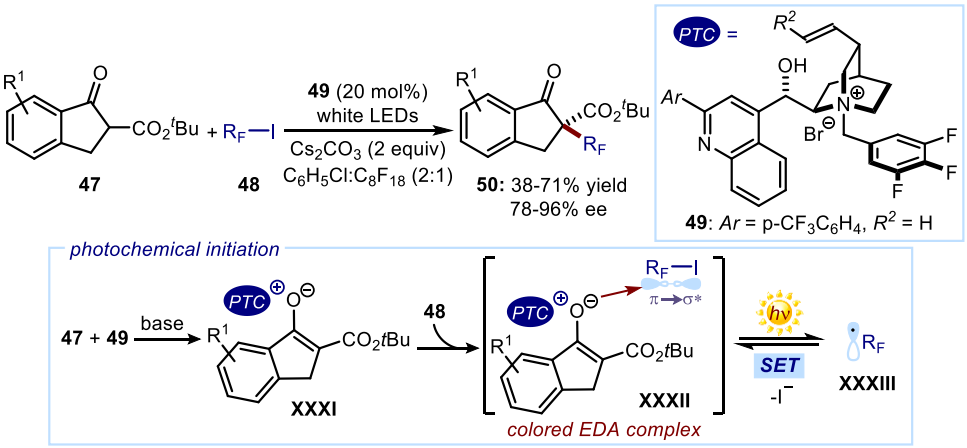

Figure 1.14. The photoactivity of the enolate-based EDA complex **XXXII** enabled the generation of perfluoroalkyl radicals **XXXIII**. These radicals could be subsequently trapped by another molecule of the chiral enolate **XXXI,** leading to the formation of the enantio-enriched ketoester products **50.** PTC: phase-transfer catalyst.

Excitation of the EDA-complex **XXXII** by visible-light led to the generation of perfluoroalkyl radicals **XXXIII** through the reductive cleavage of the C-I bond. The resulting open-shell intermediates **XXXIII** were stereoselectively trapped by another molecule of chiral enolate **XXXI**, ultimately generating the enantio-enriched ketoester products **50** bearing a perfluoroalkyl-containing quaternary stereocenter.

In the above-mentioned examples, the ability of organocatalytic intermediates *(i.e.* chiral enamines and enolates) to form colored EDA complexes was exploited to generate radicals. A second radical generation mechanism relies on the ability of these catalytically generated organic intermediates to directly reach an electronically excited state upon absorption of UV-visible light, and then act as SET reagents. Our group reported the first example of such mechanistic pathway in 2015.[26c] Specifically, we demonstrated that enamines **Ib** (Figure 1.15) could behave as potent single-electron reductants after photoexcitation by near UV-light (E_{ox}*(**Ib**$^{\cdot+}$/**Ib***)≈ -2.50 V, vs Ag/AgCl, NaCl sat.).

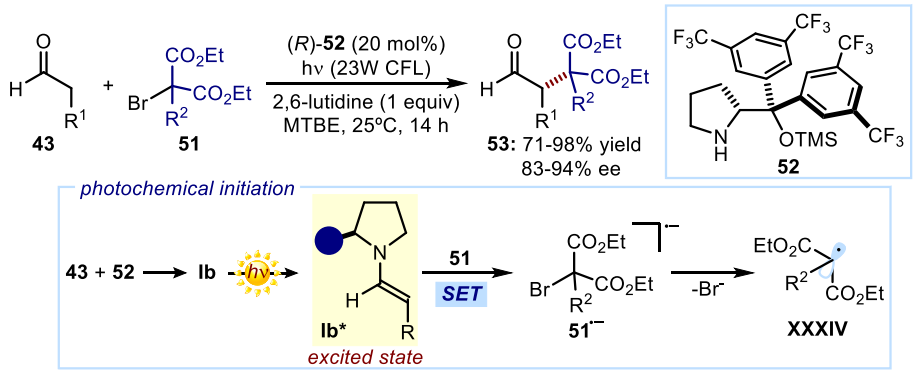

Figure 1.15. Seminal example using excited enamines **Ib*** to reduce bromomalonates **51,** and trigger the formation of electrophilic alkyl radicals (**XXXIV**).

In this transformation, a SET reduction of bromomalonates **51** from the excited enamine **Ib*** induced the formation of radicals **XXXIV**. Such electrophilic radicals were engaged in a self-propagating radical chain mechanism,[26d] giving access to enantio-enriched α-alkylated products **53** in high levels of enantiomeric excess and yield. More recently, it was also established that excited iminium ions **IIa** are capable to initiate radical-based transformations acting as strong photo-oxidants[26e] (Figure 1.16).

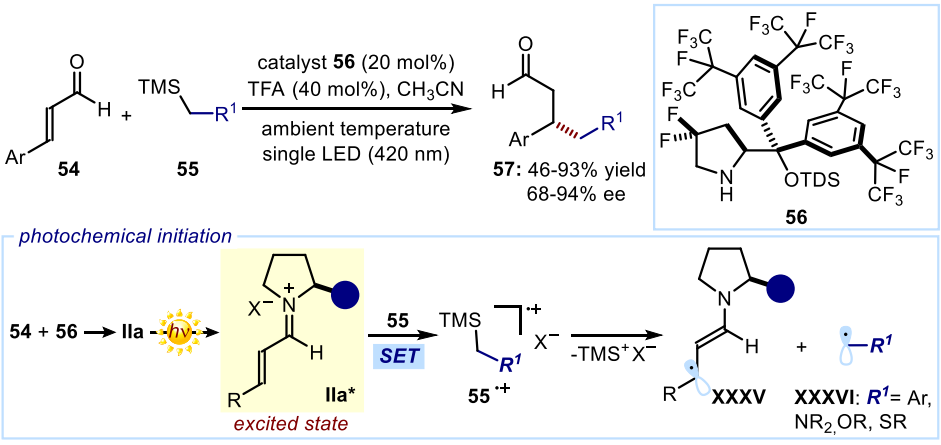

Figure 1.16. First example using excited iminium ions **IIa*** to oxidize alkyl-trimethylsilanes **55,** and trigger the simultaneous formation of the β-enaminyl radical **XXXV** and radicals **XXXVI.**

In this approach, the condensation of the chiral amine catalyst **56** with aromatic enals **54** converts an achromatic substrate (**54**) into a colored iminium ion (**IIa**). Selective excitation with a violet-light emitting diode brings the iminium ion **IIa** to an electronically excited state (**IIa***), converting an electrophilic species into a strong oxidant (E_{red}* (**IIa***/**IIa**$^{\bullet-}$)≈ +2.40 V, vs Ag/Ag+ in CH_3CN). SET oxidation of organic silanes **55** by the excited iminium ion furnishes the chiral β-enaminyl radical **XXXV** along with the radical **XXXVI**, which is

generated upon irreversible fragmentation of the carbon-silicon bond within **55**$^{\cdot+}$. A subsequent stereocontrolled coupling of **XXXV** and **XXXVI** affords the chiral β-functionalized aldehydes **57**. After this study, we have identified other substrates that can be oxidized by the excited iminium ion **IIa*** to then provide reactive radicals, including Hanstzch esters,[29] toluene derivatives,[30] or unactivated alkenes.[31] From a conceptual point of view, these examples highlighted how catalytically generated organic intermediates, containing chromophoric units, can be further exploited to trigger radical-type reactivity upon visible-light excitation.

1.3. General Objectives and Summary

The main scientific objective of this doctoral thesis was to implement organocatalytic strategies to overcome some of the limitations of well-established photochemical processes. Specifically, two known light-driven transformations have been studied: (*i*) the photoenolization of 2-alkyl-benzophenones to access transient enol-intermediates (photoenols), and (*ii*) the photolytic cleavage of stoichiometric thiocarbonyl derivatives to produce radicals.

The *photoenolization process* coupled with classical Diels-Alder chemistry (photoenolization Diels-Alder sequence) is an historical photochemical transformation discovered in 1961.[32] However, an asymmetric catalytic variant has never been realized to date. Chapter II and Chapter III describe how asymmetric organocatalysis provides simple yet effective catalytic tools to engage photoenols in highly stereoselective Diels-Alder and aldol-type processes. On the other hand, the *photolytic cleavage of thiocarbonyl-based compounds* is a known effective method for the generation of radicals. This strategy, originally introduced by Barton,[33] has provided a powerful stoichiometric methodology in radical chemistry to access synthetically relevant open-shell intermediates. However, it still relies on the use of purposely-designed thiocarbonyl-based substrates. Chapter IV details how this radical-generation strategy can be

---

[29] (a) Verrier, C.; Alandini, N.; Pezzetta, C.; Moliterno, M.; Buzzetti, L.; Hepburn, H. B.; Vega-Peñaloza, A.; Silvi, M.; Melchiorre, P. Direct Stereoselective Installation of Alkyl Fragments at the β-Carbon of Enals via Excited Iminum Ion Catalysis. *ACS Catal.* **2018**, *82*, 1062–1066.

[30] Mazzarella, D.; Crisenza, G. E. M.; Melchiorre, P. Asymmetric Photocatalytic C-H Functionalization of Toluene Derivatives. *J. Am. Chem. Soc.* **2018**, *140*, 27, 8439–8443.

[31] Bonilla, P.; Rey, Y. P.; Holden, C. M.; Melchiorre, P. Photo-Organocatalytic Enantioselective Radical Cascade Reactions of Unactivated Olefins. *Angew. Chem. Int. Ed.* **2018**, 57, 12819–12823.

[32] Yang, N. C.; Rivas, C. A New Photochemical Primary Process, the Photochemical Enolization of *o*-Substituted Benzophenones. *J. Am. Chem. Soc.* **1961**, *83*, 2213.

[33] (a) Barton, D. H. R.; Crich, D.; Kretzschmar, G. Formation of Carbon-Carbon Bonds with Radicals Derived from the Esters of Thiohydroxamic Acids. *Tetrahedron Lett.* **1984**, 25, 1055–1058. (b) Barton, D. H. R.; Jaszberenyl, J. C.; Tang, D. Photolytic Generation of Carbon Radicals from Barton Esters: Recent Developments. *Tetrahedron Lett.* **1993**, *34*, 3381–3384. (c) Delduc, P.; Tailhan, C.; Zard, S. Z. A Convenient Source of Alkyl and Acyl Radicals. *J. Chem. Soc., Chem. Commun*. **1988**, 308–310.

translated into a catalytic manifold using a dithiocarbamate anion-based organic catalyst. This new organocatalyst can be used to initiate radical-based processes under mild reaction conditions, starting from readily available starting materials.

1.3.1. An Organocatalytic Strategy for the Enantioselective Diels-Alder Trapping of Photoenols

An organocatalytic strategy to perform a highly stereoselective photoenolization/Diels-Alder (PEDA) sequence is described in Chapter II. This light-driven process has demonstrated its synthetic potential in the total synthesis of naturally-occurring and biologically active substances.[34] However, there is a lack of catalytic asymmetric strategies to perform the PEDA sequence in highly enantioselective manner. Here, we detail how a chiral organic catalyst, derived from natural cinchona alkaloids, can be used to activate maleimides **59** toward highly stereoselective Diels-Alder reactions with photoenols **XXXVII** (Figure 1.17).

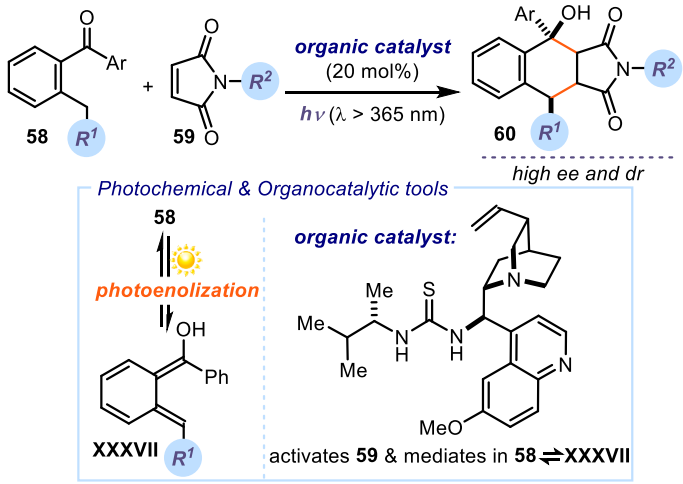

Figure 1.17. Organocatalytic enantioselective Diels-Alder trapping of photochemically generated hydroxy-*o*-quinodimethanes **XXXVII**.

[34] (a) Nicolau, K. C.; Gray, D.; Tae, J. Total Synthesis of Hamigerans: Part 1. Development of Synthetic Technology for the Construction of Benzannulated Polycyclic Systems by the Intramolecular Trapping of Photogenerated Hydroxy-*o*-quinodimethanes and Synthesis of Key Building Blocks. *Angew. Chem. Int. Ed.* **2001**, *40*, 3675–3678. (b) Nicolau, K. C.; Gray, D.; Tae, J. Total Synthesis of Hamigerans: Part 2. Implementation of the Intramolecular Diels-Alder Trapping of Photochemically Generated Hydroxy-*o*-quinodimethanes; Strategy and Completion of the Synthesis. *Angew. Chem. Int. Ed.* **2001**, *40*, 3679–3683. (c) Nicolau, K. C.; Gray, D. L. F.; Tae, J. Total Synthesis of Hamigerans and Analogues Thereof. Photochemical Generation and Diels-Alder Trapping of Hydroxy-*o*-quinodimethanes. *J. Am. Chem. Soc*. **2004**, *126*, 613–627.

Mechanistic investigations disclosed an unconventional mechanism of stereocontrol, wherein the organocatalyst is actively involved in both the photochemical pathway, by leveraging the formation of the reactive photoenol **XXXVII**, and the stereoselectivity-defining event.

This project was undertaken in collaboration with Dr. Luca Dell'Amico, who was involved in the discovery and optimization of the process, and Dr. Alberto Vega Peñaloza, who was involved in the optimization of the process and carried out part of the scope. I directly participated in the optimization process, individually conducting a high-throughput screening of the chiral organocatalysts, and I performed the transient absorption spectroscopy studies with the assistance of Dr. Javier Pérez Hernández (Manager of the Photophysics Unit at ICIQ).

1.3.2. Extending the Reactivity of Photoenols to Enantioselective Aldol-type Processes

After establishing that organocatalytic approaches are suitable for the stereoselective trapping of photoenols, we aimed to exploit the high reactivity of these intermediates in other asymmetric intermolecular addition processes. Chapter III discusses how the high reactivity of photoenols can be used to enable a desymmetric intermolecular aldol process with achiral 2-fluoro-substituted cyclopentane 1,3-diketones **61** (Figure 1.18). The photoenolization-aldol sequence can be performed with high levels of enantioselectivity using a simple chiral organocatalyst, which can differentiate between the two enantiotopic carbonyl groups within the 1,3-diketone **61**. This transformation provides a strategy for the stereoselective construction of valuable fluorine-containing quaternary stereocenters.

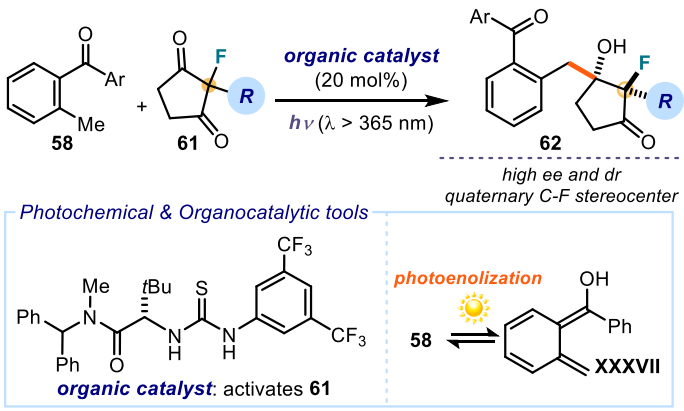

Figure 1.18. Light-driven aldol desymmetrization of prochiral 2-alkyl-2-fluoro cyclopentane-1,3-diketones **61.**

This project was undertaken in collaboration with Dr. Luca Dell'Amico, who was involved in preliminary studies.

1.3.3. A Visible-light Mediated Three-component Radical Process Using Dithiocarbamate Anion Catalysis

Chapter IV details a different type of photochemical process: the photoinduced fragmentation of thiocarbonyl-based compounds to deliver alkyl radicals. This technology uses stoichiometric amounts of easy-to make thiocarbonyl-based substrates, capable of triggering the formation of open-shell intermediates upon direct light-excitation.[33] This chapter describes how this radical generation strategy can be translated into a substoichiometric form by designing a nucleophilic dithiocarbamate (DTC)-based organic catalyst, adorned with a chromophoric unit. This catalyst is able to activate alkyl electrophiles via an S_N2 pathway, and form photo-absorbing intermediates **XXXVIII** that can deliver radicals, upon homolytic cleavage induced by visible light (Figure 1.19). This new catalytic radical generation method has allowed the design of a photoinduced three-component radical process, which couples readily available alkyl chlorides **63**, maleimides **59**, and heteroaromatic fragments **64,** to rapidly generate complex chiral products **65** with high diastereocontrol. The redox-neutral conditions of this process make it tolerant of redox-sensitive substrates and allow the installation of multiple biologically relevant heterocycles within the cascade products **65**.

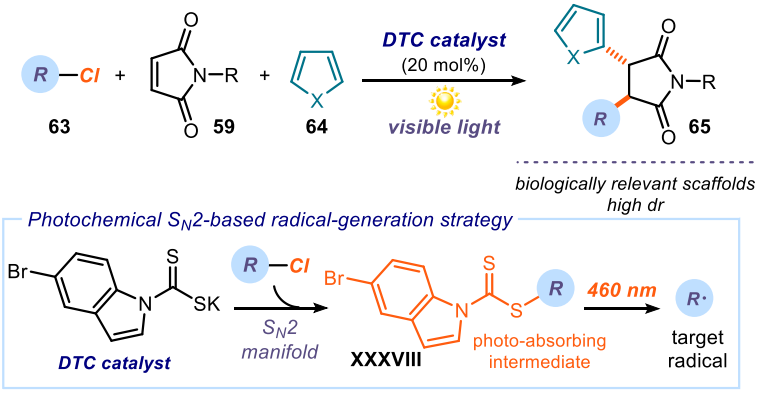

Figure 1.19. Photoinduced three-component radical process mediated by dithiocarbamate anion catalysis.

This project has been undertaken together with Dr. Matthew A. Horwitz, who was involved in the discovery of the reaction and carried out part of the scope, and Dr. Bertrand Schweitzer-Chaput, who originally designed the dithiocarbamate anion catalyst.

Chapter II

An Organocatalytic Strategy for the Enantioselective Diels-Alder Trapping of Photoenols

Target

Development of an organocatalytic strategy to perform a photoenolization/Diels-Alder sequence with high stereoselectivity.

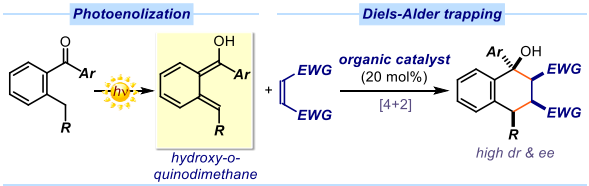

Tools

Use of a chiral hydrogen-bond-donor organic catalyst to activate dienophiles towards a stereoselective Diels-Alder reaction with photoenols.[1]

2.1. Introduction

Photochemical reactions have the potential to generate complex molecular structures from simple building blocks and in a single step. One such reaction is the photoenolization of *ortho*-alkyl aromatic ketones or aldehydes **1** to afford transient hydroxy-*o*-quinodimethanes **I**, a well-known photochemical process[2] established in 1961 (Figure 2.1). The distinctive reactivity of the photo-generated enols **I** (photoenols), which can act as dienes in [4+2]-cycloaddition reactions with electron-poor alkenes **2**, provides a photochemical alternative to classical Diels-Alder chemistry. The resulting chiral benzannulated carbocyclic products **3** are privileged cores found in many biologically relevant compounds. Because of the versatility and the synthetic potential of the photoenolization/Diels-Alder (PEDA) sequence,

[1] The project discussed in this chapter has been conducted in collaboration with Dr. Luca Dell'Amico and Dr. Alberto Vega Peñaloza. We were all involved in the synthesis of a library of hydrogen-bond donor organocatalysts, optimization of the stereoselective reaction, evaluation of the scope, and in performing the mechanistic investigations. I individually carried out the high-throughput screening of the chiral organocatalysts, and the transient absorption spectroscopy measurements with the assistance of Dr. Javier Pérez Hernández (Photophysics Unit-Manager in ICIQ). This work has been published: Dell'Amico, L.; Vega-Peñaloza, A.; Cuadros, S.; Melchiorre, P. Enantioselective Organocatalytic Diels-Alder Trapping of Photochemically Generated Hydroxy-*o*-Quinodimethanes. *Angew. Chem. Int. Ed.* **2016**, *55*, 3313–3317.

[2] Yang, N. C.; Rivas, C. A New Photochemical Primary Process, the Photochemical Enolization of *o*-Substituted Benzophenones. *J. Am. Chem. Soc.* **1961**, *83*, 2213.

this light-driven strategy has attracted great interest within the synthetic community over the past years.[3]

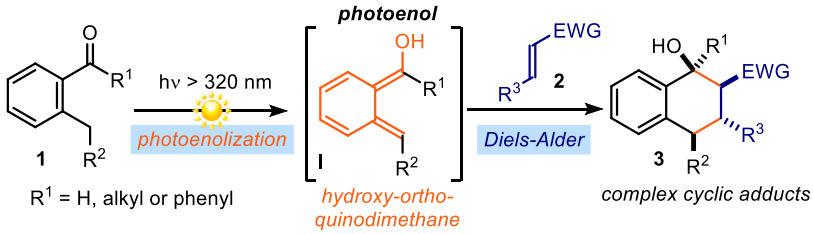

Figure 2.1. The photochemical enolization process of *ortho*-alkyl aromatic ketones and aldehydes **1** generating the reactive hydroxy-*ortho*-quinodimethanes **I**. The intermediate **I** can act as diene in Diels-Alder reactions with electron-poor alkenes, leading to the formation of cyclic adducts **3**.

2.1.1. Photoenolization/Diels-Alder (PEDA) Sequence: Historical Background

In 1961, Yang and Rivas discovered the ability of 2-methylbenzophenone **1a** to undergo a photochemical enolization process upon excitation by ultraviolet light (λ > 320 nm).[2] They observed that the photochemically generated enol intermediate was long-lived enough to allow a [4+2]-cycloaddition reaction with dimethyl acetylenedicarboxylate **4**, leading to the formation of the carbocyclic product **5** (Figure 2.2).

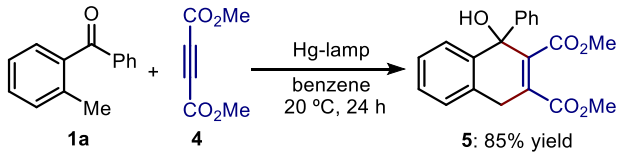

Figure 2.2. Original study by Yang and Rivas on the photoenolization/Diels-Alder (PEDA) sequence.

Their investigations on the photoenolization process were encouraged by the established photochemistry of non-substituted benzophenones. At that time, the photoreduction of benzophenone to benzopinacol was a well-studied reaction.[4] It was established that upon irradiation with UV-light, the non-substituted benzophenone **1b** reaches an electronically excited (n,π*) triplet state, which can undergo an *intermolecular* hydrogen atom transfer (HAT) from a hydrogen donor solvent (left pathway in Figure 2.3). The so-formed ketyl radical **II** rapidly dimerizes to generate the corresponding reduced benzopinacol product **6**.

---

[3] Klán, P.; Wirz, J.; Gudmundsdottir, A. Photoenolization and its Applications. Chapter 26, pp. 627–651. In CRC *Handbook of Organic Photochemistry and Photobiology*. Ed. Griesbeck, A. **2012**, CRC Press, 3rd ed.

[4] (a) Hammond, G. S.; Moore, W. M. The Role of a Triplet State in the Photoreduction of Benzophenone. *J. Am. Chem. Soc.* **1959**, *81*, 6334. (b) Pitts, J. N. Jr.; Letsinger, R. L.; Talor, R. P.; Patterson, J. M.; Recktenwald, G.; Martin, R. B. Photochemical Reactions of Benzophenone in Alcohols. *J. Am. Chem. Soc.*, **1959**, *81*, 1068–1077.

The work by Yang and Rivas revealed that this process is suppressed if benzophenone **1** bears an alkyl substituent at the *ortho*-position of one of the aromatic rings (*i.e.* benzophenones **1a** and **1c**).

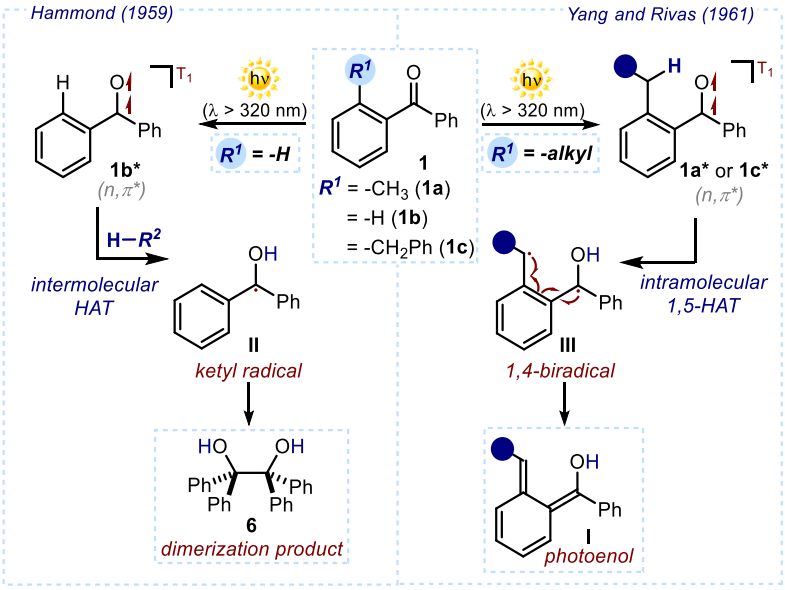

Figure 2.3. The triplet state of non-substituted benzophenones (**1b**) undergoes an intermolecular hydrogen-abstraction from a suitable solvent, leading to the formation of dimerization adducts (left pathway). The work of Yang and Rivas showed that this process is inhibited when *ortho*-alkyl substituted benzophenones (**1a** or **1c**) are employed, leading to the formation of the photoenol **I** (right pathway). HAT: hydrogen atom transfer.

In such cases, no dimerization products coming from the formation of a ketyl radical were observed. The authors rationalised this reactivity proposing an alternative pathway from the triplet state benzophenones **1a** and **1c**: they surmised that an *intramolecular* 1,5-HAT occurs from the benzylic positions of **1a** and **1c**. This produced a conjugated 1,4-biradical **III**, which relaxed to the enolic intermediate **I** (right pathway in Figure 2.3). In particular, the intramolecular 1,5-HAT of aliphatic ketones was studied by Norrish and Bamford almost 20 years before.[5] In the original work by Yang and Rivas, two experiments were performed to prove the existence of intermediate **I**: (*i*) the incorporation of deuterium at the benzylic position when *o*-benzylbenzophenone **1c** was irradiated in deuterated methanol (CH_3OD); and (*ii*) the formation of the Diels-Alder adduct **5** (depicted in Figure 2.2).

[5] Norrish, R. G. W.; Bamford, C. H. Photodecomposition of Aldehydes and Ketones. *Nature* **1937**, *140*, 195–196.

The study of Yang and Rivas unveiled an unknown photochemical primary process, allowing for the rapid formation of reactive intermediates that can be exploited in organic synthesis.[6] Ensuing studies disclosed both the detailed nature of the steps underlying the photoenolization mechanism, and the generality and utility of the photoenolization/Diels-Alder sequence for synthetic endeavours. These aspects will be discussed in the following sections.

2.1.2. The Photoenolization Process

The mechanism of formation of the photoenol intermediate has been the subject of intense research. This light-driven process is directly related with the distinctive photochemistry of carbonyl compounds.[7] The absorption of a photon by a carbonyl compound (**R**, Figure 2.4) produces an electronically excited triplet (n,π*) state (**R***). This can undergo several types of primary photochemical processes to produce an open-shell intermediate (**Int**), such as a radical pair, a biradical or a radical ion pair. Subsequently, a secondary thermal process typically occurs to yield the final closed-shell product (**P**).

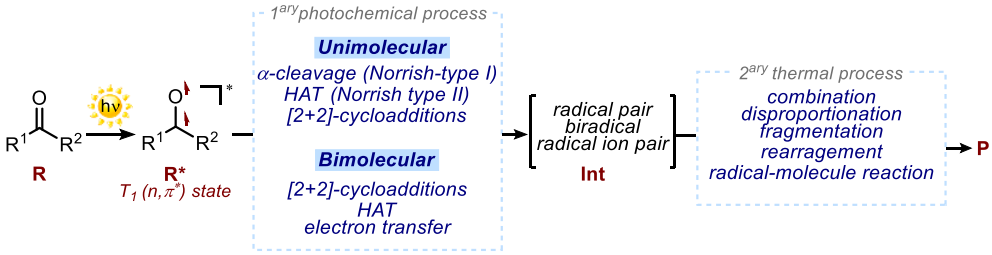

Figure 2.4. Characteristic photochemical and thermal processes of electronically excited carbonyl compounds.

The photoenolization of *o*-alkylphenyl ketones is a particular case of *Norrish-type II reactivity*. This primary photochemical process occurs through a structurally accessible, unstrained cyclic six-membered transition state, which enables a 1,5-hydrogen atom transfer (HAT) to occur from a γ-carbon atom to the carbonyl oxygen of an excited ketone or aldehyde (Figure 2.5). In terms of molecular orbital description, the Norrish-type II reaction involves the γ-hydrogen atom abstraction by the n orbital of the first T_1 (n,π*) state in **7***, to produce the conjugated 1,4-biradical **IV**. The intermediate **IV** can then undergo one of the following

[6] Segura, J. L.; Martin, N. *o*-Quinodimethanes: Efficient Intermediates in Organic Synthesis. *Chem. Rev.* **1999**, *99*, 3199–3246.

[7] Turro, N. J.; Ramamurthy, V.; Scaiano, J. C. Modern Molecular Photochemistry of Organic Molecules. Chapter 9: Photochemistry of Carbonyl Compounds, pp 629–704. **2010**, University Science Books.

secondary thermal processes: (*i*) cyclization to form cyclobutanol **8**;[8] (*ii*) C-C bond cleavage to yield enol **V** and olefin **10**; or (*iii*) disproportionation to regenerate the starting ketone **7**.

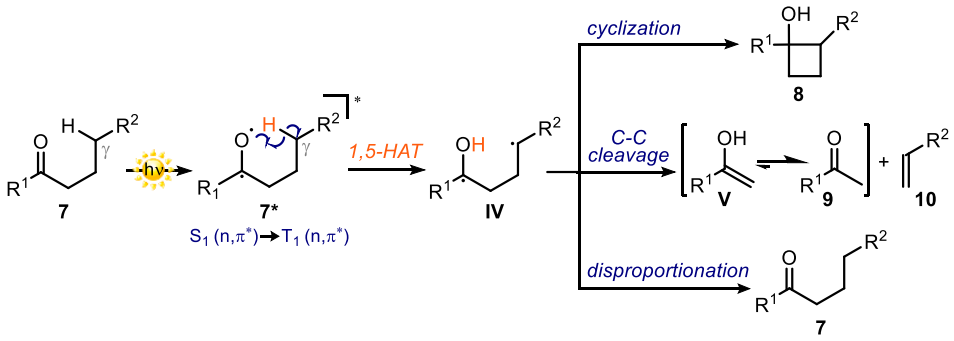

Figure 2.5. The Norrish-type II reactivity involves a 1,5-hydrogen atom transfer (1,5-HAT) from a ɣ-carbon atom to the carbonyl oxygen of the $T_1(n,\pi^*)$ state (**7***). This primary photochemical process generates the biradical **IV**, which can undergo different thermal processes: cyclization, cleavage or disproportionation.

The development of flash photolysis techniques, for which Eigen, Norrish and Porter were awarded the Nobel Prize in chemistry in 1967,[9] has allowed the detailed characterization of all the transient species implicated in the photoenolization process. The current accepted mechanistic pathway is depicted in Figure 2.6.

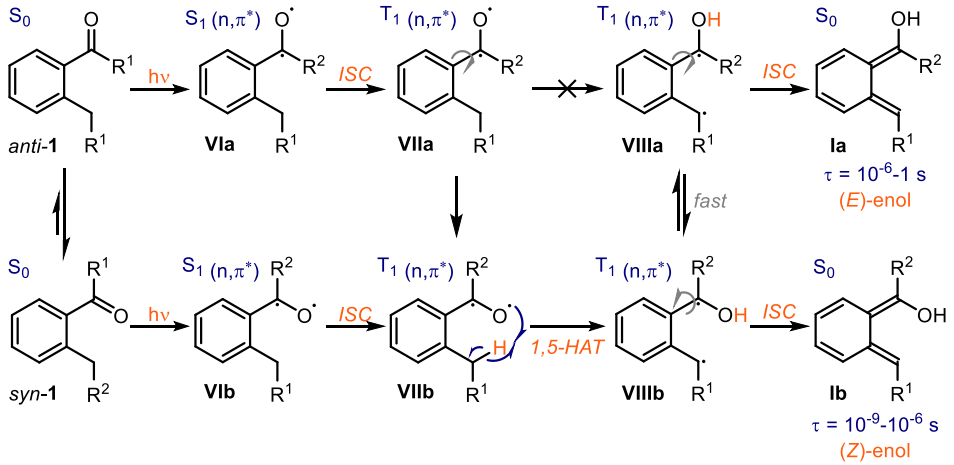

Figure 2.6. Mechanism of photoenolization. S_0: ground state; S_1 singlet excited state; T_1: triplet excited state; 1,5-HAT: 1,5-hydrogen atom transfer; ISC: intersystem crossing.

[8] Yang, N. C.; Yang, D.-D. H. Photochemical Reactions of Ketones in Solutions. *J. Am. Chem. Soc.* **1958**, *80*, 2913.

[9] Porter, G. Flash Photolysis and Some of its Applications. *Nobel Lecture*, December 11, **1967**.

Ortho-alkylbenzophenones **1** are found in solution in equilibrium between the two possible *syn*- and *anti*- conformers.[10] Under irradiation of UV-vis light ($\lambda < 365$ nm), the molecules reach an excited singlet (n,π^*) state (**VIa** and **VIb**) that rapidly decays to the triplet *n*,π^* state (**VIIa** and **VIIb**) through an intersystem crossing process (ISC). The next 1,5-HAT process necessarily occurs from the *syn* isomer of the excited 2-alkylbenzophenone (**VIIb**) through a six-membered transition state.[11] The latter event generates a 1,4-biradical **VIIIb** (or *triplet biradical*).[12] The 1,4-biradical exists in fast equilibrium with its *anti*-conformer **VIIIa**.[13] Both *syn*- and *anti*-conformers can relax to the ground state (*E*)- and (*Z*)-enols, respectively, through another ISC process (**Ia** and **Ib**, respectively).[14] The short-lived ground state (*Z*)-photoenol **Ib** reverts faster to the starting 2-alkylphenylketone *syn*-**1** *via* a 1,5-sigmatropic hydrogen transfer. In contrast, the reketonization of the (*E*)-photoenol **Ia** requires an intermolecular proton transfer. This may occur by protonation of the methylene group by an acid, or by proton transfer from the enol to the solvent or to a base, followed by carbon protonation of the dienol anion.[3] Overall, the difficult reketonization mechanism confers a longer lifetime to the (*E*)-photoenol **Ia**. Its chemical trapping with a suitable dienophile is therefore feasible.[15] The lifetimes of all the transient species are strongly solvent dependent and vary considerably depending on the substitution of the *ortho*-alkylbenzophenones.[16] The lifetime (τ) of the triplet biradicals **VIIIa** and **VIIIb** is in the nanosecond scale (10^{-9} s), the τ of the long-lived (*E*)-enol **Ia** is in the range of microseconds-seconds (10^{-6}-1 s), while the short-lived (*Z*)-enol **Ib** has a τ in the range of nanoseconds-microseconds (10^{-9}-10^{-6} s).[11]

2.1.3. Synthetic Applications of the PEDA Sequence

The applicability of the PEDA sequence within the frame of [4+2]-cycloaddition manifolds has been extensively investigated. In the past decades, the utility of this photochemical procedure has been demonstrated in the straightforward synthesis of tetralin (*i.e.* 1,2,3,4-

---

[10] Das, P. K.; Scaiano, J. C. The Formation of Two Photoenols *via* a Common Pathway in the Photochemistry of 2-Methylbenzophenone. *J. Photochem.* **1980**, *12*, 85–90.

[11] Sammes, P. G. Photoenolisation. *Tetrahedron* **1976**, *32*, 405–422, and references therein.

[12] Findlay, D. M.; Tchir, M. F. Photoenolization of *ortho*-Alkyl-S
ubstituted Acetophenones: An Evidence for the Enol Triplet State. *J. Chem. Soc., Faraday Trans.1*, **1976**, *72*, 1096–1100.

[13] Wagner, P. J.; Chen, C. P. A Rotation–controlled Excited-state Reaction. The Photoenolization of *ortho* Alkyl Phenyl Ketones. *J. Am. Chem Soc.* **1976**, *98*, 239–241.

[14] For a detailed description of the geometry adopted by the radical intermediates of the photoenolization process, see*: Synthetic Organic Photochemistry*. Chapter 2: Abstraction of ɣ-Hydrogens by Excited Carbonyls. Wagner, P. J. Eds. Griesbeck, A. G.; Mattay, J. **2005**, Marcel Dekker.

[15] Block, E.; Stevenson, R. The Irradiation of 2-Methylbenzophenone in the Presence of Dienophiles. *J. Chem. Soc., Perkin Trans. 1* **1973**, 308–313.

[16] Porter, G.; Tchir, M. F. Photoenolization of *ortho*-Substituted Benzophenones by Flash Photolysis. *J. Chem. Soc. A*. **1971**, 3772–3777.

tetrahydronaphthalene) derivatives (Figure 2.7). This core structure is the key carbon skeleton of diverse naturally occurring and biologically active substances.[17] The first contributions exploiting the use of the PEDA sequence in natural product synthesis dates back to 1970's. Sammes and co-workers first reported a synthetic protocol started by a PEDA process, which gave easy access to *justicidin E* (**11**,[18] Figure 2.7) and other structural analogues.

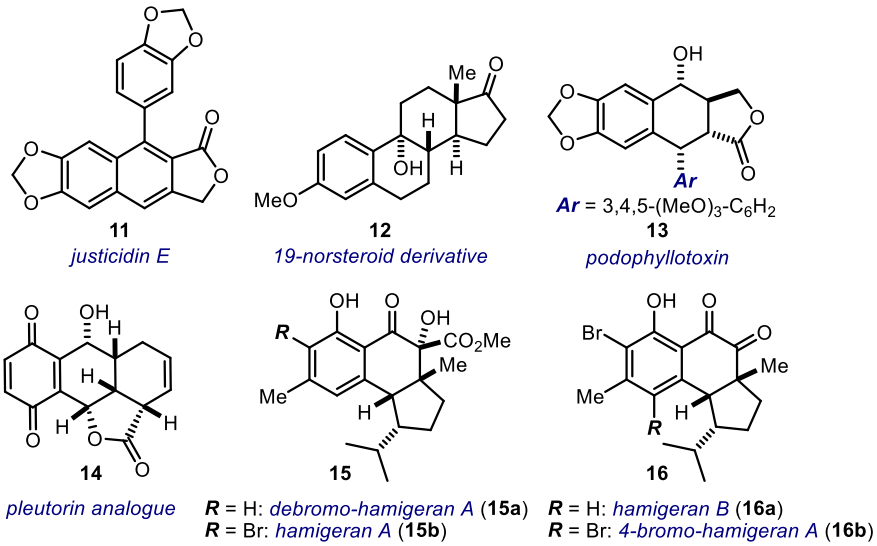

Figure 2.7. Examples of naturally occurring substances synthetized through PEDA sequences.

Years later, Quinckert successfully applied this strategy to the synthesis of stereoid derivatives (**12**).[19] Likewise, Kraus used this process for the synthesis of *podophyllotoxin*[20] (**13**) and a *pleutorin* analogue[21] (**14**). K. C. Nicolau prepared a variety of compounds belonging to the *hamigerans* family (**15** and **16**), exploiting both inter- and intra-molecular variants of the PEDA sequence.[22] Besides natural product synthesis, the PEDA sequence has also found

[17] Wright, P. M.; Seiple, I. B.; Myers, A. G. The Evolving Role of Chemical Synthesis in Antibacterial Drug Discovery. *Angew. Chem. Int. Ed.* **2014**, *53*, 8840–8869.

[18] Arnold, B. J.; Mellows, S. M.; Sammes, P. G. Photochemical Reactions. Part I. A New Route to Tetrahydropodo-phyllotoxin, Taiwanin E, and Related Compounds. *J. Chem. Soc., Perkin Trans. 1* **1974**, 401–409.

[19] Quinckert, G.; Stark, H. Stereoselective Synthesis of Enantiomerically Pure Natural Products – Estrone as Example. *Angew. Chem. Int. Ed. Engl.* **1983**, *22*, 637–655.

[20] Kraus, G. A.; Wu, Y. Hydrogen Atom Abstraction Reactions in Organic Synthesis. A Formal Total Synthesis of Racemic Podophyllotoxin. *J. Org. Chem.* **1992**, *57*, 2922–2925.

[21] Kraus, G. A.; Chen, L. Synthesis and Evaluation of a Pleutorin Analog. *Synth. Commun.* **1993**, *23*, 2041–2049.

[22] (a) Nicolau, K. C.; Gray, D.; Tae, J. Total Synthesis of Hamigerans: Part 1. Development of Synthetic Technology for the Construction of Benzaannulated Polycyclic Systems by the Intramolecular Trapping of Photogenerated Hydroxy-*o*-Quinodimethanes and Synthesis of Key Building Blocks.

applications in other synthetic scenarios, such as solid-state synthesis,[23] or the preparation of polymers.[24]

More recently, several groups have detailed synthetic protocols for the C-H functionalization of the benzylic position of *o*-alkylbenzophenones. These methods are based on the trapping of the corresponding photoenols by diverse types of electrophilic reagents. For example, the group of Murakami has reported a simple methodology for the carboxylation of the *ortho*-position of *o*-alkylphenyl ketones **1** with CO_2 (Figure 2.8).[25]

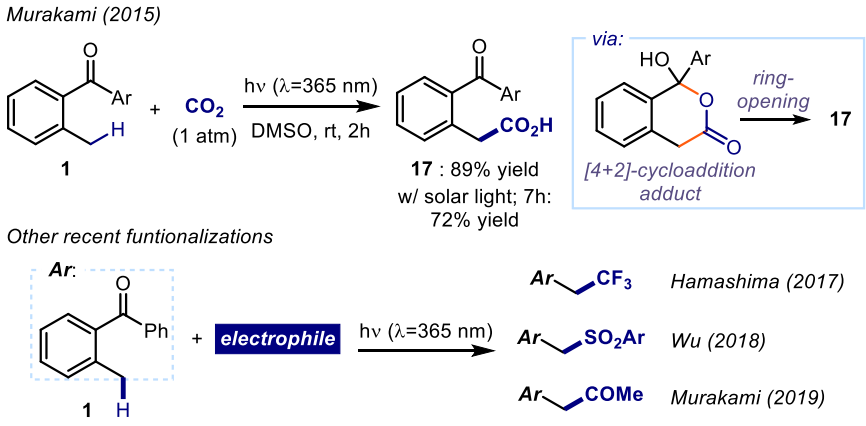

Figure 2.8. Examples of the functionalization of benzilyc C-H bonds *via* photoenol formation.

Computational studies revealed that the [4+2]-cycloaddition reaction between the photoenol and CO_2 was followed by ring opening of the corresponding cyclic adduct, ultimately affording the carboxylated product **17**. Interestingly, the reaction could also be performed using solar light.

Angew. Chem. Int. Ed. **2001**, *40*, 3675–3678. (b) Nicolau, K. C.; Gray, D.; Tae, J. Total Synthesis of Hamigerans: Part 2. Implementation of the Intramolecular Diels-Alder Trapping of Photochemically Generated Hydroxy-*o*-Quinodimethanes; Strategy and Completion of the Synthesis. *Angew. Chem. Int. Ed.* **2001**, *40*, 3679–3683. (c) Nicolau, K. C.; Gray, D. L. F.; Tae, J. Total Synthesis of Hamigerans and Analogues Thereof. Photochemical Generation and Diels-Alder Trapping of Hydroxy-*o*-Quinodimethanes. *J. Am. Chem. Soc*. **2004**, *126*, 613–627.

[23] Moorthy, J. N.; Mal, P.; Singhal, N.; Venkatakrishnan, P.; Malik, R.; Venugopalan P. Highly Diastereoselective Tandem Photoenolization-Hetero-Diels-Alder Cycloaddition Reactions of *o*-Tolualdehydes in the Solid State. *J. Org. Chem*. **2004**, 69, 8459–8466.

[24] Tyson, D. S.; Ilhan, F.; Meador, M. A. B.; Smith, D. D.; Scheiman, D. A.; Meador, M. A. Diels-Alder Trapping of Photochemically Generated *o*-Quinodimethane Intermediates: An Alternative Route to Photocured Polymer Film Development. *Macromolecules* **2005**, *38*, 3638–3646.

[25] Masuda, Y.; Ishida, N.; Murakami, M. Light-Driven Carboxylation of *o*-Alkylphenyl Ketones with CO_2. *J. Am. Chem. Soc.* **2015**, *137*, 14063–14066.

Other functionalizations of the benzylic C-H bond of **1** have been reported (Figure 2.8). These include trifluoromethylation,[26] sulfonylation,[27] and a Pd-catalyzed acylation.[28]

A recent study by Gao and co-workers has shown how the synthetic potential of the PEDA sequence can be further expanded upon combination with Lewis acid catalysis. It is worth mentioning that, in the previous examples, only 1,1- or 1,2-disubstituted alkenes could participate in the intermolecular PEDA reactions.[11,22c] Indeed, sterically hindered tri-substituted olefins were reluctant to react as dienophiles. The group of Gao has overcome this limitation by using Ti(O*i*-Pr)$_4$ to activate poorly reactive tri-substituted alkenes **19** (Figure 2.9).[29] It was hypothesized that the addition of Ti(O*i*-Pr)$_4$, which behaves as a Lewis acid, could induce the formation of a bichelate complex involving both the diene and the dienophile of the PEDA sequence. The formation of such complex would temporarily turn an otherwise intermolecular PEDA into an intramolecular one, which additionally would help to control the diastereoselective outcome of the [4+2]-cycloaddition event. This strategy has allowed the construction of scaffolds of type **20**, bearing three vicinal stereogenic centers. The authors used this PEDA method as a key step in the total synthesis of *oncocalyxone B*.

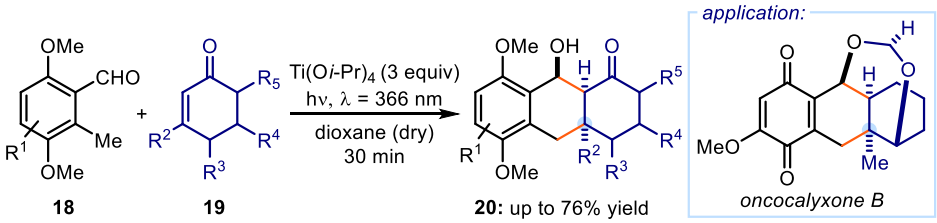

Figure 2.9. Ti(O*i*-Pr)$_4$, acting as a Lewis acid, enables the use of tri-substiuted alkenes **19** in intermolecular PEDA sequences. This strategy has been applied to the total synthesis of *oncocalyxone B*.

2.1.4. Enantioselective Variants of the PEDA Sequence

Despite its broad applications in the synthesis of biologically active compounds, designing a highly enantioselective PEDA reaction, which controls the stereochemistry of the resulting chiral benzannulated products, has proven difficult. Given the innate stereospecificity of the

---

[26] Ide, T.; Masuda, S.; Kawato, Y.; Egami, H.; Hamashima, Y. Benzylic C-H Trifluoromethylation via Photoenol. *Org. Lett.* **2017**, *19*, 4452–4455.

[27] Gong, X.; Chen, J.; Li, X.; Xie, W.; Wu, J. Sulfonylation of Benzylic C-H Bonds through the Reaction of Aryl(*o*-tolyl)methanones with Sulfonyl Hyrazides or Sulfonyl Chlorides. *Chem. Asian. J.* **2018**, *13*, 2543–2548.

[28] Masuda, Y.; Ishida, N.; Murakami, M. Light/Palladium-Promoted Benzylic C-H Acylation Using a Benzoyl Group as the Photo-Directing Group. *Chem. Asian J.* **2019**, *14*, 403–406.

[29] Yang, B.; Lin, K.; Shi, Y.; Gao, S. Ti(O*i*-Pr)$_4$ –promoted Photoenolization Diels-Alder Reaction to Construct Polycyclic Rings and its Synthetic Applications. *Nat. Comm.* **2017**, *8*, 622.

Diels-Alder process, control of the relative stereochemistry can be efficiently achieved.[30] Accordingly, on the basis of the well-defined geometry of the reactive (*E*)-photoenol (Figure 2.6), and upon judicious choice of the dienophile geometry, the *endo* or *exo* Diels-Alder adducts can be formed selectively. Nevertheless, controlling the absolute configuration of the resulting [4+2]-cycloaddition adduct presents several challenges. Specifically, two fundamental issues have historically hampered the development of a highly enantioselective PEDA sequence. The first one is *the fleeting nature of the reactive photoenols*. These intermediates has a limited lifetime ($\tau \approx 1–10^{-6}$ s), which complicates the stereoselective trapping event. The second one is *the difficulty of controlling racemic background reactions*, which occur by direct interception of the photoenol from the dienophile without the assistance of a chiral agent or catalyst. This aspect becomes crucial when considering the development of a catalytic enantioselective variant.

In 2003, the group of Bach reported an effective asymmetric method to perform a PEDA reaction.[31] In this strategy, a stoichiometric amount of a chiral complexing agent **22** was used to bind a purposely designed 2-alkyl substituted aldehyde **21**, adorned with a lactam ring serving as a hydrogen-bond (H-bond) binding site (Figure 2.10).

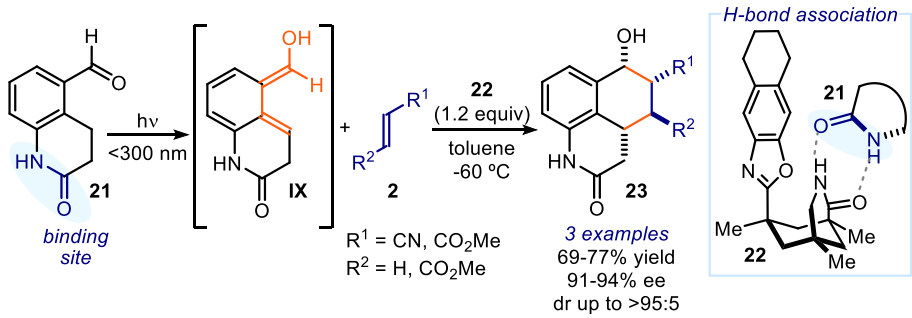

Figure 2.10. The first highly enantioselective PEDA sequence required stoichiometric amounts of the chiral complexing agent **22**.

This H-bond interaction secured an effective differentiation between the two enantiotopic faces of the photochemically generated photoenol **IX**, thus directing the PEDA sequence towards an enantioselective pattern. Nevertheless, the optimal conditions required a stoichiometric amount (at least 1.2 equivalents) of the chiral agent **22**, and a reaction temperature as low as -60 ºC to afford the cycloaddition products **23** with fairly good yields, excellent enantioselectivities, and good diastereoselectivities.

---

[30] Nicolau, K. C.; Snyder, S. A.; Montagnon, T.; Vassilikogiannakis, G. The Diels-Alder Reaction in Total Synthesis. *Angew. Chem. Int. Ed.* **2002**, *41*, 1668–1698.

[31] Grosch, B.; Orlear, C. N.; Herdtweck, E.; Massa, W.; Bach, T. Highly Enantioselective Diels-Alder Reaction of a Photochemically Generated *o*-Quinodimethane with Olefins. *Angew. Chem. Int. Ed.* **2003**, *42*, 3693–3696.

An ideal stereoselective PEDA reaction would require the use of a chiral inducer present in a catalytic amount. To this end, Nicolau and coworkers used the metal-based catalyst (*R*)-BINOL-$TiCl_2$ **26** to mediate the interception of the photoenol, generated upon excitation of aldehyde **24**, with methyl vinyl ketone **25** (Figure 2.11).[22c] Nevertheless, only the use of a high catalyst loading (0.75 equiv.) enabled the formation of the chiral product **27** with a sizeable enantiomeric excess (25% ee). These examples highlight the difficulties associated with developing asymmetric PEDA sequences within a catalytic regime.

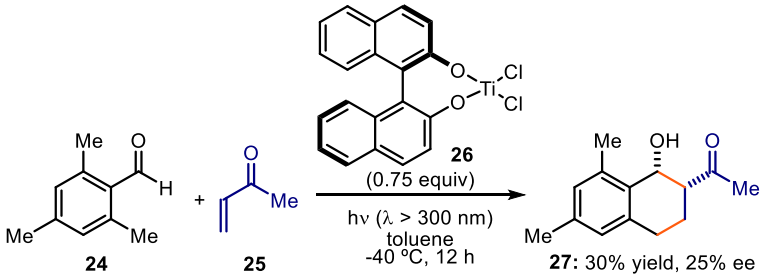

Figure 2.11. A low-enantioselective PEDA sequence using metal-based catalysis.

2.2. Design and Target of the Project

As outlined in the previous sections, the PEDA process is a well-established photochemical transformation that has demonstrated a great synthetic potential in total synthesis.[22] Almost 60 years after its discovery, no effective catalytic enantioselective variants were reported. The only effective approach reported so far has required stoichiometric amounts of the activating agent.[31] To address this limitation, we envisioned a catalytic strategy that utilizes the tools offered by asymmetric organocatalysis. We were encouraged by the fact that the modern field of organocatalysis has provided different methods to perform highly enantioselective and catalytic Diels-Alder processes,[32] some of which exploiting the *in situ* generation of *o*-quinodimethane intermediates.[33] Furthermore, our group has demonstrated that organocatalysis can be combined with photochemical processes to efficiently perform stereocontrolled C-C bond-forming transformations under mild reaction conditions[34].

---

[32] (a) Ahrendt, K. A.; Borths, C. J.; MacMillan, D. W. C. New Strategies for Organic Catalysis: The First Highly Enantioselective Diels-Alder Reaction. *J. Am. Chem. Soc.* **2000**, *122*, 4243–4244. (b) Kim, H.; Gerosa, G.; Aronow, J.; Kasaplar, P.; Ouyang, J.; Lingnau, J. B.; Guerry, P.; Farès, C.; List, B. A Multi-substrate Screening Approach for the Identification of a Broadly Applicable Diels-Alder Catalyst. *Nat. Comm.* **2019**, *10*, 770. (c) Yang, X.; Zhou, Y.-H.; Yang, H.; Wang, S.-S.; Ouyang, Q.; Luo, Q.-L.; Guo, Q.-X. Asymmetric Diels-Alder Reaction of 3-Vinylindoles and Nitroolefins Promoted by Multiple Hydrogen Bonds. *Org. Lett.* **2019**, *21*, 1161–1164.

[33] Liu, Y.; Nappi, M.; Arceo, E.; Vera, S.; Melchiorre, P. Asymmetric Catalysis of Diels-Alder Reactions with *in situ* Generated *ortho*-Quinodimethanes. *J. Am. Chem. Soc.* **2011**, *133*, 15212–15218.

[34] (a) Arceo, E.; Jurberg, I.; Álvarez, A.; Melchiorre, P. Photochemical Activity of a Key Donor-Acceptor Complex can Drive Stereoselective Catalytic α-Alkylatioin of Aldehydes. *Nat. Chem.* **2013**,

Therefore, we wondered whether asymmetric organocatalysis could also provide an effective strategy to stereoselectively intercept fleeting intermediates, such as photoenols. Our approach to make this reaction enantioselective used chiral organocatalysts that could activate dienophiles **2** by means of non-covalent interactions (see Figure 2.12).

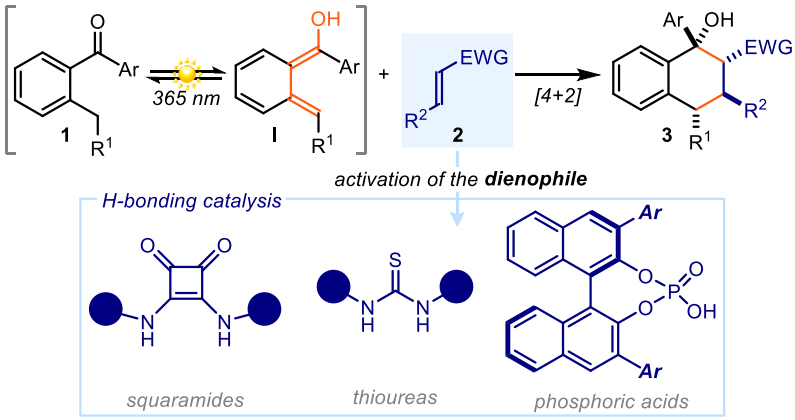

Figure 2.12. Our envisioned strategy for the development of an enantioselective catalytic PEDA process is based on the activation of dienophiles **2** by means of a H-bond donor organic catalyst. Blue dots represent chiral fragments.

A non-covalent activation mode is based on the cooperation of multiple weak attractive interactions between the organic catalyst and the substrate.[35] This is generally achieved by organocatalysts that embody H-bond donor functionalities, such as squaramides[36], thioureas[37] or phosphoric acids.[38] The success of this design plan would deliver the first catalytic system for performing an enantioselective PEDA reaction. Aside of the conceptual implications, our motivations were also fostered by the development of a procedure that uses a simple light

---

5, 750–756. (b) Silvi, M.; Arceo, E.; Jurberg, I. D.; Melchiore, P. Enantioselective Organocatalytic Alkylation of Aldehydes and Enals Driven by the Direct Photoexcitation of Enamines. *J. Am. Chem. Soc.* **2015**, *137*, 6120–6123. (c) Murphy, J. J.; Bastida, D.; Paria, S.; Fagnoni, M.; Melchiorre, P. Asymmetric Catalytic Formation of Quaternary Carbons by Iminium Ion Trapping of Radicals. *Nature* **2016**, *532*, 218–222. (d) Silvi, M.; Verrier, C.; Rey, Y. P.; Buzzetti, L.; Melchiorre, P. Visible-light Excitation of Iminium Ions Enables the Enantioselective Catalytic β-Alkylation of Enals. *Nat. Chem.* **2017**, *9*, 868–873. (e) Silvi, M.; Melchiorre, P. Enhancing the Potential of Enantioselective Organocatalysis with Light. *Nature* **2018**, *554*, 41–49.

[35] Doyle, A. G.; Jacobsen, E. N. Small Molecule H-bond Donors in Asymmetric Catalysis. *Chem. Rev.* **2007**, *107*, 5713–5743.

[36] Alemán, J.; Parra, A.; Jiang, H.; Jørgensen, K. A. Squaramides: Bridging from Molecular Recognition to Bifunctional Organocatalysis. *Chem. Eur. J.* **2011**, *17*, 6890–6899.

[37] Takemoto, Y. Recognition and Activation by Ureas and Thioureas: Stereoselective Reactions Using Ureas and Thioureas as Hydrogen-Bonding Donors. *Org. Biomol. Chem.* **2005**, *3*, 4299–4306.

[38] Zamfir, A.; Schenker, S.; Freund, M.; Tsogoeva, S. B. Chiral BINOL-derived Phosphoric Acids: Privileged Brønsted Acid Organocatalysts for C-C Bond Formation Reactions. *Org. Biomol. Chem.* **2010**, *8*, 5262–5276.

source and readily-available substrates and catalysts, avoiding the need for any tailored or purposely designed reactant.

2.3. Results and Discussions

2.3.1. Preliminary Results

We started our preliminary investigations by selecting commercially available 2-methyl benzophenone **1a** as the photoenolizable substrate. We then focused on the identification of a competent dienophile for the effective trapping of the photoenol, generated upon excitation of **1a**. Initial experiments were conducted in toluene under irradiation by three commercially available black light bulbs (BLB, λ_{max} = 365 nm, Table 1.1).

Table 1.1. Identification of a suitable dienophile to perform a stereoselective PEDA process.

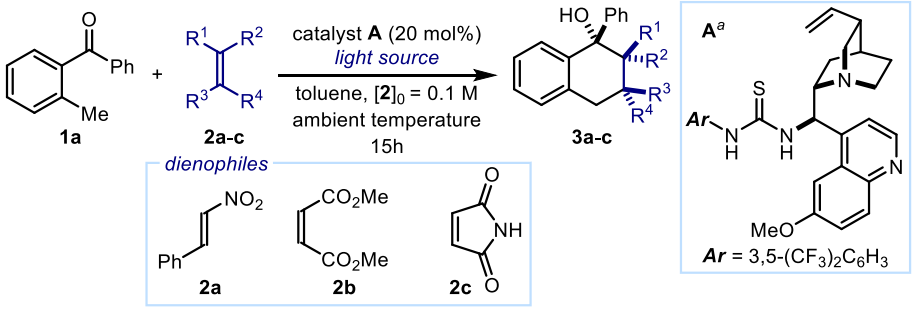

entry	dienophile	light	yield (%)[b]	dr[c]	ee (%)[d]
1	**2a**	16 W BLB[e]	10	3:1	n.d.
2	**2b**	16 W BLB	15	>20:1	n.d.
3	**2c**	16 W BLB	37	>20:1	33
4[f]	**2c**	16 W BLB	80	>20:1	-
5	**2c**	OFF	0	-	-
6	**2c**	Blue LED[g]	0	-	-
7	**2c**	23 W CFL[h]	0	-	-

Reactions performed on a 0.1 mmol scale using 3 equiv. of 2-methylbenzophenone **1a**. [a]Catalyst derived from 9-amino(9-deoxy) *epi*-quinidine. [b]Yields refer to the isolated compounds **3a-3c**. [c]Diastereomeric ratio determined by ^{1}H NMR analysis of the crude reaction mixture. [d]Enantiomeric excess determined by HPLC analysis on a chiral stationary phase. [e] Three 16 W black light bulb (λ_{max} = 365 nm) were used to irradiate the reaction vial. [f] Reaction performed in the absence of catalyst **A**. [g] One blue light emitting diode (λ_{max} = 425 nm) was used to irradiate the reaction vial. [h] Three compact fluorescence lamps (λ_{max} from 360 nm to visible frequencies) were used to illuminate the reaction vial. n.d. = not determined.

The bifunctional cinchona-thiourea catalyst **A**, derived from quinidine, was initially selected as the H-bond donor organocatalyst. This choice was dictated by the propensity of such

catalyst to activate substrates using a non-covalent catalysis mechanism.[39] We evaluated *trans*-β-styrene **2a**, dimethyl maleate **2b**, and maleimide **2c** as the electron poor dienophiles in the photochemical [4+2]-process, in the presence of 20 mol% of catalyst **A** (entries 1-3). Only maleimide **2c** provided promising levels of enantioselectivity (33% ee, entry 3) and yield (37% yield). The other dienophiles afforded the corresponding cyclization products in much lower yield and stereocontrol. Remarkably, the reaction with maleimide **2c** proceeded with complete diastereoselectivity (dr > 20:1), indicating that one of the possible *endo* or *exo* approaches was exclusively favored during the Diels-Alder process. The rate of the background process was also evaluated. In the absence of catalyst **A**, the cyclization product **3c** was obtained in 80% yield with complete diastereoselectivity (entry 4). This result confirms the challenge of channeling the PEDA sequence towards a highly enantioselective pattern. Furthermore, it was puzzling to observe that the presence of catalyst **A** clearly inhibited the formation of the Diels-Alder product (entry 3 vs. entry 4), while inducing a promising level of enantioselectivity. This observation suggested that an unconventional mechanism of stereoinduction could be operative. This prompted us towards extensive mechanistic studies, which are detailed in Section 2.5 of this Chapter. As expected, the control experiment in the dark confirmed the photochemical nature of this transformation (entry 5). Finally, other light sources with higher maximum emission wavelengths resulted in no formation of product **3c** (entries 6-7).

We next performed a screening of chiral organic catalysts based on the cinchona-thiourea scaffold or containing other H-bond-donor functionalities. The screening was performed using the CELLEX-High Throughput Experimentation (HTE) laboratory, which provides the required instrumentation to run a large number of reactions and analyze them in a short period of time. In this first stage, we tested 26 organic catalysts in order to identify a suitable primary catalyst structure. The results for some selected organic catalysts are presented in Table 1.2. A complete list of the organocatalysts tested in this screening is reported in the Experimental Section of this chapter. The best catalyst scaffold was the quinidine-thiourea derived catalyst **D**, which afforded the desired product **3c** in a promising 40% yield and 52% ee (entry 3). Cinchonine and cupreidine-based thioureas (catalysts **B** and **C**, respectively) resulted in considerably lower yields and enantioselectivity (entries 1-2). The amido-thioureas **F** and **G** gave comparable results in terms of yield, although with worse enantioselectivities. Other types of hydrogen-bond donor functionalities, such as the the squaramide **H** or the phosphoric acid **I**, provided good yields of **3c** but in nearly racemic form.

[39] Connon, S. J. Asymmetric Catalysis with Bifunctional Cinchona Alkaloid-Based Urea and Thiourea Organocatalysts. *Chem. Comm.* **2008**, *22*, 2499–2510, and references therein.

Table 1.2. Initial high-throughput screening of organic catalysts - Selected results.

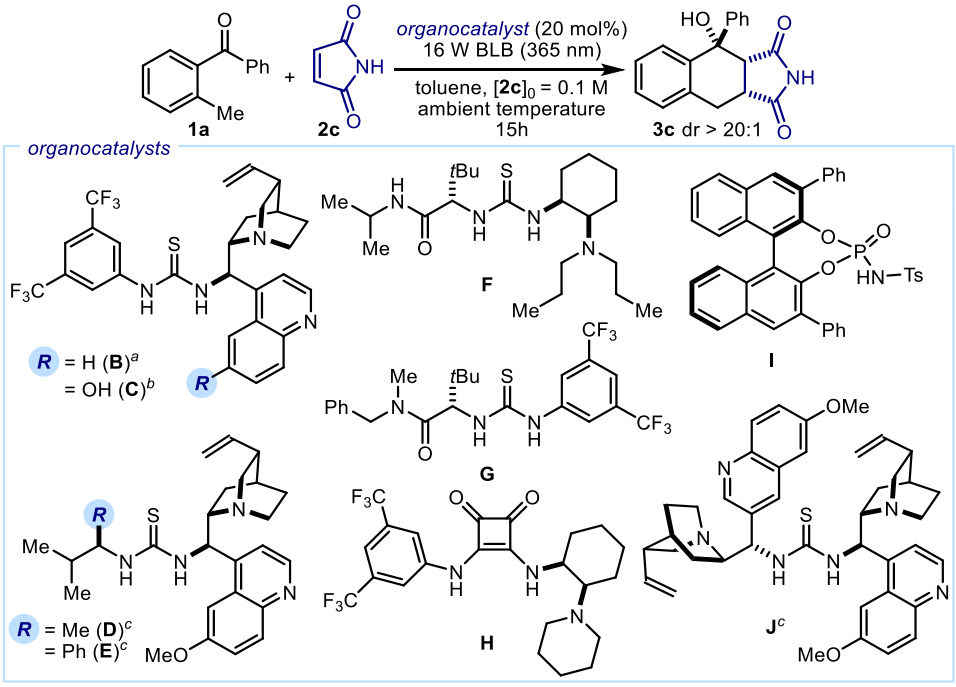

entry	catalyst	yield (%)[d]	ee (%)[e]
1	**B**	11	29
2	**C**	30	11
3	**D**	40	52
4	**E**	37	38
5	**F**	30	10
6	**G**	56	2
7	**H**	47	12
8	**I**	95	2
9	**J**	27	26

Reactions performed on a 0.1 mmol scale using 3 equiv. of 2-methylbenzophenone **1a**. Three 16 W black light bulbs (BLB, λ_{max} = 365 nm) were used to irradiate the reaction vial. [a]Catalyst derived from 9-amino(9-deoxy) *epi*-cinchonine. [b]Catalyst derived from 9-amino(9-deoxy) *epi*-cupreidine. [c]Catalyst derived from 9-amino(9-deoxy) *epi*-quinidine. [d]UltraPerformance Liquid Chromatography (UPLC) yield using biphenyl as the internal standard. [e]Ee determined by UPC² analysis on a chiral stationary phase.

In view of these preliminary results, we synthesized other quinine and quinidine-based organocatalysts bearing different alkyl chains on the thiourea moiety (Table 1.3).

Table 1.3. Evaluation of the importance of the cinchona scaffold, and the effect of an additional stereogenic center within the alkyl chain.

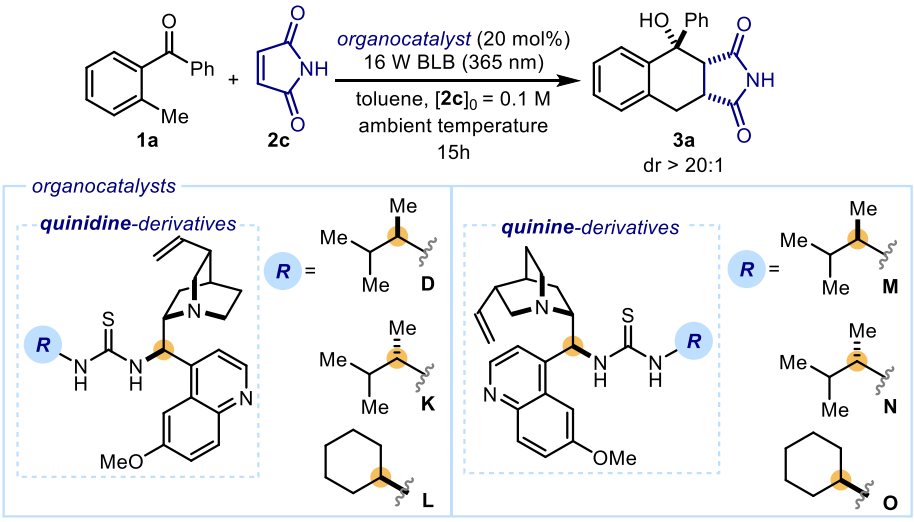

entry	catalyst	yield (%)[a]	ee (%)[b]
1	**D**	40	+52
2	**K**	57	+50
3	**L**	25	+49
4	**M**	48	-33
5	**N**	48	-30
6	**O**	35	-38

Reactions performed on a 0.1 mmol scale using 3 equiv. of 2-methylbenzophenone **1a**. Three 16 W black light bulbs (BLB, λ_{max} = 365 nm) were used to irradiate the reaction vial. [a]Yields of the isolated products after flash chromatography on silica gel. [b]Enantiomeric excess determined by HPLC analysis on a chiral stationary phase.

We evaluated the effect of an additional stereogenic center within the alkyl chain and observed that it did not have appreciable influence on the enantiocontrol of the photo-organocatalytic process (compare entry 1 *vs.* entry 2 and entry 4 *vs.* entry 5). On the other hand, the quinidine scaffold turned out to be the best compared with quinine (compare entries 1-3 vs. entries 4-6). The quinidine-based scaffold was then selected for further catalyst optimization studies.

We next evaluated the effect of other type of alkyl fragments linked to the thiourea, keeping the quinidine motif as the main catalyst structure (Table 1.4). Unexpectedly, all the catalysts with bulkier substituents resulted in the formation of **3a** with lower values of ee (entries 1-4). The substitution with a simple methyl group afforded the product **3a** in almost racemic fashion (entry 6). Only catalyst **T**, which resembles the best catalyst scaffold found in the initial

screening (*i.e.* catalyst **D**), provided comparable results in terms of enantioselectivity (entry 5, 28% yield, 49% ee).

Table 1.4. Effect of the chiral alkyl group of the thiourea moiety.

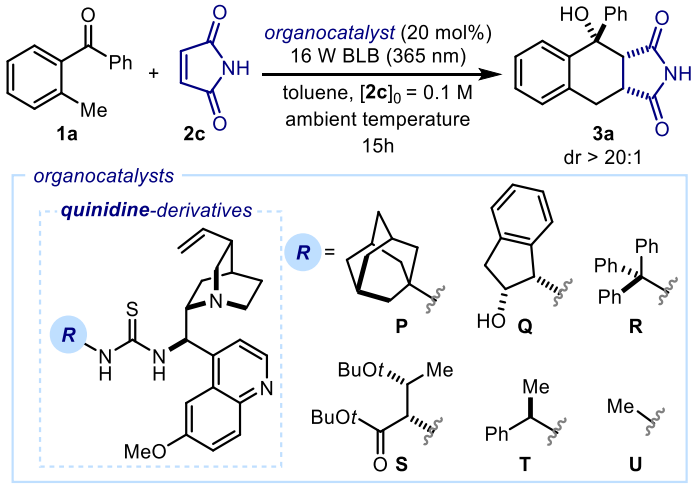

entry	catalyst	yield (%)[a]	ee (%)[b]
1	**P**	40	28
2	**Q**	22	40
3	**R**	40	3
4	**S**	20	17
5	**T**	28	49
6	**U**	47	2

Reactions performed on a 0.1 mmol scale using 3 equiv. of 2-methylbenzophenone **1a**. Three 16 W black light bulbs (BLB, λ_{max} = 365 nm) were used to irradiate the reaction vial. [a]Yields of the isolated product **3a** after flash chromatography on silica gel. [b]Enantiomeric excess determined by HPLC analysis on a chiral stationary phase.

From this study we concluded that the structure of the alkyl fragment linked to the thiourea must be similar to the ones found for catalysts **D** and **T**.

We next evaluated the effect of the protecting group of the maleimide substrate, employing catalyst **D** as the model catalyst (Table 1.5). These studies revealed that the enantioselective outcome of the reaction can be further improved by protecting the maleimide with a *tert*-butyl group. When *N*-*tert*-butylmaleimide **2f** was employed as dienophile in the PEDA sequence, the corresponding product **3f** could be obtained in an encouraging 35% yield and 75% ee (entry 3). With this result in hand, we established 2-methylbenzophenone **1a** and *N*-*tert*-butylmaleimide **2f** as the model substrates for the enantioselective PEDA sequence. A

subsequent control experiment revealed that the enantioselectivity of the process was somehow sensitive to the type of light employed.

Table 1.5. Evaluation of the effect of the N-protecting group of maleimides.

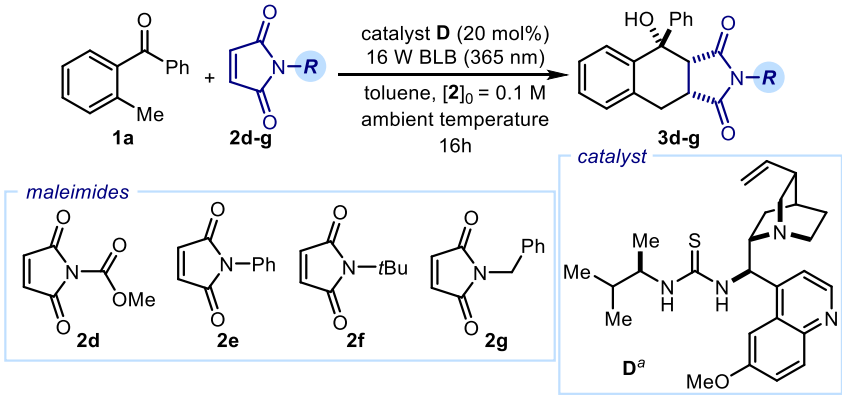

entry	maleimides	yield (%)[b]	dr[c]	ee (%)[d]
1	**2d**	12	5:1	29
2	**2e**	20	>20:1	49
3	**2f**	35	>20:1	75
4	**2g**	10	10:1	49
5[e]	**2f**	35	>20:1	84

Reactions performed on a 0.1 mmol scale using 3 equiv. of 2-methylbenzophenone **1a**. Three 16 W black light bulbs (BLB, λ_{max} = 365 nm) were used for irradiation. [a]Catalyst derived from 9-amino(9-deoxy) *epi*-quinidine. [b]Yields of the isolated products after flash chromatography on silica gel. [c]Diastereomeric ratio based on the ^{1}H NMR analysis of the reaction crude. [d]Enantiomeric excess determined by HPLC analysis on a chiral stationary phase. [e]A single black LED (λ_{max} = 365 nm) was used to irradiate the reaction vial.

Thus, we found that the use of a single black LED (light emitting diode) with an emission at 365 nm markedly increased the stereocontrol up to 84% (entry 5). The exact origin of this behaviour when using a single black LED remains unclear, but it may be likely related to a better control of the irradiance of the illumination system. This parameter undoubtedly affects the photoenolization process, and consequently, the amount of reactive photoenol formed. Therefore, the fine-tuning of the irradiance may contribute in minimizing the unwanted background racemic reaction, resulting in an enhancement of the stereoselectivity of the process.

The change of dienophile prompted us to re-evaluate the importance of the two main structural elements of the identified best catalysts. From preliminary results obtained with the unprotected maleimide **2a,** we concluded that: (*i*) thioureas based on the 9-amino(9-deoxy) *epi*-quinidine scaffold were the most appropriate organic catalysts (please refer to Table 1.3),

and (*ii*) that the alkyl fragment linked to the thiourea moiety should not be excessively bulky (please refer to Table 1.4). Considering these features, and with a more adequate light source in hand, we next focused on performing further structural tuning of the catalyst. Initially, we investigated the effect of other alkyl fragments linked to the thiourea functionality (Table 1.6).

Table 1.6. Last structural tuning of the chiral alkyl group attached to the thiourea moiety.

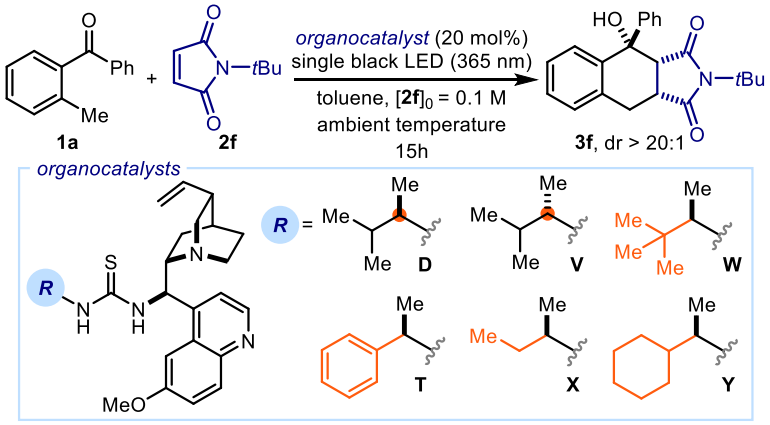

entry	catalyst	yield (%)[a]	ee (%)[b]
1	**D**	35	84
2	**V**	18	68
3	**W**	35	20
4	**T**	25	20
5	**X**	30	80
6	**Y**	25	49

Reactions performed on a 0.1 mmol scale using 3 equiv. of 2-methylbenzophenone **1a.** A single black LED (λ_{max} = 365 nm) was used to irradiate the reaction vial. [a]Yield of the isolated product **3f** after flash chromatography on silica gel. [b]Enantiomeric excess determined by HPLC analysis on a chiral stationary phase.

A matched/mismatched effect was observed when using catalyst **V**, which has an opposite configuration at the thiourea stereogenic center (entry 1 *vs.* entry 2), confirming the influence of this chiral moiety on the stereodefining event. Other substitution patterns different from the one of catalyst **D** turned to be considerable worse in terms of stereocontrol, with exception of catalyst **X**, which provided product **3f** in 80% ee (entry 1 *vs.* entry 5).

Next studies involved the evaluation of the hydrogen-bond donor functionality (Table 1.7). We observed that replacing the thiourea moiety with an urea (catalyst **Z)** or a squaramide (catalyst **AA**) resulted in much lower levels of enantiocontrol and yield (entries 1-2). Finally, modifications at the 2 position of the quinoline scaffold (catalysts **AB-AD**) were also

evaluated. Catalyst **AB** gave slightly better results in terms of ee but the yield dropped sensibly from 35% to 15%. Catalyst **AC** gave similar ee while slightly lower yield was observed. The presence of an *n*-butyl chain at position 2 of the quinoline ring (**AD**), resulted in both lower ee and yield. These last studies established catalyst **D** as the best catalyst to undergo the final cycles of optimization.

Table 1.7. Last structural tuning of the catalyst. Evaluation of both the H-bond donor functionality and substitution in the position 2 of the quinoline ring.

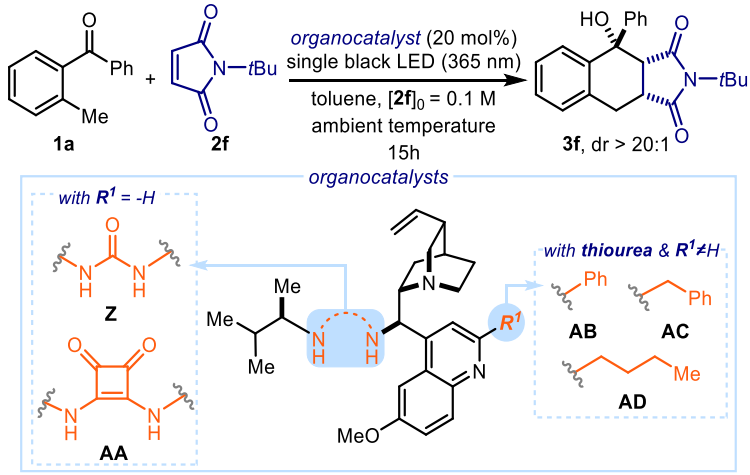

entry	catalyst	yield (%)[a]	ee (%)[b]
1	**Z**	21	24
2	**AA**	31	6
3	**AB**	15	86
4	**AC**	40	84
5	**AD**	23	82

Reactions performed on a 0.1 mmol scale using 3 equiv. of 2-methylbenzophenone **1a**. A single black LED (λ_{max} = 365 nm) was used to irradiate the reaction vial. [a]Yield of the isolated product **3f** determined after flash chromatography on silica gel. [b]Enantiomeric excess determined by HPLC analysis on a chiral stationary phase

2.3.2. Final Optimization

The preliminary studies identified 2-methylbenzophenone **1a** and *N*-*tert*-butylmaleimide **2f** as suitable candidates to participate in an enantioselective PEDA sequence mediated by 20 mol% of the thiourea cinchona catalyst **D** (Figure 2.13). Additionally, the use of a single black LED was found to be the most convenient light source. We further investigated other reaction parameters, including solvents, light intensity, reaction time, concentration and temperature.

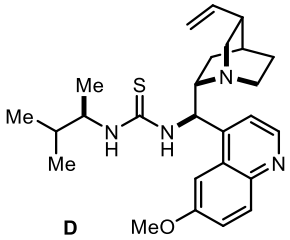

Figure 2.13. Selected organocatalyst to undergo the last cycle of optimization.

We first evaluated the effect of the reaction medium (Table 1.8). The process performed better in apolar solvents, furnishing enhanced results in terms of both yield and ee than polar media (entries 2 and 3).

Table 1.8. Solvent screening

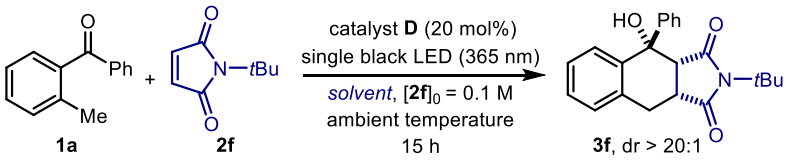

entry	solvent	yield (%)[a]	ee (%)[b]
1	toluene	35	84
2	THF	0	-
3	DMSO	16	5
4	mesitylene	30	80
5	hexane	68	71
6	cyclohexane	40	83

Reactions performed on a 0.1 mmol scale using 3 equiv. of 2-methylbenzophenone **1a**. A single black LED (λ_{max} = 365 nm) was used to irradiate the reaction vial. [a]Yield of the isolated product **3f** after flash chromatography on silica gel. [b]Enantiomeric excess determined by HPLC analysis on a chiral stationary phase.

Reactions conducted in mesitylene and cyclohexane provided the best chemical yield without affecting the stereocontrol (entries 4 and 6). On the other hand, hexane secured the desired product in higher chemical yields, but with a considerable loss of ee (entry 5). Given the better balance between reactivity and enantioselectivity offered by cyclohexane (40% yield, 83% ee), this solvent was selected for further optimization studies.

Attempts to reproduce the initial results obtained with cyclohexane were not completely satisfactory, since variations of the product yield were obtained when using different black single LED (Figure 2.14, top left). The reproducibility of an experiment is a fundamental

aspect of the scientific method.[40] In a photochemical reaction, many parameters can significantly affect its efficiency and robustness, including the intensity of the light or the distance of the light source from the reaction vessel. In the case of our reaction set-up, the distance of the light source from the reaction vial is kept constant thanks to an aluminium block fitted with the 365 nm single black LEDs (Figure 2.14, top left).

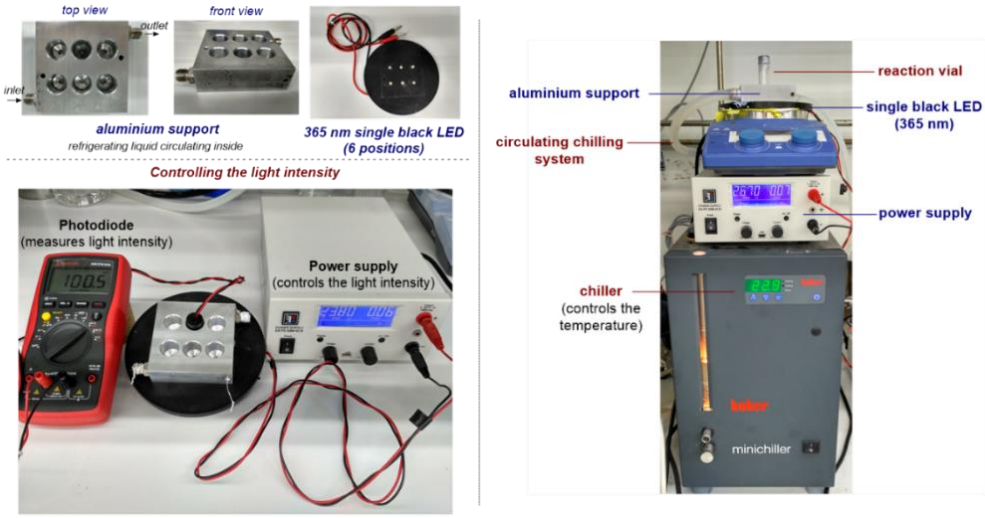

Figure 2.14. Detailed set-up and illumination system. *Top left*: aluminium support and single black LEDs; *bottom left*: photodiode, aluminium block fitted with the single black LEDs and power supply. *Right*: the connected reaction set-up.

The plate containing the single black LEDs is connected to a power supply (Figure 2.14, bottom left) that can be used to finely control the intensity of emission (irradiance, mW/cm^2). When we measured the irradiance of every single black LEDs with a photodiode light detector (device shown in Figure 2.14, bottom left), we ascertained that this parameter was not identical for the different LEDs within the same plate. This fact likely caused the irreproducibility of the results. Additionally, this observation indicated that the light intensity was another important parameter to optimize (Table 1.9). We could achieve reproducible results and better yields when setting the irradiance at 10 mW/cm^2, which was the maximum value attainable by our illumination set-up (Table 1.9, entry 3).

[40] (a) Baker, M. 1,500 Scientists Lift the Lid on Reproducibility. *Nature News* **2016**, *533*, 452–454. (b) Cooper, M. M. The Replication Crisis and Chemistry Education Research. *J. Chem. Educ.* **2018**, *95*, 1-2.

Table 1.9. Effect of light intensity, reaction time and concentration on the model reaction

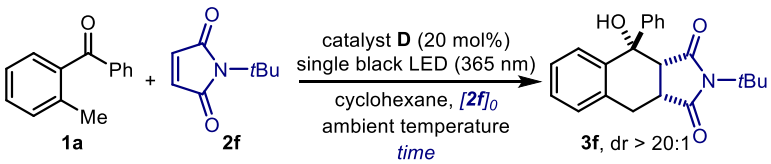

entry	irradiance (mW/cm^2)	[2f]$_0$ (M)	time (h)	yield (%)[a]	ee (%)[b]
1	7	0.1	15	40	83
2	9	0.1	15	43	85
3	10	0.1	15	50	85
4	10	0.2	15	52	82
5	10	0.5	15	52	84
6	10	0.1	30	35	86
7	10	0.1	40	37	84

Reactions performed on a 0.1 mmol scale using 3 equiv. of 2-methylbenzophenone **1a**. A single black LED (λ_{max} = 365 nm) was used to irradiate the reaction vial. [a]Yield of the isolated product **3f** after flash chromatography on silica gel. [b]Enantiomeric excess determined by HPLC analysis on a chiral stationary phase.

No improvements in chemical yields nor in enantioselectivity were obtained by increasing the concentration of **2f** up to 0.5 M (Table 1.9, entries 4-5). Extending the reaction time afforded the product in lower yield (entries 6-7). To understand this counterintuitive result, we performed investigations to evaluate the stability of product **3f** and catalyst **D** under the reaction conditions. As shown in Figure 2.15, product **3f** and catalyst **D** suffered decomposition after extensive exposure to light at ambient temperature.

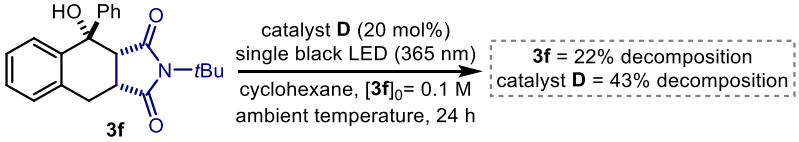

Figure 2.15. Experiment highlighting the partial instability of product **3f** ad catalyst **D** under the irradiation of the single black LED (365 nm) at ambient temperature. Percentage of decomposition calculated by ^{1}H NMR analysis using 1,3,5-trimethoxybenzene as the internal standard.

Although we could not characterize the products of the decomposition, these experiments indicated the need of preserving both the product stability and the catalyst activity. With the aim of shortening the reaction time and reducing the period of illumination, the reaction was performed at higher temperatures (Table 1.10, entry 1). However, at 40 °C the enantioselectivity was dramatically affected (70% ee). Gratifyingly, a better yield along with

an increase in enantiocontrol was obtained at 10 ºC (Table 1.10, entry 3), a likely consequence of a better product/catalyst stability under cryogenic conditions. Thus, we decided to further decrease the reaction temperature to -5 ºC. For maintaining a low temperature while irradiating, we needed an adequate combination of solvents to avoid the solidification of cyclohexane (melting point: 6.5 °C). Thus, a 1:1 cyclohexane:toluene mixture was initially used (entry 4), which gave enhanced results (66% yield, 89% ee). Further optimization of the solvent system identified that a 3:1 cyclohexane:toluene mixture afforded product **3f** with a satisfactory yield of 76% and a high enantioselectivity (90% ee, entry 7). The control experiment depicted in Figure 2.15, but performed at 0 ºC, confirmed the stability of both catalyst and product under these conditions.

Table 1.10. Evaluation of the temperature on the model reaction

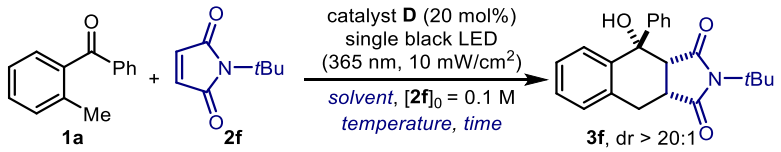

entry	temperature (ºC)	time (h)	solvent	yield (%)[a]	ee (%)[b]
1	40	15	CyH[c]	29	70
2	25	15	CyH	50	85
3	10	15	CyH	57	88
4	-5	15	CyH:Tol[d] (1:1)	66	89
5	-5	24	CyH:Tol (1:1)	80	89
6	-5	24	CyH:Tol (2:1)	75	88
7	-5	24	CyH:Tol (3:1)	76	90

Reactions performed on a 0.1 mmol scale using 3 equiv. of 2-methylbenzophenone **1a**. A single black LED (λ_{max} = 365 nm) was used to irradiate the reaction vial. [a]Yield of the isolated product **3f** after flash chromatography on silica gel. [b]Enantiomeric excess determined by HPLC analysis on a chiral stationary phase. [c]CyH: Cyclohexane. [d]Tol: toluene.

After an extensive period of optimization, the optimal conditions to perform a highly enantioselective PEDA sequence were finally identified.

2.3.3. Scope of the reaction

Adopting the optimized conditions, we demonstrated the generality of the light-driven [4+2]-cycloaddition process by evaluating a variety of 2-alkylbenzophenones **1** and maleimides **2**. As shown in Figures 2.16 and 2.17, there is significant tolerance for structural and electronic variations of the photoenolizable substrates **1** to enable access to a variety of complex tetrahydronaphthalenols (**3f-q**) bearing three or four stereogenic centers with exquisite

diastereomeric ratio and high enantiomeric excesses. Different substituents on the enolizable aromatic ring of **1** are well tolerated (products **3g**-**3i**, Figure 2.16), while a prochiral center at the *ortho*-benzylic position of **1** induces the formation of stereochemically dense products with high fidelity (products **3j**-**3l,** dr>20:1). Crystals from compound **3h** and the tetracyclic adduct **3l**[41] were suitable for X-ray analysis.

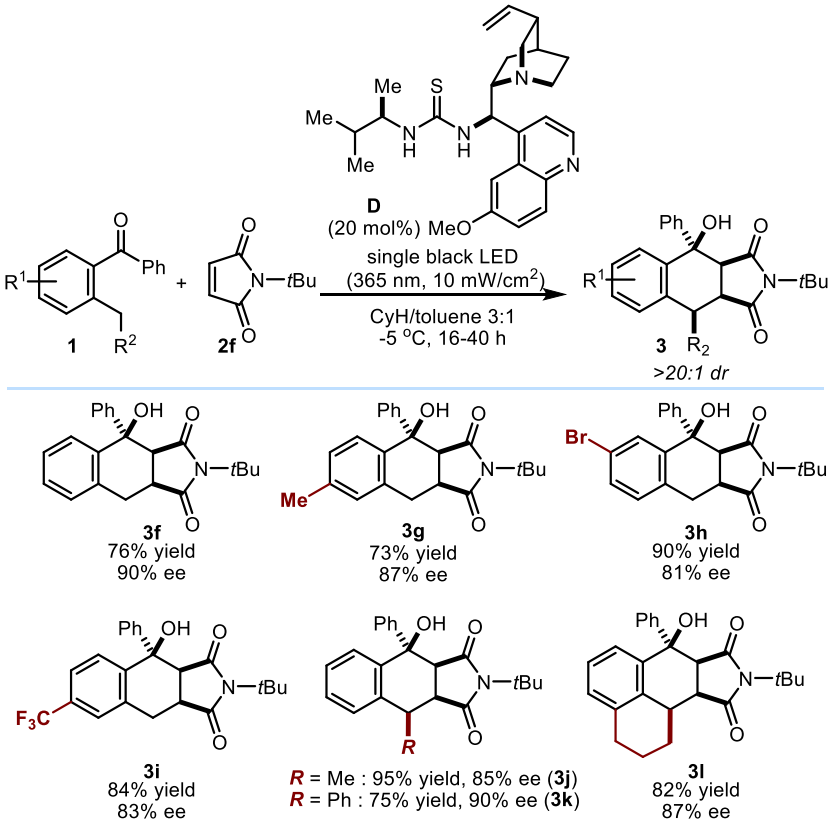

Figure 2.16. Survey of 2-alkylbenzophenones **1** that can participate in the reaction. Reactions performed on a 0.2 mmol scale; yields and enantiomeric excesses of the isolated products **3** are indicate below each entry. CyH = cyclohexane; *t*Bu =*tert*-butyl.

Modifications at the non-enolizable aryl ring in **1** are also possible, with the presence of both electron-withdrawing and donating groups furnishing products **3m-q** in high chemical and optical yields (Figure 2.17). Also maleimides with different substituents at the nitrogen atom are suitable substrates (**3r**, **3s**). One limitation of the system is that the *N*-unprotected maleimide affords the [4+2]-cycloaddition adduct **3t** with poor enantiocontrol (50% ee).

[41] Crystallographic data for compounds **3h** and **3l** have been deposited with the Cambridge Crystallographic Data Center, accession numbers CCDC 1417309 and 1417310, respectively.

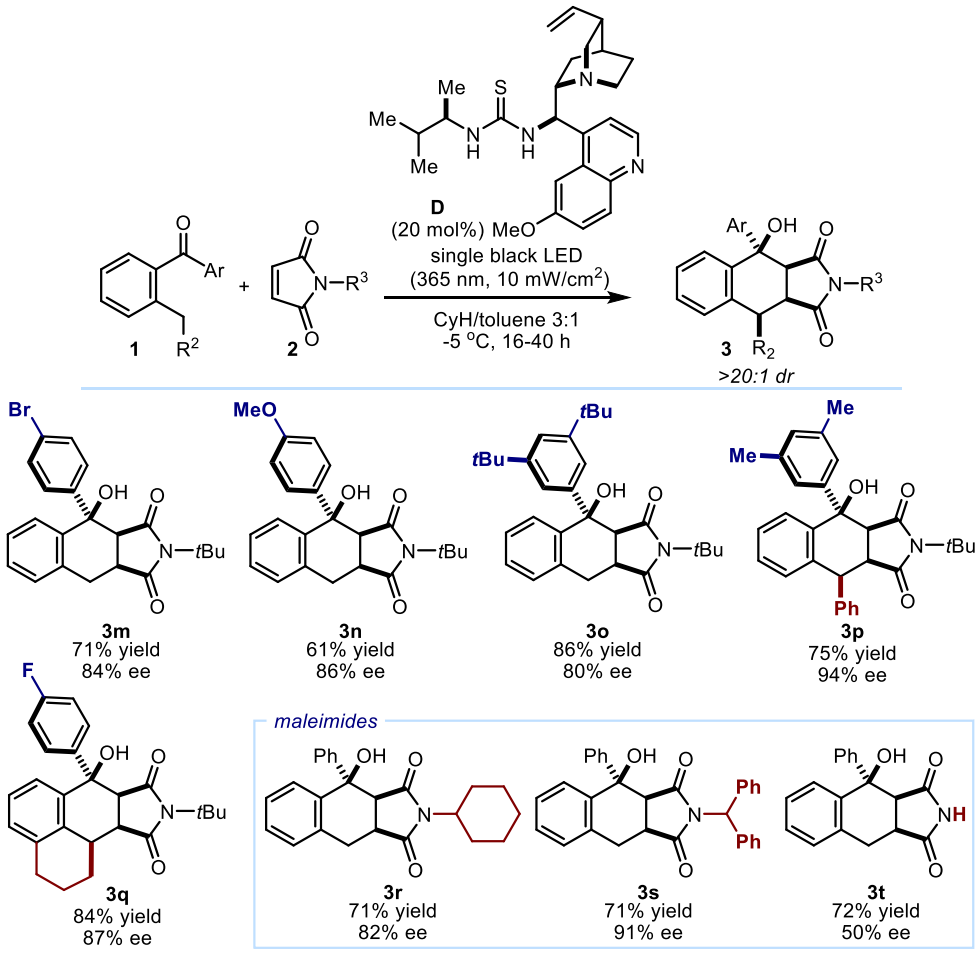

Figure 2.17. Survey of 2-alkylbenzophenones **1** (products **3m**-**q**) and maleimides (products **3r**-**3t**) that can participate in the reaction. Reactions performed on a 0.2 mmol scale; yields and enantiomeric excesses of the isolated products **3** are indicate below each entry. CyH = cyclohexane; *t*Bu =*tert*-butyl.

2.4. Origin of the Stereoselectivity

The analysis of the X-ray structures obtained from crystals of products **3h** and **3l** (Figure 2.18, left) suggested that the stereoselective [4+2] cycloaddition reaction occurs from the *Si* face of the (*E*)-photoenol and through an *endo* transition state (Figure 2.18, right). This stereochemical outcome can be rationalized on the basis of the following aspects. First, although two stereoisomeric photoenols (*i.e.* (*E*)-photoenol and (*Z*)-photoenol) can be formed during the photoenolizaton of 2-alkylbenzohpenones **1**, only the (*E*)-stereoisomer is sufficiently long-lived[11] to participate in the cycloaddition event (see discussion in section 2.1.2). A useful information comes from the spatial position of the maleimide moiety in products **3h** and **3l**, which is placed in *syn*-disposition with respect to the -OH group located

on the vicinal chiral carbon. This relative configuration can only arise from an *endo* approach of the maleimide to the long-lived (*E*)-photoenol. The *exo* approach would place the above-mentioned groups in *anti*-disposition. An alternative path leading to the same *syn*-adduct would require the reaction of the short-lived (*Z*)-enol with the maleimide to proceed through an *exo* approach. However, this pathway can be discarded on the basis of the photoenol lifetimes. Finally, considering the two enantiotopic faces of the planar (*E*)-photoenol, only the reaction ocurring from the *Si*-face (see Figure 2.18, right) leads to the observed absolute configuration.

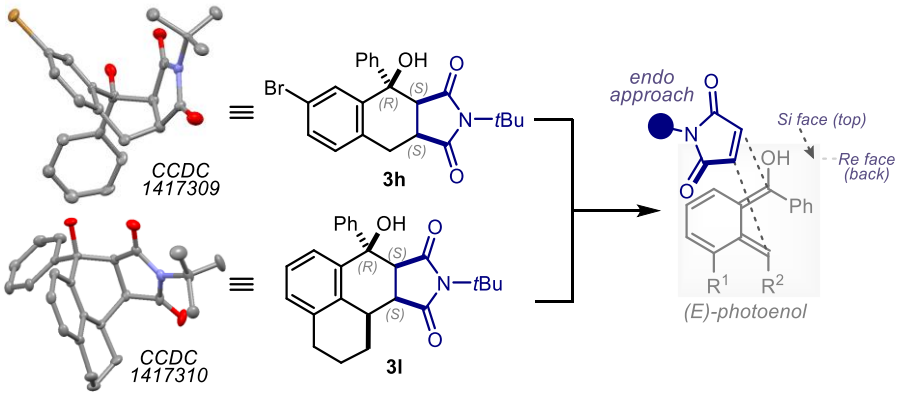

Figure 2.18. The structural analysis of products **3h** and **3l**, based on their X-ray structures, suggested that the enantioselective [4+2]-cycloaddition occurs from the *Si* face of the long-lived (*E*)-photoenol through an *endo* transition state. The mediation of the chiral H-bond donor catalyst **D** in the *endo* transition state is not shown.

2.5. Mechanistic Investigations

One of the puzzling observations during the optimization process was related with the unconventional behavior of the bifunctional thiourea-cinchona catalyst. Indeed, catalyst **D** allowed the formation of a highly enantioenriched product **3f** while greatly lowering the reaction rate in comparison with the rate of the background, uncatalyzed racemic reaction (Figure 2.19).

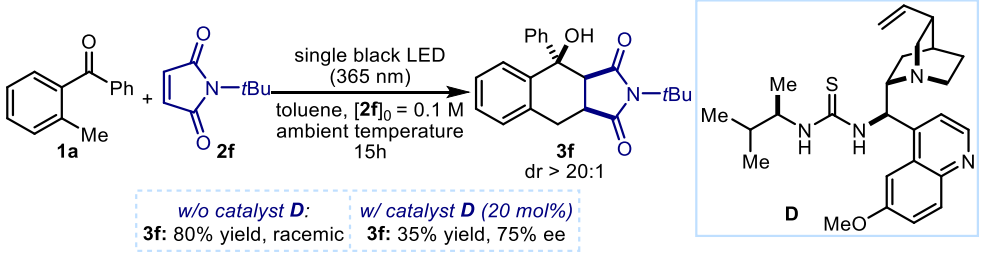

Figure 2.19. The model reaction in the absence of any catalyst and in the presence of 20 mol% of the chiral bifunctional catalyst **D**.

This intriguing result suggests that an unconventional mechanism of catalysis is likely operative in the enantioselective PEDA sequence. In asymmetric catalysis, the classical strategy to achieve high stereocontrol is to find suitable chiral catalyst and conditions that allow the catalyzed process to outcompete the racemic background reaction. Undoubtedly, this is not at the origin of stereoinduction in our developed system.

2.5.1. Conventional Pathways in Catalytic Asymmetric Photochemical Reactions

In enantioselective catalytic photochemical processes, selectivity can be achieved through different modes of action and interaction between substrate and catalyst:[42] (*i*) the substrate-catalyst aggregation can exhibit a *bathochromic shift* in its absorption, which would enable the selective irradiation of the chiral aggregate without exciting the uncomplexed substrate (Figure 2.20, *case a*); or (*ii*) the substrate-catalyst aggregate can show a significant *enhanced absorption* (higher extinction coefficient, ε) than the substrate, which would facilitate the photochemical process to proceed mainly through the chiral aggregate (Figure 2.20, *case b*). Both strategies have the same target: reducing the rate of the uncatalyzed background reaction that occurs by direct excitation of substrates while magnifying the rate of the reaction promoted by a substrate-chiral catalyst assembly.

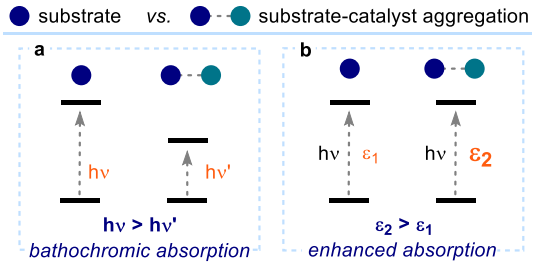

Figure 2.20. Two possible modes of action for chiral catalysts in photochemical systems.

In order to check whether an aggregation between the substrates and the chiral bifunctional cinchona-thiourea catalyst **D** was operative under our reaction conditions, we recorded the absorption spectra of the organocatalyst-substrate mixture. These studies, conducted by analyzing the absorption spectrum of all the independent components of the model reaction (2-methylbenzophenone **1a**, *N-tert*-butylmaleimide **2f** and catalyst **D**) and their combination, revealed that the main responsible for the absorption at 365 nm (the wavelength operative in our photochemical system) is 2-methylbenzophenone **1a** alone (Figure 2.21).

[42] Brimioulle, R.; Lenhart, D.; Maturi, M. M.; Bach, T. Enantioselective Catalysis of Photochemical Reactions. *Angew. Chem. Int. Ed.* **2015**, *54*, 3872–3890.

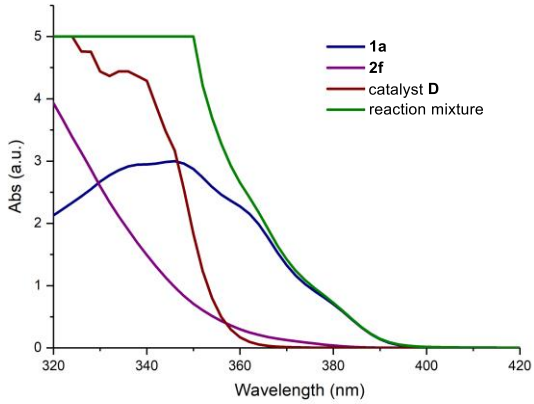

Figure 2.21. Optical absorption spectra of 2-methylbenzophenone **1a** (blue line, [**1a**] = 0.3 M), *N-tert*-butylmaleimide **2f** (purple line, [**2f**] =0.1 M), catalyst **D** (brown line, [**D**] = 0.02 M) and the reaction mixture (green line) acquired in degassed toluene using 1 mm path quartz cuvettes.

In the presence of the catalyst, no bathochromic shift or enhanced absorption of **1a** was noticed. *N-tert*-butylmaleimide **2f** can also absorb light, but at 365 nm the absorption of ketone **1a** is 10 times higher than the absorption of **2f**.

These studies excluded the possibility for the chiral catalyst **D** to form a photon-absorbing aggregate by coordination of the substrates. Thus, the conventional mechanisms of stereoinduction, generally invoked to promote stereoselective photochemical catalytic reactions (Figure 2.20), are not operative in our case. This prompted us to evaluate other possible pathways available to catalyst **D** for minimizing the racemic background process.

2.5.2. Investigating Alternative Stereoinduction Mechanisms

Our initial investigations excluded the possibility for the cinchona-thiourea catalyst **D** of using conventional mechanisms of stereoinduction: the likely hydrogen-bonding activation of the maleimide neither accelerated the reaction with respect to the background PEDA process nor induced the formation of a photoactive ground-state aggregate, which could be selectively excited. At this stage, we reconsidered the structural features of the catalyst **D**. This type of bifunctional thiourea organocatalyst have two active sites for coordination of the substrates:[43]

[43] (a) Okino, T.; Hoashi, Y.; Takemoto, Y. Enantioselective Michael Reaction of Malonates to Nitroolefins Catalyzed by Bifunctional Organocatalysts. *J. Am. Chem. Soc.* **2003**, *125*, 12672–12673. (b) McCooey, S. H.; Connon, S. J. Urea- and Thiourea-Substituted Cinchona Alkaloid Derivatives as Highly Efficient Bifunctional Organocatalysts for the Asymmetric Addition of Malonate to Nitroalkanes: Inversion of Configuration at C9 Dramatically Improves Catalyst Performance. *Angew. Chem. Int. Ed.* **2005**, *44*, 6367–6370. For a review, see: (c) Connon, S. J. Asymmetric Catalysis with

(*i*) a *Lewis acidic site*, provided by the thiourea functional group; and (*ii*) a *Lewis basic site*, offered by the quinuclidine moiety within the quinidine scaffold. On the basis of the Lewis basicity of the quinuclidine moiety, we considered another established photochemical process that could be operational in our system: the photoreduction of the benzophenone by the quinuclidine moiety. It is well-established that tertiary amines can engage in SET processes with the excited *n,π** triplet state (T_1) of benzophenones.[44] This photochemical path proceeds through an ET from the electron rich tertiary amine **28** to the excited triplet state of the benzophenone **1b**, leading to the formation of a charge-transfer complex **X** (Figure 2.22, path a). At this point, different scenarios are plausible: (*i*) a *back ET* and spin inversion, which returns the benzophenone **1b** in its ground state and the unaltered tertiary amine **28** (path b in Figure 2.22) or (*ii*) a *proton transfer* from the amine to the benzophenone radical anion, which leads to the formation of radicals **II** and **XI** (path c).

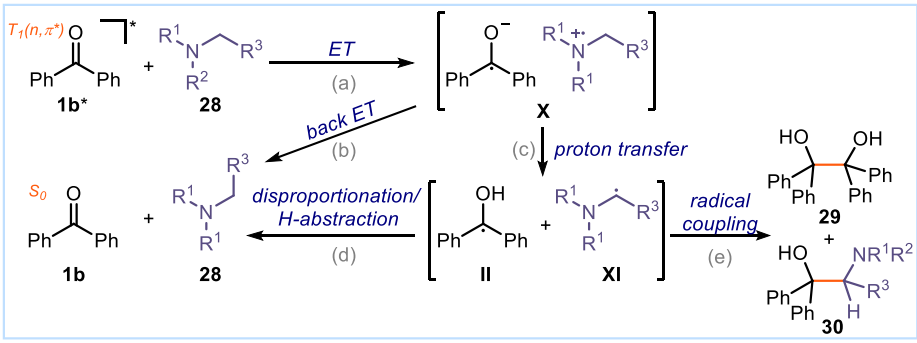

Figure 2.22. General mechanism of photoreduction of benzophenones by amines. The triplet state of benzophenone **1b** can engage in a single electron transfer (ET) with tertiary amines **28**, leading to the formation of a radical ion pair that can subsequently undergo several thermal processes.

These radicals can undergo either a disproportionation or a hydrogen transfer from **II** to **XI**, which enables the recovery of the ground state **1b** and the unaltered amine **28**. Alternatively, radicals **II** and **XI** can be coupled, yielding the homo- and heterocoupling products **29** and **30**, respectively.[7]

Let's consider this general mechanism in the context of our catalytic PEDA process. After an ET event between the triplet 2-alkylbenzophenone **1*** and the quinuclidine moiety of catalyst **D**, a radical ion pair of type **X** (Figure 2.22) would be formed. At this point, it is important to consider the geometrical features of the quinuclidine core. Precedent studies have established that geometrically constrained amines cannot undergo a proton transfer within the charge

Bifunctional Cinchona Alkaloid-based Urea and Thiourea Organocatalysts. *Chem. Commun.* **2008**, 2499–2510.

[44] (a) Scaiano, J. C. Intermolecular Photoreduction of Ketones. *J. Photochem.* **1973**, *2*, 81–118. (b) Cohen, S. G.; Parola, A.; Parsons, G. H., Jr. Photoreduction by Amines. *Chem. Rev.* **1973**, *73*, 141–161.

transfer complex **X** (*i.e.* undergo path c in Figure 2.22).[45] Indeed, this process is favored by stereoelectronic effects only when the α-C-H bond being broken is eclipsed with the nitrogen lone pair (see Figure 2.23). This conformational disposition brings about the stabilization of the product radical, allowing the formation of a coplanar 2-centre-3-electron bonding system (as in the case *(a)* in Figure 2.23). Conjugation between the unpaired electron and the nitrogen lone pair is responsible for the stabilization. The rigid cyclic structure of the quinuclidine core, however, does not allow reaching the required conformation for the formation of the 2-centre-3-electron bonding after proton loss (case *(b)* in Figure 2.23), thus preventing the proton transfer process.

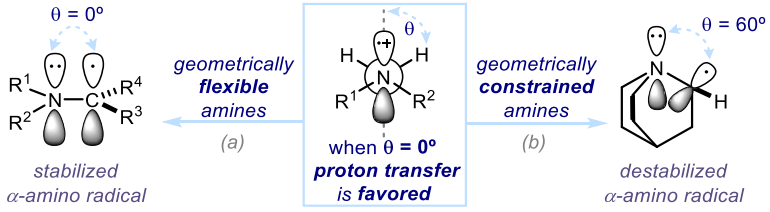

Figure 2.23. Stereoelectronic effects in the photo-induced proton transfer of amines. *Case a*: stabilization of the α-amino radical in amines with allowed C-N rotation; *case b*: absence of stabilization in geometrically constrained amines, such as quinuclidine.

Taking this into account, the only pathway that the possible charge transfer complex **Xa** (see Figure 2.24) can follow in our photo-organocatalytic system is a *back ET*, which would restore the 2-alkylbenzophenone **1** and catalyst **D**.

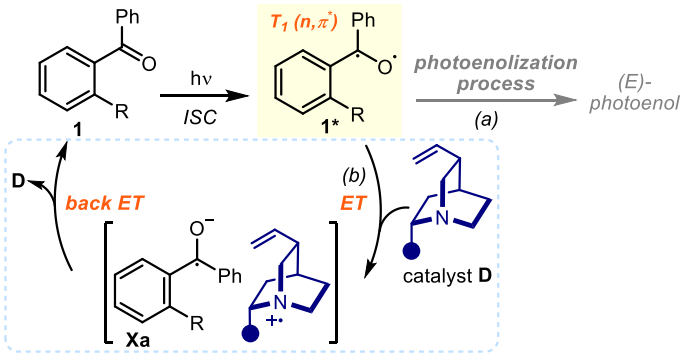

Figure 2.24. Competing pathways for the triplet state (**1***) of 2-alkylbenzophenones **1**: *(a)* the photoenolization process, and *(b)* an electron transfer (ET) quenching mechanism mediated by geometrically constrained tertiary amines, including the quinuclidine moiety of catalyst **D**.

[45] (a) Griller, D.; Howard, J. A.; Marriott, P. R.; Scaiano, J. C. Absolute Rate Constants for the Reactions of *tert*-Butoxyl, *tert*-Butylperoxyl, and Benzophenone Triplet with Amines: the Importance of a Stereoelectronic Effect. *J. Am. Chem. Soc.* **1981**, *103*, 619–623. (b) von Raumer, M.; Suppan, P.; Haselbach, E. Photoreduction of Triplet Benzophenone by Amines: Role of their Structure. *Chem. Phys. Lett.* **1996**, *252*, 263–266.

Therefore, based on this competing photochemical pathway, we envisaged the possibility for the quinuclidine moiety of catalyst **D** to *inhibit the formation of the photoenol* derived from **1**, since the tertiary amino moiety may *undergo an electron transfer to the excited triplet state of the benzophenone*, which is the key precursor intermediate in the photoenolization process.

2.5.3. Kinetic Studies

To evaluate the feasibility of this peculiar quenching mechanism from catalyst **D** (depicted in Figure 2.24), we performed a simplified kinetic study of the model reaction. Specifically, we investigated the individual effect of the quinuclidine moiety and the thiourea functionality (the two main fragments of the bifunctional organocatalyst **D**) on the rate of the model reaction (Figure 2.25). We measured the NMR yield after 4 and 8 hours in the presence of sub-stoichiometric amounts (20 mol%) of quinuclidine (**31**, brown line) and *N,N'*-dicyclohexylthiourea (**32**, violet line), and we compared the rate of product formation with the model reaction catalyzed by 20 mol% of **D** (blue line) or in the absence of the catalyst (background reaction, black line). Interestingly, the reaction was clearly inhibited by the presence of quinuclidine **31**, even in comparison with the organocatalytic regime. In contrast, a faster formation of the product was observed when the achiral thiourea **32** was added to the reaction mixture, indicating that the H-bond activation of the maleimide, which increases its dienophilic character, facilitates the photoenol trapping event. The enantioselective reaction, catalyzed by **D**, is slower than the background uncatalyzed process, but faster than the reaction in the presence of quinuclidine.

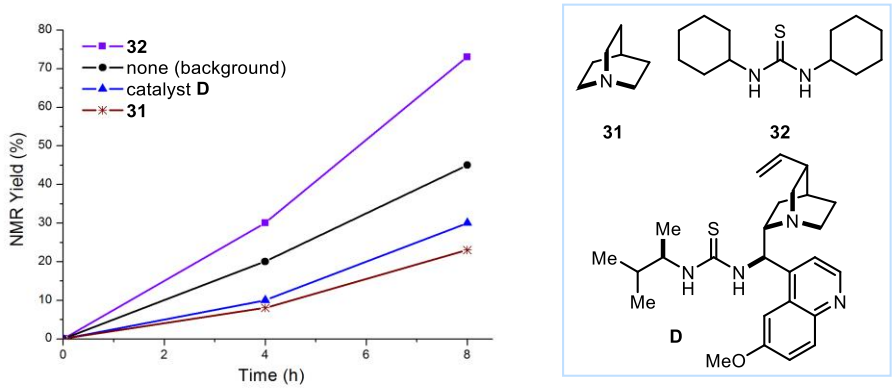

Figure 2.25. Evolution of the product **3f**'s distribution during the progress of the model reaction in the absence of any catalyst (black line), or in the presence of 20 mol% of cinchona thiourea **D** (blue line), *N,N'*-dicyclohexylthiourea **32** (purple line), and quinuclidine **31** (brown line). Reactions conducted in cyclohexane at ambient temperature.

The same studies were performed for the **D**-catalyzed reaction and the background reaction using a 3:1 mixture of cyclohexane/toluene and stirring at -5 ºC (Figure 2.26). This confirmed the presence of a faster racemic uncatalyzed process also under the optimized conditions for the enantioselective PEDA reaction.

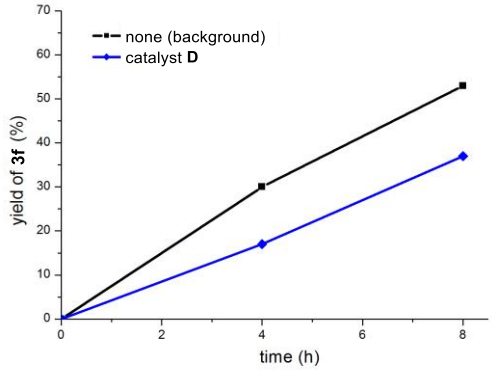

Figure 2.26. Evolution of the product **3f**'s distribution during the progress of reaction in the absence of any catalyst (black line), or in the presence of 20 mol% of cinchona thiourea **D** (blue line). Reactions conducted using a 3:1 mixture of cyclohexane/toluene and at -5 °C.

Another simple experiment was used to prove the negative effect of the quinuclidine moiety on the reaction rate. The model reaction, catalyzed by **D**, was performed in the presence of an acid, which protonates the basic quinuclidine moiety of **D**. We reasoned that, if the amine within the catalyst does not have available electrons to undergo an electron transfer with the triplet state of the 2-methylbenzophenone **1a**, the photoenolization process would not be affected. The designed experiment is depicted in Table 1.11, employing an equimolar, catalytic amount of the bifunctional thiourea catalyst **D** and benzoic acid.

Table 1.11. Effect of the addition of benzoic acid on the rate and stereocontrol of the model PEDA reaction.

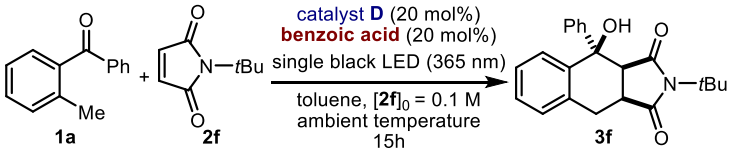

entry	catalyst D	acid	3f yield (%)[a]	3f ee (%)[b]
1	no	no	80	0
2	***yes***	no	**35**	**84**
3	yes	***yes***	**67**	**4**

Reactions performed on a 0.1 mmol scale using 3 equiv. of 2-methylbenzophenone **1a**. [a]Yield of the isolated product **3f** after flash chromatography on silica gel. [b]Enantiomeric excess determined by HPLC analysis on a chiral stationary phase.

Under these conditions, when the tertiary amine in **D** is fully protonated, the model PEDA reaction proceeded faster, while the stereoinduction was dramatically affected (compare entries 2 and 3). This result can be explained by the protonation of the tertiary amine in **D** that disabled the ET-based inhibition mechanism (please refer to Figure 2.24), thus allowing the background process to compete with the enantioselective pathway.

2.5.4. Transient Absorption Spectroscopy Studies

Transient absorption spectroscopy (TAS) is a technique used for the detection of transient intermediates formed in excited-state processes of organic molecules.[9] The transients are produced by repeated short laser pulses sent through a sample (excitation or pump pulse). Every excitation pulse, which has to be of shorter duration in comparison with the lifetime of the intermediates, is energetic enough to produce a measurable number of transients. The detection system consists of a second laser, operating after a time delay in pulse mode (probe pulse), which allows to record the absorption spectrum of the transients. The probe pulse is of lower intensity than the excitation pulse in order to avoid multiphoton/multistep processes. The overall process provides a difference absorption spectrum (ΔA), obtained by subtracting the absorption spectrum of the excited sample from the absorption spectrum of the sample in the ground state (*i.e.* $\Delta A = A_{[\text{excited state}]} - A_{[\text{ground state}]}$). By changing the time delay (τ) between the excitation pulse an the probe pulse and recording a ΔA spectrum at each delay time, a ΔA profile as a function of τ and wavelength (λ) is obtained (*i.e.* ΔA (τ, λ)).[46] This technique has found many applications spanning from kinetic studies, the determination of lifetimes of excited states, to the study of photochemical reaction mechanisms.[47] Regarding the photoenolization process, it has been extensively used for the characterization of the transient intermediates involved in the formation of the reactive photoenol.[48] Therefore, we aimed to use this spectroscopic method to detect the transient photoenol, while directly observing how its formation is affected by the presence of rigid tertiary amines, such as the quinuclidine moiety of catalyst **D**.

---

[46] Berera, R.; van Grodelle, R.; Kennis, J. T. M. Ultrafast Transient Absorption Spectroscopy: Principles and Application to Photosynthetic Systems. *Photosynth. Res.* **2009**, *101*, 10–5118.

[47] Bailey, D. N.; Hercules, D. M. XX. Flash Photolysis-A Technique for Studying Fast Reactions. *J. Chem. Educ.* **1965**, *42*, and references therein.

[48] For selected studies, see: (a) Zwicker, E. F.; Grossweiner, L. I; Yang, N. C. The Role of n-π* Triplet in the Photochemical Enolization of *o*-Benzylbenzophenone. *J. Am. Chem. Soc.* **1963**, *85*, 2671–2672. (b) Porter, G.; Tchir, M. Photoenolization of *ortho*-Substituted Benzophenones by Flash Photolysis. *J. Chem. Soc., A* **1971**, 3772–3777. (c) Uji-Ie, K.; Kikuchi, K.; Kokubun, H. Photoenolization of 2-Methylbenzophenone. *Chem. Lett.* **1977**, *5*, 499–502. (d) Uji-Ie, K.; Kikuchi, K.; Kokubun, H. The Photoenolization Mechanism of 2-Methylbenzophenone. *J. Photochem.* **1979**, *10*, 145–157. (e) Neto-Ferreira, J. C; Wintgens, V.; Scaiano, J. C. Laser Flash Photolysis Study of the Photoenols Generated from *ortho*-Benzylbenzophenone in Different Solvents. *Can. J. Chem.* **1994**, *72*, 1565–1569.

Using the TAS system available at the ICIQ[49] (specifications of the equipment can be found in the *Experimental Section* of this chapter), we observed a transient species upon selective irradiation of a $5x10^{-3}$ M solution of 2-methylbenzophenone **1a** in benzene, showing an absorption maximum at 450 nm. The half lifetime of the transient was ca. 10 ms (Figure 2.27).

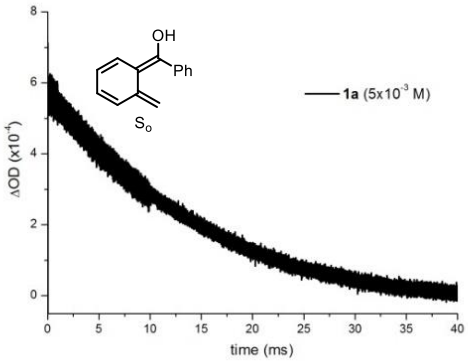

Figure 2.27. Decay of absorption at 450 nm of a transient generated upon 355 nm laser excitation of 2-methylbenzophenone **1a** ([**1a**] = $5x10^{-3}$ M in benzene). ΔOD: optical density variation. $\tau_{1/2}$= 10 ms.

The characteristics of the detected transient are in agreement with literature data obtained upon flash photolysis studies of **1a**, which identified the absorption of the ground state (*E*)-photoenol in the region of 400-450 nm. [48c-d]

We next evaluated the effect of the cinchona-thiourea catalyst **D** on the decay of the absorption of transient (*E*)-photoenol generated from **1a**. In Figure 2.28 it can be appreciated how the photoenol formation is affected by adding increasing amounts of catalyst **D**. An amount of catalyst **D** 0.0018 times lower than **1a** (ratio **1a**/**D** = 560, red line) was enough to induce a change in the (*E*)-photoenol formation. The effect is much pronounced when increasing amounts of the catalyst are added to the solution. This observation is coherent with the proposal that catalyst **D** affects the formation of the photoenol. We observed that also the lifetime of the photoenol was affected by catalyst **D**, which suggested the feasibility of an additional quenching mechanism. For example, a base-promoted deprotonation of the (*E*)-photoenol to reform the 2-alkylbenzophenone **1** could likely occur.

[49] The TAS measurements were performed with the assistance of Dr. Javier Pérez Hernández and Prof. Emilio Palomares, from ICIQ.

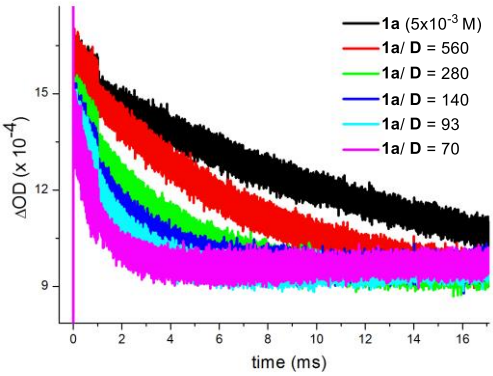

Figure 2.28. Absorption at 450 nm of the transient (*E*)-photoenol (black line) generated upon 355 nm laser excitation of 2-methylbenzophenone **1a** ($[\mathbf{1a}]_0$ = 5x10^{-3} M in cyclohexane). Absorption decays (colored lines) observed in the presence of increasing amounts of the catalyst **D**. ΔOD: optical density variation. In the legend is indicated the ratio between the moles of **1a** and **D** (mmol **1a**/ mmol **D**). The concentration of **1a** was kept constant in every measurement.

In subsequent studies, we selected a logarithmic time scale suitable for clearly showing the decay of the transient and the difference on initial concentration of the photoenol in the presence of the catalyst **D** (Figure 2.29).

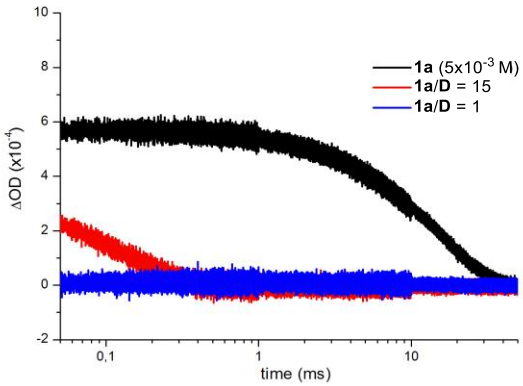

Figure 2.29. Absorption at 450 nm of the transient (*E*)-photoenol (black line) generated upon 355 nm laser excitation of 2-methylbenzophenone **1a** ($[\mathbf{1a}]_0$ = 5x10^{-3} M in benzene). Note logarithmic scale for time. The concentration of **1a** was kept constant in every measurement. Absorption decays (red and blue lines) observed in the presence of increasing amounts of the cinchona-thiourea catalyst **D**. *Red line*: note that the ratio **1a**/**D** mimics the reaction conditions. ΔOD: optical density variation.

In this case, it can be easily observed how the formation of the transient is minimized by the presence of an amount of **D** (red line) that mimics the reaction conditions. On the other hand, when an equimolar solution of 2-methylbenzophenone **1a** and catalyst **D** was irradiated, no formation of the (*E*)-photoenol was detected (blue line).

2.5.5. An Unconventional Mechanism of Stereoinduction

Reducing the rate of a racemic uncatalyzed pathway is crucial to successfully developing any photochemical asymmetric reaction. Classical strategies have relied on the formation of chiral/substrate complexes, which absorbs light at longer wavelengths or higher extinction coefficients than the free substrate. However, the initial spectroscopic studies (in section 2.5.1) have shown that our organocatalytic system does not behave following any of these classical asymmetric strategies. Preliminary kinetic studies (in section 2.5.3) and transient absorption spectroscopy measurements (in section 2.5.4) have revealed one possible pathway available to catalyst **D** for minimizing the background process. Altogether, our investigations indicate that the cinchona-thiourea **D** plays two opposite yet cooperative roles when promoting the PEDA reaction (Figure 2.30).

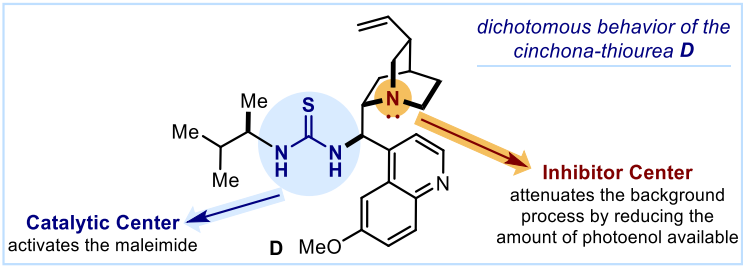

Figure 2.30. The mutualistic relationship between the two chiral fragments in catalyst **D**: the formation of a low amount of the photoenol, as controlled by the tertiary amino moiety, avoids the background reaction to compete with the enantioselective Diels-Alder trap with maleimides **2**, which is mastered by the thiourea moiety.

On the one hand, the quinuclidine moiety interferes with the photoenolization mechanism, acting as an inhibitor of the PEDA sequence. Using a light-wasting process based on an ET-back ET process (depicted in Figure 2.24), it lowers the amount of reactive photoenol available, decreasing the possibility that the background racemic reaction will take place. On the other hand, catalyst **D** uses the thiourea moiety to increase the dienophilic character of the maleimides **2** upon H-bonding activation, while channeling the Diels-Alder process toward an enantioselective pattern. While the two moieties within **D** exert opposite kinetic effects (Figure 2.30), they are both essential for achieving high stereocontrol. We are aware that the mechanism of stereoinduction could be more complicated in that **D** may use multiple weak interactions to simultaneously bind and activate both the transient (*E*)-photoenol and the maleimides **2**.

2.6. Conclusions

We have documented that a readily available chiral organic catalyst, derived from natural cinchona alkaloids, can activate maleimides towards a high stereoselective Diels-Alder reaction with light-generated hydroxy-*o*-quinodimethanes. Our investigations indicate that an unconventional mechanism of stereocontrol is operative, wherein the organocatalyst combines a quenching mechanism to decrease the formation of reactive photoenol, while acting as a non-covalent chiral activator in the stereoselectivity-defining event. This dichotomous behavior of the cinchona-derived catalyst was essential for achieving high levels of stereocontrol and allowed to develop the first catalytic asymmetric variant of the PEDA process.

2.7. Experimental Section

2.7.1. General Information

The NMR spectra were recorded at 400 MHz and 500 MHz for ^{1}H or at 100 MHz and 125 MHz for ^{13}C, respectively. The chemical shifts (δ) for ^{1}H and ^{13}C are given in ppm relative to residual signals of the solvents ($CHCl_3$ @ 7.26 ppm 1H NMR, 77.16 ppm 13C NMR). Coupling constants are given in Hz. The following abbreviations are used to indicate the multiplicity: s, singlet; d, doublet; t, triplet; q, quartet; m, multiplet; bs, broad signal.

High-resolution mass spectra (HRMS) were obtained from the ICIQ High Resolution Mass Spectrometry Unit on Waters GCT gas chromatograph coupled time-of-flight mass spectrometer (GC/MS-TOF) with electron ionization (EI) or MicroTOF II (Bruker Daltonics): HPLC-MS-TOF (ESI). UV-vis measurements were carried out on a Shimadzu UV-2401PC spectrophotometer equipped with photomultiplier detector, double beam optics and D_2 and W light sources. X-ray data were obtained from the ICIQ X-Ray Unit using a Bruker-Nonius diffractometer equipped with an APPEX 2 4K CCD area detector. Optical rotations were measured on a Polarimeter Jasco P-1030 and are reported as follows: $[\alpha]_D$ rt (c in g per 100 mL, solvent).

Studies with nanosecond transient absorption spectroscopy (TAS) were performed using an excitation source of Nd:YAG (neodymium-doped yttrium aluminium garnet) tuned with an optical parametric oscillator (OPO) from Opolette as a pump source. This laser produces 6 ns pulses of 1 mJ at a wavelength of 355 nm. The system is completed with two monochromators with double grating at the VIS an IR, and a digital recorder DSP-DAU from RAMDSP. A photodetector amplifiers and a software control complete the TAS system.

Chromatographic purification of products was accomplished using force-flow chromatography (FC) on silica gel (35-70 mesh). For thin layer chromatography (TLC) analysis throughout this work, Merck precoated TLC plates (silica gel 60 GF_{254}, 0.25 mm) were used, using UV light as the visualising agent and an acidic mixture of ceric ammonium molybdate or basic aqueous potassium permangante ($KMnO_4$), and heat as developing agents. Organic solutions were concentrated under reduced pressure on a Büchi rotary evaporator.

Determination of Diastereomeric Ratio. The diastereomeric ratio for the PEDA products **3** was determined by ^{1}H NMR analysis of the crude reaction mixture through integration of diagnostic signals, and then confirmed by HPLC analysis.

Determination of Enantiomeric Purity: HPLC analysis on chiral stationary phase was performed on an Agilent 1200-series instrumentation. Daicel Chiralpak IA, IB, ID, IC and IC-3 columns with hexane/iPrOH or hexane/iPrOH/DCM as the eluents were used. HPLC traces were compared to racemic samples prepared running the reaction in the absence of any catalyst (background process).

Materials: Commercial grade reagents and solvents were purchased at the highest commercial quality from Sigma Aldrich, Fluka, Acros Organics, and Alfa Aesar and used as received, unless otherwise stated. The bifunctional catalyst N-[3,5-bis(trifluoromethyl)phenyl]-N′-[(9*R*)-6′-methoxy-9-cinchonanyl]thiourea (**A**) is commercially available and was used without further purification. Benzophenones 2-mehtylbenzophenone **1a**, (2,4-dimethylphenyl)phenylmethanone **1b** and 2-ethylbenzphenone **1e** were purchased from Sigma-Aldrich and used without further purifications. (2-benzylphenyl)(phenyl)methanone **1f** and phenyl (5,6,7,8-tetrahydronaphthalen-1-yl)methanone **1g** were prepared according to a literature procedure.[50] The preparation of the other benzophenones is detailed in Section 2.7.2 of the Experimental Section of this chapter.

The NMR spectra and the HPLC traces are available in the published manuscript,[1] and are not reported in the present doctoral thesis.

2.7.2. Substrate Synthesis

The synthesis of benzophenones **1e**, **1f**, **1i**, **1j**, **1k**, **1l** and **1m** was performed according to one of the synthetic pathways depicted in Scheme 1.

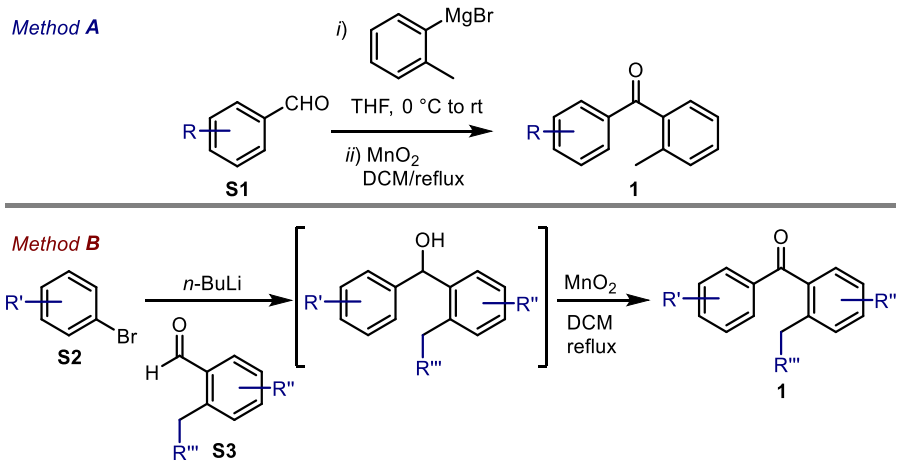

Scheme 1. Synthetic pathways for preparing **1**.

Method A: The commercially available benzaldehyde derivative **S1** (1 equiv) was dissolved in dry THF (0.25 M) under an argon atmosphere. After cooling the mixture to 0 ºC, a 0.5 M *p*-tolylmagnesium bromide solution in THF (1.2 equiv) was slowly added under vigorous stirring. The mixture was allowed to warm up to ambient temperature (rt). Upon complete consumption of the starting aldehyde **S1**, as determined by TLC analysis of the mixture, water

[50] Connolly, T. J.; Durst, T. A. Photochemically Generated Bicyclic *o*-Quinodimethanes: Photoenolization of Bicyclic Aldehydes and Ketones. *Tetrahedron* **1997**, *47*, 15969–15982.

was slowly added at 0 ºC. The biphasic system was then extracted with Et_2O (x 3). The organic phases were collected and concentrated under vacuum. The crude alcohol was dissolved in dry DCM (0.2 M solution) without any purification. Then, activated MnO_2 (7 equiv) was added at once under an argon atmosphere. The solution was refluxed for 10 h. After cooling to ambient temperature, the mixture was filtered through a pad of silica and the residue washed with DCM. The organic solution was concentrated under vacuum and the crude subjected to flash chromatography (FC) purification on silica to afford the title compound **1**.

Method B: The commercially available bromobenzene derivative **S2** (1 equiv) was dissolved in dry THF (0.25 M) under an argon atmosphere. After cooling the mixture to -30 ºC, a solution of *n*-BuLi 1.9 M in hexane (1.5 equiv) was added dropwise. After the addition, the solution was allowed to warm to ambient temperature and stirring was continued for 1 hour. The commercially available aldehyde derivative **S3** (1 equiv, 0.5 M solution in dry THF) was then added dropwise at 0 ºC, and stirring was continued over 2 hours. The reaction was then quenched by carefully adding water and extracted with Et_2O (x 3). The organic phases were collected and concentrated under vacuum. The crude alcohol was then subjected to MnO_2 oxidation as in Method A. FC purification on silica gel afforded the title compound **1**.

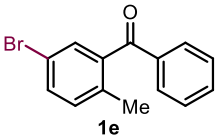

1e

(5-bromo-2-methylphenyl)(phenyl)methanone (1e). Following the procedure reported in the literature[50], **1e** was isolated by FC on silica (hexane/EtOAc: 98:2 v/v) in 55% yield as a colorless oil starting from the corresponding acid. TLC (hexane/EtOAc: 98:2 v/v): R_f = 0.35; HRMS calculated for $[C_{14}H_{11}BrO+Na]^+$: 296.9891; found: 296.9895.

^{1}H NMR (400 MHz, $CDCl_3$) δ 7.85 – 7.78 (m, 2H, Ar), 7.62 (ddt, *J* = 8.7, 6.9, 1.3 Hz, 1H, Ar), 7.55 – 7.42 (m, 4H, Ar), 7.19 (dd, *J* = 8.2, 0.8 Hz, 1H, Ar), 2.27 (s, 3H, CH_3). **^{13}C NMR (100 MHz, $CDCl_3$)** δ 196.9 (C=O), 140.5 (Cq Ar), 137.0 (Cq Ar), 135.5 (Cq Ar), 133.6 (CH Ar), 133.1 (CH Ar), 132.7 (CH Ar), 130.8 (CH Ar), 130.1 (CH Ar x2), 128.7 (CH Ar x2), 118.9 (Cq Ar), 19.5 (CH_3).

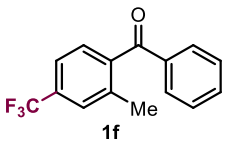

1f

(2-methyl-4-(trifluoromethyl)(phenyl)methanone (1f). Following the procedure detailed in Method B, **1f** was isolated by FC on silica (hexane/EtOAc: 98:2 v/v) in 65% yield as a colorless oil starting from the corresponding aldehyde **S3**. TLC (hexane/EtOAc: 98:2 v/v): R_f = 0.35.

^{1}H NMR (500 MHz, $CDCl_3$) δ 7.85 – 7.78 (m, 2H, Ar), 7.69 – 7.61 (m, 1H, Ar), 7.61 – 7.54 (m, 2H, Ar), 7.53 – 7.48 (m, 2H, Ar), 7.44 (m, 1H, Ar), 2.39 (s, 3H, CH_3). **^{13}C NMR (125 MHz, $CDCl_3$)** δ 197.4 (C=O), 142.1, 137.3, 136.8, 133.8, 132.0, 131.8, 130.1, 128.7, 128.3,

127.7, 127.7, 124.9, 122.7, 122.3, 122.3, 19.8 (CH_3). **^{19}F NMR decoupled ^{1}H (400 MHz, $CDCl_3$)** δ -63.0.

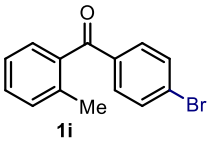

(4-bromophenyl)(*o*-tolyl)methanone (1i). Following the procedure detailed in Method A, **1i** was isolated by FC on silica (hexane/EtOAc: 98:2 v/v) in 76% yield as a colorless oil starting from the corresponding aldehyde **S1**. TLC (hexane/EtOAc: 98:2 v/v): R_f = 0.34; HRMS calculated for $[C_{14}H_{11}BrO+Na]^+$: 296.9891; found: 296.9893.

^{1}H NMR (400 MHz, $CDCl_3$) δ 7.72 – 7.65 (m, 2H, Ar), 7.64 – 7.59 (m, 2H, Ar), 7.47 – 7.38 (m, 1H, Ar), 7.36 – 7.24 (m, 4H, Ar), 2.35 (s, 1H, CH_3). **^{13}C NMR (100 MHz, $CDCl_3$)** δ 197.5 (C=O), 138.0 (Cq Ar), 136.8 (Cq Ar), 136.5 (Cq Ar), 131.8 (CH Ar x2), 131.6 (CH Ar x2), 131.2 (CH Ar), 130.5 (CH Ar), 128.5 (CH Ar), 128.4 (Cq Ar), 125.3 (CH Ar), 20.0 (CH_3).

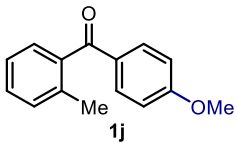

(4-methoxyphenyl)(o-tolyl)methanone (1j). Following the procedure detailed in Method A, **1j** was isolated by FC on silica (hexane/EtOAc: 98:2 v/v) in 76% yield as a colorless oil starting from the corresponding aldehyde **S1**. TLC (hexane/EtOAc: 98:2 v/v): R_f = 0.34; HRMS calculated for $[C_{15}H_{14}O_2+Na]^+$: 249.0891; found: 249.0896.

^{1}H NMR (400 MHz, $CDCl_3$) δ 7.85 – 7.77 (m, 2H, Ar), 7.43 – 7.35 (m, 1H, Ar), 7.33 – 7.21 (m, 4H, Ar), 6.99 – 6.89 (m, 2H, Ar), 3.89 (s, 3H, CH_3 OMe), 2.33 (s, 3H, CH_3). **^{13}C NMR (100 MHz, $CDCl_3$)** δ 197.4 (C=O), 163.7 (Cq Ar), 139.2 (Cq Ar), 136.2 (Cq Ar), 132.5 (CH Ar x2), 130.8 (CH Ar), 130.5 (Cq Ar), 129.8 (CH Ar), 127.9 (CH Ar), 125.2 (CH Ar), 113.7 (Cq Ar x2), 55.5 (CH_3 OMe), 19.8 (CH_3).

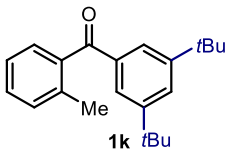

(3,5-di-*t*butylphenyl)(o-tolyl)methanone (1k). Following the procedure detailed in Method A, **1k** was isolated by FC on silica (hexane/EtOAc: 98:2 v/v) in 73% yield as a colorless oil starting from the corresponding aldehyde **S1**. TLC (hexane/EtOAc: 98:2 v/v): R_f = 0.36; HRMS calculated for $[C_{22}H_{28}O+Na]^+$: 331.2038; found: 331.2041.

^{1}H NMR (400 MHz, $CDCl_3$) δ 7.70 (s, 1H), 7.51 – 7.08 (m, 4H, Ar), 2.39 (s, 3H, CH_3), 1.36 (s, 18H, *t*Bu x2). **^{13}C NMR (100 MHz, $CDCl_3$)** δ 199.2 (C=O), 151.1 (Cq Ar x2), 139.0 (Cq Ar), 137.3 (Cq Ar), 136.9 (Cq Ar), 131.0 (CH Ar), 130.1 (CH Ar), 128.7 (CH Ar), 127.3 (CH Ar), 125.0 (CH Ar), 124.6 (CH Ar x2), 35.0 (Cq x2), 31.4 (CH_3 *t*Bu x2), 20.1 (CH_3).

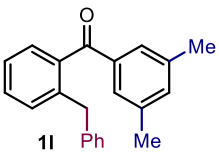

(2-benzylphenyl)(3,5-dimethylphenyl)methanone (1l). Following the procedure detailed in Method B, **1l** was isolated by FC on silica (hexane/EtOAc: 98:2 v/v) in 69% yield as a colorless oil starting from the corresponding aldehyde **S3**. TLC (hexane/EtOAc: 98:2 v/v): R_f = 0.36; HRMS calculated for $[C_{22}H_{20}O+Na]^+$: 323.1412; found: 323.1415.

^{1}H NMR (400 MHz, $CDCl_3$) δ 7.46 – 7.38 (m, 1H, Ar), 7.35 – 7.25 (m, 5H, Ar), 7.24 – 7.16 (m, 3H, Ar), 7.16 – 7.06 (m, 3H, Ar), 4.06 (s, 2H, CH_2), 2.33 (s, 6H, CH_3 x2). **^{13}C NMR (100 MHz, $CDCl_3$)** δ 199.1 (C=O), 140.5 (Cq Ar), 139.9 (Cq Ar), 139.3 (Cq Ar), 138.0 (Cq Ar x2), 137.8 (Cq Ar), 134.9 (CH Ar), 130.7 (CH Ar), 130.1 (CH Ar), 129.2 (CH Ar x2), 128.5, 128.2 (CH Ar x2), 127.9 (CH Ar x2), 126.0 (CH Ar), 125.6 (CH Ar), 38.8 (CH_2), 21.2 (CH_3).

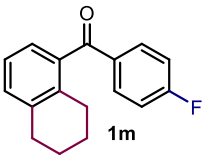

(4-fluorophenyl)(tetrahydronaphthalenyl)methanone (1m). Following the procedure detailed in Method B, **1m** was isolated by FC on silica (hexane/EtOAc: 98:2 v/v) in 71% yield as a colorless oil starting from the corresponding aldehyde **S3**. TLC (hexane/EtOAc: 98:2 v/v): R_f = 0.33.

^{1}H NMR (500 MHz, $CDCl_3$) δ 7.92 – 7.83 (m, 1H, Ar), 7.24 – 7.11 (m, 2H, Ar), 7.09 (m, 1H), 2.91 – 2.84 (m, 2H, Ar), 2.71 (m, 2H, Ar), 1.87 – 1.79 (m, 2H), 1.79 – 1.72 (m, 2H). **^{13}C NMR (125 MHz, $CDCl_3$)** δ 197.5 (C=O), δ 165.85, 138.6, 138.3, 135.3, 134.11 (d, *J* = 2.8 Hz, CH Ar), 132.8, 132.7, 131.2, 125.2, 124.8, 115.7, 115.5, 29.8 (CH_2), 27.1 (CH_2), 22.9 (CH_2), 22.7 (CH_2). **^{19}F NMR decoupled ^{1}H (400 MHz, $CDCl_3$)** δ -105.0, -115.7.

2.7.3. Catalyst Synthesis

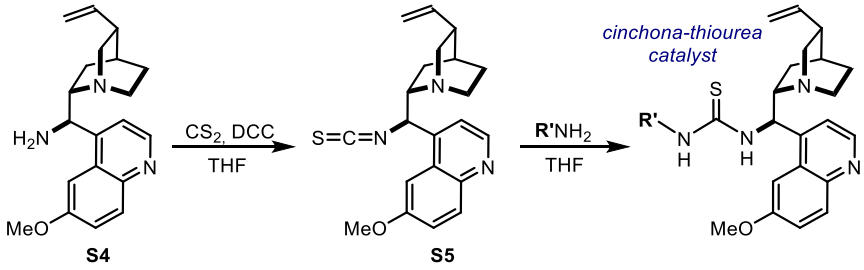

Scheme 2. General method for the synthesis of cinchona-thiourea catalysts.

General procedure: 9-amino(9-deoxy)*epi*-cinchona alkaloid **S4** was prepared from commercially available quinidine according to a literature procedure.[51] CS_2 (6 equiv) and *N*,*N*′-dicyclohexylcarbodiimide (1 equiv) were sequentially added to a stirred solution of **S4** in dry THF (1 M) at -20 °C. The reaction mixture was warmed slowly up to room temperature over a period of 3 h and then stirred overnight. The obtained solution was filtered and the solvent removed under reduced pressure. The residue was purified by flash chromatography (90:10 DCM/MeOH) yielding compound **S5** in 70-80% yield. The isothiocyanate **S5** was dissolved in dry THF (0.6 M) and then added to a stirred solution of the selected primary amine in THF (0.6 M) at ambient temperature. The reaction was stirred overnight. Then the solvent was removed under reduced pressure and the residue purified by flash chromatography (95:5 DCM/MeOH) yielding the corresponding cinchona-thiourea bifunctional organocatalyst in 65-85% yield.

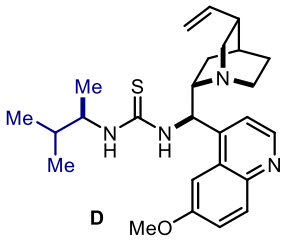

9-Amino(9-deoxy)*epi*-quinidine-derived thiourea (catalyst D). According to the general procedure described above, catalyst **D** was obtained as a white solid in 65% yield (880 mg), starting from 9-amino(9-deoxy)*epi*-quinidine **S4** (1 gr, 3 mmol, 1 equiv) and the commercially available (*R*)-(-)-2-amino-3-methylbutane (350 µl, 3 mmol, 1 equiv).

^{1}H NMR (500 MHz, $CDCl_3$) δ 8.78 (d, *J* = 4.5 Hz, 1H), 8.07 (d, *J* = 9.2 Hz, 1H), 7.62 – 7.57 (m, 1H), 7.44 (d, *J* = 2.7 Hz, 1H), 7.42 (d, *J* = 2.7 Hz, 1H), 7.40 (s, 1H), 6.44 (s, 1H), 5.99 – 5.86 (m, 1H), 5.25 – 5.14 (m, 2H), 4.00 (s, 3H), 3.18 (s, 1H), 3.13 – 2.91 (m, 4H), 2.40 (d, *J* = 8.3 Hz, 1H), 2.03 (d, *J* = 42.8 Hz, 2H), 1.78 – 1.69 (m, 2H), 1.69 – 1.53 (m, 2H), 1.36 (s, 1H), 1.05 (ddd, *J* = 14.7, 9.2, 2.8 Hz, 1H), 0.81 (s, 9H). **^{13}C NMR (125 MHz, $CDCl_3$)** δ 181.7, 158.2, 147.7, 147.0, 144.8, 139.6, 132.0, 127.7, 122.4, 115.3, 101.2, 56.2, 55.7 (x2), 55.1, 49.0, 46.8, 38.6, 32.5, 27.2, 26.1, 24.9, 18.7, 17.8, 16.3. **$[\alpha]^{26}_D$ =** + 200.9 (c = 0.5 in $CHCl_3$). **HRMS calculated for $[C_{26}H_{32}N_4OS+H]^+$**: 453.2683; **found:** 453.2685.

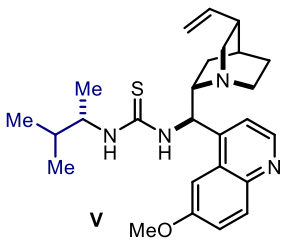

9-Amino(9-deoxy)*epi*-quinidine-derived thiourea (catalyst V). According to the general procedure described above, catalyst **V** was obtained as a white solid in 67% yield (910 mg), starting from 9-amino(9-deoxy)*epi*-quinidine **S4** (1 gr, 3 mmol, 1 equiv) and (*S*)-(+)-2-amino-3-methylbutane (350 µl, 3 mmol, 1 equiv).

[51] Cassani, C.; Martín-Rapún, R.; Arceo, E.; Bravo, F.; Melchiorre, P. Synthesis of 9-amino(9-deoxy)*epi* Cinchona Alkaloids, General Chiral Organocatalysts for the Stereoselective Functionalization of Carbonyl Compounds. *Nat. Protoc.* **2013**, *8*, 325–344.

^{1}H NMR (400 MHz, $CDCl_3$) δ 8.78 (d, J = 4.5 Hz, 1H), 8.06 (d, J = 9.3 Hz, 1H), 7.78 – 7.55 (m, 2H), 7.56 – 7.33 (m, 2H), 6.52 (s, 1H), 5.92 (ddd, J = 16.9, 10.5, 6.0 Hz, 1H), 5.52 (s, 1H), 5.33 – 5.18 (m, 2H), 4.00 (s, 3H), 3.33 (d, J = 9.5 Hz, 1H), 3.25 – 2.83 (m, 5H), 2.44 (d, J = 7.8 Hz, 1H), 1.87 – 1.46 (m, 4H), 1.32 (d, J = 36.8 Hz, 2H), 1.10 (s, 1H), 1.02 (d, J = 6.6 Hz, 2H), 0.90 (s, 1H), 0.58 (d, J = 20.4 Hz, 5H). **^{13}C NMR (100 MHz, $CDCl_3$)** δ 181.29, 158.37, 147.69, 145.00, 139.16, 132.13, 127.51, 122.54, 115.71, 101.00, 77.35, 77.03, 76.71, 55.77, 53.42, 48.96, 46.78, 38.37, 32.50, 29.69, 27.17, 25.75, 24.88, 18.26, 17.64, 16.69. **$[\alpha]^{26}_D$** = +186.4 (c = 0.3 in $CHCl_3$). **HRMS calculated for $[C_{26}H_{32}N_4OS+Na]^+$:** 453.2683; **found:** 453.2686.

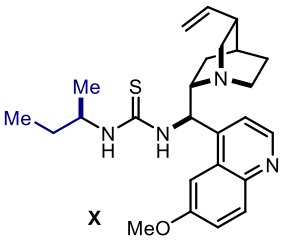

9-Amino(9-deoxy)*epi*-quinidine-derived thiourea (catalyst X). According to the general procedure described above, catalyst **X** was obtained as a white solid in 70% yield (920 mg), starting from 9-amino(9-deoxy)*epi*-quinidine **S4** (1 gr, 3 mmol, 1 equiv) and (*R*)-(-)-*sec*-butylamine (300 µl, 3 mmol, 1 equiv).

^{1}H NMR (400 MHz, $CDCl_3$) δ 8.76 (d, *J* = 4.5 Hz, 1H), 8.04 (d, *J* = 9.2 Hz, 1H), 7.67 (d, *J* = 2.1 Hz, 1H), 7.58 (s, 1H), 7.47 (d, *J* = 4.5 Hz, 1H), 7.41 (dd, *J* = 9.2, 2.6 Hz, 1H), 6.77 (s, 1H), 5.92 (ddd, *J* = 16.9, 10.5, 6.0 Hz, 1H), 5.63 (s, 1H), 5.29 – 5.15 (m, 2H), 4.00 (s, 3H), 3.34 (s, 2H), 3.24 – 2.94 (m, 4H), 2.44 (q, *J* = 7.3, 6.8 Hz, 1H), 1.81 – 1.74 (m, 1H), 1.74 – 1.54 (m, 2H), 1.54 – 1.32 (m, 3H), 1.15 – 1.04 (m, 1H), 0.99 (s, 3H), 0.86 (t, *J* = 7.4 Hz, 3H). **^{13}C NMR (100 MHz, $CDCl_3$)** δ 184.6, 181.5, 158.2, 147.7, 144.9, 139.1, 131.9, 122.4, 115.7, 101.4, 77.4, 77.0, 76.7, 61.2, 55.7, 51.9, 49.0, 46.8, 38.4, 29.3, 27.2, 25.7, 24.9, 19.6, 10.1. **$[\alpha]^{26}_D$ =** +165.1 (c = 0.5 in $CHCl_3$). **HRMS calculated for $[C_{25}H_{34}N_4OS+H]^+$:** 439.2526; **found**: 439.2522.

2.7.4. High-Throughput Screening of Organic Catalysts

The list of organocatalysts used in the high-throughput screening is shown in Scheme 3 (next page).

Procedure

1) Preparation of a library of organocatalysts. Stock solutions (0.02 M in 1,2-dichloroethane, DCE) of each catalyst were prepared. In the cases in which the catalysts were not soluble, a mixture of DCE and methanol was employed to prepare the stock solution. Then, 100 µL of each stock solution (*i.e.* 2 µmol of catalyst) were dosed in each reaction vial (0.75 mL glass vials, 8x30 mm). The solvent in every vial was removed to dryness using a parallel evaporator GeneVac.

2) Set-up of the experiments. The experiments were set-up inside a glovebox under a nitrogen atmosphere. The glass vials containing the organocatalysts (2 µmol) were initially charged into a 24-well aluminium block adapted for photochemical reactions (see Figure 2.31, left). A stock solution 0.3 M in 2-methylbenzophenone **1a** and 0.1 M in maleimide **2a**, in toluene, was prepared. 100 µL of this stock solution was dosed in every reaction vial (*i.e.* 30 µmol of **1a** and 10 µmol of **2a**). Stirring bars were then added to each reaction vial. The 24-well plate was sealed and stirred under irradiation of 365 nm black LEDs for 16 hours.

3) Analysis of the experiments. Upon opening the 24-well plate to air, 500 µL of a solution of biphenyl (used as internal standard to measure the UPLC yields) in acetonitrile (0.02 mol/L) was added to each reaction vial. The plate was covered again and the vials were stirred for 10 min to ensure good homogenization. Into a separate 96-well LC block (Figure 2.31, right) was added 500 µL of acetonitrile, followed by 20 µL of the diluted reaction mixtures. The LC block was then sealed with a silicon-rubber storage mat (shown in Figure 2.31, right) and mounted on an automated UPC^2 instrument for analysis.

Figure 2.31. *Left*: 24-well aluminium block fitted with 24 single black LEDs on the bottom. *Right:* 96-well LC block with a silicon-rubber storage mat.

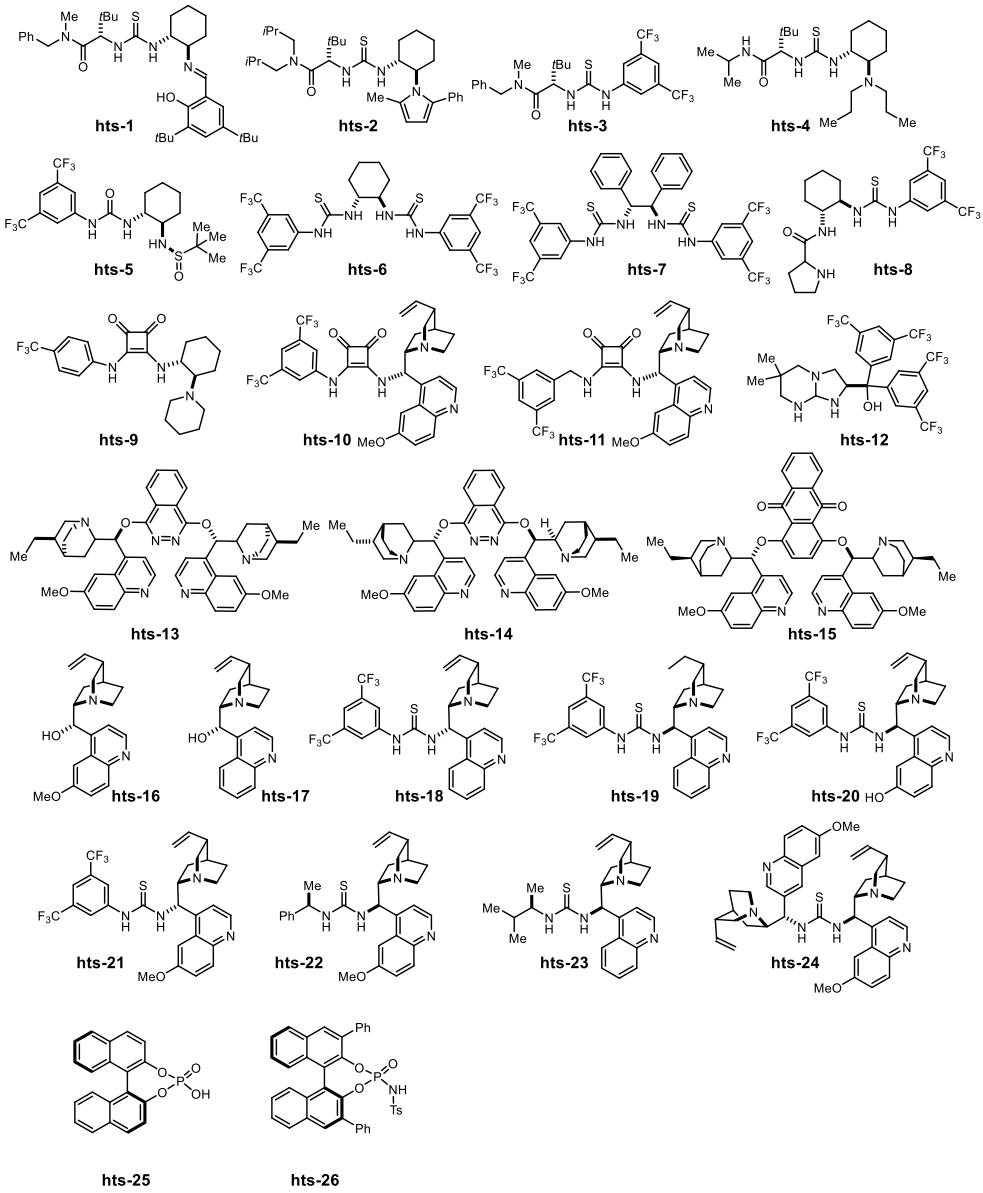

Scheme 3. Catalysts tested in the high-throughput screening.

Table 1.12. Results of the high-throughput screening of organic catalysts (see Scheme 3 for the catalyst structures)

catalyst	yield (%)[a]	ee (%)[b]	catalyst	yield (%)[a]	ee (%)[b]
hts-1	59	+3	hts-15	38	-23
hts-2	49	+2	hts-16	51	+3
hts-3	56	-2	hts-17	29	+4
hts-4	29	+10	hts-18	11	+29
hts-5	54	+3	hts-19	27	-1
hts-6	56	+3	hts-20	30	-11
hts-7	49	+2	hts-21	13	+25
hts-8	46	+3	hts-22	37	-38
hts-9	47	+3	hts-23	40	-52
hts-10	34	+6	hts-24	27	-26
hts-11	30	+6	hts-25	91	0
hts-12	40	+4	hts-26	95	+2
hts-13	38	+15			
hts-14	40	-4			

[a]UPLC (UltraPerformance Liquid Chromatography) yield using biphenyl as the internal standard. [b]Enantiomeric excess determined by UPC² (UltraPerformance Convergence Chromatography) analysis on a chiral stationary phase.

2.7.5. General Procedure for the Enantioselective Organocatalytic PEDA Reaction

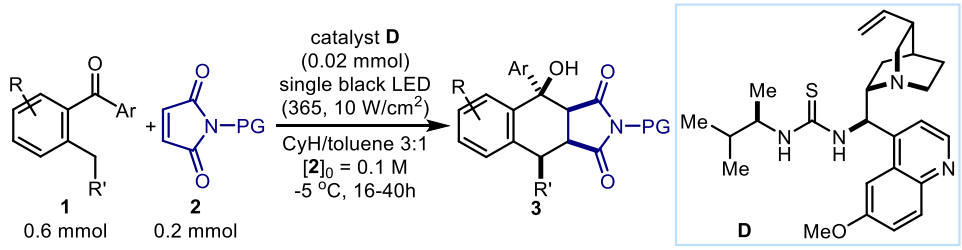

The cinchona-thiourea catalyst **D** (20 mol%, 18 mg) was added to an oven dried hand-capped vial equipped with a stirring bar, and dissolved in 1.5 mL of degassed cyclohexane. The vial was placed under an argon atmosphere, then the maleimide **2** (0.2 mmol) and 2-alkyl benzophenone **1** (0.6 mmol 3 equiv) were sequentially added. The mixture was then diluted with 0.5 mL of degassed toluene. The vial was flushed with argon, closed with a Teflon-coated cap, sealed with parafilm and placed into a single black LED plate (λ = 365 nm, irradiance = 10 mW/cm^2, as controlled by an external power supply). The light source used for illuminating the reaction vessel consisted of a single black LED (3.6 W, EOLD-365-525 LED, UV, 5 mm, λmax = 365 nm) produced by OSA OPTO Light and purchased from Farnell (http://www.farnell.com/). The temperature was kept at -5 °C with a chiller connected to the irradiation plate (the set-up is detailed in Figure 2.14 of Section 2.3.2 of this Chapter). Stirring was maintained for the indicated time (ranging from 16 to 40 hours), after this period the irradiation was stopped. The crude reaction mixture, which appeared heterogeneous, was completely solubilized by adding the minimum amount required of DCM (generally 100 µL). The overall solution was then directly charged on a flash column and subjected to chromatography purification on silica gel to afford the Diels-Alder product **3** as a single diastereoisomer and in the stated yield and enantiomeric excess.

2.7.6. Characterization Data of the PEDA Products

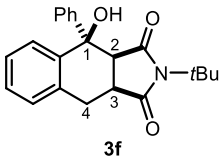

(3a*S*,4*R*,9a*S*)-2-(*t*-Butyl)-4-hydroxy-4-phenyl-tetrahydro-1H-benzoisoindole-1,3-dione (3f). Compound **3f** was prepared according to the general procedure using 2-methylbenzophenone **1a** (108 µL, 0.6 mmol, 3 equiv), N-*tert*-butyl maleimide **2f** (28 µL, 0.2 mmol, 1 equiv) and catalyst **D** (18 mg, 0.04 mmol, 0.2 equiv). Temperature: -5 °C. Time of irradiation: 24 hours. The crude mixture was purified by flash column chromatography (hexane/EtOAc, 90:10) to afford the title compound as a white solid (53 mg, 76% yield, 90% ee) and as a single diastereoisomer (dr > 20:1, as inferred by ^{1}H NMR analysis of the crude mixture). The enantiomeric excess (90% ee) was determined by HPLC analysis on a Daicel Chiralpak IC-3 column, 65:35 hexane/*i*PrOH, flow rate: 1.00

mL/min, λ = 216 nm, τ_{major}= 8.5 min, τ_{minor}= 5.9 min. $[\alpha]^{26}_D$ = + 5.7 (c = 0.5 in $CHCl_3$). HRMS calculated for $[C_{22}H_{23}NO_3+Na]^+$: 372.1576; found : 372.1570.

^{1}H NMR (500 MHz, $CDCl_3$): δ 7.90 (m, 1H, Ar), 7.43 (m, 1H, Ar), 7.36 – 7.27 (m, 4H, Ar), 7.26 – 7.21 (m, 2H, Ar), 7.12 (m, 1H Ar), 5.79 (s, 1H, OH), 3.84 (d, *J* = 9.0 Hz, 1H, H2), 3.09 (ddd, *J* = 9.0, 8.1, 1.4 Hz, 1H, H3), 2.88 (dd, *J* = 15.0, 1.4 Hz, 1H, H4 α), 2.50 (ddt, *J* = 15.0, 8.2, 1.1 Hz, 1H, H4 β), 1.30 (s, 9H, *t*-Bu). **^{13}C NMR (125 MHz, $CDCl_3$)** δ 181.8 (C=O), 180.3(C=O), 141.3 (Cq, Ar) , 141.1 (Cq, Ar), 133.0 (Cq Ar), 128.6 (Ar x2), 128.2 (Ar), 128.1 (Ar), 128.0 (Ar), 127.6 (Ar), 126.8 (Ar x2), 125.2 (Ar), 76.5 (Cq), 59.0 (Cq), 47.3 (CH), 39.1 (CH), 30.5 (CH_2), 27.9 (CH_3).

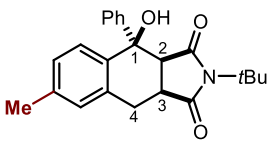

3g

(3a*S*,4*R*,9a*S*)-2-(*t*-butyl)-4-hydroxy-7-methyl-4-phenyl-tetrahydro-1H-benzoisoindole-1,3-dione (3g). Compound **3g** was prepared according to the general procedure using 2,4-dimethylbenzophenone **1d** (116 μL, 0.6 mmol, 3 equiv), *N*-*tert*-butyl maleimide **2f** (28 μL, 0.2 mmol, 1 equiv) and catalyst **D** (18 mg, 0.04 mmol, 0.2 equiv). Temperature: -5 ºC. Time of irradiation: 40 hours. The crude mixture was purified by flash column chromatography (hexane/EtOAc, 90:10) to afford the title compound as a white solid (53 mg, 73% yield, 87% ee) and as a single diastereoisomer (dr > 20:1, as inferred by ^{1}H NMR analysis of the crude mixture). The enantiomeric excess (87% ee) was determined by HPLC analysis on a Daicel Chiralpak IC-3 column, 65:35 hexane/*i*PrOH, flow rate: 1.00 mL/min, λ = 216 nm, τ_{major}= 9.4 min, τ_{minor}= 5.9 min. $[\alpha]^{26}_D$ = - 7.1 (c = 0.5 in $CHCl_3$). HRMS calculated for $[C_{23}H_{25}NO_3+Na]^+$: 386.1732; found: 386.1716.

^{1}H NMR (500 MHz, $CDCl_3$): δ 7.75 (d, *J* = 7.8 Hz, 1H, Ar), 7.35 – 7.27 (m, 3H, Ar), 7.25 – 7.21 (m, 3H, Ar), 6.94 (s, 1H), 5.72 (s, 1H, OH), 3.81 (d, *J* = 9.0 Hz, 1H, H2), 3.06 (ddd, *J* = 9.0, 8.2, 1.4 Hz, 1H, H3), 2.83 (dd, *J* = 15.0, 1.4 Hz, 1H, H4 α), 2.48 (dd, *J* = 14.9, 8.1 Hz, 1H, H4 β), 2.36 (s, 3H, CH_3), 1.31 (s, 9H, *t*-Butyl).**^{13}C NMR (125 MHz, $CDCl_3$):** δ 181.80 (C=O), 180.45 (C=O), 141.6 (Cq, Ar), 138.0 (Cq, Ar) 137.8 (Cq, Ar), 132.8 (Cq, Ar), 128.6 (Ar x2), 128.5 (Ar x2), 128.0 (Ar), 126.8 (Ar), 125.1 (Ar), 76.4 (Cq), 58.9 (Cq), 47.4 (CH), 39.1(CH), 30.4 (CH_2), 27.9 (CH_3 x3), 21.0 (CH_3).

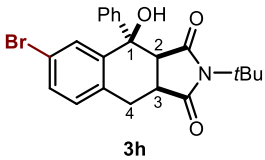

3h

(3a*S*,4*R*,9a*S*)-6-bromo-2-(*t*-butyl)-4-hydroxy-4-phenyl-tetrahydro-benzoisoindole-1,3-dione (3h). Compound **3h** was prepared according to the general procedure using 5-bromo-2-methylbenzophenone **1e** (165 mg, 0.6 mmol, 3 equiv), *N*-*tert*-butyl maleimide **2f** (28 μL, 0.2 mmol, 1 equiv) and catalyst **D** (18 mg, 0.04 mmol, 0.2 equiv). Temperature: -5 ºC. Time of irradiation: 16 hours. The crude mixture was purified by flash column chromatography (hexane/EtOAc, 90:10) to afford the

title compound as a white solid (78 mg, 90% yield, 81% ee) and as a single diastereoisomer (dr > 20:1 as inferred by ^{1}H NMR analysis of the crude mixture). The enantiomeric excess (81% ee) was determined by HPLC analysis on a Daicel Chiralpak IC column, 65:35 hexane/*i*PrOH, flow rate: 1.00 mL/min, λ = 216 nm, τ_{major}= 6.5 min, τ_{minor}= 5.0 min. $[\alpha]^{26}_D$ = - 3.2 (c = 1.3 in $CHCl_3$). HRMS calculated for $[C_{22}H_{22}BrNO_3+Na]^+$: 450.0681; found: 450.0676.

^{1}H NMR (500 MHz, $CDCl_3$): δ 8.07 (d, *J* = 2.1 Hz, 1H, Ar), 7.45 (dd, *J* = 8.0, 2.1 Hz, 1H, Ar), 7.37 – 7.30 (m, 3H, Ar), 7.23 – 7.19 (m, 2H, Ar), 7.00 (dd, *J* = 8.0, 1.0 Hz, 1H, Ar), 5.88 (s, 1H, OH), 3.84 (d, *J* = 9.1 Hz, 1H, H2), 3.09 (ddd, *J* = 9.2, 8.2, 1.3 Hz, 1H, H3), 2.87 (dd, *J* = 15.2, 1.3 Hz, 1H, H4 α), 2.46 – 2.38 (m, 1H, H4 β), 1.33 (s, 9H, *t*-Butyl). **^{13}C NMR (125 MHz, $CDCl_3$):** δ 181.5 (C=O), 179.9 (C=O), 143.4 (Cq, Ar), 140.7 (Cq. Ar), 132.0 (Cq, Ar), 131.1 (Cq, Ar), 129.6 (Ar), 128.7 (Ar x2), 128.5 (Ar), 128.4 (Ar), 126.7, (Ar x2) 121.86 (Ar), 76.3 (Cq), 59.2 (Cq) 46.9 (CH), 38.8 (CH), 29.9 (CH_2), 28.0 (CH_3 x3).

The absolute configuration for **3h** was unambiguously inferred by anomalous dispersion X-ray crystallographic analysis (CCDC 1417309), see X-ray Crystallographic Data section.

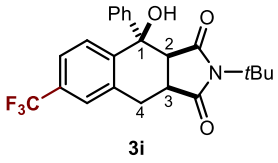

3i

(3a*S*,4*R*,9a*S*)-2-(*t*-butyl)-4-hydroxy-4-phenyl-7-(trifluoromethyl)-tetrahydro-benzoisoindole-1,3-dione (3i). Compound **3i** was prepared according to the general procedure using 2-methyl-4-trifluoromethylbenzophenone **1f** (158 mg, 0.6 mmol, 3 equiv), *N*-*tert*-butyl maleimide **2f** (28 μL, 0.2 mmol, 1 equiv) and catalyst **D** (18 mg, 0.04 mmol, 0.2 equiv). Temperature: -5 ºC. Time of irradiation: 24 hours. The crude mixture was purified by flash column chromatography (hexane/EtOAc, 90:10) to afford the title compound as a white solid (70 mg, 84% yield, 83% ee) and as a single diastereoisomer (dr > 20:1, as inferred by ^{1}H NMR analysis of the crude mixture). The enantiomeric excess (83% ee) was determined by HPLC analysis on a Daicel Chiralpak IC column, 65:35 hexane/*i*PrOH, flow rate: 0.90 mL/min, λ = 216 nm, τ_{major}= 6.0 min, τ_{minor}= 4.9 min. $[\alpha]^{26}_D$ = - 5.4 (c = 0.6 in $CHCl_3$). HRMS calculated for $[C_{23}H_{22}F_3NO_3+Na]^+$: 440.1449; found: 440.1448.

^{1}H NMR (400 MHz, $CDCl_3$): δ 8.07 (d, *J* = 8.0 Hz, 1H, Ar), 7.71 (m, 1H, Ar), 7.42 – 7.38 (m, 1H, Ar), 7.37 – 7.31 (m, 3H, Ar), 7.24 – 7.17 (m, 2H, Ar), 5.93 (s, 1H, OH), 3.89 (d, 3.14 *J* = 9.1 Hz, 1H, H2), (ddd, *J* = 9.2, 8.2, 1.4 Hz, 1H, H3), 2.97 (dd, *J* = 15.1, 1.3 Hz, 1H, H4 α), 2.53 (dd, *J* = 15.1, 8.2 Hz, 1H, H4 β), 1.29 (s, 9H, *t*-Bu). **^{13}C NMR (100 MHz, $CDCl_3$):** δ 181.5 (C=O), 179.7 (C=O), 145.4 (Cq Ar), 140.4 (Cq, Ar), 134.0 (Cq Ar), 128.8 (Ar x2), 128.6 (Cq Ar), 126.6 (Ar x2), 125.9 (Ar), 124.9 (Ar), 124.82 (Ar), 124.48 (Ar), 76.5 (Cq), 59.3 (Cq), 46.8 (CH), 38.8 (CH), 30.4 (CH_2), 27.9 (CH_3 x3).

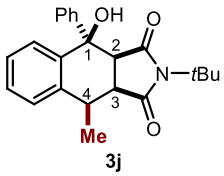

3j

(3a*S*,4*R*,9*R*,9a*S*)-2-(*t*-butyl)-4-hydroxy-9-methyl-4-phenyl-tetrahydro-1H-benzoisoindole-1,3-dione (3j). Compound **3j** was prepared according to the general procedure using 2-ethylbenzophenone **1g** (126 mg, 0.6 mmol, 3 equiv), *N*-*tert*-butyl maleimide **2f** (28 µL, 0.2 mmol, 1 equiv) and catalyst **D** (18 mg, 0.04 mmol, 0.2 equiv). Temperature: -5 ºC. Time of irradiation: 24 hours. The crude mixture was purified by flash column chromatography (hexane/EtOAc, 90:10) to afford the title compound as a white solid (67 mg, 95% yield, 85% ee) and as a single diastereoisomer (dr > 20:1 as inferred by ^{1}H NMR analysis of the crude mixture). The enantiomeric excess (85% ee) was determined by HPLC analysis on a Daicel Chiralpak IC-3 column, 65:35 hexane/*i*PrOH, flow rate: 0.8 mL/min, λ= 216 nm, τ_{major}= 12.2 min, τ_{minor}= 7.5 min. $[\alpha]^{26}_D$ = - 7.3 (c = 0.4 in $CHCl_3$). HRMS calculated for $[C_{23}H_{25}NO_3+Na]^+$: 386.1732; found: 386.1721.

^{1}H NMR (500 MHz, $CDCl_3$): δ 7.96 (m, 1H, Ar), 7.49 – 7.37 (m, 2H, Ar), 7.37 – 7.30 (m, 3H, Ar), 7.28 – 7.24 (m, 2H, Ar), 7.20 (m, 1H, Ar), 5.86 (s, 1H, OH), 3.89 (d, *J* = 8.5 Hz, 1H, H2), 3.01 (dd, *J* = 8.5, 7.6 Hz, 1H, H3), 2.66 (p, *J* = 7.2 Hz, 1H, H4), 1.41 (d, *J* = 7.1 Hz, 3H, H5), 1.23 (s, 9H, *t*-Butyl).**^{13}C NMR (125 MHz, $CDCl_3$):** δ 181.1(C=O), 177.3 (C=O), 141.2 (Cq, Ar), 141.0 (Cq, Ar), 136.3 (Cq, Ar), 128.8 (Ar x2), 128.3 (Ar), 128.1 (Ar), 127.1 (Ar), 126.6 (Ar x2), 125.1 (Ar), 124.4 (Ar), 76.3 (Cq), 58.6 (Cq), 47.8 (CH), 44.1 (CH), 31.3 (CH), 27.9 (CH_3 x3), 14.1 (CH_3).

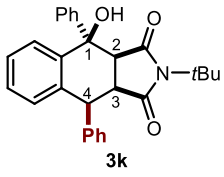

3k

(3a*S*,4*R*,9*S*,9a*S*)-2-(*t*-butyl)-4-hydroxy-4,9-diphenyl-tetrahydro-1H-benzoisoindole-1,3-dione (3k). Compound **3k** was prepared according to the general procedure using 2-benzyllbenzophenone **1c** (163.4 mg, 0.6 mmol, 3 equiv), *N*-*tert*-butyl maleimide **2f** (28 µL, 0.2 mmol, 1 equiv) and catalyst **D** (18 mg, 0.04 mmol, 0.2 equiv). Temperature: -5 ºC. Time of irradiation: 40 hours. The crude mixture was purified by flash column chromatography (hexane/EtOAc, 90:10) to afford the title compound as a white solid (63.6 mg, 75% yield, 90% ee) and as a single diastereoisomer (dr > 20:1, as inferred by ^{1}H NMR analysis of the crude mixture). The enantiomeric excess (90% ee) was determined by HPLC analysis on a Daicel Chiralpak IC-3 column, 65:35 hexane/*i*PrOH, flow rate: 0.8 mL/min, λ= 216 nm, τ_{major}= 11.7 min, τ_{minor}= 7.3 min $[\alpha]^{26}_D$ = - 40.0 (c = 0.6 in $CHCl_3$). HRMS calculated for $[C_{28}H_{27}NO_3+Na]^+$: 448.1889; found: 448.1886.

^{1}H NMR (500 MHz, $CDCl_3$): δ 8.03 (dd, *J* = 7.7, 1.4 Hz, 1H, Ar), 7.47 (m, 1H, Ar), 7.42 – 7.33 (m, 6H, Ar), 7.32 – 7.25 (m, 3H, Ar), 7.16 (m, 1H, Ar), 7.12 – 7.06 (m, 2H, Ar), 5.99 (s, 1H, OH), 3.95 (d, *J* = 8.6 Hz, 1H, H4), 3.92 (d, *J* = 8.4 Hz, 1H, H2), 3.21 (t, *J* = 8.5 Hz, 1H, H3), 1.37 (s, 9H, *t*-Butyl). **^{13}C NMR (125 MHz, $CDCl_3$):** δ 180.6 (C=O), 176.9 (C=O), 141.3 (Cq, Ar) , 141.2 (Cq, Ar), 136.0 (Cq, Ar), 134.4 (Cq, Ar), 131.2 (Ar x2), 128.8 (Ar x2), 128.4

(Ar), 127.9 (Ar x2), 127.8 (Ar), 127.8 (Ar), 127.4 (Ar), 127.0 (Ar), 126.6 (Ar x2), 125.7 (Ar), 75.6 (Cq), 58.8 (Cq), 48.6 (CH), 45.9 (CH), 45.1 (CH), 28.1 (CH_3 x3).

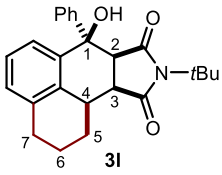

3l

(7*R*,7a*S*,10a*S*,10b*R*)-9-(*t*-butyl)-7-hydroxy-7-phenyl-hexahydronaphthoisoindole-8,10-dione (3l). Compound **3l** was prepared according to the general procedure using phenyl(5,6,7,8-tetrahydronaphthalen-1-yl)methanone **1h** (141.6 mg, 0.6 mmol, 3 equiv), *N*-*tert*-butyl maleimide **2f** (28 µL, 0.2 mmol, 1 equiv) and catalyst **D** (18 mg, 0.04 mmol, 0.2 equiv). Temperature: -5 ºC. Time of irradiation: 24 hours. The crude mixture was purified by flash column chromatography (hexane/EtOAc, 90:10) to afford the title compound as a white solid (63.6 mg, 82% yield, 87% ee) and as a single diastereoisomer (dr > 20:1, as inferred by ^{1}H NMR analysis of the crude mixture). The enantiomeric excess (87% ee) was determined by HPLC analysis on a Daicel Chiralpak IC-3 column, 65:35 hexane/*i*PrOH, flow rate: 1.00 ml/min, λ= 216 nm, τ_{major}= 12.6 min, τ_{minor}= 6.8 min. $[\alpha]^{26}_D$ = + 7.6 (c = 0.5 in $CHCl_3$). HRMS calculated for $[C_{25}H_{27}NO_3+Na]^+$: 412.1889; found: 412.1873.

^{1}H NMR (400 MHz, $CDCl_3$): δ 7.79 – 7.75 (m, 1H, Ar), 7.36 – 7.29 (m, 4H, Ar), 7.24 – 7.20 (m, 2H, Ar), 7.13 (m, 1H, Ar), 5.82 (s, 1H, OH), 3.87 (d, *J* = 8.5 Hz, 1H, H2), 2.99 (t, *J* = 8.4 Hz, 1H, H3), 2.69 (t, *J* = 6.1 Hz, 2H, H7), 2.58 (q, *J* = 8.1 Hz, 1H, H4), 1.89-1.95 (m, 2H, H5), 1.79 (m, 1H, H6 α), 1.60 – 1.48 (m, 1H, H6 β), 1.29 (s, 9H, *t*-Butyl).**^{13}C NMR (100 MHz, $CDCl_3$):** δ 180.9 (C=O), 178.1 (C=O), 141.1 (Cq, Ar), 140.9 (Cq, Ar), 137.7 (Cq, Ar), 131.1 (Cq, Ar), 128.7 (Ar x3), 128.2 (Ar), 126.7 (Ar x2), 126.5 (Ar), 123.0 (Ar), 76.0 (Cq), 58.4 (Cq), 48.1 (CH), 43.8 (CH), 32.6 (CH), 30.0 (CH_2), 28.0 (CH_3 x3), 26.1 (CH_2), 22.17 (CH_2).

The absolute configuration for **3l** was unambiguously inferred by anomalous dispersion X-ray crystallographic analysis (CCDC 1417310), see X-ray Crystallographic Data section.

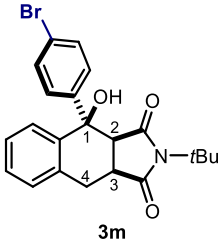

3m

(3a*S*,4*R*,9a*S*)-4-(4-bromophenyl)-2-(*t*-butyl)-4-hydroxy--tetrahydro-1H-benzoisoindole-1,3-dione (3m). Compound **3m** was prepared according to the general procedure using (4-bromophenyl)(*o*-tolyl)methanone **1i** (165 mg, 0.6 mmol, 3 equiv), *N*-*tert*-butyl maleimide **2f** (28 µL, 0.2 mmol, 1 equiv) and catalyst **D** (18 mg, 0.04 mmol, 0.2 equiv). Temperature: -5 ºC. Time of irradiation: 24 hours. The crude mixture was purified by flash column chromatography (hexane/EtOAc, 90:10) to afford the title compound as a white solid (61 mg, 71% yield, 84% ee) and as a single diastereoisomer (dr > 20:1, as inferred by ^{1}H NMR analysis of the crude mixture). The enantiomeric excess (89% ee) was determined by HPLC analysis

on a Daicel Chiralpak IC-3 column, 67:33 hexane/*i*PrOH, flow rate: 0.8 mL/min, λ= 216 nm, τ_{major}= 9.8 min, τ_{minor}= 6.8 min. $[\alpha]^{26}_D$ = + 0.3 (c = 0.5 in $CHCl_3$). HRMS calculated for $[C_{22}H_{22}BrNO_3+Na]^+$: 450.0681; found: 450.0687.

^{1}H NMR (500 MHz,$CDCl_3$) δ 7.86 (d, *J* = 6.7 Hz, 1H. Ar), 7.47 – 7.40 (m, 3H, Ar), 7.32 (m, 1H, Ar), 7.15 – 7.08 (m, 3H, Ar), 5.80 (s, 1H, OH), 3.76 (d, J=9.0 Hz, 1H, H2), 3.07 (ddd, *J* = 9.2, 8.3, 1.4 Hz, 1H, H3), 2.91 (dd, *J* = 15.1, 1.1 Hz, 1H, H4α), 2.49 (dd, *J* = 15.1, 8.2 Hz, 1H, H4β), 1.29 (s, 9H, *t*-Butyl). **^{13}C NMR (125 MHz, $CDCl_3$)** δ 181.4 (C=O), 180.1 (C=O), 140.5 (Cq Ar), 140.5 (Cq Ar) 132.9 (Cq Ar), 131.7 (CH Ar x2), 128.7 (CH Ar x2), 128.3 (CH Ar), 128.1 (CH Ar), 127.7 (CH Ar), 125.1 (CH Ar), 122.4 (Cq Ar), 76.1 (Cq), 59.1 (Cq), 47.3 (CH), 38.9 (CH), 30.4 (CH_2), 27.9 (CH_3 x3).

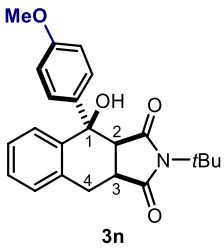

3n

(3a*S*,4*R*,9a*S*)-2-(*t*-butyl)-4-hydroxy-4-(4-methoxyphenyl)-tetrahydro-1H-benzoisoindole-1,3-dione (3n). Compound **3n** was prepared according to the general procedure using (4-methoxyphenyl)(o-tolyl)methanone **1j** (135.6 mg, 0.6 mmol, 3 equiv), *N-tert*-butyl maleimide **2f** (28 µL, 0.2 mmol, 1 equiv) and catalyst **D** (18 mg, 0.04 mmol, 0.2 equiv). Temperature: -5 ºC. Time of irradiation: 40 hours. The crude mixture was purified by flash column chromatography (hexane/EtOAc, 90:10) to afford the title compound as a white solid (46 mg, 61% yield, 86% ee) and as a single diastereoisomer (dr > 20:1 as inferred by ^{1}H NMR analysis of the crude mixture). The enantiomeric excess (86% ee) was determined by HPLC analysis on a Daicel Chiralpak IC-3 column, 65:35 hexane/*i*PrOH, flow rate: 1.00 mL/min, λ= 216 nm, τ_{major}= 16.4 min, τ_{minor}= 8.6 min. $[\alpha]^{26}_D$ = - 0.5 (c = 0.5 in $CHCl_3$). HRMS calculated for $[C_{23}H_{25}NO_4+Na]^+$: 402.1681; found: 402.1673.

^{1}H NMR (500 MHz, $CDCl_3$): δ 7.88 (dd, *J* = 7.6, 1.3 Hz, 1H, Ar), 7.42 (m, 1H, Ar), 7.30 (m, 1H, Ar), 7.17 – 7.09 (m, 3H, Ar), 6.86 – 6.81 (m, 2H, Ar), 5.73 (s, 1H, OH), 3.80 (d, *J* = 9.0 Hz, 1H, H2 overlap signal), 3.79 (s, 3H. OMe), 3.06 (ddd, *J* = 9.2, 8.2, 1.3 Hz, 1H, H3), 2.91 – 2.85 (m, 1H, H4 α), 2.52 (dd, *J* = 14.9, 8.2 Hz, 1H, H4β), 1.29 (s, 9H, *t*-Butyl).**^{13}C NMR (125 MHz, $CDCl_3$):** δ 181.8 5 (C=O), 180.4 5 (C=O), 159.3 (Cq, Ar), 141.3 (Cq, Ar), 133.5 (Cq, Ar) 132.9 (Cq, Ar), 128.1 (Ar x2), 128.0 (Ar), 127.5 (Ar), 125.1 (Ar), 113.90 (Ar x2), 76.1 (Cq), 58.9 (Cq), 55.3 (CH), 47.5 (CH_3), 39.1 (CH), 30.5 (CH_2), 28.0 (CH_3 x3).

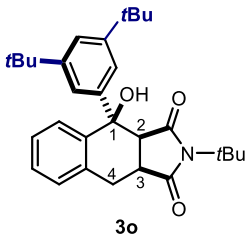

3o

(3a*S*,4*R*,9a*S*)-2-(*t*-butyl)-4-(3,5-di-tert-butylphenyl)-4-hydroxy-tetrahydrobenzoisoindole-1,3-dione (3o). Compound **3o** was prepared according to the general procedure using (3,5-di-tert-butylphenyl)(o-tolyl)methanone **1k** (186 mg, 0.6 mmol, 3 equiv), *N-tert*-butyl maleimide **2f** (28 µL, 0.2 mmol, 1 equiv) and catalyst

D (18 mg, 0.04 mmol, 0.2 equiv). Temperature: -5 ºC. Time of irradiation: 24 hours. The crude mixture was purified by flash column chromatography (hexane/EtOAc, 90:10) to afford the title compound as a white solid (79 mg, 86% yield, 80% ee) and as a single diastereoisomer (dr > 20:1, as inferred by ^{1}H NMR analysis of the crude mixture). The enantiomeric excess (80% ee) was determined by HPLC analysis on a Daicel Chiralpak IC column, 65:35 hexane/*i*PrOH, flow rate: 0.90 mL/min, λ = 216 nm, τ_{major}= 7.7 min, τ_{minor}= 5.4 min. $[\alpha]^{26}_D$ = + 8.3 (c = 0.7 in $CHCl_3$). HRMS calculated for $[C_{30}H_{39}NO_3+Na]^+$: 484.2828; found: 484.2827.

^{1}H NMR (400 MHz, $CDCl_3$): δ 7.90 (dd, *J* = 7.7, 1.3 Hz, 1H, Ar), 7.42 (m, 1H, Ar), 7.34 (m, 1H, Ar), 7.31 – 7.26 (m, 1H, Ar), 7.13 – 7.08 (m, 1H, Ar), 7.05 (m, 2H, Ar), 5.78 (s, 1H, OH), 3.86 (d, *J* = 9.0 Hz, 1H, H2), 3.06 (ddd, *J* = 9.2, 8.3, 1.3 Hz, 1H, H3), 2.86 (dd, *J* = 15.0, 1.3 Hz, 1H, H4 α), 2.53 (dd, *J* = 14.9, 8.2 Hz, 1H, H4 β), 1.30 (s, 9H, *t*-Butyl), 1.25 (s, 18H, *t*-Butyl x2). **^{13}C NMR (100 MHz, $CDCl_3$):** δ 182.0 (C=O), 180.5 (C=O), 150.7 (Cq x2, Ar), 141.5(Cq), 140.2 (Cq), 133.0 (Cq), 127.9 (Ar), 127.7 (Ar), 127.5 (Ar), 125.0 (Ar), 122.1 (Ar), 121.0 (Ar x2), 76.9 (Cq), 58.9 (Cq), 47.7 (CH), 39.3(Cq x2), 34.9 (CH), 31.4 (CH_3 x6), 30.5(CH_2), 28.0 (CH_3 x3).

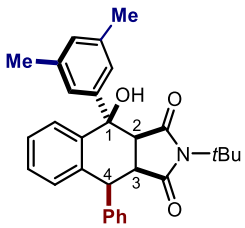

3p

(3a*S*,4*R*,9a*S*)-2-(*t*-butyl)-4-(3,5-dimethylphenyl)-4-hydroxy-tetrahydrobenzoisoindole-1,3-dione (3p). Compound **3p** was prepared according to the general procedure using (2-benzylphenyl)(3,5-dimethylphenyl)methanone **1l** (180 mg, 0.6 mmol, 3 equiv), *N*-*tert*-butyl maleimide **2f** (28 μL, 0.2 mmol, 1 equiv) and catalyst **D** (18 mg, 0.04 mmol, 0.2 equiv). Temperature: -5 ºC. Time of irradiation: 40 hours. The crude mixture was purified by flash column chromatography (hexane/EtOAc, 95:5) to afford the title compound as a white solid (68 mg, 75% yield, 94% ee) and as a single diastereoisomer (dr > 20:1, as inferred by ^{1}H NMR analysis of the crude mixture). The enantiomeric excess (94% ee) was determined by HPLC analysis on a Daicel Chiralpak IB column, 90:10 hexane/*i*PrOH, flow rate: 0.80 mL/min, λ= 216 nm, τ_{major}= 13.5 min, τ_{minor}= 8.9 min. $[\alpha]^{26}_D$ = - 40.0 (c = 0.3 in $CHCl_3$). HRMS calculated for $[C_{30}H_{31}NO_3+Na]^+$: 476.2202; found: 476.2201.

^{1}H NMR (500 MHz, $CDCl_3$): δ 8.00 (dd, *J* = 7.7, 1.4 Hz, 1H, Ar), 7.46 (m, 1H, Ar), 7.40 – 7.34 (m, 3H, Ar), 7.32 – 7.26 (m, 1H, Ar), 7.17 – 7.13 (m, 1H, Ar), 7.11 (m, 2H, Ar), 6.99 (m, 1H, Ar), 6.86 (dt, *J* = 1.5, 0.7 Hz, 2H, Ar), 5.93 (s, 1H, OH), 3.98 (d, *J* = 8.3 Hz, 1H, H4), 3.95 (d, *J* = 8.6 Hz, 1H, H2), 3.24 (t, *J* = 8.5 Hz, 1H, H3), 2.30 (s, 6H, 2Me), 1.36 (s, 9H, *t*-Butyl).**^{13}C NMR (100 MHz, $CDCl_3$):** δ 180.7 (C=O), 177.0 (C=O), 141.5 (Cq, Ar), 141.1(Cq, Ar), 138.3 (Cq, Ar x2), 136.1 (Cq, Ar), 134.3 (Cq, Ar), 131.2 (Ar x2), 130.1 (Ar), 127.9 (Ar x2), 127.7 (Ar), 127.6 (Ar), 127.3 (Ar), 126.9 (Ar), 125.7 (Ar), 124.3 (Ar x2), 75.6 (Cq), 58.7 (Cq), 48.6 (CH), 46.0 (CH), 45.0 (CH), 28.1 (CH_3 x3), 21.5 (CH_3 x2).

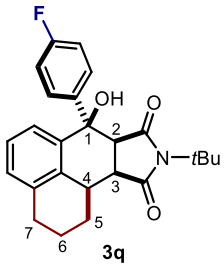

3q

(7*R*,7a*S*,10a*S*,10b*R*)-9-(*t*-butyl)-7-(4-fluorophenyl)-7-hydroxy-hexahydronaphthoisoindole-8,10-dione (3q). Compound **3q** was prepared according to the general procedure using (4-fluorophenyl)-(5,6,7,8-tetrahydronaphthalenyl)methanone **1m** (152.6 mg, 0.6 mmol, 3 equiv), *N*-*tert*-butyl maleimide **2f** (28 µL, 0.2 mmol, 1 equiv) and catalyst **D** (18 mg, 0.04 mmol, 0.2 equiv). Temperature: -5 ºC. Time of irradiation: 24 hours. The crude mixture was purified by flash column chromatography (hexane/EtOAc, 90:10) to afford the title compound as a white solid (70 mg, 84% yield, 87% ee) and as a single diastereoisomer (dr > 20:1 as inferred by ^{1}H NMR analysis of the crude mixture). The enantiomeric excess (87% ee) was determined by HPLC analysis on a Daicel Chiralpak IC-3 column, 65:35 hexane/ *i*PrOH, flow rate: 0.90 mL/min, λ= 216 nm, τ_{major}= 10.5 min, τ_{minor}= 6.4 min. $[\alpha]^{26}_D$ = + 14.2 (c = 0.7 in $CHCl_3$). HRMS calculated for $[C_{25}H_{26}FNO_3+Na]^+$: 430.1794; found: 430.1789.

^{1}H NMR (500 MHz,$CDCl_3$): δ 7.75 (m, 1H, Ar), 7.32 (m, 1H, Ar), 7.22 – 7.16 (m, 2H, Ar), 7.03 – 6.97 (m, 2H, Ar), 5.84 (s, 1H, OH), 3.81 (d, *J* = 8.5 Hz, 1H, H2), 2.97 (t, *J* = 8.4 Hz, 1H, H3), 2.70 (t, *J* = 6.1 Hz, 2H, H7), 2.56 (q, *J* = 8.1 Hz, 1H, H4), 1.97 – 1.89 (m, 2H, H5), 1.84 – 1.75 (m, 1H, H6 α), 1.59 – 1.51 (m, 1H, H6 β), 1.29 (s, 9H, *t*-But). **^{13}C NMR (125 MHz, $CDCl_3$):** δ 180.7 (C=O), 177.9 (C=O), 140.6 (Cq Ar), 137.8 (Cq, Ar), 131.0 (Cq, Ar), 128.8 (Ar x2), 128.6 (Cq), 128.5 (Ar x2), 126.6 (Ar), 122.9 (Ar), 115.6 (Ar), 115.43 (Ar), 75.5 (Cq), 58.5 (Cq), 48.3 (CH), 43.7 (CH), 32.7 (CH), 29.9 (CH_2), 28.0 (CH_3 x3), 26.11 (CH_2), 22.18 (CH_2).

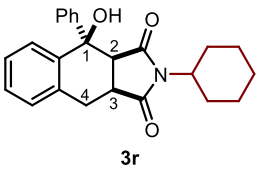

3r

(3a*S*,4*R*,9a*S*)-2-cyclohexyl-4-hydroxy-4-phenyl-tetrahydro-1H-benzoisoindole-1,3-dione (3r). Compound **3r** was prepared according to the general procedure using 2-methylbenzophenone **1a** (109µL, 0.6 mmol, 3 equiv), *N*-cyclohexyl maleimide **2g** (35.8 mg, 0.2 mmol, 1 equiv) and catalyst **D** (18 mg, 0.04 mmol, 0.2 equiv). Temperature: -5 ºC. Time of irradiation: 24 hours. The crude mixture was purified by flash column chromatography (hexane/EtOAc, 90:10) to afford the title compound as a white solid (53 mg, 71% yield, 82% ee) and as a single diastereoisomer (dr > 20:1, as inferred by ^{1}H NMR analysis of the crude mixture). The enantiomeric excess (82% ee) was determined by HPLC analysis on a Daicel Chiralpak IC-3 column, 65:35 hexane/*i*PrOH, flow rate: 0.80 mL/min, λ= 216 nm, τ_{major}= 11.1 min, τ_{minor}= 8.2 min. $[\alpha]^{26}_D$ = + 5.2 (c = 0.5 in $CHCl_3$). HRMS calculated for $[C_{24}H_{25}NO_3+Na]^+$: 398.1732; found: 398.1734.

^{1}H NMR (500 MHz, $CDCl_3$): δ 7.88 (m, 1H, Ar), 7.42 (m, 1H, Ar), 7.37 – 7.27 (m, 4H, Ar), 7.26 – 7.22 (m, 2H, Ar), 7.10 (m, 1H, Ar), 5.68 (s, 1H, OH), 3.92 (d, *J* = 8.7 Hz, 1H, H2), 3.73 (tt, *J* = 12.3, 3.8 Hz, 1H, H5), 3.17 (td, *J* = 8.4, 1.4 Hz, 1H, H3), 2.90 (dd, *J* = 14.9, 1.4 Hz, 1H, H4 α), 2.52 (ddt, *J* = 14.9, 8.1, 1.1 Hz, 1H, H4 β), 1.83 (m, 2H, Cy), 1.75 – 1.55 (m,

2H, Cy), 1.13 (m, 6H, Cy). **^{13}C NMR (125 MHz, $CDCl_3$):** δ 180.7 (C=O), 179.4 (C=O), 141.2 (Cq, Ar), 140.9 (Cq, Ar), 132.8 (Cq, Ar), 128.6 (Ar x2), 128.2 (Ar), 128.1 (Ar), 128.1 (Ar), 127.7 (Ar), 126.8 (Ar x2), 125.06 (Ar), 76.5 (Cq), 51.9 8 (CH), 47.4 (CH), 38.9 (CH), 30.3 (CH_2), 28.4 (CH_2), 28.1 (CH_2), 25.6 (CH_2), 25.6 (CH_2), 24.9 (CH_2).

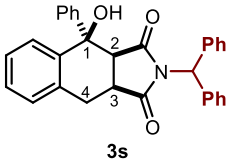

3s

(3a*S*,4*R*,9a*S*)-2-benzhydryl-4-hydroxy-4-phenyl-tetrahydro-1H-benzoisoindole-1,3-dione (3s). Compound **3s** was prepared according to the general procedure using 2-methylbenzophenone **1a** (109 μL, 0.6 mmol, 3 equiv), *N*-dibenzylmaleimide **2h** (53 mg, 0.2 mmol, 1 equiv) and catalyst **D** (18 mg, 0.04 mmol, 0.2 equiv). Temperature: -5 ºC. Time of irradiation: 24 hours. The crude mixture was purified by flash column chromatography (hexane/EtOAc, 90:10) to afford the title compound as a white solid (70 mg, 71% yield, 91% ee) and as a single diastereoisomer (dr > 20:1, as inferred by ^{1}H NMR analysis of the crude mixture). The enantiomeric excess (91% ee) was determined by HPLC analysis on a Daicel Chiralpak IC-3 column, 65:35 hexane/*i*PrOH, flow rate: 0.90 mL/min, λ= 216 nm, τ_{major}= 10.5 min, τ_{minor}= 6 min. $[\alpha]^{26}_D$ = + 24.6 (c = 0.1 in $CHCl_3$). HRMS calculated for $[C_{31}H_{25}NO_3+Na]^+$: 482.1732; found: 482.1719.

^{1}H NMR (500 MHz, $CDCl_3$): δ 7.86 (dd, *J* = 7.7, 1.3 Hz, 1H, Ar), 7.46 (m, 1H, Ar), 7.33 (m, 1H, Ar), 7.25 – 7.09 (m, 9H, Ar), 7.04 (m, 3H, Ar), 6.90 (m, 2H, Ar), 6.45 (m, 2H, Ar), 6.24 (s, 1H, H5), 5.47 (s, 1H, OH), 3.87 (d, *J* = 8.9 Hz, 1H, H2), 3.16 (td, *J* = 8.6, 1.2 Hz, 1H, H3), 2.87 (d, *J* = 15.1 Hz, 1H, H4 α), 2.47 (dd, *J* = 15.0, 8.3 Hz, 1H, H4 β). **^{13}C NMR (125 MHz,):** δ 180.1 (C=O), 178.8 (C=O), 141.2 (Cq, Ar), 141.1 (Cq, Ar), 137.0 (Cq, Ar), 136.2 (Cq, Ar), 133.1 (Cq, Ar), 128.9 (Ar x2), 128.7 (Ar x2), 128.6 (Ar), 128.5 (Ar), 128.4 (Ar x2), 128.3 (Ar x2), 128.0 (Ar), 128.0 (Ar), 127.5 (Ar x2), 127.4 (Ar), 126.8 (Ar x2), 125.48 (Ar), 76.44 (Cq), 58.5 (CH), 47.7 (CH), 39.1 (CH), 30.1 (CH_2).

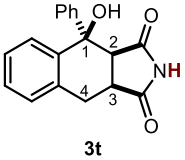

3t

(3a*S*,4*R*,9a*S*)-4-Hydroxy-4-phenyl-tetrahydrobenzoisoindole-1,3-dione (3t) . Compound **3t** was prepared according to general procedure using 2-methylbenzophenone **1a** (109 μL, 0.6 mmol, 3 equiv)**,** maleimide **2a** (19 mg, 0.2 mmol, 1 equiv) and catalyst **D** (18 mg, 0.04 mmol, 0.2 equiv). Temperature: -5 °C. Time of irradiation: 24 hours. The crude mixture was purified by flash column chromatography (hexane: EtOAc 70:30) to afford the title compound (21 mg, 72% yield, 50% ee) as a white solid and as the only detected diastereoisomer (dr > 20:1, as inferred by ^{1}H NMR analysis of the crude mixture). The enantiomeric excess was determined by HPLC analysis on a Daicel Chiralpak IC column, 70:30 hexane/*i*PrOH, flow rate: 1.00 mL/min, λ= 216 nm, τ_{major}= 35 min (50% ee), τ_{minor}= 28 min. $[\alpha]^{26}_D$ = + 6.2 (c = 0.4 in $CHCl_3$). HRMS calculated for $[C_{18}H_{15}NO_3+Na]^+$: 316.0950; found: 316.0945.

^{1}H NMR (500 MHz, $CDCl_3$): δ 8.03 (s, 1H, NH), 7.87 (dd, J = 7.6, 1.3 Hz, 1H, Ar), 7.46 – 7.42 (m, 1H, Ar), 7.37 – 7.31 (m, 4H, Ar), 7.22 (m, 2H, Ar), 7.16 (d, J = 7.4 Hz, 1H, Ar), 5.28 (s, 1H, OH), 4.05 (d, J = 9.0 Hz, 1H, H2), 3.27 (ddd, J = 8.7, 1.6 Hz, 1H, H3), 2.96 (dd, J = 15.3, 1.6 Hz, 1H, H4α), 2.58 (ddt, J = 15.2, 8.6, 1.1 Hz, 1H, H4β). **^{13}C ($CDCl_3$, 125 MHz):** δ 180.2 (C=O), 178.8 (C=O), 141.0 (Cq, Ar), 140.7 (Cq, Ar), 132.8 (Cq, Ar), 128.7 (Ar x2), 128.43 (Ar, x2), 128.39 (Ar), 128.37 (Ar), 127.9 (Ar), 126.8 (Ar), 125.3 (CH, Ar), 76.2 (Cq), 49.3 (CH), 40.3 (CH), 29.7 (CH_2).

2.7.7. Preparation of the Samples for TAS measurements

In a typical transient absorption spectroscopy experiment, independent solutions with different ratios of **1a** and catalyst **D** were prepared. Every freshly prepared solution was added to a screw-top 3.0 mL quartz cuvette and upon 355 nm laser excitation, the decay of absorption at 450 nm of the transient (*E*)-photoenol was collected.

Two stock solutions were prepared:

(i) *Stock Solution **SS1*** (0.3 M of 2-methylbenzophenone **1a**) was prepared by adding 110 µL of 2-methylbenzophenone to a total volume of 2 mL of degassed benzene

(ii) *Stock Solution **SS2*** (0.05 M of catalyst **D**) was prepared by adding 22.6 mg of catalyst **D** to a total volume of 1 mL of degassed benzene

The volumes of stock solutions employed in the preparation of the every independent sample are compiled in Table 1.13.

Table 1.13. Volumes of stock solutions **SS1** and **SS2** employed in the preparation of the samples for TAS measurements

Samples in Figure 2.28

sample	ratio **1a**/ **D**	volume of **SS1** (µL)	volume of **SS2** (µL)
1	0	50	0
2	600	50	5
3	300	50	10
4	150	50	20
5	60	50	50
6	30	50	100

Samples in Figure 2.29

sample	ratio **1a**/ **D**	volume of **SS1** (µL)	volume of **SS2** (µL)
1	0	50	0
2	15	50	20
3	1	50	300

After the addition of corresponding volume of stock solutions **SS1** and **SS2**, the volume of every independent sample was raised to 3 mL using degassed benzene. It is of note that the concentration of **1a** was kept constant for every measurement.

2.7.8. X-Ray Crystallographic Data

2.7.8.1. Single Crystal X-ray Diffraction Data for compound 3h

X-ray structure determinations: Crystals of compound **3h** were obtained by slow diffusion of hexane into a saturated dichloromethane solution. Measurements were made on a Bruker-Nonius diffractometer equipped with an APPEX 2 4K CCD area detector, a FR591 rotating anode with $Mo_{K\alpha}$ radiation, Montel mirrors and a Cryostream Plus low temperature device (T = 100K). Full-sphere data collection was used with ω and φ scans.

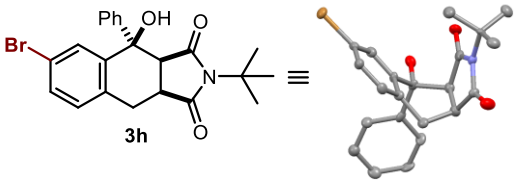

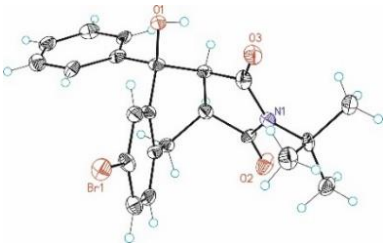

Table 1.14. Crystal data and structure refinement for **3h** at 100 K: **CCDC 1417309**

Identification code	AV-01_b-05
Empirical formula	C22 H22 Br N O3
Formula weight	428.31
Temperature	100(2) K
Wavelength	0.71073 Å
Crystal system	Monoclinic
Space group	P2(1)
Unit cell dimensions	a = 7.4637(7)Å; α= 90°. b = 7.7570(8)Å; β = 96.453(5)°. c = 16.7383(16)Å; γ = 90°.
Volume	962.94(16) $Å^3$
Z	2
Density (calculated)	1.477 Mg/m^3
Absorption coefficient	2.157 mm^{-1}
F(000)	440
Crystal size	0.10 x 0.04 x 0.01 mm^3
Theta range for data collection	8.210 to 28.774°.
Index ranges	-9<=h<=9,-10<=k<=10,-22<=l<=13
Reflections collected	3000
Independent reflections	3000[R(int) = ?]
Completeness to theta =28.774°	85.7%
Absorption correction	Multi-scan
Max. and min. transmission	0.979 and 0.753
Refinement method	Full-matrix least-squares on F^2
Data / restraints / parameters	3000/ 14/ 249

Goodness-of-fit on F^2	1.069
Final R indices [I>2sigma(I)]	R1 = 0.0717, wR2 = 0.1698
R indices (all data)	R1 = 0.0823, wR2 = 0.1830
Flack parameter	x =0.016(19)
Largest diff. peak and hole	1.593 and -1.097 e.Å^{-3}

2.7.8.2. Single Crystal X-ray Diffraction Data for compound 3l

X-ray structure determinations: Crystals of compound **3l** were obtained by slow diffusion of hexane into a saturated dichloromethane solution. Measurements were made on a Rigaku XtaLab P200 diffractometer equipped with a Pilatus 200K area detector, a Microfocus-HF007 rotating anode with $Mo_{K\alpha}$ radiation, Confocal Max Flux optic and a Cryostream Plus low temperature device (T = 100K). Full-sphere data collection was used with ω and φ scans. For the absolute configuration determination of the light-atom molecule **3l**, a methodology described in the literature has been followed.[52]

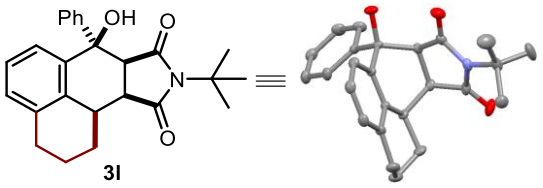

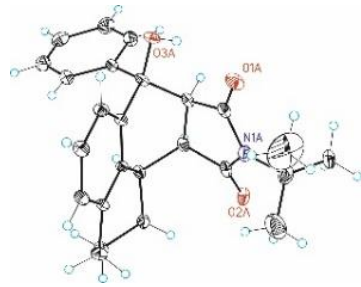

Table 1.15. Crystal data and structure refinement for **3l** at 100 K: **CCDC 1417310**

Identification code	AV_86B_c
Empirical formula	C25 H27 N O3
Formula weight	389.47
Temperature	100(2) K
Wavelength	0.71073 Å
Crystal system	Monoclinic
Space group	P2(1)
Unit cell dimensions	a = 10.7595(14)Å; α= 90°. b = 9.5651(11)Å; β = 100.741(3)°. c = 19.866(3)Å; γ = 90°.
Volume	2008.7(4) Å^3
Z	4
Density (calculated)	1.288 Mg/m^3
Absorption coefficient	0.084 mm^{-1}
F(000)	832
Crystal size	0.50 x 0.40 x 0.30 mm^3
Theta range for data collection	1.926 to 52.156°.
Index ranges	-23<=h<=23,-21<=k<=21,-43<=l<=43

[52] Escudero-Adán, E. C.; Benet-Buchholz, J.; Ballester, P. The Use of Mo Kα Radiation in the Assignment of the Absolute Configuration of Light-atom Molecules; the Importance of High-resolution Data. *Acta Cryst. B* **2014**, *70*, 660–668.

Reflections collected	131105
Independent reflections	35471[R(int) = 0.0317]
Completeness to theta =52.156°	80.7%
Absorption correction	Multi-scan
Max. and min. transmission	0.975 and 0.75
Refinement method	Full-matrix least-squares on F^2
Data / restraints / parameters	35471/ 817/ 826
Goodness-of-fit on F^2	1.067
Final R indices [I>2sigma(I)]	R1 = 0.0503, wR2 = 0.1467
R indices (all data)	R1 = 0.0568, wR2 = 0.1514
Flack parameter	x =-0.11(10)
Largest diff. peak and hole	0.658 and -0.327 e.$Å^{-3}$

Chapter III

Extending the Reactivity of Photoenols to Enantioselective Aldol-type Processes

Target

Development of an organocatalytic strategy to perform the enantioselective Aldol-type trapping of photoenols with electrophilic ketones.

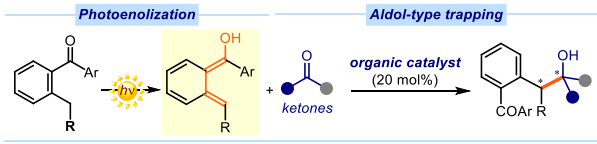

Tools

Use of a chiral hydrogen-bond donor organic catalyst that could activate ketones towards an enantioselective aldol-type addition of photoenols.[1]

3.1. Introduction

The previous Chapter has described an organocatalytic strategy to perform the classical photoenolization/Diels-Alder (PEDA) sequence in a stereoselective manner. The investigations led to the discovery of an unconventional mechanism of stereoinduction, in which a cinchona-thiourea-derived catalyst was actively involved in both the photoenolization process and the stereoselectivity-defining event.[2] Encouraged by these findings, our research group has explored other chiral organocatalytic intermediates that could stereoselectively intercept the fleeting photoenols. These studies have shown that the chemistry of these intermediates is not limited to [4+2]-cycloaddition processes. Rather, it can be expanded to develop intermolecular addition reactions that stereoselectively form one carbon-carbon bond, including Michael[3] and Mannich-type[4] reactions (Figure 3.1).

[1] The work discussed in this Chapter has been published: Cuadros, S.; Dell'Amico, L.; Melchiorre, P. Forging Fluorine-Containing Quaternary Stereocenters by a Light-Driven Organocatalytic Aldol Desymmetrization Process. *Angew. Chem. Int. Ed.* **2017**, 56, 11875–11879.

[2] Dell'Amico, L.; Vega-Peñaloza, A.; Cuadros, S.; Melchiorre, P. Enantioselective Organocatalytic Diels-Alder Trapping of Photochemically Generated Hydroxy-*o*-Quinodimethanes. *Angew. Chem. Int. Ed.* **2016**, 55, 3313 –3317.

[3] Dell'Amico, L.; Fernández-Álvarez, V. M.; Maseras, F.; Melchiorre, P. Light-Driven Enantioselective Organocatalytic β-Benzylation of Enals. *Angew. Chem. Int. Ed.* **2017**, 56, 3304–3308.

[4] Hepburn, H. B.; Magagnano, G.; Melchiorre, P. Light-Triggered Enantioselective Organocatalytic Mannich-Type Reaction. *Synthesis* **2017**, 49, 76–86.

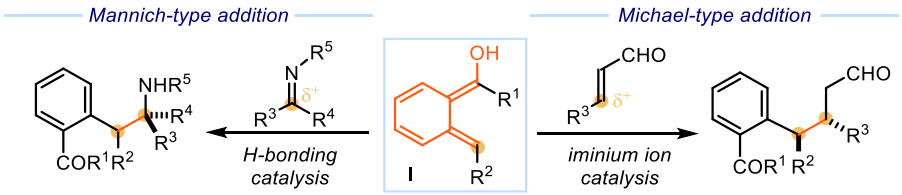

Figure 3.1. Previous studies from our research group demonstrating that the photogenerated enols **I** can participate in direct intermolecular enantioselective Michael-type and Mannich-type addition reactions catalyzed by chiral organic molecules.

Expanding upon these precedents, we aimed to extend the reactivity pathways available to **I** to include *aldol-type processes*. Our target was to develop an organocatalytic strategy to perform the aldol-type trapping of these highly reactive intermediates in a *stereocontrolled manner*. To better contextualize the background in which the enantioselective aldol-type trapping of **I** was developed, the following section will briefly discuss the previous organocatalytic strategies developed by our group that enabled the enantioselective intermolecular trapping of photoenols through an *addition pathway*.

3.2. Photoenols in Enantioselective Intermolecular Addition Processes

3.2.1. Enantioselective Michael-type Trapping of Photoenols

Iminium ion activation[5] is an established mode of organocatalytic reactivity that has found wide applications in enantioselective conjugate additions of soft nucleophiles to unsaturated carbonyl compounds. It relies on the electrophilic character of the iminium ion intermediate of type **IIa** (Figure 3.2), generated upon condensation of an α,β-unsaturated aldehyde **1** with a chiral amine catalyst.

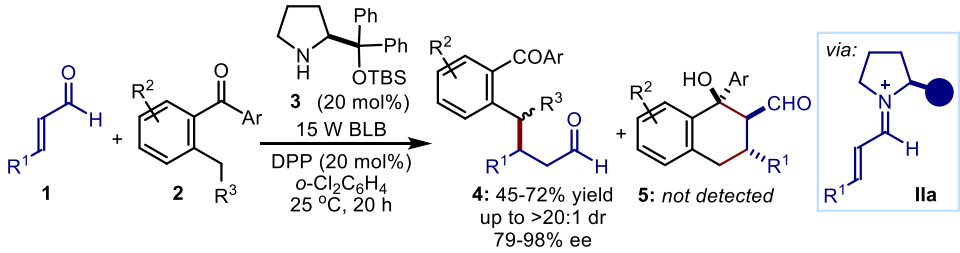

Figure 3.2. The photoenolization/β-benzylation sequence developed in our group: it follows an unconventional Michael-type addition manifold. TBS = *tert*-butyldimethylsilyl, BLB = black light bulb, DPP = diphenylphosphoric acid, *o*-$Cl_2C_6H_4$ = 1,2-dichlorobenzene. Filled blue circle in **IIa** represents the diphenylsyloxy- group of the chiral amine catalyst **3**.

---

[5] (a) Lelais, G.; MacMillan, D. W. C. Modern Strategies in Organic Catalysis: The Advent and Development of Iminum Activation. *Aldrichim. Acta* **2006**, *39*, 79–87. (b) Donslund, B. S.; Johansen, T. K.; Poulsen, P. H.; Halskov, K. S.; Jørgensen, K. A. The Diarylprolinol Silyl Ethers: Ten Years After. *Angew. Chem. Int. Ed.* **2015**, *54*, 13860–13874.

Our research group recently found that the reaction between **1** and *ortho*-methylbenzophenones **2** in the presence of 20 mol% of the diphenylprolinol trimethylsilylether **3**, and under the irradiation by a 15W black light bulb (λ= 365 nm), led to the exclusive formation of β-benzylated aldehydes **4** with good yields and high enantioselectivity.[3] No traces of the cycloaddition product **5** was observed. From a synthetic perspective, this chemistry provided a straightforward method for the direct enantioselective β-benzylation of enals **1**, a transformation for which a few effective catalytic enantioselective precedents are available.[6] This reaction was mechanistically intriguing because of the uncommon ability of the photoenol to exclusively undergo a conjugate addition manifold. The formation of **4** can be rationalized on the basis of a [4+2]-cycloaddition between **IIa** and the photoenol to afford **5**, followed by ring-opening.[7] However, no evidence for the formation of the cycloaddition intermediate **5** was found during our investigations. For example, when submitting an authentic sample of intermediate **5a**, synthesized according to a reported procedure,[8] to the optimized conditions of the enantioselective photoenolization/β-benzylation sequence, no traces of the open product **4a** could be detected (Figure 3.3). This experimental evidence excluded a possible ring-opening step as responsible for the formation of **4a**.

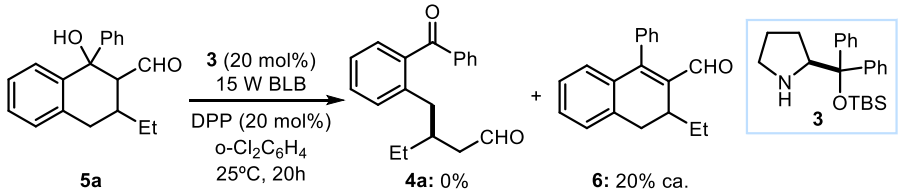

Figure 3.3. Control experiment showing the inability of the pre-formed cyclic adduct **5a** to undergo a ring-opening process under the optimized conditions of the photoenolization/β-benzylation sequence.

The mechanism was studied computationally by using density functional theory (DFT), which suggested the crucial role of water in dictating the formation of product **4** (Figure 3.4). The computational studies revealed that the intrinsic preference for the cycloaddition product was offset by a network of proton transfer mechanisms, facilitated by the presence of water.

---

[6] Silvi, M.; Verrier, C.; Rey, Y. P.; Buzzetti, L.; Melchiorre, P. Visible-Light Excitation of Iminium Ions Enables the Enantioselective β-Benzylation of Enals. *Nat. Chem.* **2017**, *9*, 868–873.

[7] (a) Masuda, Y.; Ishida, N.; Murakami, M. Light-Driven Carboxylation of *o*-Alkylphenyl Ketones with CO_2. *J. Am. Chem. Soc.* **2015**, *137*, 14063–14066. (b) Marshall Wilson, R.; Hannemann, K.; Heineman, W. R.; Kirchhoff, J. R. Laser-Jet Delayed Trapping: Electron Transfer Trapping of the Photoenol from 2-Methylbenzophenone. *J. Am. Chem. Soc.* **1987**, *109*, 4743–4745.

[8] Block, E.; Stevenson, R. The Irradiation of 2-Methylbenzophenone in the Presence of Dienophiles. *J. Chem. Soc., Perkin Trans. 1* **1973**, 308–313.

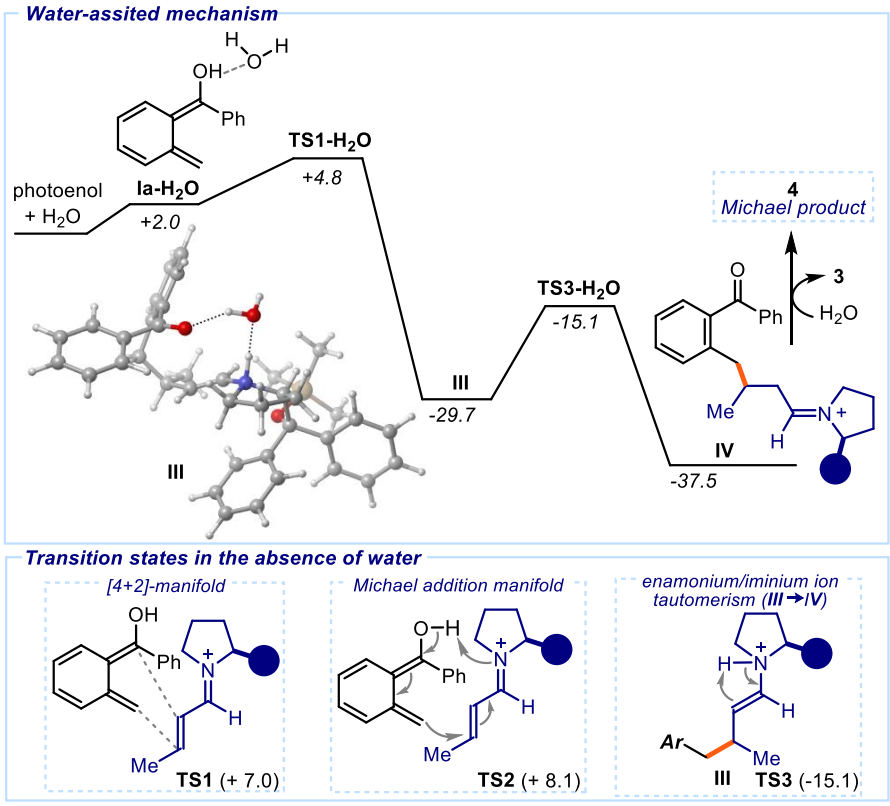

Figure 3.4. *Upper panel*: Free energy profile of the Michael-type trapping of the photoenol **Ia** with iminium ions assisted by water acting as a proton shuttle. The optimized structure **III** (at -29.7 kcal·mol^{-1}) is highlighted. *Lower panel*: Optimized transition states of different reaction manifolds, in the absence of water. Free energies indicated in kcal·mol^{-1}, and computed with the M06-2X functional and the 6-311++G(d,p) basis set, with solvent contributions added using the SMD model. Filled blue circle represents the diphenylsyloxy- group of the chiral amine catalyst **3**. *Ar*: 2-COPh(C_6H_4).

Specifically, in the computed preferred pathway for the reaction between the fleeting photoenol **Ia** and the chiral iminium ion **IIa**, a water molecule engaged in a hydrogen-bonding network with **Ia** to form adduct **Ia-H$_2$O** (Figure 3.4, upper panel).The approach of **Ia-H$_2$O** to the iminium ion **IIa** led to the transition state (**TS1-H$_2$O**), which is 2.2 kcal·mol^{-1} lower than the free energy of the Diels-Alder transition state in the absence of a proton-shuttle (see **TS1**, in Figure 3.4, lower panel), and 3.3 kcal·mol^{-1} lower than the Michael-addition transition state **TS2**. This explained why the Michael addition dominated over the classical cycloaddition mechanism. **TS1-H$_2$O** exclusively relaxed to intermediate **III**, with the proton being transferred from the photoenol to the iminium ion nitrogen atom *via* a water-assisted proton shuttle mechanism. From the enammonium ion intermediate **III**, an intramolecular proton transfer readily formed the iminium ion intermediate **IV**, which released the Michael addition product **4** and the catalyst **3** after hydrolysis.

A similar Michael addition mechanism was later reported by Ye and coworkers.[9] They described how the chiral iminium ions **IIb** (Figure 3.5), generated upon condensation of cyclic enones **7** with the chiral amino ester catalyst **8**, could stereoselectively capture the photoenols derived from *ortho*-alkylbenzophenones **2**. A variety of cyclic enones of different sizes was tolerated, giving access to the corresponding β-benzylated ketones **9** in moderate to good yields (32-72% yield), and excellent enantioselectivities (up to 99% ee).

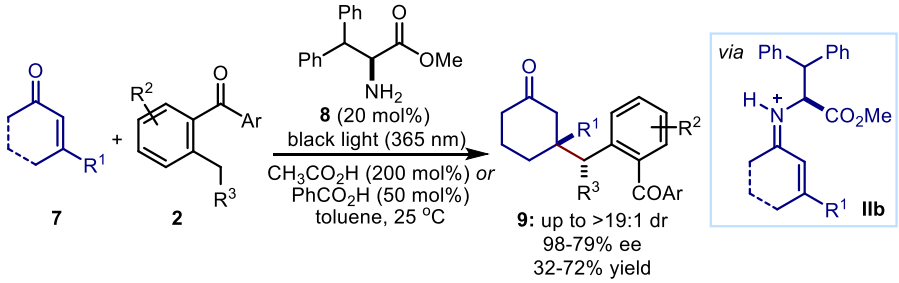

Figure 3.5. Organocatalytic enantioselective photoenolization/Michael addition sequence using cyclic α,β-unsaturated ketones (**7**) as Michael acceptors.

3.2.2. Enantioselective Mannich-type Trapping of Photoenols

After the demonstration that the photoenols can participate in enantioselective Michael addition reactions,[3] our research group explored whether these fleeting intermediates could also engage in stereoselective Mannich-type transformations. Therefore, imines were selected as the electrophilic trapping reagents. Since these substrates are primed to non-covalent mechanisms of organocatalytic activations,[10] we considered feasible the realization of an enantioselective photoenolization/Mannich addition sequence. Investigations[4] showed that the highly electrophilic cyclic benzoxathiazine-2,2-diones **10** could intercept the photoenols generated upon irradiation of **2** by a single black-light-emitting diode (black LED, λ_{max}= 365 nm), with the intermediacy of the dimeric cinchona alkaloid derivative $(DHQ)_2PHAL$ **11** (Figure 3.6). This catalyst (**11**) is commonly used as a ligand for the Sharpless asymmetric dihydroxylation.[11]

---

[9] Yuan, X.; Dong, S.; Liu, Z.; Wu, G.; Zou, C.; Ye, J. Enantioselective Michael Addition of Photogenerated *o*-Quinodimethanes to Enones Catalyzed by Chiral Amino Acid Esters. *Org. Lett.* **2017**, 19, 2322–2325.

[10] Merino, P.; Delso, I.; Tejero, T.; Roca-López, D.; Isasi, A.; Matute, R. Organocatalytic Activation of Imines and Related Compounds Through Hydrogen-Bond Activations. *Curr. Org. Chem.* **2011**, *15*, 2184–2209.

[11] Amberg, W.; Bennani, Y. L.; Chadha, R. K.; Crispino, G. A.; Davies, W. D.; Hartung, J.; Jeong, K. S.; Ogino, Y.; Shibata, T.; Sharpless, K. B. Syntheses and Crystal Structures of the Cinchona Alkaloid Derivatives Used as Ligands in the Osmium-Catalyzed Asymmetric Dihydroxylation of Olefins. *J. Org. Chem.* **1993**, *58*, 844–849.

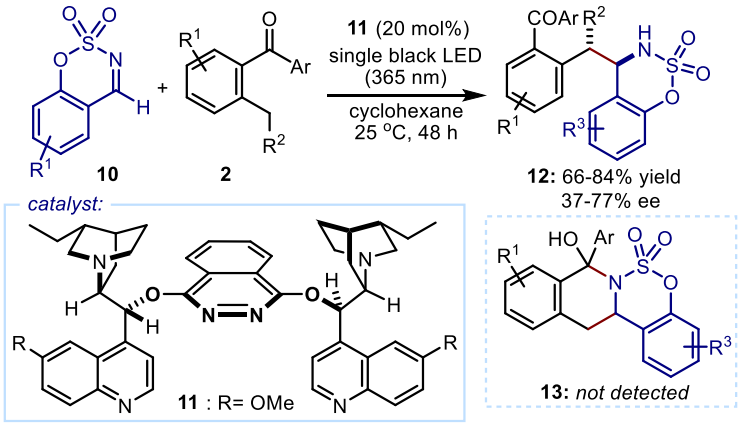

Figure 3.6. Organocatalytic enantioselective photoenolization/Mannich addition sequence using cyclic benzoxathiazine-2,2-diones **10** as electrophiles.

The reaction led to the exclusive formation of the chiral amine products **12** with moderate levels of enantioselectivity (up to 77% ee) and good yields (66-84%). Here too, no formation of the [4+2]-cycloaddition adduct **13** was detected. However, given the well-established tendency of both photogenerated hydroxy-*o*-quinodimethanes and cyclic imines of type **10**[12] to participate in hetero-Diels-Alder pathways, the possibility for a [4+2]-cycloaddition manifold, followed by the spontaneous collapse of the hemiaminal **13**, could not be discarded. Indeed, a related hetero-Diels-Alder/ring opening sequence was proposed (and supported by calculations) as the underlying mechanism of the light-driven carboxylation[7a] of ketones **2**, proceeding via the trapping of the corresponding photoenol **I** with CO_2 (example depicted in Figure 2.8 of Chapter II).

As for the mechanism of stereocontrol, flash photolysis studies revealed that the generation of the transient photoenol was not affected by the presence of catalyst **11** (contrary to what was observed in the organocatalytic enantioselective PEDA sequence described in Chapter II). This suggested that **11** controlled the stereochemical outcome of the reaction solely by interacting with the imine **10**.

3.3. Target of the Project (I)

Our research group established that the trapping of the reactive photoenols can proceed through Michael- or Mannich-type addition manifolds. Furthermore, these intermolecular addition processes can be channeled towards an enantioselective pattern by choosing adequate organocatalytic strategies. Building upon these precedents, we wondered whether the

[12] Liu, Y.; Kang, T.-R.; Liu, Q.-Z.; Chen, L.-M.; Wang, Y.-C.; Liu, J.; Xie, Y.-M.; Yang, J.-L.; He, L. Enantioselective [4+2] Cycloaddition of Cyclic *N*-Sulfimines and Acyclic Enones or Ynones: A Concise Route to Sulfamidate-Fused 2,6-Disubstiuted Piperidin-4-ones. *Org. Lett.* **2013**, *15*, 6090–6093.

reactivity framework available to the photoenols could be expanded to develop enantioselective aldol-type addition processes. Specifically, we selected symmetric 1,3-diketones of type **14** as aldol acceptors (Figure 3.7a). These symmetric ketones have a long history in asymmetric organocatalysis since they were used in the Hajos-Parrish-Eder-Sauer-Wiechert[13] reaction (Figure 3.7b), the first example of enamine-mediated proline catalysis.[14] This historical transformation proceeds through an enamine-catalyzed desymmetric aldol cyclization of **14a**, furnishing the bycyclic adduct **16** in quantitative yields and high enantioselectivities.

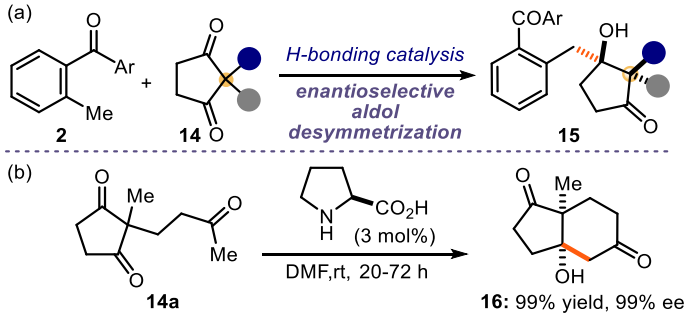

Figure 3.7. (a) Our envisioned substrate combination to develop an aldol-type trapping of photoenols. (b) The Hajos-Parrish-Eder-Sauer-Wiechert reaction is based on an enamine-catalyzed desymmetric aldol cyclization of the 1,3-diketone **14a**.

The symmetric 1,3-diketones of type **14** have been largely used in desymmetric aldol processes, but always reacted in an *intra*-molecular fashion (like in the Hajos-Parrish-Eder-Sauer-Wiechert reaction).[15] In contrast, their use in *inter*-molecular aldol pathways has never been reported. We found that such type of 1,3-diketones **14** could serve as suitable aldol acceptors for developing an enantioselective process with photoenols, based on an *inter*-molecular path.

3.3.1. Identification of the Aldol Acceptor

The idea of using 1,3-diketones **14** for developing an enantioselective aldol-type trapping of photoenols was conceived during related studies on enantioselective PEDA sequences. Specifically, after the work described in the previous Chapter II, we aimed to use symmetric

---

[13] (a) Hajos, Z. G.; Parrish, D. R. Asymmetric Synthesis of Optically Active Polycyclic Organic Compounds. German Patent, **1971**, DE 2102623. (b) Eder, U.; Sauer, G.; Wiechert, R. New Type of Asymmetric Cyclization to Optically Active Stereoid CD Partial Structures. *Angew. Chem. Int. Ed. Engl.* **1971**, *10*, 496–497. (c) Hajos, Z. G.; Parrish, D. R. Asymmetric Synthesis of Bicyclic Intermediates of Natural Product Chemistry. *J. Org. Chem.* **1974**, *39*, 1615–1621.

[14] MacMillan, D. W. C. The Advent and Development of Organocatalysis. *Nature* **2008**, *455*, 304–308.

[15] Zeng, K.-P.; Cao, Z.-Y.; Wang, Y.-H.; Zhou, F.; Zhou, J. Catalytic Enantioselective Desymmetrization Reactions to All-Carbon Quaternary Stereocenters. *Chem. Rev.* **2016**, *116*, 7330–7396.

dienophiles of type **17** (see Figure 3.8) in [4+2]-cycloadditions with photoenols. The use of these substrates (**17**) in a stereoselective PEDA sequence would furnish carbocyclic products **18** with up to five stereogenic centers. If two different alkyl groups were placed in the prochiral carbon of **17**, a carbon quaternary center could be stereoselectively forged within the cyclic adduct **18** upon desymmetrization.

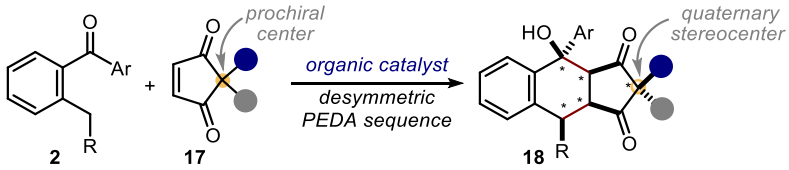

Figure 3.8. Our envisioned strategy to perform a catalytic enantioselective PEDA sequence using 2,2-disubstituted cyclopentene,1-3-diones **17**.

Dienophiles **17** have been exploited in other enantioselective desymmetric C-C bond forming processes, including 1,3-dipolar cycloadditions,[16] transition metal-catalyzed alkylation[17] and arylation[18] reactions, and organocatalytic nucleophilic additions.[19] During these studies,[20] we found that the reaction between 2-methylbenzphenone **2a** and the 2,2-disubstiuted cyclopentene-1,3-dione **17a**, in the presence of 20 mol% of catalyst **A**, furnished the adduct **18a** in 20% yield, 91% ee, and complete diastereoselectivity (dr > 20:1, Figure 3.9).

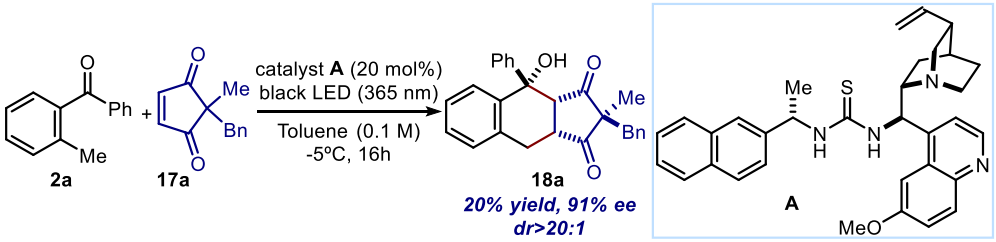

Figure 3.9. Stereoselective PEDA sequence using 2-benzyl-2-methyl cyclopentene-1,3-dione **17a** as dienophile. Bn: benzyl.

---

[16] Liu, H.-C.; Liu, K.; Xue, Z.-Y.; He, Z.-L.; Wang, C.-J. Silver (I)-Catalyzed Enantioselective Desymmetrization of Cyclopentenediones: Access to Highly Functionalized Bicyclic Pyrrolidines. *Org. Lett.* **2015**, *17*, 5440–5443.

[17] Aikawa, K.; Okamoto, T.; Mikami, K. Copper(I)-Catalyzed Asymmetric Desymmetrization: Synthesis of Five-Membered-Ring Compounds Containing All-Carbon Quaternary Stereocenters. *J. Am. Chem. Soc.* **2012**, *134*, 10329–10332.

[18] Walker, S. E.; Lamb, C. J. C.; Beattie, N. A.; Nikodemiak, P.; Lee, A.-L. Oxidative Heck Desymmetrization of 2,2-Disubstituted Cyclopentene-1,3-diones. *Chem. Commun.* **2015**, *51*, 4089–4092.

[19] (a) Manna, M. S.; Mukherjee, S. Remarkable Influence of Secondary Catalyst Site on Enantioselective Desymmetrization of Cyclopentenedione. *Chem. Sci.* **2014**, *5*, 1627–1633. (b) Manna, M. S.; Mukherjee, S. Organocatalytic Enantioselective Formal C(sp^2)-H Alkylation. *J. Am. Chem. Soc.* **2015**, *137*, 130–133.

[20] Unpublished results.

The excellent stereoselective outcome of this transformation demonstrated that cyclopentene-1,3-diones of type **17a** can be efficiently activated through non-covalent interactions with the cinchona-thiourea catalyst **A**, and that a desymmetrization process was possible. After screening several conditions, we could not improve the yield of the cycloaddition reaction. We therefore modified the dienophile scaffold in order to increase its reactivity. The judicious introduction of fluorine atoms in organic molecules is a powerful strategy to tune the reactivity of the substrates.[21] We accordingly planned the synthesis of the fluorinated cyclopentene-1,3-dione **17b** through the procedure depicted in Figure 3.10. Fluorination with Selectfluor of the commercially available diketone **19** gave **14b** in 85% yield. We next tried to perform the oxidation of **14b** to the alkene derivative **17b**, following a procedure reported for non-fluorinated cyclopenta-1,3-dione analogues.[17] The desired alkene **17b** was formed in low yields (15% yield *ca.*) and its purification resulted extremely difficult. In contrast, we could easily isolate the fluorinated cyclopenta-1,3-dione **14b**. We become curious of the possibility to intercept the nucleophilic photoenol with the supposedly highly electrophilic carbonyl **14b**.

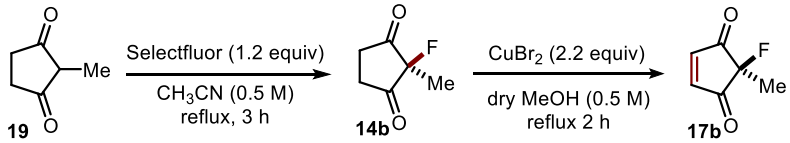

Figure 3.10. Proposed synthetic route to access 2-fluoro-2-methylcyclopentene-1,3-dione **17b**.

To our delight, when 2-methylbenzophenone **2a** and the diketone **14b** were mixed in toluene at -5 ºC under irradiation of a 365 nm LED and in the presence of catalyst **A**, we observed the exclusive formation of the corresponding aldol-type product **15a** in 86% yield, although with poor levels of stereoselectivity (dr = 2:1, 8% ee_{major}, 5% ee_{minor}; Figure 3.11). No traces of the hetero-Diels product **20** were observed.

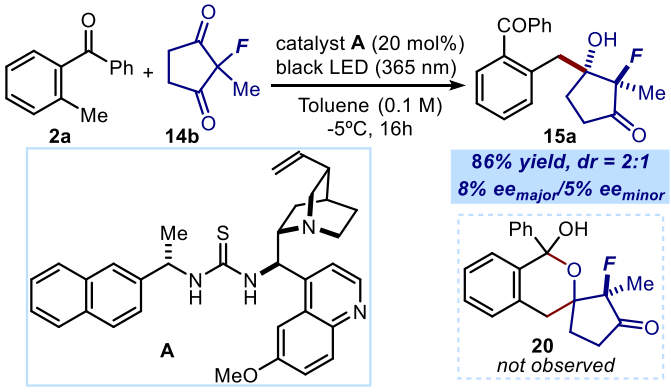

Figure 3.11. Initial hit for the development of an enantioselective aldol-type trapping of photoenols.

[21] Cahard, D.; Bizet, V. The Influence of Fluorine in Asymmetric Catalysis. *Chem. Soc. Rev.* **2014**, *43*, 135–147

This experiment proved that the reactivity of photoenols can be extended to include aldol-type processes. It also indicated that an *inter*-molecular aldol desymmetrization of 1,3-diketones **14** was feasible. Our interest in this process was increased by the possibility to forge a fluorine-containing quaternary stereocenter within the aldol-product **15a**. This is an interesting feature of the overall process, since the stereoselective construction of such chiral centers is synthetically difficult.[22] The next section will provide a brief overview of the methods available to stereoselectively form F-containing quaternary carbon centers.

3.4. Catalytic Stereoselective Construction of Fluorine-Containing Quaternary Stereocenters

Organofluorine compounds have a distinguished role in medicinal chemistry, agrochemistry, and material science.[23] Given the importance of these substrates in different areas of chemistry, synthetic strategies to build new chiral fluorinated molecules are of high interest. Significant improvements have been made in the asymmetric incorporation of fluorine to form F-containing tertiary carbons.[24] However, the stereoselective construction of F-containing quaternary carbons is still synthetically difficult, especially employing catalytic methods.[22] Successful catalytic enantioselective strategies can be classified in two main groups: (*i*) methods based on the direct enantioselective introduction of F atoms (examples in Section 3.4.1); and (*ii*) methods based on enantioselective C-C bond forming processes using racemic molecules with pre-installed C-F units (discussed in Section 3.4.2).

3.4.1. Direct Enantioselective Introduction of Fluorine Atoms

The majority of the catalytic procedures reported to date for the formation of C-F quaternary stereocenters are based on stereoselective C-F bond forming processes employing electrophilic sources of fluorine.[25] The development of bench-stable and easy-to-handle

---

[22] Zhu, Y.; Han, J.; Wang, J.; Shibata, N.; Sodeoka, M.; Soloshonok, V. A.; Coelho, J. A. S.; Toste, F. D. Modern Approaches for Asymmetric Construction of Carbon-Fluorine Quaternary Stereogenic Centers: Synthetic Challenges and Pharmaceutical Needs. *Chem. Rev*. **2018**, *118*, 388–73964.

[23] (a) Kirsch, P. *Modern Fluororganic Chemistry*; Wiley-VCH: Weinheim, **2013**. (b) Müller, K.; Faeh, C.; Diederich, F. Fluorine in Pharmaceuticals: Looking Beyond Intuition. *Science* **2007**, *317*, 1881–1886. (c) Wang, J.; Sánchez-Roselló, M.; Aceña, J. L.; del Pozo, C.; Sorochinky, A. E.; Fustero, S.; Soloshonok, V. A.; Liu, H. Fluorine in Pharmaceutical Industry: Fluorine-containing Drugs Introduced to the Market in the Last Decade (2001–2011). *Chem. Rev.* **2014**, *114*, 2432–2506.

[24] (a) Yang, X.; Wu, T.; Phipps, R. J.; Toste, F. D. Advances in Catalytic Enantioselective Fluorination, Mono-, Di-, and Trifluoromethylation, and Trifluoromethylthiolation Reactions. *Chem. Rev*. **2015**, *115*, 826–870. (b) Ma, J.-A.; Cahard, D. Asymmetric Fluorination, Trifluoromethylation, and Perfluoroalkylation Reactions. *Chem. Rev.* **2004**, *104*, 6119–6146.

[25] (a) Lin, J.-H.; Xiao, J.-C. Recent Advances in Asymmetric Fluorination and Fluoroalkylation Reactions via Organocatalysis. *Tetrahedron Lett.* **2014**, *55*, 6147–6155. (b) Lectard, S.; Hamashima, Y.; Sodeoka, M. Recent Advances in Catalytic Enantioselective Fluorination Reactions. *Adv. Synth. Catal.* **2010**, *352*, 2708–2732.

reagents, such as Selectfluor, *N*-fluorobenzenesulfonimide (NFSI), or *N*-fluoropyridinium salts (in Figure 3.12), have triggered considerable progress in the area of enantioselective fluorination.

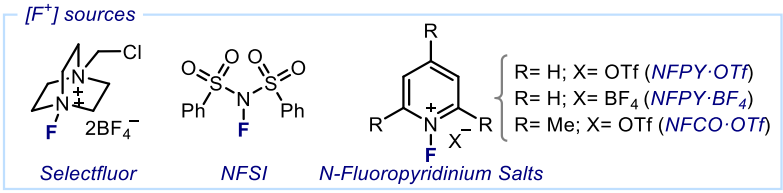

Figure 3.12. Commercially available electrophilic fluorinating reagents

Togni and Hintermann[26] reported the first example of a catalytic enantioselective fluorination strategy leading to the formation of a F-containing quaternary stereocenter (Figure 3.13). They used a catalytic amount of the Ti-TADDOL complex **24** to activate β-ketoesters **21** through the formation of a chiral enolate intermediate.

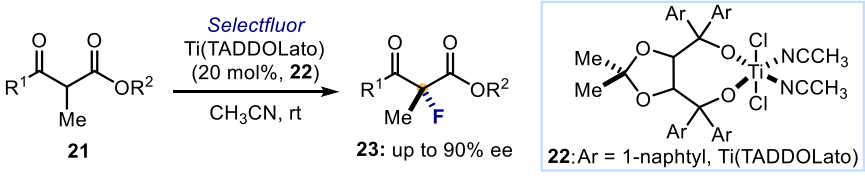

Figure 3.13. First example of a catalytic enantioselective fluorination reaction leading to the formation of C-F quaternary stereocenters.

Selectfluor was employed as the electrophilic fluorine source. This combination of reagents resulted in the formation of the chiral fluorinated products **23** in quantitative yields and up to 90% ee. Besides representing a milestone for asymmetric fluorination, this study provided an early example of catalytic asymmetric soft enolization strategy. This breakthrough in enantioselective catalytic fluorination has inspired the design of other catalytic systems that have employed a transition metal catalyst or organocatalyst in combination with an enolizable carbonyl compound.[22,24]

The enantioselective fluoro-functionalization of olefins by electrophilic fluorinating reagents[27] has also offered an alternative path for the construction of C-F quaternary stereocenters. Here, mainly cyclic alkenes have been used as substrates. For example, Shiro

---

[26] Hintermann, L.; Togni, A. Catalytic Enantioselective Fluorination of β-Ketoesters. *Angew. Chem. Int. Ed.* **2000**, *39*, 4359–4362.

[27] Wu, J.; Wang, Y.-M.; Drljevic, A.; Rauniyar, V.; Phipps, R. J.; Toste, F. D. A Combination of Directing Groups and Chiral Anion Phase-Transfer Catalysis for Enantioselective Fluorination of Alkenes. *Proc. Natl. Acad. Sci. U. S. A.* **2013**, *110*, 13729–13733.

and coworkers[28] reported the catalytic enantioselective fluorination of allyl silanes **24** and silyl enol ethers **25** (Figure 3.14), mediated by cinchona alkaloid catalysts. The overall process implied the fluorodesilylation of the electron-rich alkenes **24** or **25**, furnishing the chiral fluorinated indane derivative **27** with up to 95% ee.

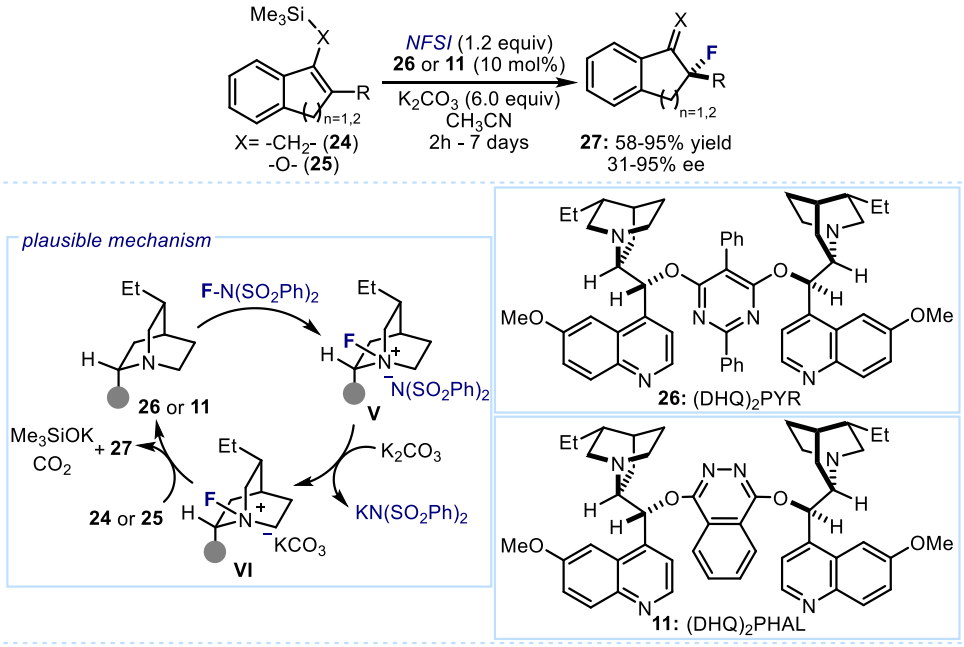

Figure 3.14. Example of catalytic enantioselective fluorination of activated cyclic alkenes, mediated by cinchona alkaloids.

In the proposed catalytic cycle, a stable *N*-fluoroammonium salt **V**,[29] derived from the combination of NFSI and bis-cinchona alkaloids (**26** or **11**), undergoes anion exchange with K_2CO_3 leading to the formation of the corresponding *N*-fluoroammonium KCO_3^- salt **VI**. The fluorodesilylation of substrates **24** or **25** is then triggered by KCO_3^-, followed by the enantioselective transfer fluorination from the *N*-fluoroammonium ion **VI** to the substrates **24** or **25**. In the absence of K_2CO_3, the reactivity of the *N*-fluoroammonium salt **V** with the substrates **24** or **25** was very low, thereby confirming that the formation of intermediate **VI** was crucial. A related approach uses cyclic alkenes bearing tethered nucleophilic

[28] Ishimaru, T.; Shibata, N.; Horikawa, T.; Yasuda, N.; Nakamura, S.; Toru, T.; Shiro, M. Cinchona Alkaloid Catalyzed Enantioselective Fluorination of Allyl Silanes, Silyl Enol Ethers, and Oxindoles. *Angew. Chem. Int. Ed.* **2008**, *47*, 4157–4161.

[29] Baudequin, C.; Loubassou, J.-F.; Plaquevent, J.-C.; Cahard, D. Enantioselective Electrophilic Fluorination: A Study of the Fluorine-Transfer from Achiral N-F reagents to Cinchona Alkaloids. *J. Fluorine Chem.* **2003**, *122*, 189–193.

functionalities, which can participate in a cyclization event.[30] The first successful catalytic process of this type was reported by the group of Gouverneur (Figure 3.15).[31] They used the indole **28** with a pendant hetero-nucleophile tethered at the C3 position as the model substrate, and NFSI as the "F^+" source. After a screening of chiral organocatalysts, they identified $(DHQ)_2PHAL$ **11** as the best structure to perform the enantioselective fluorocyclization of **28**.

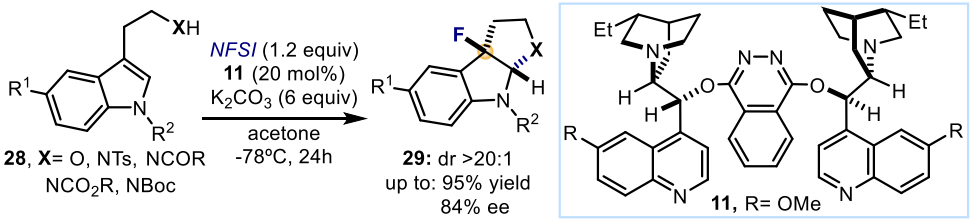

Figure 3.15. Example of enantioselective fluoro-cyclization of alkenes leading to the construction of a fluorine-containing quaternary stereocenter.

Although better results in terms of enantioselectivity were obtained using stoichiometric amounts of **11** (72-90% ee), only a slight decrease of ee was observed under catalytic conditions (20 mol%), without compromising the yields of the tetrahydrofuroindole derivatives **29** (up to 95% yield).

3.4.2. Enantioselective C-C Bond Forming Processes

A second effective strategy to forge F-containing quaternary stereocenters is based on stereoselective C-C bond forming processes using substrates bearing a pre-installed C-F stereogenic unit. The majority of strategies uses enolizable α-fluoro carbonyl compounds of type **30** (Figure 3.16).[22]

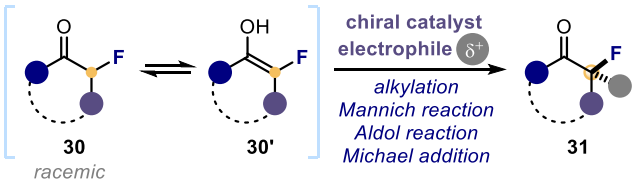

Figure 3.16. An alternative approach for the construction of C-F quaternary stereocenters involves the use of racemic α-fluorocarbonyl compounds **30**, which can participate in enantioselective alkylation-, Mannich-, aldol- or Michael addition processes with the intermediacy of a suitable chiral catalyst.

---

[30] Wolstenhulme, J. R.; Gouverneur, V. Asymmetric Fluorocyclizations of Alkenes. *Acc. Chem. Res.* **2014**, *47*, 3560–3570. (b) Egami, H.; Niwa, T.; Sato, H.; Hotta, R.; Rouno, D.; Kawato, Y.; Hamashima, Y. *J. Am. Chem. Soc.* **2018**, *140*, 2785–2788.

[31] Lozano, O.; Blessley, G.; Martinez del Campo, T.; Thompson, A. L.; Giuffredi, G. T.; Bettati, M.; Walker, M.; Borman, R.; Gouverneur, V. Organocatalyzed Enantioselective Fluorocyclizations. *Angew. Chem. Int. Ed.* **2011**, *50*, 8105–8109.

These substrates (**30**) can undergo different enantioselective processes in the presence of a suitable chiral catalyst, including alkylation reactions,[32] Mannich-,[33] aldol-,[34] or Michael-type additions.[35] Recent investigations have exploited other type of prochiral fluorinated substrates. In 2018, Butcher and Hartwig[36] reported the first enantioselective allylic substitution of the fluorinated electrophilic substrates **33** (Figure 3.17). An iridium catalyst **34** was suited for this transformation because it favored the nucleophilic attack of soft carbon nucleophiles (**32**) at the more substituted end of the π-allyl intermediates **VII**. The corresponding tertiary allylic fluorides **35** were obtained with high regioselectivity and enantioselectivity (branched:linear >50:1; ee up to 96% ee).

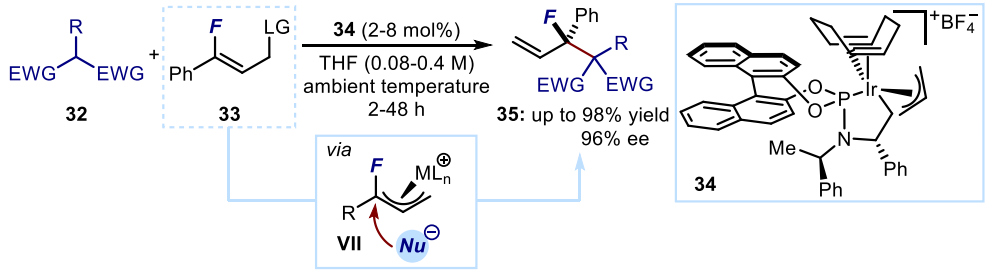

Figure 3.17. First enantioselective allylic substitution reaction using fluorinated electrophiles **33**.

In 2019, Toste and Sigman[37] used alkenyl fluorides **36** in Heck-type reactions with aryl boronic esters **37** (Figure 3.18), leading to the formation of tertiary carbon-fluoride bonds within **38** with high levels of enantioselectivity. This transformation proceeds through a site-selective[38] migratory insertion of the alkene **36** into the organometallic complex **VIII**, giving access to the Pd-intermediate **IX**. Then, a sequential β-hydride elimination/migratory-insertion process enables the migration of Pd towards the terminal alcohol group (*i.e.* from **IX** to **XII**), which ultimately releases the carbonyl compound **XIV**.

---

[32] Jiao, Z.; Beiger, J. J.; Jin, Y.; Ge, S.; Zhou, J. S.; Hartwig, J. F. Palladium-Catalyzed Enantioselective α-Arylation of α-Fluoroketones. *J. Am. Chem. Soc.* **2016**, *138*, 15980–15986.

[33] Cosimi, E.; Engl, O. D.; Saadi, J.; Ebert, M. O.; Wennemers, H. Stereoselective Organocatalyzed Synthesis of α-Fluorinated β-Amino Thioesters and Their Application in Peptide Synthesis. *Angew. Chem. Int. Ed.* **2016**, 55, 13127–13131.

[34] Xie, C.; Wu, L.; Han, J.; Soloshonok, V. A.; Pan, Y. Assembly of Fluorinated Quaternary Stereogenic Centers through Catalytic Enantioselective Detrifluoroacetylative Aldol Reactions. *Angew. Chem. Int. Ed.* **2015**, 54, 6019–6023.

[35] Cosimi, E.; Saadi, J.; Wennemers, H. Stereoselective Synthesis of α-Fluoro-γ-nitro Thioesters under Organocatalytic Conditions. *Org. Lett.* **2016**, *18*, 6014–6017.

[36] Butcher, T. W.; Hartwig, J. Enantioselective Synthesis of Tertiary Allylic Fluorides by Iridium-Catalyzed Allylic Fluoroalkylation. *Angew. Chem. Int. Ed.* **2018**, 57, 13125–13129.

[37] Liu, J.; Yuan, Q.; Toste, F. D.; Sigman, M. S. Enantioselective Construction of Remote Tertiary Carbon-Fluorine Bonds. *Nat. Chem.* **2019**, 11, 710–715.

[38] Mei, T.-S.; Patel, H. H.; Sigman, M. S. Enantioselective Construction of Remote Quaternary Stereocenters. *Nature* **2014**, *508*, 340–344.

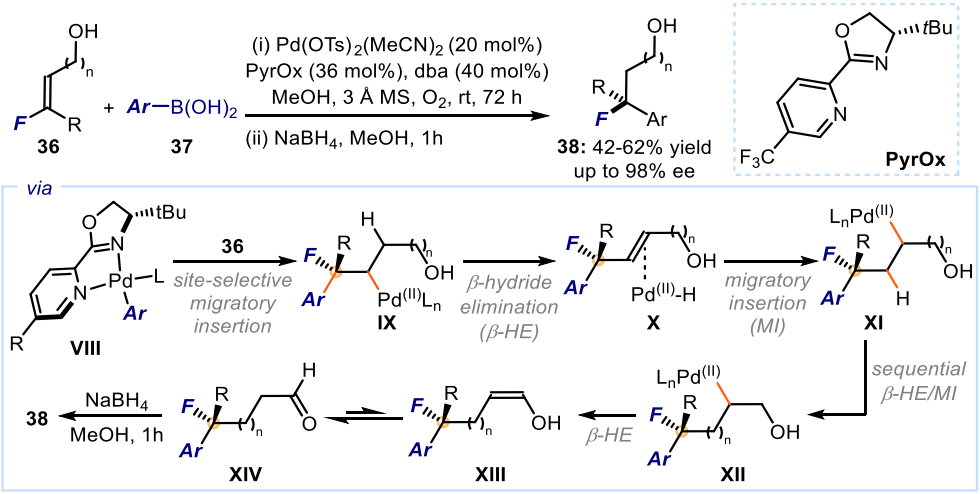

Figure 3.18. Enantioselective construction of remote fluorine-containing quaternary stereocenters. dba: dibenzylideneacetone.

To avoid issues of decomposition associated with the isolation of the fluorinated aldehyde products, **XIV** was reduced in situ with $NaBH_4$ to form the corresponding alcohol product **38**. Overall, this strategy allows to set fluorine-containing quaternary stereocenters in a remote position from a pre-existing functional group.

The enantioselective desymmetrization of symmetric compounds bearing a pre-installed quaternary C-F prochiral carbon has been rarely exploited. One effective method was developed by the research group of Gaunt (Figure 3.19).[39]

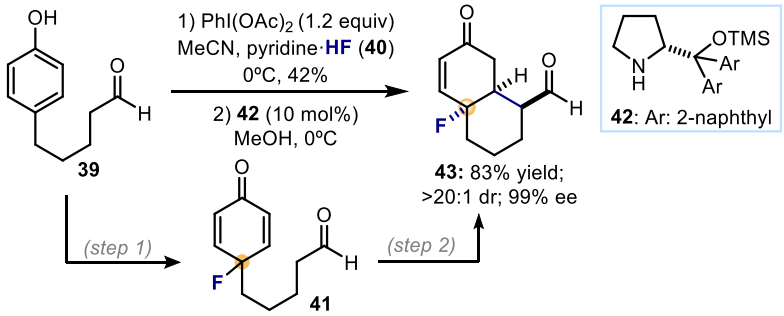

Figure 3.19. Catalytic construction of fluorine-containing quaternary stereocenters through a desymmetrization strategy. This sequence involves the nucleophilic fluorination of phenol **39** to generate the cyclohexadiene **41,** followed by an intramolecular enamine catalyzed desymmetrizing Michael reaction.

[39] Vo, N. T.; Pace, R. D. M.; O'Har, F.; Gaunt, M. J. An Enantioselective Organocatalytic Oxidative Dearomatization Strategy. *J. Am. Chem. Soc.* **2008,** *130*, 404–405.

The strategy was based on a two-step sequence. The first step involved the oxidation of phenol **39** in the presence of the nucleophilic HF-pyridine complex **40**, leading to the fluorinated cyclohexadiene **41**. Afterwards, the prochiral substrate **41** was engaged in a desymmetric enantioselective Michael addition reaction catalyzed by the chiral diarylprolinol catalyst **42**. The following process yielded the chiral fluorinated product **43** in good yield (83% yield) and excellent diastereo- and enantioselectivity (>20:1 dr, 99% ee). This desymmetric strategy to forge a F-containing quaternary center was reported only for the substrate **39**.

Enzymes have been also applied in desymmetrization processes or in kinetic resolutions with racemic substrates containing a quaternary C-F prochiral carbon. However, few examples have been reported so far.[22] Takeuchi and co-workers described an enantioselective desmmetric hydrolysis of 2-fluorinated diacetates **44** catalyzed by the lipase from porcine pancreas (PPL, **45**), which afforded the corresponding chiral alcohol **46** in up to 96% ee and 65% yield (Figure 3.20, a).[40]

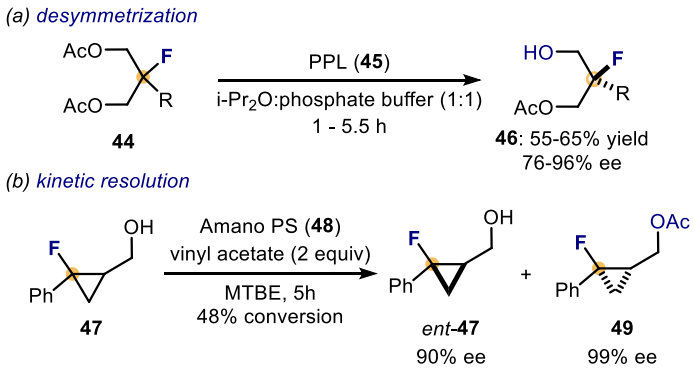

Figure 3.20. Examples of enzyme-catalyzed reactions that use racemic substrates bearing a quaternary C-F prochiral unit. PPL: porcine pancreas lipase; Amano PS: *Pseudomonas cepacia* lipase.

The Haufe group documented the enzymatic kinetic resolution of racemic 2-fluoro-2-phenylcyclopropyl derivatives **47** (Figure 3.20, b). The lipase *Pseudomonas cepacia* (Amano PS, **48**) provided the best results for accessing the chiral acylated cyclopropane **49** in nearly enantiopure form.[41]

3.5. Target of the Project (II)

The desymmetrization of symmetric compounds bearing a pre-installed C-F unit has been rarely exploited for the stereoselective formation of F-containing quaternary stereocenters.

---

[40] Yokoyama, H.; Hyodo, R.; Nakada, A.; Yamaguchi, S.; Hirai, Y.; Kometani, T.; Goto, M.; Shibata, N.; Takeuchi, Y. Asymmetric Synthesis of Chiral 2-Fluorinated 1,3-Propanediols and Its Application to the Preparation of Monofluorinated Chiral Synthon. *Tetrahedron Lett.* **1998**, *39*, 7741–7744.

[41] Rosen, T. C.; Haufe, G. Synthesis of Enantiopure Mono-Fluorinated Phenylcyclopropanes by Lipase-Catalyzed Kinetic Resolution. *Tetrahedron Asymmetr.* **2002**, *13*, 1397–1405.

Only few examples have been reported so far, mainly using enzymes as catalysts. Another example based on an *intra*-molecular enamine catalyzed desymmetrizing Michael reaction has been reported by the Gaunt group (Section 3.4.2, Figure 3.19). Within this context, we wondered whether *H-bonding catalysis* could be successfully used to selectively activate one of the two enantiotopic groups within the fluorinated 1,3-diketone **14**, thereby facilitating an enantioselective *inter*-molecular aldol process with the photoenols (Figure 3.21).

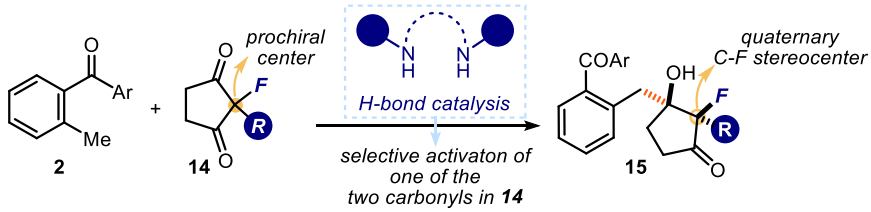

Figure 3.21. The proposed strategy for forging fluorine-containing quaternary stereocenters by a desymmetrizing aldol reaction of photoenols generated from 2-alkylbenzophenones **2** and achiral 2-fluoro-substituted cyclopentane-1,3-diketones **14**. Blue dots represent fragments on the chiral scaffold of the organic catalyst.

The next section will detail our efforts to identify a suitable chiral H-bond donor catalyst that could channel this light-driven aldol-desymmetrization process through a stereoselective pattern.

3.6. Results and Discussions

3.6.1. Optimization Studies

As discussed in Section 3.3.1, we initially found that the 1,3 diketone **14b** furnished the corresponding aldol product **15a** in 86% yield, 2:1 dr, and in nearly racemic form (Table 1, entry 1). This initial experiment was conducted in the presence of 20 mol% of the chiral organic catalyst **A**, in toluene at -5 ºC, and under the irradiation by a single black LED (λ_{max} = 365 nm). A similar catalyst could induce good levels of enantioselectivity in the stereoselective PEDA sequence described in the previous Chapter II.

We initially tested the performance of other photoenolizable substrates **2** in the aldol-desymmetrization process of 1,3-diketones **14** (Table 3.1).

Table 3.1. Evaluation of other 1,3-diketones **14** and photoenolizable compounds **2**.

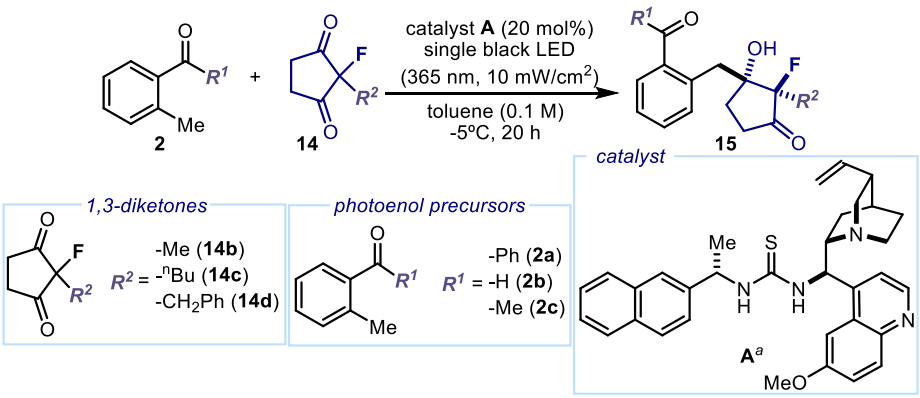

entry	1,3-diketone (14)	photoenol precursor (2)	product (15)	yield (%)[b]	dr[c]	ee$_{major}$ / ee$_{minor}$(%)[d]
1	**14b**	**2a**	**15a**	86	2:1	8 / 5
2	**14c**	**2a**	**15b**	52	3:1	5 / 4
3	**14d**	**2a**	**15c**	53	>20:1	14 / -
4	**14d**	**2b**	**15d**	0	-	-
5	**14d**	**2c**	**15e**	0	-	-
6[e]	**14d**	**2a**	**15c**	0	-	-
7[f]	**14d**	**2a**	**15c**	20	>20:1	0 / 0

Reactions performed on a 0.1 mmol scale using 3 equiv. of the photoenol precursor **2**. [a]Catalyst derived from 9-amino(9-deoxy) *epi*-quinidine. [b]Yields of the isolated products after flash chromatography on silica gel. [c]Diastereomeric ratio determined by ^{1}H NMR analysis of the crude reaction mixture. [d]Enantiomeric excess determined by UltraPerformance Convergence Chromatography (UPC^2) analysis on a chiral stationary phase. [e]Reaction performed in the dark. [f]Reaction performed in the absence of catalyst **A** (background reaction).

The use of 2-butyl-2-fluorocyclopentane-1,3-dione **14c** in the aldol reaction with 2-alkylbenzophenone **2a** afforded the corresponding product **15b** in lower yields (52% yield, entry 2), although with a slightly enhanced diastereoselective outcome (dr = 3:1). Pleasingly, the aldol product **15** was obtained with complete diastereoselectivity when substrate **14d** was used as the aldol-type acceptor. In this case, the corresponding product **15c** was obtained in 53% yield and 14% ee (entry 3). Other photoenol precursors (**2b**-**2c**) did not provide the desired aldol products (entries 4-5). We then performed control experiments using 2-methylbenzophenone **2a** and the 1,3-diketone **14d** as the model substrates. As expected, the reaction did not proceed in the dark, thus confirming the photochemical nature of the process (entry 6). We also evaluated the rate of the background process. In the absence of catalyst **A**, the corresponding aldol product **15c** was obtained in 20% yield, indicating that the

background reaction is slower than the catalyzed regime. This result indicated the feasibility to develop a catalytic enantioselective variant. Overall, these preliminary studies established the diketone **14d** and the benzophenone derivative **2a** as suitable candidates for further optimization studies.

We next performed an extensive screening of different type of H-bond donor organocatalysts. Specifically, we used the CELLEX-High Throughput Experimentation (HTE) laboratory of ICIQ to determine the efficiency of a library of 49 novel and known organocatalysts in this desymmetric aldol process. The results for some selected organic catalysts are presented in Table 3.2, while a complete list of results is provided in the Experimental Section of this Chapter.

Table 3.2. Initial high-throughput screening of organic catalysts. Selected results.

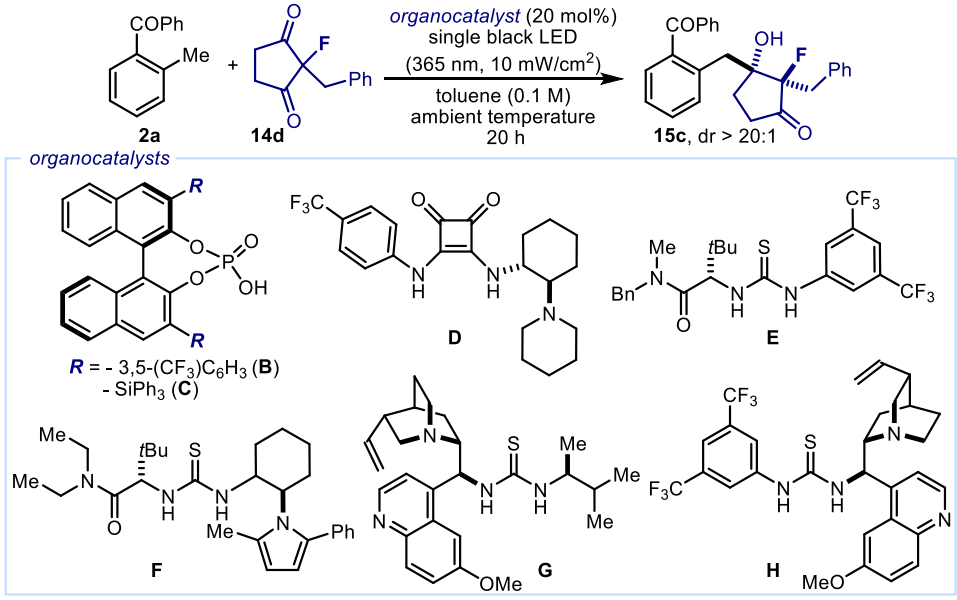

entry	catalyst	yield (%)[a]	ee (%)[b]
1	**B**	11	29
2	**C**	10	19
3	**D**	13	68
4	**E**	50	76
5	**F**	27	38
6	**G**	17	41
7	**H**	10	27

Reactions performed on a 0.1 mmol scale using 3 equiv. of 2-methylbenzophenone **2a**. [a]Yields determined by UPLC analysis using biphenyl as the internal standard. [b]Enantiomeric excess determined by UPC² analysis on a chiral stationary phase.

The use of phosphoric acids (catalysts **B-C**, entries 1-2) resulted in the formation of product **15c** with low yield and enantioselectivity. The squaramide-based catalyst **D** offered encouraging levels of enantioselectivity (68% ee), albeit at the expense of reactivity (10% yield, entry 3). The amido-thiourea catalyst **E** afforded the product **15c** with promising yield (50% yield) and enantioselectivity (76% ee, entry 4). Catalysts of type **E** have been successfully used in asymmetric Strecker reactions.[42] Other catalyst structures based on the cinchona-thiourea scaffold (catalysts **G-H**, entries 6-7) afforded product **15c** with worse results (10-17% yield, 27-41% ee). This screening study established catalyst **E** as the benchmark catalyst structure for next studies.

We next investigated the effect of the temperature in the model reaction. A clear trend was observed when lowering the temperature of the aldol process (Table 3.3): the enantioselective outcome of the process was gradually enhanced, while the reactivity was negatively affected.

Table 3.3. Temperature effect

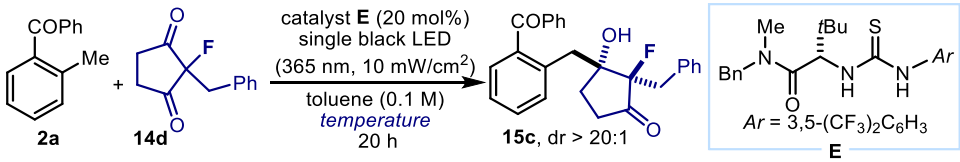

entry	Temperature (°C)	yield (%)[a]	ee (%)[b]
1	25	50	76
2	15	46	80
3	5	39	87
4	-5	27	90
5	-10	20	92

Reactions performed on a 0.1 mmol scale using 3 equiv. of 2-methylbenzophenone **2a**. [a]Yields of the isolated products after flash chromatography on silica gel. [b]Enantiomeric excess determined by UPC² analysis on a chiral stationary phase.

We then analyzed the effect of structural modifications within the amido-thiourea catalyst **E** (in Figure 3.22). We synthesized other catalysts bearing different benzyl amide-moieties (catalysts **I-L**), and we evaluated their performance in the model reaction at room temperature. An additional stereogenic center imparted a slightly higher stereoinduction, but with a minimal matched/mismatched effect (catalysts **I** and **J**, 83% and 87% ee, respectively). These results suggested that the steric profile of the tertiary benzyl amide component could play a more prominent role than the presence of a second stereocontrol element in dictating the

[42] Zuend, S. J.; Coughlin, M. P.; Lalonde, M. P.; Jacobsen, E. N. Scaleable Catalytic Asymmetric Strecker Syntheses of Unnatural α-Amino Acids. *Nature* **2009**, *461*, 968–970.

reaction's stereoselectivity. In consonance with this reasoning, the best results were obtained with catalysts **K** and **L**, both containing a more encumbered amide moiety but a single stereogenic center. Specifically, the *N*-benzhydryl substituted amido-thiourea catalyst **K** enabled the formation of product **15c** in 45% yield and 89% ee. Because of the good balance between reactivity and enantioselectivity, catalyst **K** was selected for final optimization studies.

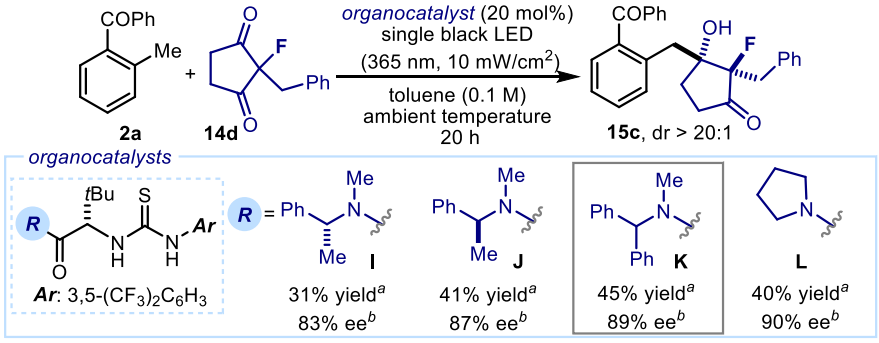

Figure 3.22. Structural tuning of the amido-thiourea catalyst. Reactions performed on a 0.1 mmol scale using 3 equiv. of 2-methylbenzophenone **2a**. [a]Yield of the isolated product **15c** after flash chromatography on silica gel. [b]Enantiomeric excess determined by UPC² analysis on a chiral stationary phase.

We next performed a solvent screening using catalyst **K** (Table 3.4), identifying *o*-chlorobenzene as the best reaction medium. By using this solvent, the product **15c** could be obtained in 83% yield, complete diastereoselectivity, and 91% ee (entry 5).

Table 3.4. Solvent screening

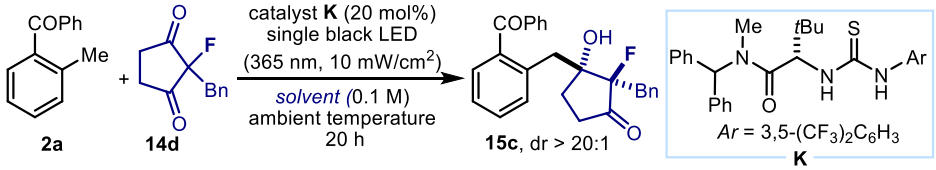

entry	solvent	conversion (%)	yield (%)[a]	ee (%)[b]
1	acetonitrile	13	15	-
2	THF	0	0	-
3	Benzene	35	24	-
4	Mesitylene	73	65	-
5	*o*-dichlorobenzene	90	83 (69)	91

Reactions performed on a 0.1 mmol scale using 3 equiv. of **2a**. [a]Yield determined by ^{1}H NMR analysis using 1-fluoro-2-nitrobenzene as internal standard. [b]Enantiomeric excess determined by UPC² analysis on a chiral stationary phase. Values in parenthesis are referred to the isolated material **15c**. Bn: benzyl.

Our last investigations focused on the fine-tuning of the reaction conditions (Table 3.5). By extending the reaction time from 20 to 30 hours, we could reach 89% yield of the desired product **15c**, without affecting the stereoselective outcome (90% ee, entry 2). Further extending the reaction time did not provide any improvement (entry 3). Worse results were obtained by decreasing the catalyst loading, varying the initial concentration of **14d**, or decreasing the equivalents of photoenol precursor (entries 4-7). The reaction was sensitive to oxygen (entry 8). This is congruent with the notion that oxygen can react with the ground-state photoenol or some of its precursors.[43] However, good reactivity can be obtained by adding all the components in the reaction vessel under an argon atmosphere (entry 1), without the necessity of performing the freeze-pump-thaw technique to degas the initial solution (entry 9). Since our illumination system consisted of a black LED connected to an external power supply, we could finely tune and control the intensity of the light emission (see Experimental Section of this Chapter for details of the illumination set-up).

Table 3.5. Final optimization

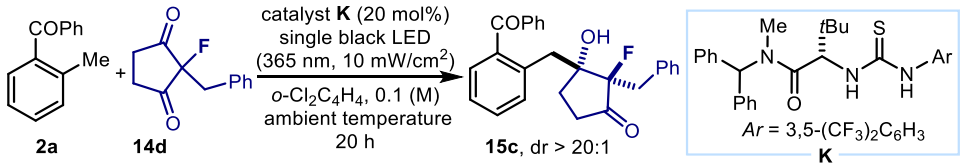

2a **14d** **15c**, dr > 20:1 **K**

entry	deviation from standard conditions	r.s.m (%)	yield (%)[a]	ee (%)[b]
1	none	17	83 (69)	91
2	30 h	10	89 (82)	90
3	40 h	<10	86	n.d.
4	15 mol% of catalyst **K**	26	71	83
5	0.05 M	42	56	n.d.
6	0.15 M	25	75	n.d.
7	**2a**:**14d** = 2:1	65	32	n.d.
8	aerobic conditions	70	28	n.d.
9	freeze-pump-thaw	20	80	n.d.
10	15 mW/cm^2 ; 30 h	traces	97 (89)	90
11	no catalyst **K**	85	15	0

Reactions performed on a 0.1 mmol scale using 3 equiv. of **2a**. [a]NMR-yield determined by ^{19}F NMR analysis of the crude reaction mixture using 1-fluoro-2-nitrobenzene as internal standard. Values in parenthesis refer to the yield of the isolated product **15c** after chromatography. [b]Enantiomeric excess determined by UPC^2 analysis on a chiral stationary phase. r.s.m.= remaining starting material. n.d.= not determined.

[43] Sammes, P. G. Photoenolisation. *Tetrahedron* **1976**, *32*, 405–422.

Increasing the irradiance from 10±1 mW/cm^2 (used in the benchmark reaction) to 15±1 mW/cm^2 while keeping the reaction time to 30 hours provided the isolated product **15c** in 89% yield, as a single diastereoisomer, and with 90% ee (entry 10). In the absence of catalyst **K**, the racemic adduct **15c** could be isolated in 15% yield (entry 11). This last result, along with the high stereocontrol achieved with the chiral amido-thiourea **K**, implies that the rate acceleration provoked by **K** is large enough to overcome a racemic background process.

3.6.2. Scope of the Reaction

With the optimal conditions in hand (Table 3.5, entry 10), we then evaluated the generality of the light-driven organocatalytic aldol desymmetrization process (Figures 3.23 and 3.24).

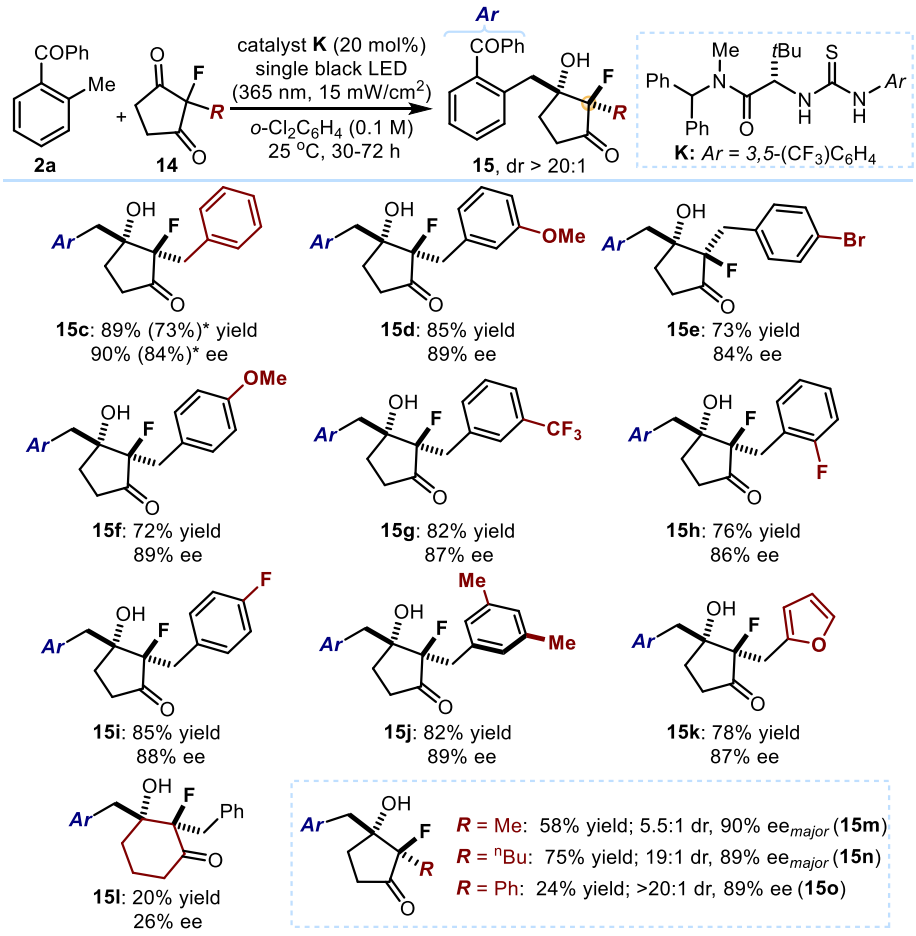

Figure 3.23. Survey of the 2-fluoro-substituted 1,3-diketones **14** that can participate in the photochemical organocatalytic desymmetrization aldol process. Reactions performed on a 0.1 mmol scale using 3 equiv. of **2a**. Unless otherwise specified, the diastereoisomeric ratio (dr) of products **15** is >20:1 (inferred by ^{19}F NMR analysis of the crude reaction mixture). Yields and enantiomeric excesses of the isolated products **15** are indicated below each entry (average of two runs). *Performed on a 1 mmol scale.

We first studied the reactivity of a variety of achiral 2-substituted-2-fluorocyclopentane-1,3-diketones **14**. As depicted in Figure 3.23, different substituents at the aromatic ring of the benzyl moiety in **15** could be used, regardless of their electronic and steric properties or position on the phenyl ring (products **15c-j**). X-ray crystallographic analysis performed on crystals from adduct **15e**[44] secured the assignment of the absolute configuration for the newly formed fluorine-containing quaternary stereogenic center while establishing the stereochemical outcome of the aldol-based desymmetrization (see Section 3.7). This system also showed some limitations. The presence of a 2-phenyl substituent in **14** greatly affected the reactivity, although the stereoselectivity was preserved (adduct **15o**). Additionally, the six-member ring product **15l** could be obtained only in poor yield and enantiomeric excess. We next evaluated the scope of the 2-alkylbenzophenones **2** that can participate in the reaction by acting as donors upon photochemical generation of the reactive photoenol intermediates. (Figure 3.24).

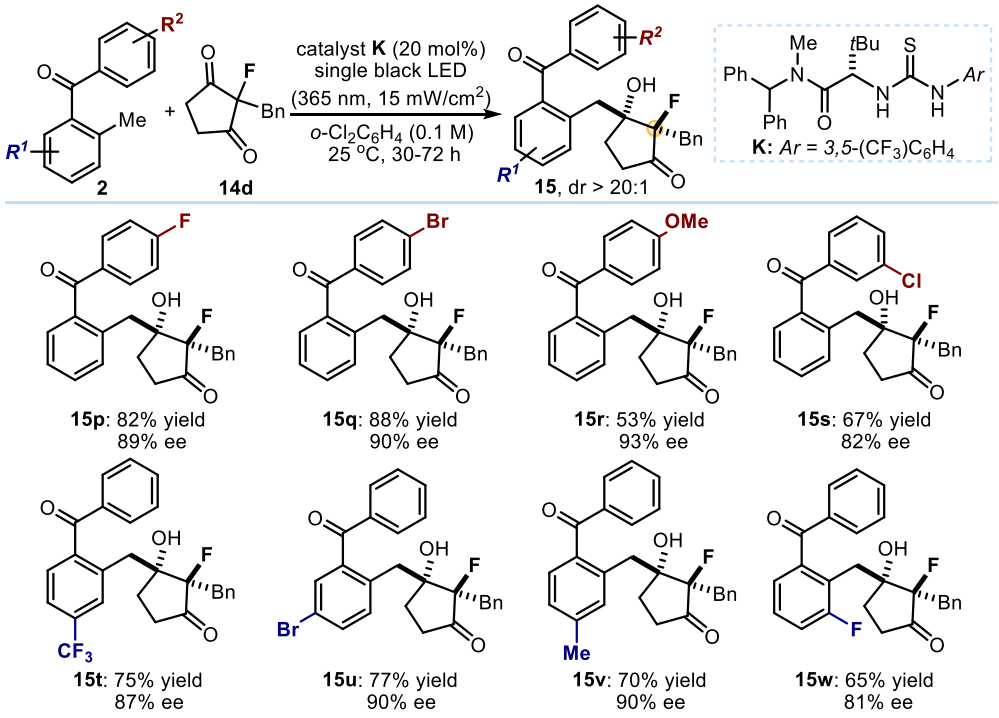

Figure 3.24. Survey of the 2-alkylbenzophenones **2** that can participate in the photochemical organocatalytic desymmetrization aldol process. Reactions performed on a 0.1 mmol scale using 3 equiv. of **2**. Unless otherwise specified, the diastereoisomeric ratio (dr of products **15** is >20:1 (inferred by ^{19}F NMR analysis of the crude reaction mixture). Yields and enantiomeric excesses of the isolated products **15** are indicated below each entry (average of two runs). Bn: benzyl.

[44] Crystallographic data for compound **15e** has been deposited with the Cambridge Crystallographic Data Center, accession number CCDC 1552622.

A wide range of substituents at both the non-enolizable (products **15p**-**15s**) and the enolizable (products **15t**-**15w**) aromatic ring of **2** are well tolerated, granting access to chiral 2-fluoro-3-hydroxycyclopentanones **15p**-**w**.

3.7. Origin of Stereoselectivity

The X-ray structure obtained from crystals of product **15e** places the fluorine atom and the hydroxyl group of the contiguous carbon in an *anti*-disposition (Figure 3.25, *left panel*).

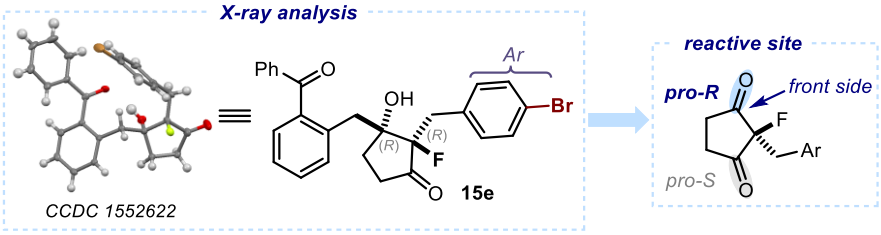

Figure 3.25. The analysis of the X-ray structure of product **15e** (*left panel*) showed that the enantioselective desymmetric aldol reaction occurs at the *pro-R* carbonyl group, from the side where the F atom is located (highlighted in blue in the *right panel*).

The excellent diastereoselective outcome is likely due to the different steric hindrance provided by the two groups situated on the prostereogenic quaternary center, which forces the aldol addition process to occur preferentially from the side where the smallest group is located (in this case, the fluorine atom). In consonance with this proposal, the diastereoselectivity of the process was affected when the prochiral center contained substituents of similar size, such as a methyl group and a fluorine atom (case of product **15m**, in Figure 3.23). This suggests that the methyl group is not large enough to effectively inhibit the addition over the side where it is placed.

The analysis of the absolute configuration suggests that catalyst **K** facilitates the aldol-type addition of the photoenol to the *pro-R* carbonyl within the 1,3-diketone (Figure 3.25, *right panel*).

3.8. Product Manipulations

We applied the photochemical organocatalytic desymmetrization strategy to the one-pot synthesis of the highly functionalized Hajos-Parrish-type ketone **50** (Figure 3.26). For that purpose, we initially checked the individual behavior of the two reactions required to access **50**. First, we submitted 2-methylbenzophenone **2a** and 2-fluoro-2-(3-oxobutyl)cyclopentane-1,3-dione **14o** to the optimal conditions of the light-driven desymmetric aldol process. Adduct **15x** was formed in 73% yield, complete diastereoselectivity, and 70% ee after 24 hours. We then tested the ability of the isolated compound **15x** to undergo an enamine-catalyzed aldol cyclization by using 50% of pyrrolidine as the amine catalyst and *o*-dichlorobenzene as

solvent. Complete conversion of the precursor **15x** to form the target product **50** was observed after 16 hours. With these two individual results in hand, we next performed the one-pot synthesis of **50**. The one-pot process implied the direct addition of 50 mol% of pyrrolidine to the reaction vessel, once the photochemical step was concluded (*i.e.* after 24 hours of light-irradiation of **2a** and **14o**), and without isolation of the intermediate **15x**. Product **50** was obtained in 61% yield, as a single diastereoisomer and 70% ee. This result indicates that the stereochemical information is fully transmitted throughout the enamine-mediated cyclization step.

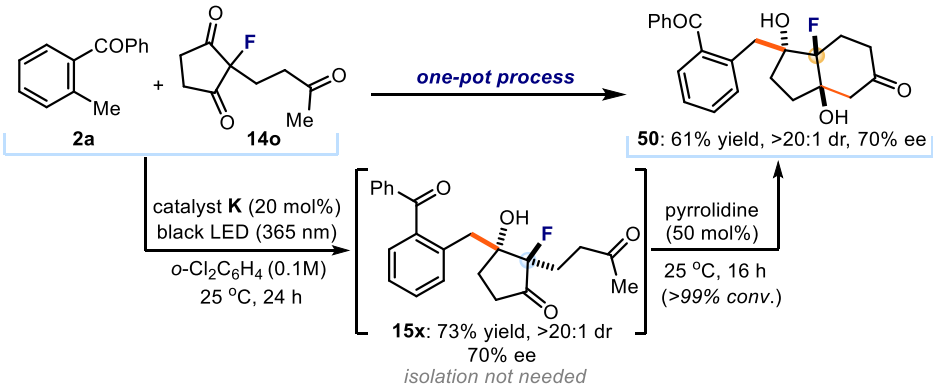

Figure 3.26. One-pot organocatalytic enantioselective synthesis of the fluorinated Hajos-Parrish-type ketone **50** proceeding through an intermolecular desymmetrizing aldol reaction of **14o** followed by enamine-mediated intramolecular aldol cyclization of **15x**.

3.9 Attempts to Extend the Scope of the Light-Driven Aldol-Desymmetrization Strategy

After demonstrating that the enantioselective aldol-type desymmetrization of 2-alkyl-2-fluorocyclopentane-1,3-diones can be used to forge F-containing quaternary centers, we wondered whether other substitution patterns in the prochiral center (different from fluorine) could be tolerated. To this end, we synthesized the 1,3-diketones **14p**-**14r** (Figure 3.27) and we submitted them to the optimized conditions of the aldol-desymmetrization process. Unfortunately, no traces of the corresponding aldol products **15**, nor of the hetero-Diels-Alder products **20**, were detected. Instead, the starting materials were recovered. These results highlight the crucial role of fluorine in triggering the aldol-type addition of photoenols to the 1,3-diketones **14**. Since the C-F bond is highly polarized,[45] strong electronic effects likely account for the unique reactivity observed with 2-alkyl-2-fluorocyclopentane-1,3-diones.

[45] O'Hagan, D. Understanding Organofluorine Chemistry. An Introduction to the C-F Bond. *Chem. Soc. Rev*. **2008**, 37, 308–319.

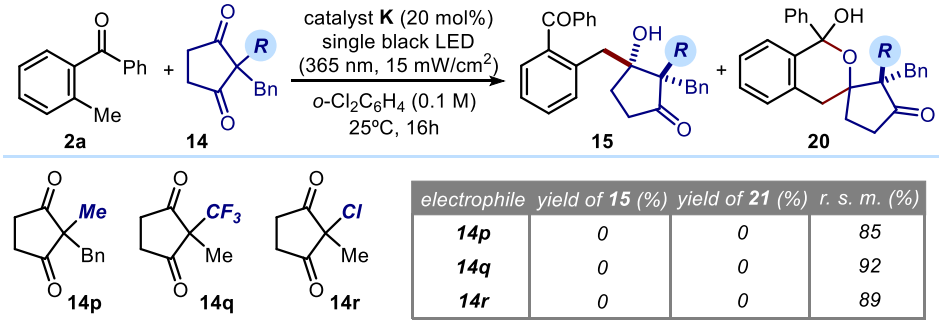

electrophile	yield of **15** (%)	yield of **21** (%)	r. s. m. (%)
14p	*0*	*0*	*85*
14q	*0*	*0*	*92*
14r	*0*	*0*	*89*

Figure 3.27. Evaluation of other 2-alkyl-2-substituted 1,3-diketones **15**.

3.10. Conclusions

We have demonstrated that the chemistry of photoenols can be expanded to enantioselective *inter*-molecular aldol-type addition processes. Specifically, we have used these photochemically generated intermediates in a desymmetric aldol-type reaction with achiral 2-fluoro-substituted cyclopentane-1,3-diketones. In order to make this process enantioselective, we have exploited the ability of a readily available amido-thiourea catalyst to selectively activate one of the two enantiotopic carbonyl groups within the symmetric 2-substituted-2-fluorocyclopentane-1,3-diones, while facilitating the aldol-type addition with the highly reactive photoenols. This transformation provides a strategy to forge fluorine-containing quaternary stereocenters at the carbon adjacent to the reactive site.

3.11. Experimental Section

3.11.1. General Information

The NMR spectra were recorded at 400 MHz and 500 MHz for ^{1}H, 100 MHz or 125 MHz for ^{13}C and 376 MHz for ^{19}F. The chemical shift (δ) for ^{1}H and ^{13}C are given in ppm relative to residual signals of the solvents ($CHCl_3$ @ 7.26 ppm ^{1}H NMR, 77.16 ppm ^{13}C NMR, and tetramethylsilane @ 0 ppm). Coupling constants are given in Hertz. The following abbreviations are used to indicate the multiplicity: s, singlet; d, doublet; t, triplet; q, quartet; m, multiplet; bs, broad signal.

High-resolution mass spectra (HRMS) were obtained from the ICIQ High Resolution Mass Spectrometry Unit on MicroTOF Focus and Maxis Impact (Bruker Daltonics) with electrospray ionization. X-ray data were obtained from the ICIQ X-Ray Unit using a Bruker-Nonius diffractometer equipped with an APPEX 2 4K CCD area detector. Optical rotations were measured on a Polarimeter Jasco P-1030 and are reported as follows: $[\alpha]_D^T$ (c in g per 100 mL, solvent).

General Procedures. All reactions were set up under an argon atmosphere in oven-dried glassware using standard Schlenk techniques, unless otherwise stated. Synthesis grade solvents were used as purchased. Anhydrous solvents were taken from a commercial SPS solvent dispenser. Chromatographic purification of products was accomplished using force-flow chromatography (FC) on silica gel (35-70 mesh). For thin layer chromatography (TLC) analysis throughout this work, Merck precoated TLC plates (silica gel 60 GF_{254}, 0.25 mm) were used, using UV light as the visualizing agent and an acidic mixture of *p*-anisaldehyde or basic aqueous potassium permangante ($KMnO_4$), and heat as developing agents. Organic solutions were concentrated under reduced pressure on a Büchi rotary evaporator (in vacuo at 40 ºC, ~5 mbar).

Determination of Diastereomeric Ratio. The diastereomeric ratio was determined by ^{19}F NMR and ^{1}H NMR analysis of the crude reaction mixture through integration of diagnostic signals.

Determination of Enantiomeric Purity: UPC^2 analysis on chiral stationary phase was performed on a Waters ACQUITY® UPC^2 instrument, using a AMY1 and IA chiral columns. The exact conditions for the analyses are specified within the characterisation section. UPC^2 traces were compared to racemic samples prepared performing the reactions in the absence of the chiral catalyst.

Materials: Commercial grade reagents and solvents were purchased at the highest commercial quality from Sigma Aldrich, Fluka, Acros Organics, Alfa Aesar or Fluorochem, and used as received, unless otherwise stated. The preparation of the 2-fluoro-2-alkylsubstitued cyclopentane-1,3-diones **14** is detailed in Section 3.11.2. Cyclopentane-1,3-dione **S1**, aldehydes **S2**, the Hanztsch ester **S3**, and Selectfluor® were purchased from

Fluorochem or Sigma Aldrich and used without further purification. Ethyl 4-chloro-4-oxobutyrate **S5**, benzyl magnesium chloride **S6**, and 2-methylbenzophenone **2a** were purchased from Sigma Aldrich and used without further purification. 2-trimethylsiloxypropene **S10** was purchased from Fluorochem and used without further purification. The preparation of benzophenones **2d-k** was described in the Experimental Section 2.7.2 of Chapter II. The organocatalysts **E**, **I**, **J**, **K**, **L** were synthesized according to described procedures.[42,46] The amido-thiourea catalyst **E** is also commercially available from Sigma Aldrich.

The NMR spectra and the UPC² traces are available in the published manuscript,[1] and are not reported in the present doctoral thesis.

3.11.2. Synthesis of 2-Fluoro-2-alkylsubstituted Cyclopentane-1,3-diones

General Procedure

Step 1: one-pot Knoevenagel condensation / reduction sequence

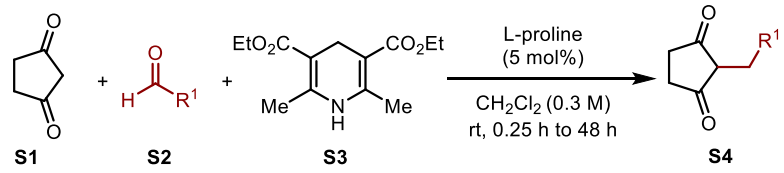

Step 2: Electrophilic fluorination

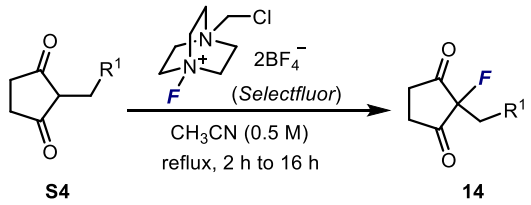

Scheme 1. Preparation of 2-fluoro-2-alkyl-substituted-1,3-diketones **14**.

Step 1: Substrates **S4** were synthesized according to a procedure described in the literature[47] for similar compounds: cyclopentane-1,3-dione **S1** (1 equiv.), aldehyde **S2** (3 equiv.) and the Hantzsch ester **S3** (1 equiv.) were dissolved in dichloromethane (0.3 M). Then, L-proline (0.05 equiv., 5 mol%) was added, and the reaction mixture was stirred at 25 ºC during 2-24 hours, until complete consumption of **S1**, as judged by TLC analysis. The reaction mixture was concentrated *in vacuo* to afford a brown solid. Crystallization of the solid from methanol

[46] Reisman, S. E.; Doyle, A. G.; Jacobsen, E. N. Enantioselective Thiourea-catalyzed Additions to Oxocarbenium ions. *J. Am. Chem. Soc.* **2008**, *130*, 7198–7199.

[47] Ramachary, D. B.; Kishor, M. Direct Amino Acid-catalyzed Cascade Biomimetic Reductive Alkylation: Application to the Asymmetric Synthesis of Hajos-Parrish Ketones Analogues. *Org. Biomol. Chem.* **2008**, *6*, 4176–4187.

gave substrates **S4** as white solids that displayed spectrosocopic data consistent with those reported in the literature.[47] Some intermediates **S4** were purified by flash column chromatography on SiO_2 gel (details are reported in the Characterization Data below).

Step 2: Substrates **14** were prepared following a literature procedure for similar compounds:[48] the 2-substituted-cyclopentane-1,3-dione **S4** (1 equiv.) and Selectfluor® (1 equiv.) were dissolved in acetonitrile (0.5 M) under an argon atmosphere. The solution was heated to reflux and stirred until complete consumption of **S4**, as judged by TLC analysis (6-24 hours). Then, the crude reaction mixture was cooled to ambient temperature and concentrated *in vacuo*. The residue was diluted with ethyl acetate, washed with saturated sodium bicarbonate, water, brine, dried ($MgSO_4$) and concentrated *in vacuo*. Purification of the residue by flash column chromatography (90:10 hexanes/EtOAc) gave the title compound **14**.

Characterization Data

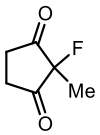

14b

2-methyl-2-fluorocyclohexane-1,3-dione (14b)

Compound **14b** was synthesized according to the general procedure (only the *step 2* is required) using 2-methylcyclopenta-1,3-dione (560 mg, 5 mmol, 1 equiv). The crude mixture of *step 2* was purified by flash column chromatography on silica gel (gradient from 90:10 hexanes/EtOAc to 70:30 hexanes/EtOAc) to give **14b** as a white solid (85% yield).

^{1}H NMR (400 MHz, $CDCl_3$) δ: 3.06 – 2.90 (m, 2H), 2.90 – 2.73 (m, 2H), 1.55 (s, 3H). **^{13}C NMR (100 MHz, $CDCl_3$)** δ: 204.4 (d, *J* = 345.3 Hz, C=O x2), 33.2 (d, *J* = 2.3 Hz, -CH_2 x2), 19.2 (d, *J* = 26.3 Hz). **^{19}F NMR decoupled ^{1}H (376 MHz, $CDCl_3$)** δ: -173.05. **HRMS** calculated for $[C_6H_7FO_2+CH_3OH+Na]^+$**:**185.0584; found: 185.0585.

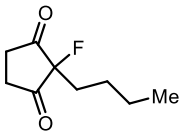

14c

2-butyl-2-fluorocyclopentane-1,3-dione (14c). Compound **14c** was synthesized according to the general procedure using cyclopenta-1,3-dione (560 mg, 5 mmol, 1 equiv) and butanal (1.5 mL, 15 mmol, 3 equiv) in *step 1*. The crude mixture in *step 1* was purified by flash column chromatography on silica gel (gradient from 50:50 hexanes/EtOAC to 100% EtOAc) to give the corresponding intermediate **S4** as a white solid. The crude mixture of *step 2* was purified by flash column chromatography on silica gel (80:20 hexanes/EtOAc) to give **14c** as a white solid (35% yield over two steps).

[48] Patent: Bristol-Meyers Squibb Company; Stephen, T. W.; Brown, G. D.; Doweyko, L. M.; Duan, J.; Guo, J.; Hynes, J.; Jian, B.; Kempson, J.; Lin, S.; Lu, Z.; Spergel, S. H.; Tokarski, J. S.; Wu, H.; Yang, B. V. Patent: WO2012/125886A1, **2012**. Location in patent: page/page column 174.

^{1}H NMR (400 MHz, $CDCl_3$) δ: 3.01 – 2.89 (m, 2H), 2.85 – 2.72 (m, 2H), 1.97 – 1.83 (m, 2H), 1.47 – 1.27 (m, 4H), 0.90 (t, *J* = 7.2 Hz, 3H). **^{13}C NMR (125 MHz, $CDCl_3$)** δ: 205.8 (d, *J* = 15.4 Hz, C=O x2), 95.8 (d, *J* = 208.6 Hz), 33.6, 33.4 (d, *J* = 2.8 Hz), 24.0 (d, *J* = 3.1 Hz), 22.6, 13.8. **^{19}F NMR decoupled ^{1}H (376 MHz, $CDCl_3$)** δ: -182.17. **HRMS** calculated for $[C_9H_{13}FO_2+H]^+$: 173.0972; found: 173.0975.

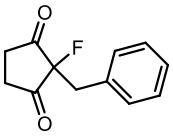

14d

2-benzyl-2-fluorocyclopentane-1,3-dione (14d). Compound **14d** was synthesized according to the general procedure using benzaldehyde (1.5 mL, 15 mmol, 3 equiv.) in *step 1*. The crude mixture of *step 2* was purified by flash column chromatography on silica gel (90:10 hexanes/EtOAc) to give **14d** as a white solid (65% yield over two steps).

^{1}H NMR (400 MHz, $CDCl_3$) δ: 7.33 – 7.28 (m, 3H), 7.11 (m, 2H), 3.26 (d, *J* = 14.8 Hz, 2H), 2.72 – 2.55 (m, 2H), 2.41 – 2.23 (m, 2H). **^{13}C NMR (100 MHz, $CDCl_3$)** δ: 207.1 (d, *J* = 15.1 Hz, C=O x2), 130.5 (d, *J* = 9.0 Hz), 130.1, 129.2, 128.4, 93.3 (d, *J* = 207.1 Hz), 40.8 (d, *J* = 26.0 Hz), 34.4 (d, *J* = 2.5 Hz, -CH_2 x2). **^{19}F NMR decoupled ^{1}H (376 MHz, $CDCl_3$)** δ: -168.53. **HRMS** calculated for $[C_{12}H_{11}FO_2+Na+CH_3OH]^+$: 261.0897; found: 261.0903.

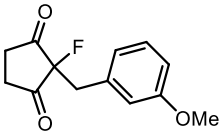

14e

2-fluoro-2-(3-methoxybenzyl)cyclopentane-1,3-dione (14e). Compound **14e** was synthesized according to the general procedure using *m*-anisaldehyde (1.8 mL, 15 mmol, 3 equiv.) in *step 1*. The crude mixture of *step 2* was purified by flash column chromatography on silica gel (90:10 hexanes/EtOAc) to give **14e** as a white solid (31% yield over two steps).

^{1}H NMR (500 MHz, $CDCl_3$) δ: 7.23 (m, 1H), 6.84 (m, 1H), 6.69 (d, *J* = 7.5 Hz, 1H), 6.65 (m, *J* = 2.1 Hz, 1H), 3.78 (s, 3H), 3.24 (d, *J* = 14.1 Hz, 2H), 2.72 – 2.57 (m, 2H), 2.41 – 2.27 (m, 2H). **^{13}C NMR (125 MHz, $CDCl_3$)** δ: 207.2 (d, *J* = 15.1 Hz, C=O x2), 160.1, 131.9 (d, *J* = 9.5 Hz), 130.3, 122.3, 115.8, 113.9, 93.0 (d, *J* = 206.7 Hz), 55.4, 40.9 (d, *J* = 26.2 Hz), 34.5 (d, *J* = 2.5 Hz, -CH_2 x2). **^{19}F NMR decoupled ^{1}H (376 MHz, $CDCl_3$)** δ: -167.50. **HRMS** calculated for $[C_{13}H_{13}FO_3+Na+CH_3OH]^+$: 291.1003; found: 291.0999.

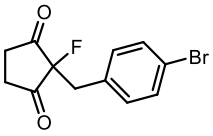

14f

2-fluoro-2-(4-bromobenzyl)cyclopentane-1,3-dione (14f). Compound **14f** was synthesized according to the general procedure using 4-bromobenzaldehyde (1850 mg, 30 mmol, 3 equiv) in *step 1*. The crude mixture of *step 2* was purified by flash column chromatography on silica gel (90:10 hexanes/EtOAc) to give **14f** as a white solid (38% yield over two steps).

^{1}H NMR (500 MHz, $CDCl_3$) δ: 7.48 – 7.41 (m, 2H), 7.00 (d, *J* = 8.3 Hz, 2H), 3.21 (d, *J* = 16.0 Hz, 2H), 2.79 – 2.65 (m, 2H), 2.54 – 2.41 (m, 2H).

^{13}C NMR (125 MHz, $CDCl_3$) δ: 206.3 (d, *J* = 15.2 Hz, C=O x2), 132.3 (x2), 131.9 (x2), 129.6 (d, *J* = 8.0 Hz), 122.7, 92.6 (d, *J* = 206.8 Hz), 39.6 (d, *J* = 26.1 Hz), 34.3 (d, *J* = 2.3 Hz, -CH_2 x2). **^{19}F NMR decoupled ^{1}H (376 MHz, $CDCl_3$)** δ: -168.80. **HRMS** calculated for $[C_{12}H_{10}BrFO_2+CH_3OH+Na]^+$**:** 339.0003; found: 339.9993.

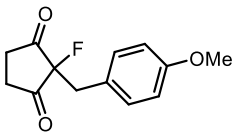

14g

2-fluoro-2-(4-methoxybenzyl)cyclopentane-1,3-dione (14g). Compound **14g** was synthesized according to the general procedure using *p*-anisaldehyde (1.8 mL, 15 mmol, 3 equiv.) in *step 1*. The crude mixture of *step 2* was purified by flash column chromatography on silica gel (90:10 hexanes/EtOAc) to give **14g** as a white solid (54% yield over two steps).

^{1}H NMR (400 MHz, $CDCl_3$) δ: 7.06 – 7.01 (m, 2H), 6.86 – 6.81 (m, 2H), 3.79 (s, 1H), 3.22 (d, *J* = 14.1 Hz, 2H), 2.71 – 2.54 (m, 2H), 2.42 – 2.23 (m, 2H). **^{13}C NMR (100 MHz, $CDCl_3$)** δ: 207.4 (d, *J* = 15.1 Hz, C=O x2), 159.6, 131.3 (x2), 122.1 (d, *J* = 9.5 Hz), 114.6 (x2), 93.1 (d, *J* = 206.9 Hz), 55.4, 40.1 (d, *J* = 26.1 Hz), 34.4 (d, *J* = 2.5 Hz, -CH_2 x2). **^{19}F NMR decoupled ^{1}H (376 MHz, $CDCl_3$)** δ: -167.59. **HRMS** calculated for $[C_{13}H_{13}FO_3+Na]^+$: 259.0741; found: 259.0747.

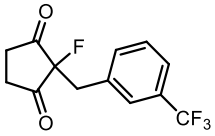

14h

2-fluoro-2-(3-(trifluoromethyl)benzyl)cyclopentane-1,3-dione (14h). Compound **14h** was synthesized according to the general procedure using 3-trifluoromethylbenzaldehyde (2.0 mL, 15 mmol, 3 equiv) in *step 1*. The crude mixture of *step 2* was purified by flash column chromatography on silica gel (90:10 hexanes/EtOAc) to give **14h** as a white solid (34% yield over two steps).

^{1}H NMR (500 MHz, CD_3CN) δ: 7.63 (d, *J* = 7.9 Hz, 1H), 7.55 – 7.42 (m, 3H), 3.29 (d, *J* = 24.6 Hz, 2H), 3.11 – 2.96 (m, 2H), 2.78 – 2.64 (m, 2H). **^{13}C NMR (125 MHz, CD_3CN)** δ: 206.6 (d, *J* = 15.0 Hz, C=O x2), 135.3, 134.6 (d, *J* = 1.0 Hz), 130.9 (d, *J* = 32.0 Hz), 130.2, 128.4 – 127.8 (q), 126.5 – 125.3 (q), 122.8 (q, *J* = 339.8, 276.8, 241.2 Hz, -CF_3), 96.4 (d, *J* = 210.5 Hz), 39.1 (d, *J* = 23.5 Hz), 34.1 (d, *J* = 3.0 Hz, -CH_2 x2). **^{19}F NMR decoupled ^{1}H (376 MHz, CD_3CN)** δ: -63.27 (-CF_3), -180.94. **HRMS** calculated for $[C_{13}H_{10}F_4O_2+CH_3OH+Na]^+$: 329.0771; found: 329.0780.

14i

2-fluoro-2-(2-fluorobenzyl)cyclopentane-1,3-dione (14i). Compound **14i** was synthesized according to the general procedure using 2-fluorbenzaldehyde (1.6 mL, 15 mmol, 3 equiv) in *step 1*. The crude mixture of *step 2* was purified by flash column chromatography on silica gel (90:10 hexanes/EtOAc) to give **14i** as a white solid (27% yield over two steps).

^{1}H NMR (500 MHz, $CDCl_3$) δ: 7.31 (dddd, *J* = 8.3, 7.3, 5.4, 1.8 Hz, 1H), 7.28 – 7.23 (m, 1H), 7.14 (td, *J* = 7.5, 1.2 Hz, 1H), 7.04 (ddd, *J* = 9.7, 8.2, 1.2 Hz, 1H), 3.28 (dd, *J* = 21.6, 1.4 Hz, 2H), 3.00 – 2.85 (m, 2H), 2.82 – 2.68 (m, 2H). **^{13}C NMR (125 MHz, $CDCl_3$)** δ: 205.1 (d, *J* = 15.1 Hz, C=O x2), 161.0 (d, *J* = 245.6 Hz), 132.9 (d, *J* = 3.7 Hz), 130.4 (d, *J* = 8.4 Hz), 124.8 (d, *J* = 3.7 Hz), 118.3 (dd, *J* = 15.4, 2.9 Hz), 115.5 (d, *J* = 21.9 Hz), 94.4 (d, *J* = 211.1 Hz), 33.5 (d, *J* = 2.8 Hz, -CH_2 x2), 33.2 (dd, *J* = 25.5, 2.7 Hz). **^{19}F NMR decoupled ^{1}H (376 MHz, $CDCl_3$)** δ: -116.22 (Ar), -177.16. **HRMS** calculated for $[C_{12}H_{10}F_2O_2+Na+CH_3OH]^+$: 279.0803; found: 279.0804.

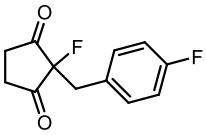

14j

2-fluoro-2-(2-chlorobenzyl)cyclopentane-1,3-dione (14j). Compound **14j** was synthesized according to the general procedure using 4-fluorobenzaldehyde (3.4 mL, 30 mmol, 3 equiv.) in *step 1*. The crude mixture of *step 2* was purified by flash column chromatography on silica gel (90:10 hexanes/EtOAc) to give **14j** as a white solid (33% yield over two steps).

^{1}H NMR (400 MHz, CD_3CN) δ: 7.19 (dd, *J* = 8.4, 5.5 Hz, 2H), 7.06 (t, *J* = 8.9 Hz, 2H), 3.21 (d, *J* = 23.7 Hz, 2H), 2.99 – 2.85 (m, 2H), 2.76 – 2.60 (m, 2H). **^{13}C NMR (100 MHz, CD_3CN)** δ: 206.9 (d, *J* = 15.0 Hz, C=O x2), 163.3 (d, *J* = 244.1 Hz), 133.1 (d, *J* = 8.2 Hz, x2), 129.3 – 129.0 (m), 116.0 (d, *J* = 21.6 Hz, x2), 96.7 (d, *J* = 210.0 Hz), 39.0 (d, *J* = 23.9 Hz), 34.1 (d, *J* = 2.9 Hz, -CH_2 x2). **^{19}F NMR decoupled ^{1}H (376 MHz, CD_3CN)** δ: -116.57 (Ar), -180.16. **HRMS** calculated for $[C_{12}H_{10}F_2O_2+CH_3OH+Na]^+$: 279.0803; found: 279.0808.

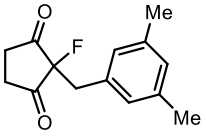

14k

2-(3,5-dimethylbenzyl)-2-fluorocyclopentane-1,3-dione (14k). Compound **14k** was synthesized according to the general procedure using 3,5-dimethylbenzaldehyde (2 mL, 15 mmol, 3 equiv.) in *step 1*. The crude mixture of *step 2* was purified by flash column chromatography on silica gel (90:10 hexanes/EtOAc) to give **14k** as a white solid (13% yield over two steps).

^{1}H NMR (400 MHz, $CDCl_3$) δ: 6.93 (s, 1H), 6.71 (s, 2H), 3.19 (d, *J* = 14.0 Hz, 2H), 2.70 – 2.53 (m, 2H), 2.38 – 2.18 (m, 8H, -CH_3 x2 + -CH_2). **^{13}C NMR (100 MHz, $CDCl_3$)** δ: 207.4 (d, *J* = 15.1 Hz, C=O x2), 138.9, 130.2 (d, *J* = 9.5 Hz), 130.1 (x2), 127.8 (x2), 93.5 (d, *J* = 207.0 Hz), 41.0 (d, *J* = 26.0 Hz), 34.5 (d, *J* = 2.6 Hz, -CH_2 x2), 21.3 (-CH_3 x2). **^{19}F NMR**

decoupled ^{1}H (376 MHz, $CDCl_3$) δ: -168.13. **HRMS** calculated for $[C_{14}H_{15}FO_2+CH_3OH+Na]^+$: 289.1210; found: 289.1214.

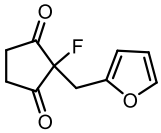

14l

2-fluoro-2-(furan-2-ylmethyl)cyclopentane-1,3-dione (14l). Compound **14l** was synthesized according to the general procedure using 2-furaldehyde (1.2 mL, 15 mmol, 3 equiv) in *step 1*. The crude mixture in *step 1* was purified by flash column chromatography on silica gel (gradient from 50:50 hexanes/EtOAC to 100% EtOAc) to give the corresponding intermediate **S4** as a brown solid. The crude mixture of *step 2* was purified by flash column chromatography on silica gel (80:20 hexanes/EtOAc) to give **14l** as a white solid (20% yield over two steps).

^{1}H NMR (400 MHz, $CDCl_3$) δ: 7.35 (dd, *J* = 1.9, 0.8 Hz, 1H), 6.34 (dd, *J* = 3.3, 1.9 Hz, 1H), 6.22 – 6.20 (m, 1H), 3.36 (d, *J* = 12.8 Hz, 2H), 2.78 – 2.62 (m, 2H), 2.62 – 2.45 (m, 2H). **^{13}C NMR (100 MHz, $CDCl_3$)** δ: 206.4 (d, *J* = 14.9 Hz, C=O x2), 145.0 (d, *J* = 12.5 Hz), 143.2, 111.4, 110.3 (d, *J* = 1.1 Hz), 90.8 (d, *J* = 207.0 Hz), 34.1 (d, *J* = 2.3 Hz, -CH_2 x2), 33.4 (d, *J* = 29.2 Hz). **^{19}F NMR decoupled ^{1}H: (376 MHz, $CDCl_3$)** δ: -169.18. **HRMS** calculated for $[C_{10}H_9FO_3+CH_3OH+Na]^+$: 251.0690; found: 251.0694.

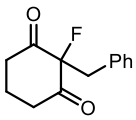

14m

2-benzyl-2-fluorocyclohexane-1,3-dione (14m). Compound **14m** was synthesized according to the general procedure using cyclohexane-1,3-dione (560 mg, 5 mmol, 1 equiv) and benzaldehyde (1.5 mL, 15 mmol, 3 equiv) in *step 1*. The corresponding intermediate **S4** in *step 1* was crystallized from methanol to give a white solid (596 mg, 59 % yield). The crude mixture of *step 2* was purified by flash column chromatography on silica gel (hexanes:EtOAc 70/30) to give **14m** as a white solid (56% yield over two steps).

^{1}H NMR (400 MHz, $CDCl_3$) δ: 7.34 – 7.27 (m, 3H), 7.22 – 7.18 (m, 2H), 3.37 (d, *J* = 24.2 Hz, 2H), 2.83 – 2.77 (m, 4H), 2.16 – 2.05 (m, 1H), 1.87 – 1.69 (m, 1H). **^{13}C NMR (100 MHz, $CDCl_3$)** δ: 200.9 (d, *J* = 17.3 Hz, C=O x2), 132.0, 130.0 (d, *J* = 1.3 Hz, x2), 128.9 (x2), 128.2, 103.8 (d, *J* = 205.2 Hz), 41.7 (d, *J* = 23.0 Hz), 38.8 (-CH_2, x2), 18.2. **^{19}F NMR decoupled ^{1}H (376 MHz, $CDCl_3$)** δ: -169.14. **HRMS calculated for $[C_{13}H_{13}FO_3+Na]^+$**: 243.0792; found: 243.0796.

3.11.2.1. Synthesis of 2-fluoro-2-substituted cyclopentane-1,3-diones 14n and 140

2-fluoro-2-phenylcyclopentane-1,3-dione (14n)

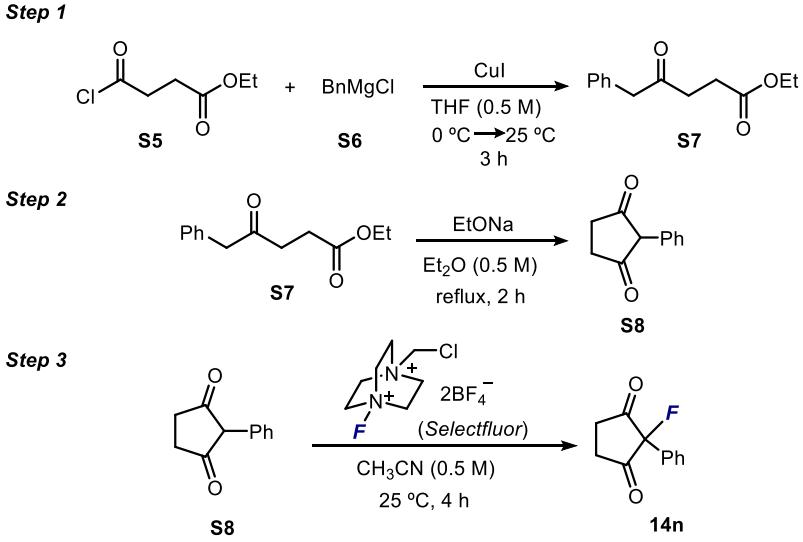

Scheme 2. Preparation of 2-fluoro-2-phenylcyclopentane-1,3-dione **14n.**

Compound **14n** was synthesized according to procedures described in the literature:[49]

Step 1: To a solution of CuI (1 equiv.) and ethyl 4-chloro-4-oxobutyrate **S5** in THF (0.5 M) was slowly added a 1.0 M solution of BnMgCl **S6** in THF (1 equiv.) at 0 ºC (time of addition: 1 hour). After stirring for 3 hours at ambient temperature, the reaction was quenched with saturated aqueous NH_4Cl. The mixture was extracted with EtOAc, and the organic layers were dried over anhydrous Na_2SO_4, filtered and concentrated. The residue was purified by flash column chromatography on SiO_2 gel (gradient from 100% hexane to 90:10 hexane/EtOAc) to give ethyl 4-oxo-5-phenylpentanoate **S7** as a pale yellow oil (56% yield).

Step 2: Compound **S7** was heated at reflux with 2 equivalents of EtONa in diethyl ether (0.5 M), under an N_2 atmosphere. A white precipitate was formed after 2 hours. The diethyl ether was removed *in vacuo*. The residue was suspended in CH_2Cl_2 and filtered to afford 2-phenylcyclopentane-1,3-dione **S8** as a white solid (79% yield).

---

[49] (a) Nakatsuji, H.; Sawamura, Y.; Sakakura, A.; Ishihara, K. Cooperative Activation with Chiral Nucleophilic Catalysts and N-haloimides: Enantioselective Iodolactonization of 4-Arylmethyl-4-pentenoic Acids. *Angew. Chem. Int. Ed.* **2014**, *53*, 6974–6977. (b) Betts, B. E.; Davey, W. Cyclohexane-1,3-diones. Part VI. Structural Requirements for the Displacement of the Alkoxyl by the Cyano-group in the Enol Ethers of Cyclic β-Diketones. *J. Chem. Soc.,* **1961**, 3333–3340. (c) Born, H.; Pappo, R.; Szmuszkovicz, J. 366. Synthesis of Cyclohexenones. *J. Chem. Soc.,* **1953**, 1779–1782.

Step 3: the fluorination of **S8** was accomplished following the general procedure (only *step 2*) described in Section 3.11.2. The crude mixture after *step 3* was purified by flash column chromatography on silica gel (gradient from 100% hexane to 90:10 hexane/EtOAc) to give **14n** as a pale brown solid (30% yield).

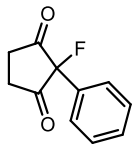

14n

2-phenyl-2-fluorocyclopentane-1,3-dione (14n):

^{1}H NMR (400 MHz, $CDCl_3$) δ: 7.55 – 7.44 (m, 1H), 7.41 (dt, *J* = 8.2, 1.6 Hz, 1H), 3.06 – 2.91 (m, 1H), 2.91 – 2.76 (m, 1H). **^{13}C NMR (100 MHz, $CDCl_3$)** δ: 204.3 (d, *J* = 17.7 Hz, C=O x2), 131.3 (d, *J* = 3.4 Hz), 129.7 (d, *J* = 1.9 Hz), 127.7 (d, *J* = 3.2 Hz), 33.8 (d, *J* = 2.4 Hz. $-CH_2$ x2). **^{19}F NMR decoupled ^{1}H (376 MHz, $CDCl_3$)** δ: -160.70. **HRMS** calculated for $[C_{11}H_9FO_2+Na+CH_3OH]^+$: 247.0741; found: 247.0732.

2-fluoro-2-(3-oxobutyl)cyclopentane-1,3-dione (14o)

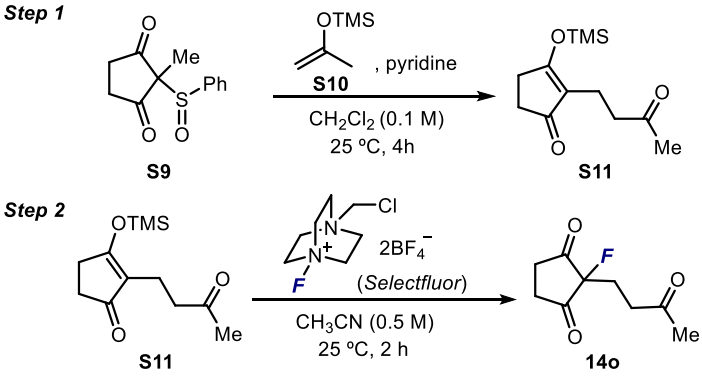

Scheme 3. Preparation of 2-fluoro-2-(3-oxobutyl)cyclopentane-1,3-dione **14o.**

Compound **14o** was synthesized according to procedures described in the literature:[50]

Step 1: To a solution 0.1 M of sulfoxide **S9**[50a] in dry dichloromethane and under an argon atmosphere was added pyridine (12 equiv), and the mixture was stirred at room temperature until all solids were dissolved (5 minutes). Then, 2-trimethylsiloxypropene **S10** (1.2 equiv.) was added to this bright yellow solution, and the stirring was continued for 4 hours. The solvents were removed *in vacuo* and the residue was directly subjected to flash column

[50] (a) Eaton, P. E.; Bunnelle, W. H. Synthesis of Dodecahedrane Precursors. 3. Synthesis of Alkylidene-1,3-Cyclopentanediones and Attempts to Roof Peristylanes. *Can J. Chem.* **1984**, 62, 2612–2626. (b) Bunnelle, W. H.; Meyer, L. A. Reactions of 2-Methylene-1,3-cyclopentanedione with Electron-rich Alkenes. *J. Org. Chem.* **1988**, 53, 4038–4042.

chromatography purification (gradient from 80:20 to 60:40 hexane/EtOAc) to give **S11** as a pale yellow oil (45% yield).

Step 2: Fluorination of **S11** was accomplished following the general procedure (only *step 2*) described in Section 3.11.2. The crude mixture after *step 2* was purified by flash column chromatography on silica gel (gradient from 90:10 to 60:40 hexane/EtOAc) to give **14o** as a white solid (25% yield).

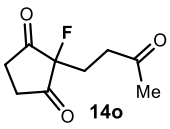

2-fluoro-2-(3-oxobutyl)cyclopentane-1,3-dione (14o).

^{1}H NMR (400 MHz, $CDCl_3$) δ: 3.21 – 3.00 (m, 2H), 2.82 – 2.63 (m, 4H), 2.25 (t, *J* = 6.2 Hz, 1H), 2.19 (t, *J* = 6.2 Hz, 1H), 2.14 (s, 3H). **^{13}C NMR (100 MHz, $CDCl_3$)** δ: 206.8, 205.6 (d, *J* = 15.4 Hz, C=O x2), 94.0 (d, *J* = 206.3 Hz), 35.3 (d, *J* = 1.7 Hz), 33.1 (d, *J* = 2.7 Hz, -CH_2 x2), 29.8, 26.5 (d, *J* = 24.5 Hz). **^{19}F NMR decoupled ^{1}H (376 MHz, $CDCl_3$)** δ: -180.98. **HRMS** calculated for $[C_9H_{11}FO_3+Na]^+$: 209.0584; found: 209.0579.

3.11.3. High-Throughput Screening of Organic Catalysts

Procedure

1) *Preparation of a library of organocatalysts*. Stock solutions (0.02 M in 1,2-dichloroethane, DCE) of each catalyst were prepared. In the cases in which the catalysts were not soluble, a mixture of DCE and methanol was employed to prepare the stock solution. Then, 100 µL of each stock solution (*i.e.* 2 µmol of catalyst) were dosed in each reaction vial (0.75 mL glass vials, 8x30 mm). The solvent in every vial was removed to dryness using a parallel evaporator GeneVac. The list of dosed organocatalysts is shown in Scheme 4 (next page).

2) *Set-up of the experiments.* Experiments were set-up inside of a glovebox under a nitrogen atmosphere. The glass vials containing the pre-dosed catalysts (2 µmol) were initially charged into a 24-well aluminium block adapted for photochemical reactions (see Figure 2.31 in Section 2.7.4 of Chapter II). Then, the 1,3-diketone **14d** (10 µmol/reaction) and 2-methylbenzophenone **2a** (30 µmol/reaction) were dosed in toluene (50 µL of each substrate, total volume of 100 µL). Stirring bars were added to each reaction vial. The 24-well plate was then sealed and stirred under irradiation of 365 nm black LEDs for 20 hours.

3) *Analysis of the experiments.* Upon opening the 24-well plate to air, 500 µL of a solution of biphenyl (used as internal standard to measure the UPLC yields) in acetonitrile (0.02 mol/L) was added to each reaction vial. The plate was covered again and the vials were stirred for 10 min to ensure good homogenization. Into a separate 96-well LC block (see Figure 2.31 in Section 2.7.4 of Chapter II) was added 500 µL of acetonitrile, followed by 20

µL of the diluted reaction mixtures. The LC block was then sealed with a silicon-rubber storage mat and mounted on an automated UPC^2 instrument for analysis.

Scheme 4. Catalysts tested in the high-throughput screening. List of abbreviations: Ar = 3,5-$(CF_3)_2C_6H_3$; QN = quinidine ; CN = cinchonine; HQD = hydroquinidine; HQN = hydroquinine.

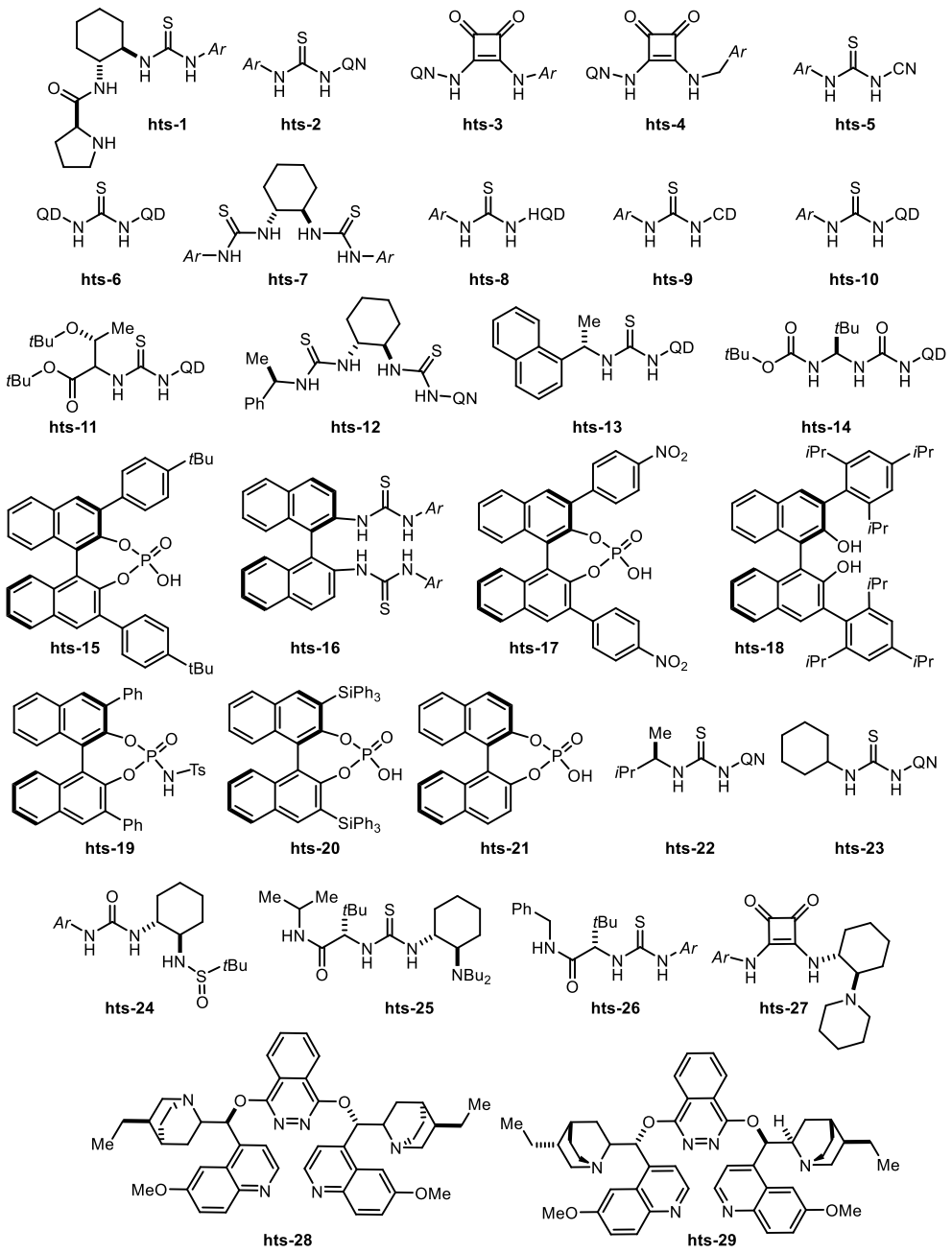

(continue in next page)

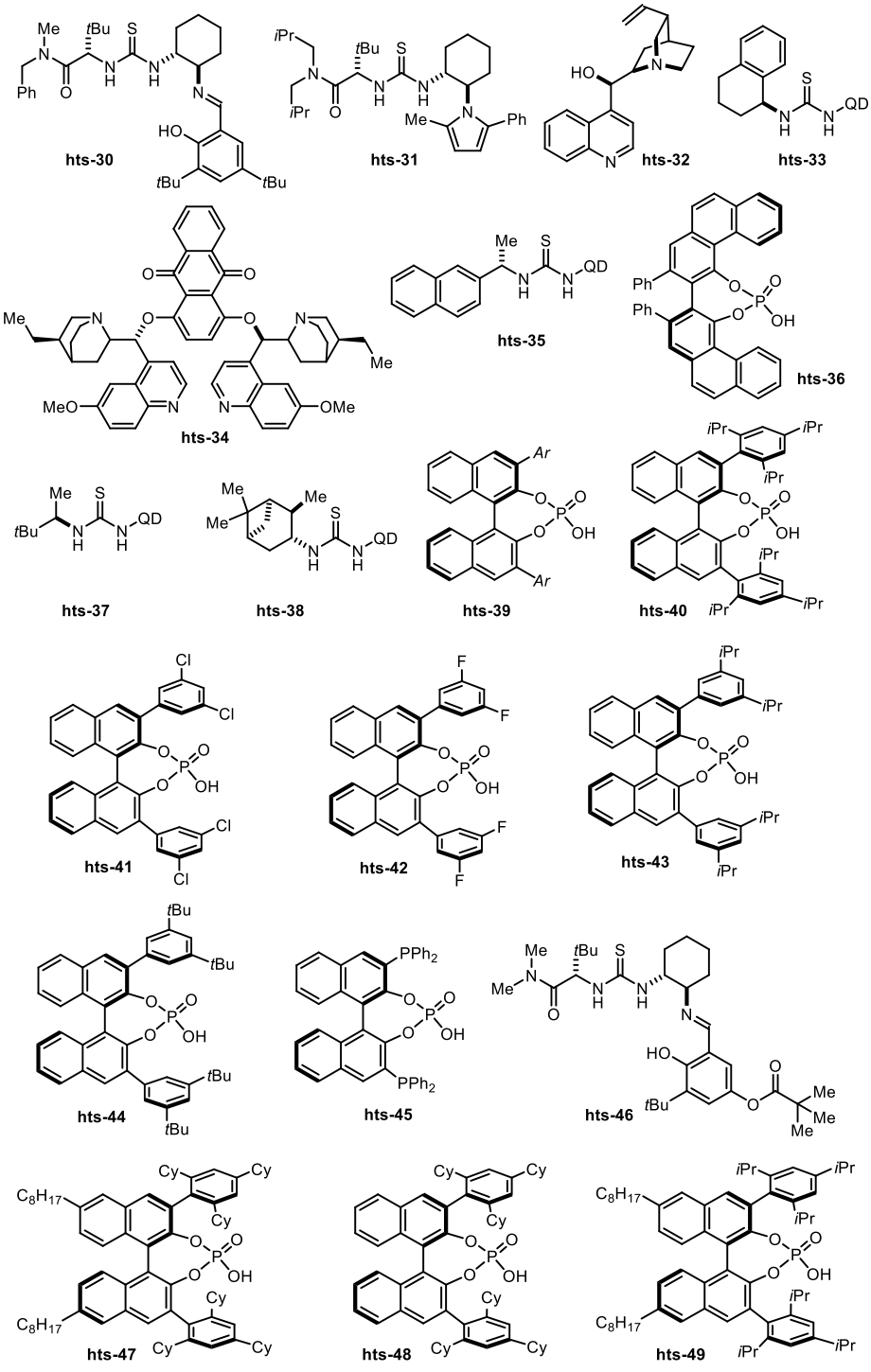
hts-30
hts-31
hts-32
hts-33
hts-34
hts-35
hts-36
hts-37
hts-38
hts-39
hts-40
hts-41
hts-42
hts-43
hts-44
hts-45
hts-46
hts-47
hts-48
hts-49

Table 3.6. Results of the high-throughput screening of organic catalysts (catalyst structures shown in Scheme 4)

catalyst	16c yield (%)[a]	ee (%)[b]	catalyst	16c yield (%)[a]	ee (%)[b]
hts-1	15	+10	hts-25	17	+2
hts-2	12	+36	hts-26	50	-76
hts-3	8	-7	hts-27	13	-68
hts-4	21	-1	hts-28	47	+-59
hts-5	12	+27	hts-29	19	+57
hts-6	12	+35	hts-30	10	-7
hts-7	7	-6	hts-31	27	-38
hts-8	11	-13	hts-32	33	+5
hts-9	11	19	hts-33	35	-24
hts-10	10	-27	hts-34	21	+24
hts-11	11	-13	hts-35	40	-24
hts-12	11	47	hts-36	26	-4
hts-13	16	-4	hts-37	40	-1
hts-14	27	-45	hts-38	23	-39
hts-15	13	-16	hts-39	11	+29
hts-16	7	-32	hts-40	13	-5
hts-17	<5	n.d.	hts-41	13	+30
hts-18	<5	n.d.	hts-42	7	+12
hts-19	6	41	hts-43	19	+5
hts-20	<5	n.d.	hts-44	24	2
hts-21	7	-18	hts-45	<5	n.d.
hts-22	17	-41	hts-46	7	19
hts-23	20	-43	hts-47	12	10
hts-24	53	+2	hts-48	12	14
			hts-49	8	17

[a]UPLC yield using biphenyl as the internal standard. [b]Enantiomeric excess determined by UPC² analysis on a chiral stationary phase.

3.11.4. Light-driven Aldol Desymmetrization of 2-Fluoro-2-alkylsubstituted cyclopentane-1,3-diones

General Procedure

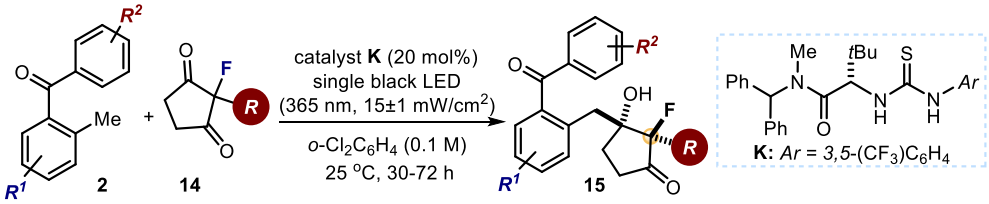

A 5 mL argon-purged glass vial containing a stirring bar, the organocatalyst **K** (11.6 mg, 0.02 mmol, 20 mol%) and the 2-fluoro-2-alkylsubstituted cyclopentane-1,3-dione **14** (0.1 mmol, 1 equiv) was closed with a Teflon-coated cap and flushed with argon. Then, degassed 1,2-dichlorobenzene (1 mL) and 2-alkylbenzophenone **2** (0.3 mmol, 3 equiv) were added under an argon atmosphere. The vial was sealed with parafilm and placed into a single black LED plate (λ = 365 nm, irradiance = 15±1 mW/cm^2, as controlled by an external power supply and measured using a photodiode light detector at the start of each reaction; the set-up is detailed in Chapter 2, Section 2.3.2, Figure 2.14). This set-up secured a reliable irradiation while keeping a constant distance between the reaction vessel and the light source.

The reaction mixture was stirred under light irradiation at 25 ºC for the indicated time (30-72 hours). The temperature was controlled at 25 ºC with a chiller connected to the irradiation plate (as detailed in Chapter 2, Section 2.3.2, Figure 2.14). Then, the irradiation was stopped and the crude reaction mixture was analyzed by NMR to infer the diastereomeric ratio. The crude mixture was purified by column chromatography on silica gel to furnish the product **15** in the stated yield and enantiomeric purity.

Characterization Data

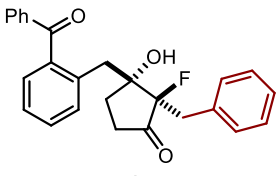

15c

(2*R*, 3*R*)-3-(2-benzoylbenzyl)-2-benzyl-2-fluoro-3-hydroxycyclopentan-1-one (15c). The title compound **15c** was prepared according to the general procedure using 2-benzyl-2-fluorocyclopentane-1,3-dione **14d** (20.6 mg, 0.1 mmol, 1 equiv), 2-methylbenzophenone **2a** (54 µL, 0.3 mmol, 3 equiv), and the organocatalyst **K** (11.6 mg, 0.02 mmol, 20 mol%). Time of irradiation: 30 hours. The crude mixture was purified by flash column chromatography (98:2 hexane/acetone) to afford the title compound **15c** as a white foam (35.9 mg, 89% yield, 90% ee, average of two runs) and as a single diastereoisomer (dr > 20:1, as inferred by ^{1}H NMR and ^{19}F NMR analysis of the crude mixture). The enantiomeric excess was determined by UPC^2 analysis on a Daicel Chiralpak AMY1 column: gradient from 100% CO_2 to 60:40 CO_2: *i*PrOH over 5 minutes, curve 6, flow rate: 2 mL/min, λ= 250 nm, τ_{major}= 4.79 min (90% ee),

τ_{minor}= 5.68 min. $[\alpha]_D^{26}$ = + 190.7 (c = 1.8 in $CHCl_3$). Absolute configuration determined in comparison to compound **15e**. HRMS calculated for $[C_{26}H_{23}FO_3+Na]^+$: 425.1523; found: 425.1533.

^{1}H NMR (500 MHz, $CDCl_3$) δ: 7.80 – 7.75 (m, 2H), 7.69 – 7.63 (m, 1H), 7.49 (ddd, *J* = 8.8, 7.5, 1.6 Hz, 3H), 7.38 – 7.27 (m, 5H), 7.08 – 6.98 (m, 3H), 6.21 (s, 1H), 3.40 (dd, *J* = 18.7, 15.1 Hz, 1H), 3.24 (dd, *J* = 30.3, 15.1 Hz, 1H), 2.80 (d, *J* = 14.2 Hz, 1H), 2.66 (dd, *J* = 14.2, 2.2 Hz, 1H), 2.47 – 2.42 (m, 2H), 2.25 (m, 1H), 1.89 – 1.82 (m, 1H). **^{13}C NMR (125 MHz, $CDCl_3$)** δ: 211.5 (d, *J* = 16.6 Hz), 200.2, 138.5, 137.5, 136.6, 135.1 (d, *J* = 2.2 Hz), 134.1, 132.9, 131.3 (d, *J* = 1.6 Hz, x2), 131.3 (x2), 131.2, 130.8, 128.6 (x2), 127.9 (x2), 126.6, 126.0, 97.9 (d, *J* = 188.1 Hz), 79.2 (d, *J* = 22.6 Hz), 36.6 (d, *J* = 3.4 Hz), 33.6 (d, *J* = 20.9 Hz), 32.8, 31.4. **^{19}F NMR decoupled ^{1}H (376 MHz, $CDCl_3$)** δ: -164.66.

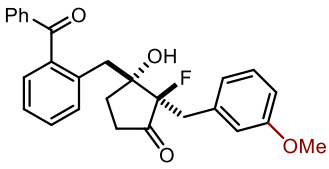

15d

(2*R*, 3*R*)-3-(2-benzoylbenzyl)-2-fluoro-3-hydroxy-2-(3-methoxybenzyl) cyclopentan-1-one (15d). The title compound **15d** was prepared according to the general procedure using 2-fluoro-2-(3-methoxybenzyl)cyclopentane-1,3-dione **14e** (23.6 mg, 0.1 mmol, 1 equiv), 2-methylbenzophenone **2a** (54 µL, 0.3 mmol, 3 equiv), and the organocatalyst **K** (11.6 mg, 0.02 mmol, 20 mol%). Time of irradiation: 72 hours. The crude mixture was purified by flash column chromatography (98:2 hexane/EtOAc,) to afford the title compound **15d** as a white foam (37.1 mg, 85% yield, 89% ee, average of two runs) and as a single diastereoisomer (dr > 20:1, as inferred by ^{1}H NMR and ^{19}F NMR analysis of the crude mixture). The enantiomeric excess was determined by UPC[2] analysis on a Daicel Chiralpak AMY1 column: gradient from 100% CO_2 to 60:40 CO_2:*i*PrOH over 5 minutes, curve 6, flow rate: 2 mL/min, λ= 250 nm, τ_{major}= 4.95 min (89% ee), τ_{minor}= 5.80 min. $[\alpha]_D^{26}$ = +131.0 (c = 1.2 in $CHCl_3$). Absolute configuration determined in comparison to compound **15e**. HRMS calculated for $[C_{27}H_{25}FO_4+Na]^+$: 455.1629; found: 455.1627.

^{1}H NMR (500 MHz, $CDCl_3$) δ: 7.78 – 7.74 (m, 2H), 7.68 – 7.63 (m, 1H), 7.51-7.47 (m, 3H), 7.37 (dd, *J* = 7.8, 1.5 Hz, 3H), 7.33 – 7.28 (m, 3H), 6.98 – 6.90 (m, 3H), 6.57 (dt, *J* = 7.0, 2.5 Hz, 1H), 6.28 (s, 1H), 3.61 (s, 3H), 3.39 (dd, *J* = 17.9, 15.1 Hz, 2H), 3.21 (dd, *J* = 31.3, 15.1 Hz, 1H), 2.84 (d, *J* = 14.2 Hz, 2H), 2.69 (dd, *J* = 14.2, 2.1 Hz, 1H), 2.45 (ddd, *J* = 8.7, 6.6, 1.9 Hz, 1H), 2.25 (qd, *J* = 9.6, 4.1 Hz, 1H), 1.88 – 1.81 (m, 1H). **^{13}C NMR (100 MHz, $CDCl_3$)** δ: 211.5 (d, *J* = 16.5 Hz), 200.2, 159.3, 138.4, 137.6, 136.8, 136.7 (d, *J* = 1.8 Hz), 134.0, 133.0, 131.3, 131.1, 128.8, 128.5, 126.0, 123.7 (d, *J* = 1.5 Hz), 116.6 (d, *J* = 1.7 Hz), 113.4, 112.4, 97.9 (d, *J* = 187.8 Hz), 79.3 (d, *J* = 22.5 Hz), 55.1, 36.6 (d, *J* = 3.1 Hz), 33.6 (d, *J* = 20.7 Hz), 32.8, 31.5. **^{19}F NMR decoupled ^{1}H (376 MHz, $CDCl_3$)** δ: -164.10.

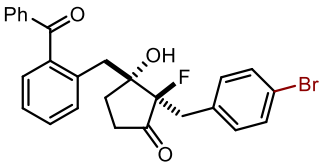

15e

(2*R*, 3*R*)-3-(2-benzoylbenzyl)-2-fluoro-2-(4-bromobenzyl)-3-hydroxycyclopentan-1-one (15e). The title compound **15e** was prepared according to the general procedure using 2-fluoro-2-(4-bromobenzyl)cyclopentane-1,3-dione **14f** (28.5 mg, 0.1 mmol, 1 equiv), 2-methylbenzophenone **2a** (54 µL, 0.3 mmol, 3 equiv), and the organocatalyst **K** (11.6 mg, 0.02 mmol, 20 mol%). Time of irradiation: 72 hours. The crude mixture was purified by flash column chromatography (gradient from 100% to 90:10, hexane: EtOAc) to afford the title compound **15e** as a white foam (35.0 mg, 73% yield, 84% ee, average of two runs) and as a single diastereoisomer (dr > 20:1, as inferred by ^{1}H NMR and ^{19}F NMR analysis of the crude mixture). The enantiomeric excess was determined by UPC^2 analysis on a Daicel Chiralpak AMY1 column: gradient from 100% CO_2 to 60:40 CO_2:*i*PrOH over 5 minutes, curve 6, flow rate: 2 mL/min, λ= 250 nm, τ_{major}= 5.06 min (84% ee), τ_{minor}= 6.03 min. $[\alpha]_D^{26}$ = +210.0 (c = 1.2 in $CHCl_3$). HRMS calculated for $[C_{26}H_{22}BrF_2O_3+Na]^+$: 503.0629; found: 503.0634.

^{1}H NMR (500 MHz, $CDCl_3$) δ: 7.79 – 7.75 (m, 2H), 7.70 – 7.65 (m, 1H), 7.55 – 7.47 (m, 3H), 7.39 – 7.29 (m, 3H), 7.24 – 7.13 (m, 4H), 6.24 (s, 1H), 3.34 (dd, *J* = 18.9, 15.2 Hz, 1H), 3.18 (dd, *J* = 30.1, 15.2 Hz, 1H), 2.77 – 2.65 (m, 2H), 2.45 (ddd, *J* = 8.7, 6.6, 1.9 Hz, 2H), 2.31 – 2.20 (m, 1H), 1.94 – 1.84 (m, 1H). **^{13}C NMR (125 MHz, $CDCl_3$)** δ: 211.3 (d, *J* = 16.5 Hz), 200.4, 138.5, 137.4, 136.4, 134.3, 134.2 (d, *J* = 1.6 Hz), 133.0 (d, *J* = 1.5 Hz, x2), 132.8, 131.2, 131.2 (x2), 131.0 (x2), 130.7, 128.7 (x2), 126.1, 120.7, 97.5 (d, *J* = 187.6 Hz), 79.1 (d, *J* = 22.5 Hz), 36.7 (d, *J* = 3.0 Hz), 32.9 (d, *J* = 20.8 Hz), 32.9, 31.7. **^{19}F NMR decoupled ^{1}H (376 MHz, $CDCl_3$)** δ: -164.47.

*The absolute configuration for **15e** was unambiguously inferred by anomalous dispersion X-ray crystallographic analysis (CCDC 1552622), see X-ray Crystallographic Data section.*

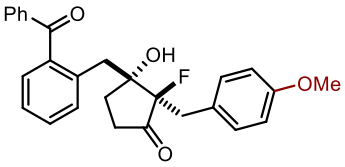

15f

(2*R*, 3*R*)-3-(2-benzoylbenzyl)-2-fluoro-3-hydroxy-2-(4-methoxybenzyl) cyclopentan-1-one (15f). The title compound **15f** was prepared according to the general procedure using 2-fluoro-2-(4-methoxybenzyl)cyclopentane-1,3-dione **14g** (23.6 mg, 0.1 mmol, 1 equiv), 2-methylbenzophenone **2a** (54 µL, 0.3 mmol, 3 equiv), and the organocatalyst **K** (11.6 mg, 0.02 mmol, 20 mol%). Time of irradiation: 50 hours. The crude mixture was purified by flash column chromatography (toluene: acetone, 99:1) to afford the title compound **15f** as a white foam (30.9 mg, 71% yield, 89% ee, average of two runs) and as a single diastereoisomer (dr > 20:1, as inferred by ^{1}H NMR and ^{19}F NMR analysis of the crude mixture). The enantiomeric excess was determined by UPC^2 analysis on a Daicel Chiralpak

AMY1 column: gradient from 100% CO_2 to 60:40 CO_2:*i*PrOH over 5 minutes, curve 6, flow rate: 2 mL/min, λ= 250 nm, τ_{major}= 4.96 min (89% ee), τ_{minor}= 5.98 min. $[\alpha]_D^{26}$ = +178.5 (c = 1.0 in $CHCl_3$). Absolute configuration determined in comparison to compound **15e**. HRMS calculated for $[C_{27}H_{25}FO_4+Na]^+$: 455.1629; found: 455.1644.

^{1}H NMR (500 MHz, $CDCl_3$) δ: 7.81 – 7.76 (m, 2H), 7.68 – 7.63 (m, 1H), 7.53 – 7.46 (m, 3H), 7.38 – 7.23 (m, 5H), 6.60 – 6.54 (m, 2H), 6.21 (s, 1H), 3.51 (s, 3H), 3.35 (dd, *J* = 18.1, 15.3 Hz, 1H), 3.18 (dd, *J* = 31.7, 15.2 Hz, 1H), 2.75 (d, *J* = 14.3 Hz, 1H), 2.64 (dd, *J* = 14.3, 2.2 Hz, 1H), 2.44 (ddd, *J* = 8.9, 6.3, 1.6 Hz, 2H), 2.25 (ddd, *J* = 13.2, 9.5, 4.1 Hz, 1H), 1.90 – 1.81 (m, 1H). **^{13}C NMR (125 MHz, $CDCl_3$)** δ: 211.7 (d, *J* = 16.4 Hz), 200.1, 158.3, 138.4, 137.5, 136.7, 134.0, 132.9, 132.2, 131.3, 131.2, 130.7, 128.6, 127.0, 125.9, 113.4, 97.9 (d, *J* = 187.1 Hz), 79.2 (d, *J* = 22.5 Hz), 55.0, 36.6 (d, *J* = 3.3 Hz), 32.9, 32.7 (d, *J* = 21.1 Hz), 31.5. **^{19}F NMR decoupled ^{1}H (376 MHz, $CDCl_3$)** δ: -164.39.

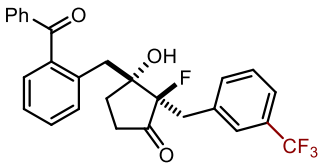

15g

(2*R*, 3*R*)-3-(2-benzoylbenzyl)-2-fluoro-3-hydroxy-2-(3-(trifluoromethyl)benzyl)-3-hydroxycyclopentan-1-one (15g). The title compound **15g** was prepared according to the general procedure using 2-fluoro-2-(3-trifluorofluorobenzyl)cyclopentane-1,3-dione **14h** (27.4 mg, 0.1 mmol, 1 equiv), 2-methylbenzophenone **2a** (54 µL, 0.3 mmol, 3 equiv), and the organocatalyst **K** (11.6 mg, 0.02 mmol, 20 mol%). Time of irradiation: 50 hours. The crude mixture was purified by flash column chromatography (99:1 toluene/ acetone) to afford the title compound **15g** as a white foam (38.6 mg, 82% yield, 87% ee, average of two runs) and as a single diastereoisomer (dr > 20:1, as inferred by ^{1}H NMR and ^{19}F NMR analysis of the crude mixture). The enantiomeric excess was determined by UPC^2 analysis on a Daicel Chiralpak AMY1 column: gradient from 100% CO_2 to 60:40 CO_2:*i*PrOH over 5 minutes, curve 6, flow rate: 2 mL/min, λ= 250 nm, τ_{major}= 4.02 min (87% ee), τ_{minor}= 4.54 min. $[\alpha]_D^{26}$ = + 168.7 (c = 1.2 in $CHCl_3$). Absolute configuration determined in comparison to compound **15e**. HRMS calculated for $[C_{27}H_{22}F_4O_3+Na]^+$: 493.1397; found: 493.1394.

^{1}H NMR (500 MHz, $CDCl_3$) δ: 7.78 – 7.74 (m, 2H), 7.69 – 7.61 (m, 2H), 7.57 (d, *J* = 7.8 Hz, 1H), 7.54 – 7.47 (m, 3H), 7.40 (dd, *J* = 7.8, 1.4 Hz, 1H), 7.36 – 7.30 (m, 3H), 7.19 (t, *J* = 7.8 Hz, 1H), 6.41 (s, 1H), 3.45 (dd, *J* = 19.6, 15.2 Hz, 1H), 3.31 (dd, *J* = 27.7, 15.1 Hz, 1H), 2.86 (d, *J* = 14.0 Hz, 1H), 2.73 (dd, *J* = 14.1, 2.3 Hz, 1H), 2.47 (ddd, *J* = 8.5, 6.5, 1.9 Hz, 2H), 2.33 – 2.21 (m, 1H), 1.94 – 1.85 (m, 1H). **^{13}C NMR (125 MHz, $CDCl_3$)** δ: 211.1 (d, *J* = 16.5 Hz), 200.4, 138.2, 137.5, 136.6, 136.3 (d, *J* = 2.0 Hz), 134.8, 134.1, 132.9, 131.5, 131.4, 131.3, 130.3 (d, *J* = 32.1 Hz), 128.6, 128.3, 128.0 – 127.8 (m), 126.1, 123.5 (d, *J* = 3.9 Hz), 97.4 (d, *J* = 187.8 Hz), 79.1 (d, *J* = 22.5 Hz), 36.7 (d, *J* = 3.0 Hz), 33.2 (d, *J* = 20.6 Hz), 32.9, 31.7. **^{19}F NMR decoupled ^{1}H (376 MHz, $CDCl_3$)** δ: -62.76 (-CF_3), -164.64.

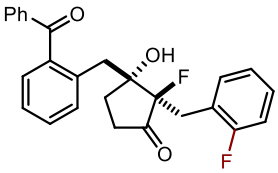

15h

(2*R*, 3*R*)-3-(2-benzoylbenzyl)-2-fluoro-2-(2-fluorobenzyl)-3-hydroxycyclopentan-1-one (15h). The title compound **15h** was prepared according to the general procedure using 2-fluoro-2-(2-fluorobenzyl)cyclopentane-1,3-dione **14i** (22.4 mg, 0.1 mmol, 1 equiv), 2-methylbenzophenone **2a** (54 µL, 0.3 mmol, 3 equiv), and the organocatalyst **K** (11.6 mg, 0.02 mmol, 20 mol%). Time of irradiation: 72 hours. The crude mixture was purified by flash column chromatography (toluene: acetone, 99:1) to afford the title compound **15h** as a white foam (30.6 mg, 76% yield, 86% ee, average of two runs) and as a single diastereoisomer (dr > 20:1, as inferred by ^{1}H NMR and ^{19}F NMR analysis of the crude mixture). The enantiomeric excess was determined by UPC^2 analysis on a Daicel Chiralpak AMY1 column: gradient from 100% CO_2 to 60:40 CO_2:*i*PrOH over 5 minutes, curve 6, flow rate: 2 mL/min, λ= 250 nm, τ_{major}= 4.98 min (86% ee), τ_{minor}= 5.61 min. $[\alpha]_D^{26}$ = +130.1 (c = 1.0 in $CHCl_3$). Absolute configuration determined in comparison to compound **15e**. HRMS calculated for $[C_{26}H_{22}F_2O_3+Na]^+$: 443.1429; found: 443.1430.

^{1}H NMR (500 MHz, $CDCl_3$) δ: 7.82 – 7.76 (m, 2H), 7.68 – 7.61 (m, 1H), 7.57 – 7.52 (m, 1H), 7.52 – 7.46 (m, 2H), 7.45 – 7.38 (m, 2H), 7.38 – 7.31 (m, 2H), 7.17 – 7.08 (m, 1H), 7.01 – 6.89 (m, 2H), 6.15 (s, 1H), 3.53 – 3.30 (m, 2H), 3.13 (d, *J* = 14.2 Hz, 1H), 2.77 – 2.70 (m, 1H), 2.56 (m, 1H), 2.43 (ddd, *J* = 19.4, 9.5, 4.8 Hz, 1H), 2.30 (dtd, *J* = 13.0, 9.0, 3.8 Hz, 1H), 1.95 (ddd, *J* = 14.0, 9.8, 4.8 Hz, 1H). **^{13}C NMR (100 MHz, $CDCl_3$)** δ: 210.8 (d, *J* = 17.1 Hz), 200.2, 162.9, 160.4, 138.4, 137.6, 136.6, 134.0, 133.4 (dd, *J* = 4.0, 1.5 Hz), 132.9, 131.4, 131.3, 128.7, 128.6, 128.6, 126.2, 123.8 (d, *J* = 3.6 Hz), 122.0 (dd, *J* = 15.5, 1.7 Hz), 115.2, 115.0, 99.0 (d, *J* = 193.6 Hz), 79.2 (d, *J* = 21.0 Hz), 36.1 (d, *J* = 4.9 Hz), 32.5, 30.4, 27.4 (dd, *J* = 22.5, 2.6 Hz). **^{19}F NMR decoupled ^{1}H (376 MHz, $CDCl_3$)** δ: -115.80 (d, *J* = 8.8 Hz, Ar), -169.63 (d, *J* = 7.5 Hz).

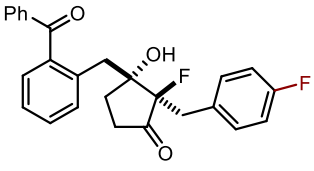

15i

(2*R*, 3*R*)-3-(2-benzoylbenzyl)-2-fluoro-2-(4-fluorobenzyl)-3-hydroxycyclopentan-1-one (15i). The title compound **15i** was prepared according to the general procedure using 2-fluoro-2-(4-fluorobenzyl)cyclopentane-1,3-dione **14j** (22.4 mg, 0.1 mmol, 1 equiv), 2-methylbenzophenone **2a** (54 µL, 0.3 mmol, 3 equiv), and the organocatalyst **K** (11.6 mg, 0.02 mmol, 20 mol%). Time of irradiation: 50 hours. The crude mixture was purified by flash column chromatography (toluene: acetone, 99:1) to afford the title compound **15i** as a white foam (35.1 mg, 83% yield, 88% ee, average of two runs) and as a single diastereoisomer (dr > 20:1, as inferred by ^{1}H NMR and ^{19}F NMR analysis of the crude mixture). The enantiomeric excess was determined by UPC^2 analysis on a Daicel Chiralpak AMY1 column: gradient from 100% CO_2 to 60:40 CO_2:*i*PrOH over 5 minutes, curve 6, flow rate: 2 mL/min, λ= 250 nm, τ_{major}= 4.48 min (88%

ee), τ_{minor}= 5.41 min. $[\alpha]_D^{26}$ = +210.8 (c = 1.1 in $CHCl_3$). Absolute configuration determined in comparison to compound **15e**. HRMS calculated for $[C_{26}H_{22}F_2O_3+Na]^+$: 443.1429; found: 443.1432.

^{1}H NMR (500 MHz, $CDCl_3$) δ: 7.77 (d, *J* = 8.3 Hz, 2H), 7.70 – 7.65 (m, 1H), 7.50 (t, *J* = 7.8 Hz, 3H), 7.39 – 7.27 (m, 5H), 6.77 – 6.70 (m, 2H), 6.24 (s, 1H), 3.36 (dd, *J* = 18.9, 15.2 Hz, 1H), 3.22 (dd, *J* = 30.0, 15.2 Hz, 1H), 2.78 (d, *J* = 14.2 Hz, 1H), 2.68 (dd, *J* = 14.2, 2.2 Hz, 1H), 2.45 (ddd, *J* = 8.9, 6.7, 2.0 Hz, 2H), 2.30 – 2.20 (m, 1H), 1.91 – 1.83 (m, 1H).**^{13}C NMR (125 MHz, $CDCl_3$)** δ: 211.4 (d, *J* = 16.6 Hz), 200.4, 161.9 (d, *J* = 244.6 Hz), 138.4, 137.5, 136.5, 134.2, 132.9, 132.7 (dd, *J* = 7.8, 1.5 Hz, x2), 131.3, 131.2 (x2), 130.8, 130.8 (dd, *J* = 3.2, 2.0 Hz), 128.7 (x2), 126.1, 114.7 (d, *J* = 21.1 Hz, x2), 97.6 (d, *J* = 187.3 Hz), 79.1 (d, *J* = 22.5 Hz), 36.7 (d, *J* = 3.2 Hz), 32.9, 32.7 (d, *J* = 20.9 Hz), 31.6. **^{19}F NMR decoupled ^{1}H (376 MHz, $CDCl_3$)** δ: -116.92 (-F, Ar), -164.82.

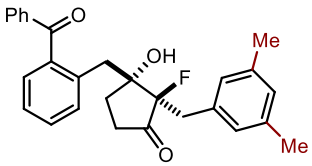

15j

(2*R*, 3*R*)-3-(2-benzoylbenzyl)-2-(3,5-dimethylbenzyl)-2-fluoro-3-hydroxycyclopentan-1-one (15j). The title compound **15j** was prepared according to the general procedure using 2-(3,5-dimethylbenzyl)-2-fluorocyclopentane-1,3-dione **14k** (23.4 mg, 0.1 mmol, 1 equiv), 2-methylbenzophenone **2a** (54 µL, 0.3 mmol, 3 equiv), and the organocatalyst **K** (11.6 mg, 0.02 mmol, 20 mol%). Time of irradiation: 50 hours. The crude mixture was purified by flash column chromatography (gradient from 100% to 99:1, toluene: acetone) to afford the title compound **15j** as a white foam (35.3 mg, 82% yield, 89% ee, average of two runs) and as a single diastereoisomer (dr > 20:1, as inferred by ^{1}H NMR and ^{19}F NMR analysis of the crude mixture). The enantiomeric excess was determined by UPC^2 analysis on a Daicel Chiralpak AMY1 column: gradient from 100% CO_2 to 60:40 CO_2:*i*PrOH over 5 minutes, curve 6, flow rate: 2 mL/min, λ= 250 nm, τ_{major}= 4.59 min (89% ee), τ_{minor}= 5.31 min. $[\alpha]_D^{26}$ = +107.6 (c = 1.2 in $CHCl_3$). Absolute configuration determined in comparison to compound **15e**. HRMS calculated for $[C_{28}H_{27}FO_3+Na]^+$: 453.1836; found: 453.1841.

^{1}H NMR (500 MHz, $CDCl_3$) δ: 7.79 – 7.75 (m, 2H, Ar), 7.67 – 7.61 (m, 1H, Ar), 7.49 (qd, *J* = 7.5, 1.6 Hz, 3H, Ar), 7.40 – 7.28 (m, 3H, Ar), 6.97 (s, 2H), 6.69 (s, 1H), 6.37 (s, 1H, -OH), 3.34 (dd, *J* = 16.8, 15.0 Hz, 1H), 3.19 (dd, *J* = 31.8, 15.0 Hz, 1H), 2.94 (d, *J* = 14.2 Hz, 1H), 2.67 (dd, *J* = 14.2, 2.1 Hz, 1H), 2.45 (ddd, *J* = 9.2, 6.5, 2.3 Hz, 2H), 2.30 – 2.21 (m, 1H), 2.05 (s, 6H, -CH_3 x2), 1.89 – 1.81 (m, 1H). **^{13}C NMR (125 MHz, $CDCl_3$)** δ: 211.6 (d, *J* = 16.6 Hz), 200.1, 138.3, 137.7, 137.4 (x2), 137.1, 134.9 (d, *J* = 1.9 Hz), 133.9, 133.0, 131.3 (x2), 131.3 (x2), 129.2 (d, *J* = 1.0 Hz, x2), 128.5 (x2), 128.3, 125.9, 97.8 (d, *J* = 187.4 Hz), 79.3 (d, *J* = 22.5 Hz), 36.6 (d, *J* = 3.1 Hz), 33.1 (d, *J* = 20.9 Hz), 32.8, 31.4, 21.1 (-CH_3, x2). **^{19}F NMR decoupled ^{1}H (376 MHz, $CDCl_3$)** δ: -164.14.

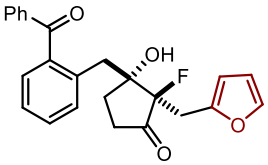

15k

(2*R*, 3*R*)-3-(2-benzoylbenzyl)-2-fluoro-2-(furan-2-ylmethyl)-3-hydroxycyclopentan-1-one (15k). The title compound **15k** was prepared according to the general procedure using 2-fluoro-2-(furan-2-ylmethyl)cyclopentane-1,3-dione **14l** (19.6 mg, 0.1 mmol, 1 equiv), 2-methylbenzophenone **2a** (54 µL, 0.3 mmol, 3 equiv), and the organocatalyst **K** (11.6 mg, 0.02 mmol, 20 mol%). Time of irradiation: 50 hours. The crude mixture was purified by flash column chromatography (gradient from 100% to 99:1, toluene: acetone) to afford the title compound **15k** as a white foam (30.9 mg, 78% yield, 88% ee, average of two runs) and as a single diastereoisomer (dr > 20:1, as inferred by ^{1}H NMR and ^{19}F NMR analysis of the crude mixture). The enantiomeric excess was determined by UPC^2 analysis on a Daicel Chiralpak AMY1 column: gradient from 100% CO_2 to 60:40 CO_2:*i*PrOH over 5 minutes, curve 6, flow rate: 2 mL/min, λ= 250 nm, τ_{major}= 4.55 min (87% ee), τ_{minor}= 5.36 min. $[\alpha]_D^{26}$ = +333.7 (c = 0.8 in $CHCl_3$). Absolute configuration determined in comparison to compound **15e**. HRMS calculated for $[C_{24}H_{21}FO_4+Na]^+$: 415.1316; found: 415.1314.

^{1}H NMR (500 MHz, $CDCl_3$) δ: 7.81 – 7.77 (m, 2H), 7.68 – 7.62 (m, 1H), 7.54 – 7.46 (m, 3H), 7.35 (dtd, *J* = 24.6, 7.7, 1.4 Hz, 3H), 7.12 (d, *J* = 2.3 Hz, 1H), 6.21 (d, *J* = 3.1 Hz, 1H), 6.09 (dd, *J* = 3.2, 1.9 Hz, 1H), 6.07 (s, 1H), 3.44 – 3.25 (m, 2H), 2.88 – 2.75 (m, 2H), 2.49 – 2.43 (m, 2H), 2.30 – 2.20 (m, 1H), 1.90 – 1.83 (m, 1H). **^{13}C NMR (125 MHz, $CDCl_3$)** δ: 210.9 (d, *J* = 16.3 Hz), 200.0, 149.3 (d, *J* = 3.6 Hz), 141.5, 138.5, 137.5, 136.5, 134.0, 132.9, 131.2 (x2), 131.2, 130.8, 128.6 (x2), 126.1, 110.5, 109.4, 97.0 (d, *J* = 188.5 Hz), 78.8 (d, *J* = 22.0 Hz), 36.0 (d, *J* = 3.3 Hz), 32.9, 31.4, 26.5 (d, *J* = 22.8 Hz). **^{19}F NMR decoupled ^{1}H (376 MHz, $CDCl_3$)** δ: -164.15.

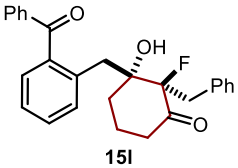

15l

(2*R*, 3*R*)-3-(2-benzoylbenzyl)-2-benzyl-2-fluoro-3-hydroxycyclohexan-1-one (15l). The title compound **15l** was prepared according to the general procedure using 2-fluoro-2-benzyl-2-fluorocyclohexane-1,3-dione **14m** (22.0 mg, 0.1 mmol, 1 equiv), 2-methylbenzophenone **2a** (54 µL, 0.3 mmol, 3 equiv), and the organocatalyst **K** (11.6 mg, 0.02 mmol, 20 mol%). Time of irradiation: 120 hours. The crude mixture was purified by flash column chromatography (*first purification:* gradient from 100% to 99:1 toluene/acetone; *second purification*: gradient from 100% to 90:10 hexane/EtOAc) to afford the title compound **15l** as a white foam (8.2 mg, 20% yield, 26% ee, average of two runs) and as a single diastereoisomer (dr > 20:1, as inferred by ^{1}H NMR and ^{19}F NMR analysis of the crude mixture). The enantiomeric excess was determined by UPC^2 analysis on a Daicel Chiralpak AMY1 column: gradient from 100% CO_2 to 60:40 CO_2:*i*PrOH

over 5 minutes, curve 6, flow rate: 2 mL/min, λ= 250 nm, τ_{major}= 5.82 min (26% ee), τ_{minor}= 6.29 min. HRMS calculated for $[C_{27}H_{25}FO_3+Na]^+$: 439.1680; found: 439.1677.

^{1}H NMR (500 MHz, $CDCl_3$) δ: 7.79 – 7.75 (m, 2H), 7.65 – 7.60 (m, 1H), 7.53 (td, *J* = 7.5, 1.5 Hz, 1H), 7.49 – 7.45 (m, 2H), 7.41 (dd, *J* = 8.0, 1.5 Hz, 1H), 7.36 – 7.27 (m, 4H), 7.25 – 7.17 (m, 3H), 6.22 (s, 1H), 3.68 (t, *J* = 14.8 Hz, 1H), 3.50 – 3.34 (m, 2H), 2.70 (d, *J* = 14.2 Hz, 1H), 2.59 – 2.51 (m, 2H), 2.18 – 2.10 (m, 1H), 2.09 – 2.00 (m, 1H), 2.00 – 1.84 (m, 2H). **^{13}C NMR (125 MHz, $CDCl_3$)** δ: 200.2, 190.1 (d, *J* = 67.2 Hz), 138.5, 137.6, 136.7, 135.0, 133.8, 132.8, 131.1 (x2), 131.1 (x2), 130.2 (d, *J* = 1.8 Hz), 129.5, 128.4 (x2), 128.2 (x2), 126.8, 125.9, 89.6 (d, *J* = 208.1 Hz), 79.4 (d, *J* = 20.5 Hz), 38.8, 37.2 (d, *J* = 22.7 Hz), 35.1 (d, *J* = 7.2 Hz), 32.0 (d, *J* = 3.2 Hz), 20.4. **^{19}F NMR decoupled ^{1}H (376 MHz, $CDCl_3$)** δ: -169.85.

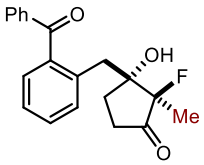

15m

(2*R*, 3*R*)-3-(2-benzoylbenzyl)-2-methyl-2-fluoro-3-hydroxycyclopentan-1-one (15m). The title compound **15m** was prepared according to the general procedure using 2-fluor-2-methylcyclopentane-1,3-dione **14b** (13.0 mg, 0.1 mmol, 1 equiv), 2-methylbenzophenone **2a** (54 µL, 0.3 mmol, 3 equiv), and the organocatalyst **K** (11.6 mg, 0.02 mmol, 20 mol%). Time of irradiation: 14 hours. The crude mixture was purified by flash column chromatography (gradient from 90:10 to 80:20 hexane/EtOAc) to afford the major diastereoisomer of **15m** as a white foam (12.8 mg, 40% yield, 90% ee, average of two runs). The diastereoisomeric ratio (d.r. = 5.5:1) was inferred by ^{19}F NMR analysis of the crude mixture. The enantiomeric excess was determined for the *major diastereoisomer* by UPC^2 analysis on a Daicel Chiralpak AMY1 column: gradient from 100% CO_2 to 60:40 CO_2: *i*PrOH over 5 minutes, curve 6, flow rate: 2 mL/min, λ= 250 nm, τ_{major}= 3.94 min (90% ee), τ_{minor}= 4.36 min. $[\alpha]_D^{26}$ = + 165.2 (c = 0.6 in $CHCl_3$). Absolute configuration determined in comparison to compound **15e**. HRMS calculated for $[C_{20}H_{19}FO_3+Na]^+$: 349.1210; found: 349.1203.

^{1}H NMR (400 MHz, $CDCl_3$) δ: 7.82 – 7.76 (m, 2H), 7.68 – 7.62 (m, 1H), 7.60 – 7.51 (m, 1H), 7.52 – 7.41 (m, 4H), 7.35 (td, *J* = 7.5, 1.3 Hz, 1H), 5.91 (d, *J* = 1.7 Hz, 1H), 3.26 (d, *J* = 13.9 Hz, 1H), 2.99 (dd, *J* = 13.9, 2.7 Hz, 1H), 2.53 – 2.37 (m, 2H), 2.28 (m, 1H), 2.08 – 1.98 (m, 1H), 1.50 (d, *J* = 24.0 Hz, 3H). **^{13}C NMR (125 MHz, $CDCl_3$)** δ: 211.9 (d, *J* = 16.9 Hz), 200.4, 138.1, 137.8, 137.0, 134.0, 132.7, 131.6, 131.5, 131.3 (x2), 128.6 (x2), 126.1, 97.6 (d, *J* = 178.0 Hz), 78.4 (d, *J* = 22.4 Hz), 36.4 (d, *J* = 2.4 Hz), 33.1, 31.9, 12.2 (d, *J* = 23.7 Hz). **^{19}F NMR decoupled ^{1}H (376 MHz, $CDCl_3$)** δ: -157.03.

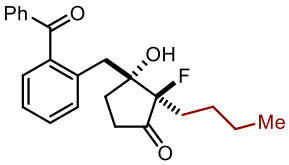

15n

(2*R*, 3*R*)-3-(2-benzoylbenzyl)-2-butyl-2-fluoro-3-hydroxycyclopentan-1-one (15n). The title compound **15n** was prepared according to the general procedure using 2-butyl-2-fluorocyclopentane-1,3-dione **14c** (17.2 mg, 0.1 mmol, 1 equiv), 2-methylbenzophenone **2a** (54 µL, 0.3 mmol, 3 equiv), and the organocatalyst **K** (11.6 mg, 0.02 mmol, 20 mol%). Time of irradiation: 48 hours. The crude mixture was purified by flash column chromatography (gradient from 100% to 90:10 hexane/EtOAc) to afford the title compound **15n** as a white foam (27.6 mg, 75% yield, 89% ee, average of two runs), in a distereomeric ratio = 19:1 (as inferred by ^{1}H NMR and ^{19}F NMR analysis of the crude mixture). The enantiomeric excess of the *major diastereoisomer* was determined by UPC^2 analysis on a Daicel Chiralpak AMY1 column: gradient from 100% CO_2 to 60:40 CO_2: *i*PrOH over 5 minutes, curve 6, flow rate: 2 mL/min, λ= 250 nm, τ_{major}= 4.18 min (88% ee), τ_{minor}= 5.14 min. $[\alpha]_D^{26}$ = + 135.3 (c = 0.9 in $CHCl_3$). Absolute configuration determined in comparison to compound **15e**. HRMS calculated for $[C_{23}H_{25}FO_3+Na]^+$: 391.1680; found: 391.1686.

^{1}H NMR (400 MHz, $CDCl_3$) δ: 7.79 (dd, *J* = 8.3, 1.4 Hz, 2H), 7.67 – 7.61 (m, 1H), 7.55 (td, *J* = 7.5, 1.5 Hz, 1H), 7.52 – 7.45 (m, 2H), 7.42 (ddd, *J* = 11.7, 7.9, 1.1 Hz, 2H), 7.35 (td, *J* = 7.5, 1.3 Hz, 1H), 5.91 (s, 1H), 3.31 (d, *J* = 14.0 Hz, 1H), 2.86 (dd, *J* = 14.0, 2.2 Hz, 1H), 2.48 – 2.38 (m,2H), 2.27 (dtd, *J* = 13.0, 8.9, 3.6 Hz, 1H), 2.04 – 1.86 (m, 3H), 1.73 – 1.58 (m, 1H), 1.52 (ddd, *J* = 10.8, 8.6, 5.6 Hz, 1H), 1.44 – 1.32 (m, 2H), 0.92 (t, *J* = 7.3 Hz, 3H). **^{13}C NMR (125 MHz, $CDCl_3$)** δ: 212.3 (d, *J* = 17.3 Hz), 200.3, 138.2, 137.8, 137.0, 133.9, 132.8, 131.5, 131.4, 131.3 (x2), 128.6 (x2), 126.1, 99.4 (d, *J* = 187.1 Hz), 79.2 (d, *J* = 22.0 Hz), 36.4 (d, *J* = 4.4 Hz), 33.1, 31.0, 27.8 (d, *J* = 22.6 Hz), 24.5 (d, *J* = 5.9 Hz), 23.6, 14.1. **^{19}F NMR decoupled ^{1}H (376 MHz, $CDCl_3$)** δ: -170.71.

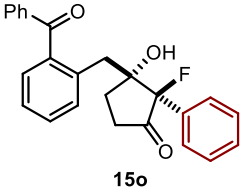

15o

(2*R*, 3*R*)-3-(2-benzoylbenzyl)-2-fluoro-2-phenyl-3-hydroxycyclopentan-1-one (15o). The title compound **15o** was prepared according to the general procedure using 2-fluoro-3-phenylcyclopentane-1,3-dione **14n** (17.2 mg, 0.1 mmol, 1 equiv), 2-methylbenzophenone **2a** (54 µL, 0.3 mmol, 3 equiv), and the organocatalyst **K** (11.6 mg, 0.02 mmol, 20 mol%). Time of irradiation: 40 hours. The crude mixture was purified by flash column chromatography (gradient from 100% to 90:10 hexane/EtOAc) to afford the title compound **15o** as a white foam (9.3 mg, 24% yield, 92% ee, average of two runs), and as a single diastereoisomer (dr > 20:1, as inferred by ^{1}H NMR and ^{19}F NMR analysis of the crude mixture). The enantiomeric excess was determined by UPC^2 analysis on a Daicel Chiralpak IA column: gradient from 100% CO_2 to 60:40 CO_2:*i*PrOH over 5 minutes, curve 6, flow rate: 3 mL/min, λ= 250 nm,

τ_{major}= 4.51 min (92% ee), τ_{minor}= 5.37 min. $[\alpha]_D^{26}$ = + 155.4 (c = 0.3 in $CHCl_3$). Absolute configuration determined in comparison to compound **15e**. HRMS calculated for $[C_{25}H_{21}FO_3+Na]^+$: 411.1367; found: 411.1367.

^{1}H NMR (400 MHz, $CDCl_3$) δ: 7.62 – 7.58 (m, 3H), 7.57 – 7.51 (m, 1H), 7.47 – 7.39 (m, 8H), 7.37 – 7.30 (m, 2H), 5.50 (d, *J* = 2.0 Hz, 1H), 3.13 (dd, *J* = 13.8, 2.9 Hz, 1H), 2.92 (d, *J* = 13.8 Hz, 1H), 2.72 – 2.64 (m, 2H), 2.55 – 2.42 (m, 1H), 2.17 – 2.06 (m, 1H). **^{13}C NMR (100 MHz, $CDCl_3$)** δ 210.5 (d, *J* = 15.9 Hz), 199.2, 138.0, 137.3, 136.2, 133.5, 132.4, 131.8 (d, *J* = 21.3 Hz), 130.9 (d, *J* = 28.6 Hz, x2), 130.9 (x2), 128.5, 128.3 (x2), 127.6 (x2), 127.5, 125.9, 98.7 (d, *J* = 182.5 Hz), 79.4 (d, *J* = 24.4 Hz), 36.1 (d, *J* = 1.6 Hz), 34.0, 31.7. **^{19}F NMR decoupled ^{1}H (376 MHz, $CDCl_3$)** δ: -160.0.

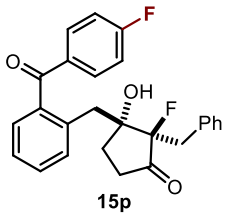

15p

(2*R*, 3*R*)-2-benzyl-2-fluoro-3-(2-(4-fluorobenzoyl)benzyl)-3-hydroxycyclopentan-1-one (15p). The title compound **15p** was prepared according to the general procedure using 2-benzyl-2-fluorocyclopentane-1,3-dione **14d** (20.6 mg, 0.1 mmol, 1 equiv), 4-fluorophenyl(*o*-tolyl)methanone **2d** (47 µL, 0.3 mmol, 3 equiv), and the organocatalyst **K** (11.6 mg, 0.02 mmol, 20 mol%). Time of irradiation: 50 hours. The crude mixture was purified by flash column chromatography (gradient from 100% to 99:1 toluene/acetone) to afford the title compound **15p** as a white foam (35.9 mg, 82% yield, 89% ee, average of two runs) and as a single diastereoisomer (dr > 20:1, as inferred by ^{1}H NMR and ^{19}F NMR analysis of the crude mixture). The enantiomeric excess was determined by UPC^2 analysis on a Daicel Chiralpak AMY1 column: gradient from 100% CO_2 to 60:40 CO_2: *i*PrOH over 5 minutes, curve 6, flow rate: 2 mL/min, λ= 250 nm, τ_{major}= 4.60 min (89% ee), τ_{minor}= 5.35 min. $[\alpha]_D^{26}$ = + 258.5 (c = 1.3 in $CHCl_3$). Absolute configuration determined in comparison to compound **15e**. HRMS calculated for $[C_{26}H_{22}F_2O_3+Na]^+$: 443.1431; found: 443.1429.

^{1}H NMR (500 MHz, $CDCl_3$) δ: 7.84 – 7.79 (m, 2H), 7.50 (td, *J* = 7.3, 2.0 Hz, 1H), 7.36 – 7.29 (m, 5H), 7.17 (t, *J* = 8.6 Hz, 2H), 7.09 – 6.98 (m, 3H), 6.09 (s, 1H), 3.40 (dd, *J* = 18.5, 15.1 Hz, 1H), 3.23 (dd, *J* = 30.9, 15.1 Hz, 1H), 2.75 (d, *J* = 14.2 Hz, 1H), 2.65 (dd, *J* = 14.3, 2.1 Hz, 1H), 2.48 – 2.41 (m, 2H), 2.29 – 2.19 (m, 1H), 1.87 – 1.80 (m, 1H). **^{13}C NMR (125 MHz, $CDCl_3$)** δ: 211.4 (d, *J* = 16.6 Hz), 198.5, 166.4 (d, *J* = 257.1 Hz), 138.2, 136.6, 135.1 (d, *J* = 1.7 Hz), 134.0 (d, *J* = 9.6 Hz, x2), 133.8 (d, *J* = 2.9 Hz), 133.0, 131.3 (x2), 130.5, 128.0 (x2), 126.6, 126.1, 115.9 (d, *J* = 22.0 Hz, x2), 97.9 (d, *J* = 188.0 Hz), 79.2 (d, *J* = 22.6 Hz), 36.6 (d, *J* = 3.4 Hz), 33.6 (d, *J* = 21.0 Hz), 32.8, 31.4. **^{19}F NMR decoupled ^{1}H (376 MHz, $CDCl_3$)** δ: -103.22 (Ar), -164.48.

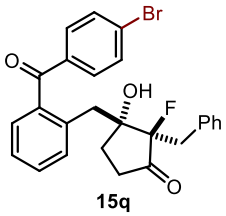

15q

(2*R*, 3*R*)-2-benzyl-2-fluoro-3-(2-(4-bromobenzoyl)benzyl)-3-hydroxycyclopentan-1-one (15q). The title compound **15q** was prepared according to the general procedure using 2-benzyl-2-fluorocyclopentane-1,3-dione **14d** (20.6 mg, 0.1 mmol, 1 equiv), 4-bromophenyl(*o*-tolyl)methanone **2e** (51 µL, 0.3 mmol, 3 equiv), and the organocatalyst **K** (11.6 mg, 0.02 mmol, 20 mol%). Time of irradiation: 30 hours. The crude mixture was purified by flash column chromatography (gradient from 100% to 99:1 toluene/ acetone) to afford the title compound **15q** as a white foam (42.3 mg, 88% yield, 90% ee, average of two runs) and as a single diastereoisomer (dr > 20:1, as inferred by ^{1}H NMR and ^{19}F NMR analysis of the crude mixture). The enantiomeric excess was determined by UPC^2 analysis on a Daicel Chiralpak IA column: gradient from 100% CO_2 to 60:40 CO_2: *i*PrOH over 5 minutes, curve 6, flow rate: 2 mL/min, λ= 250 nm, τ_{major}= 4.99 min (90% ee), τ_{minor}= 5.65 min. $[\alpha]_D^{26}$ = + 60.5 (c = 1.2 in $CHCl_3$). Absolute configuration determined in comparison to compound **15e**. HRMS calculated for $[C_{26}H_{22}BrFO_3+Na]^+$: 503.0629; found: 503.0626.

^{1}H NMR (500 MHz, $CDCl_3$) δ: 7.66 (s, 4H), 7.53 (ddd, *J* = 7.5, 6.5, 2.5 Hz, 1H), 7.38 – 7.31 (m, 5H), 7.12 – 7.04 (m, 3H), 6.00 (s, 1H), 3.43 (dd, *J* = 18.5, 15.1 Hz, 1H), 3.25 (dd, *J* = 30.9, 15.1 Hz, 1H), 2.78 (d, *J* = 14.2 Hz, 1H), 2.68 (dd, *J* = 14.2, 2.2 Hz, 1H), 2.50 – 2.44 (m, 2H), 2.31 – 2.20 (m, 1H), 1.88 – 1.82 (m, 1H). **^{13}C NMR (125 MHz, $CDCl_3$)** δ: 211.4 (d, *J* = 16.5 Hz), 199.0, 137.9, 136.8, 136.2, 135.1 (d, *J* = 1.9 Hz), 133.0, 132.6 (x2), 132.0 (x2), 131.4, 131.3 (d, *J* = 1.2 Hz, x2), 130.7, 129.5, 128.0 (x2), 126.7, 126.1, 97.9 (d, *J* = 187.9 Hz), 79.3 (d, *J* = 22.5 Hz), 36.6 (d, *J* = 3.5 Hz), 33.6 (d, *J* = 21.0 Hz), 32.8, 31.4. **^{19}F NMR decoupled ^{1}H (376 MHz, $CDCl_3$)** δ: -164.35.

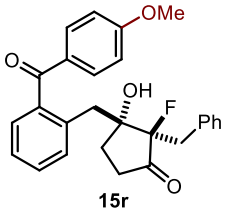

15r

(2*R*, 3*R*)-2-benzyl-2-fluoro-3-(2-(4-methoxybenzoyl)benzyl)-3-hydroxycyclopentan-1-one (15r). The title compound **15r** was prepared according to the general procedure using 2-benzyl-2-fluorocyclopentane-1,3-dione **14d** (20.6 mg, 0.1 mmol, 1 equiv), 4-methoxyphenyl(*o*-tolyl)methanone **2f** (47 µL, 0.3 mmol, 3 equiv), and the organocatalyst **K** (11.6 mg, 0.02 mmol, 20 mol%). Time of irradiation: 50 hours. The crude mixture was purified by flash column chromatography (*first purification*: gradient from 100% to 99:1 toluene/acetone; *second purification*: gradient from 100% to 90:10 hexane/EtOAc) to afford the title compound **15r** as a white foam (22.0 mg, 53% yield, 93% ee, average of two runs) and as a single diastereoisomer (dr > 20:1, as inferred by ^{1}H NMR and ^{19}F NMR analysis of the crude mixture). The enantiomeric excess was determined by UPC^2 analysis on a Daicel Chiralpak AMY1 column: gradient from 100% CO_2 to 60:40 CO_2: *i*PrOH over 5 minutes, curve 6, flow rate: 2 mL/min, λ= 290 nm, τ_{major}= 5.18

min (93% ee), τ_{minor}= 6.18 min. $[\alpha]_D^{26}$ = + 163.9 (c = 0.7 in $CHCl_3$). Absolute configuration determined in comparison to compound **15e**. HRMS calculated for $[C_{27}H_{25}FO_4+Na]^+$: 455.1629; found: 455.1629.

^{1}H NMR (500 MHz, $CDCl_3$) δ: 7.78 (d, *J* = 8.8 Hz, 2H), 7.51 – 7.44 (m, 1H), 7.35 (dq, *J* = 6.7, 2.2 Hz, 3H), 7.32 – 7.27 (m, 2H), 7.09 – 7.00 (m, 3H), 6.99 – 6.94 (m, 2H), 6.45 (s, 1H), 3.92 (s, 3H), 3.40 (dd, *J* = 18.4, 15.1 Hz, 1H), 3.24 (dd, *J* = 30.6, 15.1 Hz, 1H), 2.77 (s, 1H), 2.63 (dd, *J* = 14.2, 2.2 Hz, 1H), 2.44 (ddd, *J* = 8.0, 6.5, 1.6 Hz, 2H), 2.32 – 2.18 (m, 1H), 1.91 – 1.81 (m, 1H). **^{13}C NMR (125 MHz, $CDCl_3$)** δ: 211.6 (d, *J* = 16.5 Hz), 198.6, 164.5, 138.8, 136.2, 135.2 (d, *J* = 1.9 Hz), 133.8 (x2), 132.7, 131.3 (d, *J* = 1.2 Hz, x2), 130.7, 130.3, 130.1, 127.9 (x2), 126.5, 125.9, 113.9 (x2), 98.0 (d, *J* = 187.9 Hz), 79.0 (d, *J* = 22.5 Hz), 55.8, 36.6 (d, *J* = 3.2 Hz), 33.5 (d, *J* = 21.0 Hz), 32.9, 31.5. **^{19}F NMR decoupled ^{1}H (376 MHz, $CDCl_3$)** δ: -164.84.

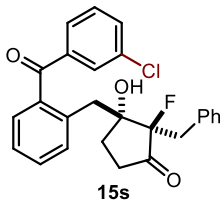

15s

(2*R*, 3*R*)-2-benzyl-3-(2-(3-chlorobenzoyl)benzyl)-2-fluoro-3-hydroxycyclopentan-1-one (15s). The title compound **15s** was prepared according to the general procedure using 2-benzyl-2-fluorocyclopentane-1,3-dione **14d** (20.6 mg, 0.1 mmol, 1 equiv), 3-chlorophenyl(*o*-tolyl)methanone **2g** (64 µL, 0.3 mmol, 3 equiv), and the organocatalyst **K** (11.6 mg, 0.02 mmol, 20 mol%). Time of irradiation: 48 hours. The crude mixture was purified by flash column chromatography (*first purification*: gradient from 100% to 99:1 toluene/acetone; *second purification*: gradient from 100% to 90:10 hexane/EtOAc) to afford the title compound **15s** as a white foam (28.7 mg, 67% yield, 82% ee, average of two runs) and as a single diastereoisomer (dr > 20:1, as inferred by ^{1}H NMR and ^{19}F NMR analysis of the crude mixture). The enantiomeric excess was determined by UPC^2 analysis on a Daicel Chiralpak AMY1 column: gradient from 100% CO_2 to 60:40 CO_2: *i*PrOH over 5 minutes, curve 6, flow rate: 2 mL/min, λ= 250 nm, τ_{major}= 4.99 min (82% ee), τ_{minor}= 5.70 min. $[\alpha]_D^{26}$ = + 104.1 (c = 1.0 in $CHCl_3$). Absolute configuration determined in comparison to compound **15e**. HRMS calculated for $[C_{26}H_{22}ClFO_3+Na]^+$: 459.1132; found: 459.1134.

^{1}H NMR (500 MHz, $CDCl_3$) δ: 7.76 (t, *J* = 1.9 Hz, 1H), 7.65 – 7.61 (m, 2H), 7.54 – 7.50 (m, 1H), 7.44 (t, *J* = 7.9 Hz, 1H), 7.36 – 7.31 (m, 5H), 7.09 (dd, *J* = 8.2, 6.4 Hz, 2H), 7.06 – 7.01 (m, 1H), 5.88 (s, 1H), 3.40 (dd, *J* = 18.7, 15.1 Hz, 1H), 3.23 (dd, *J* = 30.7, 15.1 Hz, 1H), 2.77 (d, *J* = 14.2 Hz, 1H), 2.67 (dd, *J* = 14.3, 2.1 Hz, 1H), 2.45 (ddd, *J* = 11.9, 6.5, 2.6 Hz, 2H), 2.29 – 2.16 (m, 1H), 1.87 – 1.79 (m, 1H). **^{13}C NMR (125 MHz, $CDCl_3$)** δ: 211.2 (d, *J* = 16.6 Hz), 198.6, 139.0, 137.7, 136.7, 134.9 (d, *J* = 1.8 Hz), 134.8, 133.8, 132.9, 131.4, 131.1 (d, *J* = 1.3 Hz, x2), 130.8, 130.6, 129.8, 129.2, 127.9 8 (x2), 126.5, 126.1, 97.8 (d, *J* = 188.1 Hz),

79.2 (d, *J* = 22.5 Hz), 36.5 (d, *J* = 3.3 Hz), 33.5 (d, *J* = 21.0 Hz), 32.7, 31.3. **^{19}F NMR decoupled ^{1}H (376 MHz, $CDCl_3$)** δ: -164.30.

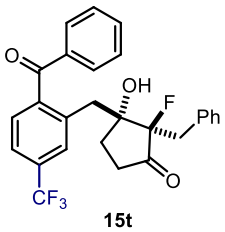

15t

(2*R*, 3*R*)- 3-(2-benzoyl-5-(trifluoromethyl)benzyl)-2-benzyl-2-fluoro-3-hydroxycyclopentan-1-one (15t). The title compound **15t** was prepared according to the general procedure using 2-benzyl-2-fluorocyclopentane-1,3-dione **14d** (20.6 mg, 0.1 mmol, 1 equiv), 2-methyl-4-(trifluoromethyl)phenyl)(phenyl)methanone **2h** (64 µL, 0.3 mmol, 3 equiv), and the organocatalyst **K** (11.6 mg, 0.02 mmol, 20 mol%). Time of irradiation: 48 hours. The crude mixture was purified by flash column chromatography (*first purification*: gradient from 100% to 99:1 toluene/acetone; *second purification*: gradient from 100% to 90:10 hexane/EtOAc) to afford the title compound **15t** as a white foam (32.9 mg, 75% yield, 87% ee, average of two runs) and as a single diastereoisomer (dr > 20:1, as inferred by ^{1}H NMR and ^{19}F NMR analysis of the crude mixture). The enantiomeric excess was determined by UPC^2 analysis on a Daicel Chiralpak AMY1 column: gradient from 100% CO_2 to 60:40 CO_2: *i*PrOH over 5 minutes, curve 6, flow rate: 2 mL/min, λ= 250 nm, τ_{major}= 3.96 min (87% ee), τ_{minor}= 4.30 min. $[\alpha]_D^{26}$ = + 131.0 (c = 1.0 in $CHCl_3$). Absolute configuration determined in comparison to compound **15e**. HRMS calculated for $[C_{27}H_{22}F_4O_3+Na]^+$: 493.1397; found: 493.1397.

^{1}H NMR (500 MHz, $CDCl_3$) δ: 7.76 (dd, *J* = 8.3, 1.4 Hz, 2H), 7.71 (tt, *J* = 7.3, 1.3 Hz, 1H), 7.58 (d, *J* = 9.1 Hz, 2H), 7.55 – 7.50 (m, 2H), 7.47 (d, *J* = 7.9 Hz, 1H), 7.34 – 7.29 (m, 2H), 7.05 – 6.94 (m, 3H), 5.65 (s, 1H), 3.41 (dd, *J* = 17.3, 15.2 Hz, 1H), 3.18 (dd, *J* = 32.5, 15.1 Hz, 1H), 2.72 (s, 2H), 2.54 – 2.38 (m, 2H), 2.30 – 2.19 (m, 1H), 1.87 – 1.77 (m, 1H). **^{13}C NMR (100 MHz, $CDCl_3$)** δ: 210.9 (d, *J* = 16.4 Hz), 199.1, 141.8, 137.5, 136.6, 134.9 (d, *J* = 1.7 Hz), 134.8 (x2), 133.4 – 132.1 (q, C_{Ar}-CF_3), 131.2 (x2), 130.4, 129.4 (d, *J* = 3.7 Hz), 128.9 (x3), 128.0 (x2), 126.7, 122.2-130.2 (q, *J* = 272.8 Hz, -CF_3), 123.0 (q, *J* = 3.7 Hz), 97.5 (d, *J* = 187.1 Hz), 79.1 (d, *J* = 22.8 Hz), 36.7 (d, *J* = 3.1 Hz), 33.4 (d, *J* = 20.7 Hz), 32.8, 31.6. **^{19}F NMR decoupled ^{1}H (376 MHz, $CDCl_3$)** δ: -63.16 (-CF_3), -163.38.

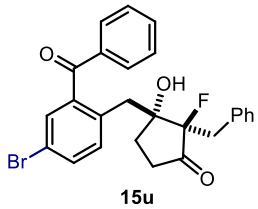

15u

(2*R*, 3*R*)-3-(2-benzoyl-4-bromobenzyl)-2-benzyl-2-fluoro-3-hydroxycyclopentan-1-one (15u). The title compound **15u** was prepared according to the general procedure using 2-benzyl-2-fluorocyclopentane-1,3-dione **14d** (20.6 mg, 0.1 mmol, 1 equiv), (5-bromo-2-methylphenyl)(phenyl)methanone **2i** (82.5 mg, 0.3 mmol, 3 equiv), and the organocatalyst **K** (11.6 mg, 0.02 mmol, 20 mol%). Time of irradiation: 70 hours. The crude mixture was purified by flash column

chromatography (gradient from 100% to 95:5 hexane/EtOAc) to afford the title compound **15u** as a white foam (37.1 mg, 77% yield, 90% ee, average of two runs) and as a single diastereoisomer (dr > 20:1, as inferred by ^{1}H NMR and ^{19}F NMR analysis of the crude mixture). The enantiomeric excess was determined by UPC^2 analysis on a Daicel Chiralpak AMY1 column: gradient from 100% CO_2 to 60:40 CO_2: *i*PrOH over 5 minutes, curve 6, flow rate: 2 mL/min, λ= 250 nm, τ_{major}= 5.10 min (90% ee), τ_{minor}= 5.69 min. $[\alpha]_D^{26}$ = + 215.4 (c = 1.2 in $CHCl_3$). Absolute configuration determined in comparison to compound **15e**. HRMS calculated for $[C_{26}H_{22}BrFO_3+Na]^+$: 503.0622; found: 503.0629.

^{1}H NMR (400 MHz, $CDCl_3$) δ: 7.81 – 7.76 (m, 2H), 7.74 – 7.68 (m, 1H), 7.58 – 7.47 (m, 4H), 7.37 (dt, *J* = 7.9, 1.4 Hz, 2H), 7.31 – 7.24 (m, 1H), 7.12 – 7.01 (m, 3H), 6.03 (s, 1H), 3.44 (dd, *J* = 18.3, 15.1 Hz, 1H), 3.24 (dd, *J* = 31.0, 15.1 Hz, 1H), 2.78 (d, *J* = 14.2 Hz, 1H), 2.66 (dd, *J* = 14.2, 2.1 Hz, 1H), 2.54 – 2.47 (m, 2H), 2.33 – 2.21 (m, 1H), 1.95 – 1.87 (m, 1H). **^{13}C NMR (100 MHz, $CDCl_3$)** δ: 211.1 (d, *J* = 16.5 Hz), 199.2, 139.0, 137.3, 137.1, 135.7, 134.9 (d, *J* = 1.9 Hz), 134.4, 132.0, 131.2 (d, *J* = 1.4 Hz, x2), 131.2 (x2), 129.3, 128.7 (x2), 128.0 (x2), 126.6, 125.9, 97.7 (d, *J* = 187.7 Hz), 79.2 (d, *J* = 22.6 Hz), 36.5 (d, *J* = 3.2 Hz), 33.5 (d, *J* = 20.9 Hz), 32.8, 31.5. **^{19}F NMR decoupled ^{1}H (376 MHz, $CDCl_3$)** δ: -163.98.

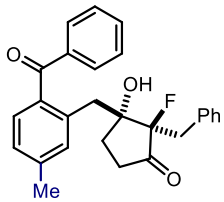

15v

(2*R*, 3*R*)-3-(2-benzoyl-5-methylbenzyl)-2-benzyl-2-fluoro-3-hydroxycyclopentan-1-one (15v). The title compound **15v** was prepared according to the general procedure using 2-benzyl-2-fluorocyclopentane-1,3-dione **14d** (20.6 mg, 0.1 mmol, 1 equiv), (2,4-dimethylphenyl)(phenyl)methanone **2j** (58 µL, 0.3 mmol, 3 equiv), and the organocatalyst **K** (11.6 mg, 0.02 mmol, 20 mol%). Time of irradiation: 50 hours. The crude mixture was purified by flash column chromatography (gradient from 100% to 90:10 hexane/EtOAc) to afford the title compound **15v** as a white foam (27.9 mg, 70% yield, 90% ee, average of two runs) and as a single diastereoisomer (dr > 20:1, as inferred by ^{1}H NMR and ^{19}F NMR analysis of the crude mixture). The enantiomeric excess was determined by UPC^2 analysis on a Daicel Chiralpak AMY1 column: gradient from 100% CO_2 to 60:40 CO_2: *i*PrOH over 5 minutes, curve 6, flow rate: 2 mL/min, λ= 253 nm, τ_{major}= 4.67 min (90% ee), τ_{minor}= 5.52 min. $[\alpha]_D^{26}$ = + 238.5 (c = 0.9 in $CHCl_3$). Absolute configuration determined in comparison to compound **15e**. HRMS calculated for $[C_{27}H_{25}FO_3+Na]^+$: 439.1680; found: 439.1686.

^{1}H NMR (400 MHz, $CDCl_3$) δ: 7.95 – 7.87 (m, 2H), 7.83 – 7.74 (m, 1H), 7.63 (t, *J* = 7.8 Hz, 2H), 7.54 – 7.47 (m, 2H), 7.45 – 7.38 (m, 1H), 7.29 – 7.14 (m, 5H), 6.55 (s, 1H), 3.62 – 3.33 (m, 1H), 3.01 (d, *J* = 14.1 Hz, 1H), 2.77 (dd, *J* = 14.1, 2.2 Hz, 1H), 2.64 – 2.52 (m, 5H, -CH_3 + -CH_2), 2.47 – 2.32 (m, 1H), 2.05 – 1.96 (m, 1H). **^{13}C NMR (100 MHz, $CDCl_3$)** δ: 211.6 (d, *J* = 16.7 Hz), 200.1, 141.9, 137.9, 137.0, 135.6, 135.1 (d, *J* = 2.2 Hz), 133.8, 133.6, 131.5,

131.3 (d, *J* = 1.5 Hz, x2), 131.2 (x2), 128.5 (x2), 127.9 (x2), 126.8, 126.6, 98.1 (d, *J* = 188.4 Hz), 79.2 (d, *J* = 22.3 Hz), 36.5 (d, *J* = 3.4 Hz), 33.7 (d, *J* = 21.2 Hz), 32.9, 31.4, 21.7. **^{19}F NMR decoupled ^{1}H (376 MHz, $CDCl_3$)** δ: -165.00.

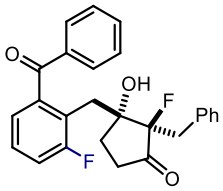

15w

(2*R*, 3*R*)-3-(2-benzoyl-6-fluorobenzyl)-2-benzyl-2-fluoro-3-hydroxycyclopentan-1-one (15w) The title compound **15w** was prepared according to the general procedure using 2-benzyl-2-fluorocyclopentane-1,3-dione **14d** (20.6 mg, 0.1 mmol, 1 equiv), (3-fluoro2-methylphenyl)(phenyl)methanone **2k** (64.3 mg, 0.3 mmol, 3 equiv) and the organocatalyst **K** (11.6 mg, 0.02 mmol, 20 mol%). Time of irradiation: 65 hours. The crude mixture was purified by flash column chromatography (gradient from 100% to 90:10 hexane/EtOAc) to afford the title compound **15w** as a white foam (27.1 mg, 65% yield, 81% ee, average of two runs) and as a single diastereoisomer (dr > 20:1, as inferred by ^{1}H NMR and ^{19}F NMR analysis of the crude mixture). The enantiomeric excess was determined by UPC^2 analysis on a Daicel Chiralpak AMY1 column: gradient from 100% CO_2 to 60:40 CO_2: *i*PrOH over 5 minutes, curve 6, flow rate: 2 mL/min, λ= 250 nm, τ_{major}= 4.55 min (81% ee), τ_{minor}= 5.33 min. $[\alpha]_D^{26}$ = + 140.2 (c = 0.9 in $CHCl_3$). Absolute configuration determined in comparison to compound **15e**. HRMS calculated for $[C_{26}H_{22}F_2O_3+Na]^+$: 443.1429; found: 443.1436.

^{1}H NMR (500 MHz, $CDCl_3$) δ: 7.78 – 7.71 (m, 2H), 7.68 (ddt, *J* = 8.7, 7.3, 1.3 Hz, 1H), 7.54 – 7.46 (m, 2H), 7.36 – 7.25 (m, 4H), 7.18 (dd, *J* = 7.4, 1.5 Hz, 1H), 7.07 – 6.97 (m, 3H), 6.06 (s, 1H), 3.39 (dd, *J* = 19.4, 15.1 Hz, 1H), 3.24 (dd, *J* = 29.4, 15.1 Hz, 1H), 3.00 (dt, *J* = 14.4, 1.7 Hz, 1H), 2.60 (dd, *J* = 14.4, 2.6 Hz, 1H), 2.52 – 2.36 (m, 2H), 2.35 – 2.24 (m, 1H), 1.86 – 1.76 (m, 1H). **^{13}C NMR (125 MHz, $CDCl_3$)** δ: 211.5 (d, *J* = 16.5 Hz), 199.1 (d, *J* = 2.5 Hz), 161.9 (d, *J* = 247.0 Hz), 140.5 (d, *J* = 3.8 Hz), 137.2, 135.0 (d, *J* = 2.1 Hz), 134.4, 131.2, 131.2 (d, *J* = 1.3 Hz), 128.7, 128.0, 127.7 (d, *J* = 8.9 Hz), 126.6, 126.5 (d, *J* = 3.3 Hz), 124.2 (d, *J* = 17.9 Hz), 118.6 (d, *J* = 24.3 Hz), 98.3 (d, *J* = 190.3 Hz), 79.6 (d, *J* = 21.9 Hz), 34.0 (d, *J* = 21.4 Hz), 32.9 (d, *J* = 1.6 Hz), 31.0 (d, *J* = 6.1 Hz), 29.8 (d, *J* = 4.1 Hz). **^{19}F NMR decoupled ^{1}H (376 MHz, $CDCl_3$)** δ: -110.78, -165.03.

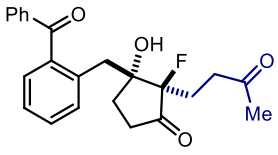

15x

(2*R*, 3*R*)-3-(2-benzoylbenzyl)-2-fluoro-3-hydroxy-2-(3-oxobutyl)cyclopentan-1-one (15x). The title compound **15x** was prepared according to the general procedure using 2-fluoro-2-(3-oxobutyl)cyclopentane-1,3-dione **14o**, 2-methylbenzophenone **2a** (54 µL, 0.3 mmol, 3 equiv) and the organocatalyst **K** (11.6 mg, 0.02 mmol, 20 mol%). Time of irradiation: 24 hours. The crude

mixture was purified by flash column chromatography (gradient from 90:10 to 70:30 hexane/EtOAc) to afford the title compound **15x** as a white foam (28.1 mg, 73% yield, 70% ee, average of two runs) and as a single diastereoisomer (dr > 20:1, as inferred by ^{1}H NMR and ^{19}F NMR analysis of the crude mixture). The enantiomeric excess was determined by UPC^2 analysis on a Daicel Chiralpak IA column: gradient from 100% CO_2 to 60:40 CO_2: *i*PrOH over 5 minutes, curve 6, flow rate: 3 mL/min, λ= 250 nm, τ_{major}= 4.30 min (70% ee), τ_{minor}= 4.64 min. $[\alpha]_D^{26}$ = + 84.7 (c = 0.9 in $CHCl_3$). HRMS calculated for $[C_{23}H_{23}FO_4+Na]^+$: 443.1473; found: 405.1469.

^{1}H NMR (400 MHz, $CDCl_3$) δ: 7.80 – 7.76 (m, 2H), 7.67 – 7.61 (m, 1H), 7.55 (td, *J* = 7.5, 1.5 Hz, 1H), 7.51 – 7.32 (m, 5H), 6.06 – 6.02 (m, 1H), 3.28 (d, *J* = 14.0 Hz, 1H), 2.96 (dt, *J* = 18.3, 7.3 Hz, 1H), 2.87 – 2.79 (m, 1H), 2.72 (dt, *J* = 18.4, 7.1 Hz, 1H), 2.58 – 2.39 (m, 2H), 2.39 – 2.21 (m, 3H), 2.17 (s, 3H), 2.02 – 1.91 (m, 1H). **^{13}C NMR (125 MHz, $CDCl_3$)** δ: 211.5 (d, *J* = 16.5 Hz), 199.1 (d, *J* = 2.5 Hz), 161.9 (d, *J* = 247.0 Hz), 140.5 (d, *J* = 3.8 Hz), 137.2, 135.0 (d, *J* = 2.1 Hz), 134.4, 131.2, 131.2 (d, *J* = 1.3 Hz), 128.7, 128.0, 127.7 (d, *J* = 8.9 Hz), 126.6, 126.5 (d, *J* = 3.3 Hz), 124.2 (d, *J* = 17.9 Hz), 118.6 (d, *J* = 24.3 Hz), 98.3 (d, *J* = 190.3 Hz), 79.6 (d, *J* = 21.9 Hz), 34.0 (d, *J* = 21.4 Hz), 32.9 (d, *J* = 1.6 Hz), 31.0 (d, *J* = 6.1 Hz), 29.8 (d, *J* = 4.1 Hz). **^{19}F NMR decoupled ^{1}H (376 MHz, $CDCl_3$)** δ: -170.56

3.11.5. Product Manipulations: One-pot synthesis of Hajos-Parrish type Ketone 50.

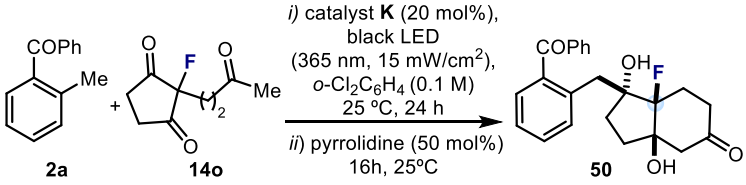

A glass hand-capped vial containing a stirring bar, the organocatalyst **K** (11.6 mg, 0.02 mmol, 20 mol%) and 2-fluoro-2-(3-oxobutyl)cyclopentane-1,3-dione **14o** (19.6 mg, 0.1 mmol, 1 equiv) was closed with a Teflon-coated cap and flushed with argon. Then, degassed 1,2-dichlorobenzene (1 mL) and the 2-methylbenzophenone **2a** (54 µL, 0.3 mmol, 3 equiv) were added under an argon atmosphere. The vial was sealed with parafilm, placed into a single black LED plate (λ= 365 nm, irradiance = 15±1 mW/cm^2) and stirred during 24 hours at 25 ºC (the complete set-up is detailed in Chapter 2, Section 2.3.2, Figure 2.14). Then, the irradiation was stopped, and pyrrolidine (4 µL, 0.05 mmol, 50 mol%) was added to the vial. The reaction mixture was stirred over 16 hours (during this period the reaction becomes dark-brown). The crude reaction mixture was directly purified by flash column chromatography (gradient from 90:10 to 60:40 hexane/EtOAc) to afford the product **50** as a white solid (23.2

mg, 61 % yield, 70% ee) and as a single diastereoisomer (dr > 20:1, as inferred by ^{1}H NMR and ^{19}F NMR analysis of the crude mixture).

The enantioenriched fluorinated 3-hydroxyketone **15x**, generated form the organocatalytic desymmetrization of 2-fluoro-2-(3-oxobutyl) cyclopentane 1,3-dione **14o**, was isolated in 70% ee (see Section 3.11.4 for the characterization data), thus showing that the stereochemical information is fully transmitted throughout the enamine-mediated cyclization step.

Characterization Data

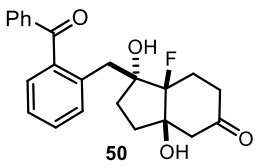

50

(1*R*, 3a*R*, 7a*R*)-1-(2-benzoylbenzyl)-7a-fluoro-1,3a-dihydroxyoctahydro-5H-inden-5-one (50). The enantiomeric excess of **50** was determined by UPC^2 analysis on a Daicel Chiralpak IA column: gradient from 100% CO_2 to 60:40 CO_2: *i*PrOH over 5 minutes, curve 6, flow rate: 3 mL/min, λ= 250 nm, τ_{major}= 5.14 min (70% ee), τ_{minor}= 5.63 min. $[\alpha]_D^{26}$ = + 68.8 (c = 0.7 in $CHCl_3$). HRMS calculated for $[C_{23}H_{23}FO_4+Na]^+$: 405.1473; found: 405.1472.

^{1}H NMR (400 MHz, $CDCl_3$) δ: 7.81 – 7.75 (m, 2H), 7.65 (ddt, *J* = 7.8, 7.0, 1.3 Hz, 1H), 7.55 (td, *J* = 7.5, 1.5 Hz, 1H), 7.52 – 7.45 (m, 3H), 7.41 (dd, *J* = 7.8, 1.5 Hz, 1H), 7.33 (td, *J* = 7.5, 1.3 Hz, 1H), 6.13 (d, *J* = 1.6 Hz, 1H), 3.20 (d, *J* = 13.8 Hz, 1H), 3.05 (dd, *J* = 13.8, 3.6 Hz, 1H), 2.87 – 2.68 (m, 3H), 2.67 – 2.53 (m, 2H), 2.51 – 2.38 (m, 1H), 2.22 (dtd, *J* = 11.2, 5.2, 4.7, 2.7 Hz, 1H), 2.17 – 1.98 (m, 2H), 1.89 (ddt, *J* = 13.9, 9.3, 1.1 Hz, 1H), 1.76 (ddd, *J* = 12.5, 7.9, 1.8 Hz, 1H). **^{13}C NMR (100 MHz, $CDCl_3$)** δ: 210.7, 200.8, 138.0, 137.8, 137.7, 134.1, 132.6, 131.7, 131.4, 131.3, 128.7, 126.1, 104.3 (d, *J* = 187.9 Hz), 82.2 (d, *J* = 25.0 Hz), 80.9 (d, *J* = 16.4 Hz), 51.1 (d, *J* = 2.2 Hz), 37.5 (d, *J* = 3.7 Hz), 37.5, 34.8, 34.0, 23.9 (d, *J* = 25.7 Hz). **^{19}F NMR decoupled ^{1}H (376 MHz, $CDCl_3$)** δ: -164.80.

3.11.6. X-ray Crystallographic Data

Single Crystal X-ray Diffraction Data for the Compound 15e

X-ray structure determinations: Crystals of compound **15e** were obtained dissolving the compound in dichloromethane and storing at room temperature for 1 day.

Data Collection. Measurements were made on a Bruker-Nonius diffractometer equipped with an APPEX 2 4K CCD area detector, a FR591 rotating anode with $Mo_{K\alpha}$ radiation, Montel mirrors and a Cryostream Plus low temperature device (*T* = 100K). Full-sphere data collection was used with ω and φ scans.

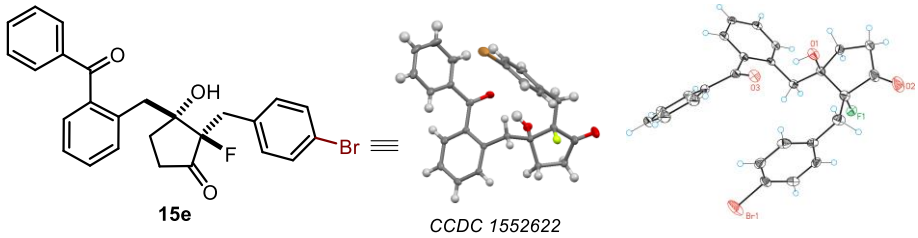

Table 3.7. Crystal data and structure refinement for **15e.** ***CCDC 1552622***

Empirical formula	C26 H22 Br F O3
Formula weight	481.34
Temperature	100(2) K
Wavelength	0.71073 Å
Crystal system	Orthorhombic
Space group	P2(1)2(1)2(1)
Unit cell dimensions	a = 5.7122(3) Å; α= 90°.
	b = 16.4421(7) Å; β = 90°.
	c = 23.2902(8) Å; γ = 90°.
Volume	2187.43(17) $Å^3$
Z	4
Density (calculated)	1.462 Mg/m^3
Absorption coefficient	1.913 mm^{-1}
F(000)	984
Crystal size	0.5 x 0.1 x 0.1 mm^3
Theta range for data collection	2.477 to 28.941°.
Index ranges	-7<=h<=6,-22<=k<=20,-24<=l<=31
Reflections collected	12995
Independent reflections	4857[R (int) = 0.0319]
Completeness to theta =28.941°	89.8%
Absorption correction	Multi-scan
Max. and min. transmission	0.832 and 0.64
Refinement method	Full-matrix least-squares on F^2
Data / restraints / parameters	4857/ 0/ 284
Goodness-of-fit on F^2	1.047
Final R indices [I>2sigma(I)]	R1 = 0.0385, wR2 = 0.0738
R indices (all data)	R1 = 0.0499, wR2 = 0.0767
Flack parameter	x =0.002(5)
Largest diff. peak and hole	0.690 and -0.746 $e.Å^{-3}$

Chapter IV

A Visible-Light Mediated Three-Component Radical Process Using Dithiocarbamate Anion Catalysis

Target

Development of a three component radical process that couples readily available alkyl chlorides, maleimides, and heteroaromatic fragments to rapidly generate complex chiral products with high diastereocontrol.

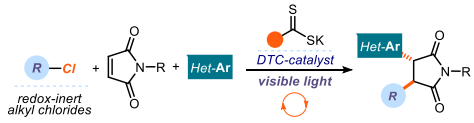

Tool

Use of a dithiocarbamate anion catalyst able to initiate radical processes under redox-neutral conditions.[1]

4.1. Introduction

Multicomponent reactions (MCRs) are important in synthetic chemistry since they can rapidly generate high levels of molecular complexity from simple substrates and in a single step.[2] MCRs have provided a suitable technology to prepare biologically active molecules in a rapid and efficient manner.[3] While chemists have predominantly developed methods based on polar pathways, radical reactivity provides a powerful alternative.[4] Methods to initiate radical MCRs have traditionally required unstable initiators or stoichiometric oxidants or reductants (Figure 4.1).[5] The relatively harsh reaction conditions for generating open-shell intermediates

[1] The project discussed in this chapter has been conducted in collaboration with Dr. Matthew A. Horwitz and Dr. Bertrand Schweitzer-Chaput. This work has been published: Cuadros, S.; Horwitz, M. A.; Schweitzer-Chaput, B.; Melchiorre, P. A Visible-Light Mediated Three Component Process Using Dithiocarbamate Anion Catalysis. *Chem. Sci.* **2019**, *10*, 5484–5488.

[2] Tietze, L. F.; Brasche, G.; Gericke, K. M. Eds.; *Domino Reactions in Organic Synthesis*, Wiley-VCH, Weinheim, 2006.

[3] Dömling, A.; Wang, W.; Wang, K. Chemistry and Biology of Multicomponent Reactions. *Chem. Rev.* **2012**, *112*, 3083–3135.

[4] (a) Studer, A.; Curran, D. P. Catalysis of Radical Reactions: A Radical Chemistry Perspective. *Angew. Chem. Int. Ed.* **2016**, *55*, 58–102. (b) Yan, M.; Lo, J. C.; Edwards, J. T.; Baran, P. S. Radicals: Reactive Intermediates with Translational Potential. *J. Am. Chem. Soc.* **2016**, *138*, 12692–12714. (c) V. Liautard and Y. Landais, Free-radical Multicomponent Processes in *Multicomponent Reactions in Organic Synthesis*, ed. J. Zhu, Q. Wang and M.-X. Wang, Wiley-VCH, **2015**, Ch. 14, pp. 401–438. (d) Godineau, E.; Landais, Y. Radical and Radical-Ionic Multicomponent Processes. *Chem. Eur. J.* **2009**, *15*, 3044–3055.

[5] J. Lalevée and J. P. Fouassier, 'Overview of Radical Initiation', in *Encyclopedia of Radicals in Chemistry, Biology and Materials*, ed. C. Chatgilialoglu and A. Studer, John Wiley & Sons, **2012**, vol. 1, pp. 37–56.

(*i.e.* high temperatures, toxic reagents, or strong redox active reagents) may significantly affect the selectivity and the functional group tolerance of the overall radical cascade processes.

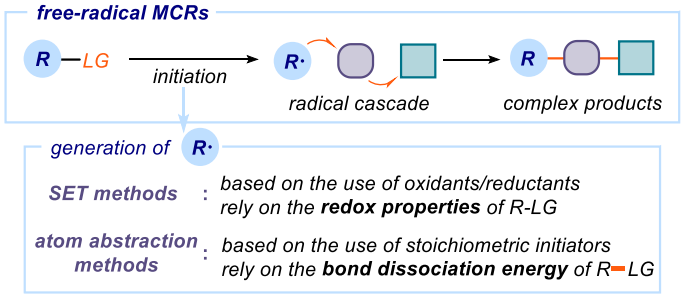

Figure 4.1. Classical radical-generating strategies to initiate free-radical based multicomponent reactions (MCRs) require precursors (R-LG) with suitable redox properties or bond-dissociation energies (BDE).

In the last decade, the field of photoredox catalysis[6] has provided some solutions to these limitations, offering effective tools to trigger radicals MCRs under mild conditions while avoiding the use of stoichiometric metals or harsh atoms abstractors.[7] Photoredox catalysis mainly activates substrates via SET pathways, thus relying on their redox properties.[8] This intrinsic feature poses a voltage-gated limit to the generality of the radical precursors that can be used.

Our laboratory has recently developed a novel photochemical catalytic strategy that harnesses different physical properties of the substrates used as precursors of open-shell intermediates.[9] Specifically, we designed a dithiocarbamate (DTC) anion catalyst able to activate alkyl electrophiles by displacing a variety of leaving groups *via* an S_N2 pathway (Figure 4.2). The resulting photo-absorbing intermediate **I** generates radicals upon excitation by visible-light and homolytic cleavage of the C-S bond. This new catalytic methodology does not rely on the

---

[6] Shaw, M. H.; Twilton, J.; MacMillan, D. W. C. Photoredox Catalysis in Organic Chemistry. *J. Org. Chem.* **2016**, *81*, 6898–6926.

[7] (a) Plesniak, M. P.; Huang, H.-M.; Procter. D. J. Radical Cascade Reactions Triggered by Single Electron Transfer. *Nat. Rev. Chem.* **2017**, *1*, 0077. (b) Sebren, L. J.; Devery, J. J.; Stephenson, C. R. J. Catalytic Radical Domino Reactions in Organic Synthesis. *ACS Catal.* **2014**, *4*, 703–716. (c) S. Garbino, D. Ravelli, S. Protti and A. Basso. Photoinduced Multicomponent Reactions. *Angew. Chem. Int. Ed.* **2016**, 55, 15476–15484.

[8] Roth, H. G.; Romero, N. A.; Nicewicz, D. A. Experimental and Calculated Electrochemical Potentials of Common Organic Molecules for Applications to Single-Electron Redox Chemistry. *Synlett* **2016**, *27*, 714–723.

[9] Schweitzer-Chaput, B.; Horwitz, M. A.; de Pedro Beato, E.; Melchiorre, P. Photochemical Generation of Radicals from Alkyl Electrophiles Using a Nucleophilic Organic Catalyst. *Nat. Chem.* **2019**, *11*, 129–135.

redox properties of the precursors, so it can grant access to radical species from substrates that would be incompatible with or inert to classical radical-generating strategies, including photoredox catalysis.

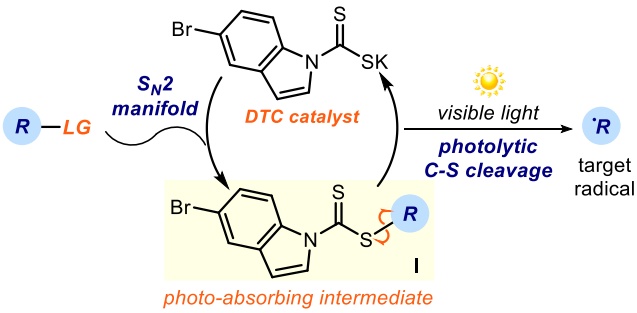

Figure 4.2. Photochemical S_N2-based radical-generation strategy. LG: leaving group.

To better contextualize this recently developed radical generation strategy, the present Chapter will start with a discussion on the existing methodologies for the production of open-shell intermediates. Then, general aspects and the synthetic potential of this new S_N2-based radical-generation method will be detailed. Finally, this Chapter will discuss the successful implementation of this strategy in the design of a MCR that uses redox-inert alkyl chlorides as radical precursors, and redox-sensitive substrates as coupling partners.

4.2. General Overview of Radical Generation Methods

Free-radical chemistry is a powerful tool in synthetic organic chemistry.[10] Open-shell intermediates have enabled access to chemical space that was previously unattainable, and their use has facilitated the design of concise routes to target structures.[11] Advances within the field of free radical chemistry have been spurred by the development of effective and mild radical-generating strategies. The following sections will provide an overview of the four general pathways available for the production of open-shell intermediates.

4.2.1. Methods Based on Atom Abstraction Processes

The generation of radicals has traditionally required the use of stoichiometric amounts of initiators.[5,12] These substrates (represented as *In-In* in Figure 4.3) contain one or several weak

[10] Renaud, P.; Sibi, M. P. (eds) Radicals in Organic Synthesis (Wiley-VCH, Weinheim, Germany, 2001).

[11] (a) Yan, M.; Lo, J. C.; Edwards, J. T.; Baran, P. S. Radicals: Reactive Intermediates with Translational Potential. *J. Am. Chem. Soc.* **2016**, *138*, 12692–12714. (b) Studer, A.; Curran, D. P. Catalysis of Radical Reactions: A Radical Chemistry Perspective. *Angew. Chem. Int. Ed.* **2016**, *55*, 58–102.

[12] Denisov, E. T.; Denisova, T. G.; Pokidova, T. S. *Handbook of Free Radical Initiators*. John Wiley & Sons, **2005**.

bonds with bond dissociation energies (BDE)[13] in the range of 30-50 kcal·mol^{-1}. These bonds can be homolytically cleaved upon heating or irradiation with high-energy light (UV-light), producing free radicals (*In*·). These ensuing reactive species can then abstract a hydrogen or a halogen atom from a substrate, leading to the formation of a radical (R·). Peroxides and azo-compounds (structures shown in the lower panel of Figure 4.3) are commonly used radical initiators (*In-In*). This radical-generating strategy ultimately relies on the *BDE of the substrates* used as precursors of the target radicals.

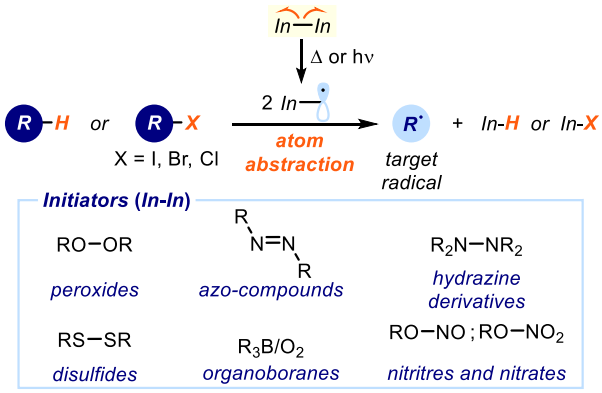

Figure 4.3. The generation of radicals through atom abstraction mechanisms have traditionally required the use of stoichiometric initiators (In-In) and precursors (R-H and R-X) with suitable bond dissociation energies (BDE).

4.2.2. Methods Based on SET Processes

Radicals can be also generated via redox processes, through either the reduction or oxidation of an appropriate precursor (represented as R-Y in Figure 4.4). In such processes, the radical ions formed after a SET event can subsequently fragment to deliver the target radical species (R·).

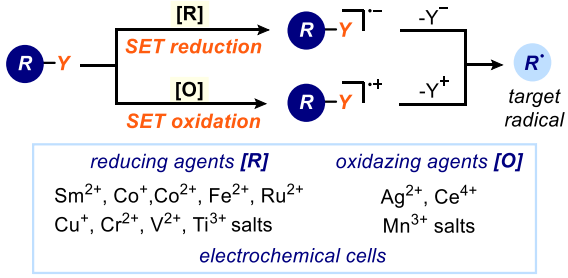

Figure 4.4. The generation of radicals through redox processes requires the use of precursors (R-Y) with suitable redox potentials.

[13] Luo, Y. R. *Handbook of Bond Dissociation Energies in Organic Compounds*. 2002, CRC press.

Stoichiometric amounts of metal salts (typically based on Ce^{4+}, Mn^{3+} or Ag^{2+} for oxidations; and Fe^{2+}, Co^{2+}, Cu^{+}, Cr^{2+} or Ti^{3+} for reductions) have traditionally been used as redox chemical agents. On the other hand, electrochemical methods[14] provide an alternative way to produce open-shell intermediates through SET processes. This approach uses electrodes connected to a power source, which allows the direct application of an electrical potential on the reaction mixture. Here, the SET process with the radical precursors occurs over the surface of the electrodes. In both cases (chemical or electrochemical means), the *redox potential* (E_{redox})[8] of the substrates must be primarily considered when selecting a suitable radical precursor.

4.2.3. Methods Based on Photoredox Catalysis

The advent and development of photoredox catalysis has enormously expanded the conditions by which radical-type reactivity can be accessed.[6] This photochemical method relies on the ability of transition-metal complexes and organic dyes (represented as **PC** in Figure 4.5) to absorb visible-light and reach an electronically excited state (**PC***). The excited photocatalyst (**PC***) can then participate in SET or HAT[15] processes with simple bench-stable substrates, which ultimately leads to the formation of radical intermediates. Therefore, a photoredox catalyst can generate radicals applying both mechanisms discussed above. After the first SET or HAT event, the modified photocatalyst (**PC'**) is turned over to its initial state (**PC**) by means of a secondary SET or HAT process, thus establishing a catalytic regime.[4a]

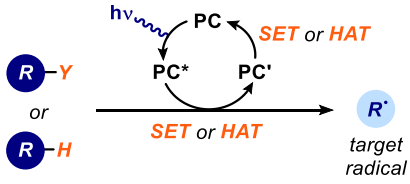

Figure 4.5. Photoredox catalysis enables the mild generation of radicals using substoichiometric amounts of light-activated transition-metal complexes and organic dyes. This radical generation strategy proceeds through single-electron transfer (SET) or hydrogen atom abstraction (HAT) processes with the radical precursors. PC: photocatalyst.

Photoredox catalysis is nowadays a widely used method for developing new radical based-transformations under mild conditions. However, this technology still relies on the redox properties or the BDE of the radical precursors, which limits the repertoire of substrates that can be used when designing new radical-based processes.

---

[14] Yan, M.; Kawamata, Y.; Baran, P. S. Synthetic Organic Electrochemical Methods since 2000: On the Verge of a Renaissance. *Chem. Rev.* **2017**, *117*, 13230–13319.

[15] Tzirakis, M. D.; Lykakis, I. N.; Orfanopoulos, M. Decatungstate as an Efficient Photocatalyst in Organic Chemistry. *Chem. Soc. Rev.* **2009**, *38*, 2609–2621.

4.2.4. Methods Based on the Homolytic Cleavage of Thiocarbonyl Derivatives

A crucial step towards milder and more selective radical-generating methods has been the use of substrates bearing thiocarbonyl groups.[16] In the early 80's, Barton and collaborators[17] identified *N*-hydroxypyridine-2-thione esters **3** as a versatile source of open-shell intermediates (Figure 4.6). These substrates, commonly known as *Barton esters*, are easily obtained from the corresponding carboxylic acids or acyl chlorides (**1**) and the commercially available *N*-hydroxy-2-thiopyridone **2** or its sodium salt.

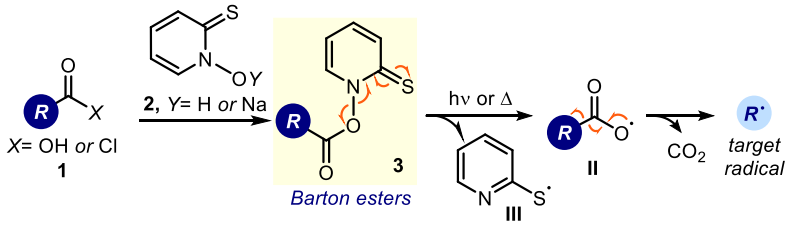

Figure 4.6. The thermolysis or photolysis of *N*-hydroxypyridine-2-thione esters **3**, synthesized from carboxylic acids or acid chlorides (**1**) and *N*-hydroxy-2-thiopyridone (**2**), enables a mild and selective generation of radicals.

Barton esters contain a weak N-O bond[17c] that can be homolytically cleaved at room temperature by UV-visible light irradiation. This is because these substrates (**3**) exhibit an absorption profile matching the emission spectra of common UV-visible lamps (*e.g.* Hg or Xe lamps, compact fluorescent bulbs, LEDs, etc).[18] For example, the computed BDE of the N-O bond in substrate **3**, where R = Me, is 28.2 kcal·mol^{-1}.[19] The energy of one mole of photons at λ = 365 nm is 78.7 kcal (obtained through the equation $E \cdot N_A = h \cdot c \cdot \lambda^{-1}$, where N_A is the Avogadro constant, 6.0223x10^{23}; *h* is the Planck's constant, 6.63x10^{-34} J·s; and *c* the speed of light, 3x10^{8} m·s^{-1}). This energy value is large enough for breaking the N-O bond of one mole

[16] Crich, D.; Quintero, L. Radical Chemistry Associated with the Thiocarbonyl Group. *Chem. Rev.* **1989**, *89*, 1413–1432.

[17] (a) Barton, D. H. R.; Crich, D.; Motherwell, W. B. New and Improved Methods for the Radical Decarboxylation of Acids. *J. Chem. Soc., Chem. Commun.* **1983**, 939–941. (b) Barton, D. H. R.; Hervé, Y.; Potier, P.; Thierry, J. Reductive Radical Decarboxylation of Amino-Acids and Peptides. *J. Chem. Soc., Chem. Commun.* **1984**, 1298–1299. (c) Barton, D. H. R.; Crich, D.; Motherwell, W. B. The Invention of New Radical Chain Reactions. Part VII. Radical Chemistry of Thiohydroxamic Esters: A New Method for the Generation of Carbon Radicals from Carboxylic Acids. *Tetrahedron* **1985**, *41*, 3901–3924.

[18] (a) Barton, D. H. R.; Blundell, P.; Jaszberenyi, J. C. Quantum Yields in the Photochemically Induced Radical Chemistry of Acyl Derivatives of Thiohydroxamic Acids. *J. Am. Chem. Soc.* **1991**, *113*, 6937–6942. (b) Barton, D. H. R.; Jaszberenyl, J. C.; Tang, D. Photolytic Generation of Carbon Radicals from Barton Esters: Recent Developments. *Tetrahedron Lett.* **1993**, *34*, 3381–3384.

[19] For computational details, see: Allonas, X.; Dietlin, C.; Fouassier, J.-P.; Casiraghi, A.; Visconti, M.; Norcini, G.; Bassi, G. Barton Esters as New Radical Photoinitiators for Flat Panel Display Applications. *J. Photopolym. Sci. Technol.* **2008**, *21*, 505–509.

of **3**. The cleavage of the N-O bond in **3** furnishes an acyloxy radical **II**, which rapidly decarboxylates to afford the target radical **R**·, and the 2-pyridylthiyl radical **III**.[20] **R**· can undergo radical combination with **III**, affording the corresponding pyridyl sulfide,[18b] or can be captured by a radical-trapping agent in inter- or intra-molecular manner.[21] An intra-molecular trapping implies that the structure of the carboxylic acid derivative **1** contains a tethered radical-trapping fragment (*e.g.* an alkene or alkyne). The homolytic cleavage of the N-O bond in **3** can also be induced directly upon heating, or through the addition of a thiophilic radical (*e.g.* $R_3Sn^{\cdot}$, $RS^{\cdot}$) to the sulfur of the thiocarbonyl function within **3** (Figure 4.7). [16]

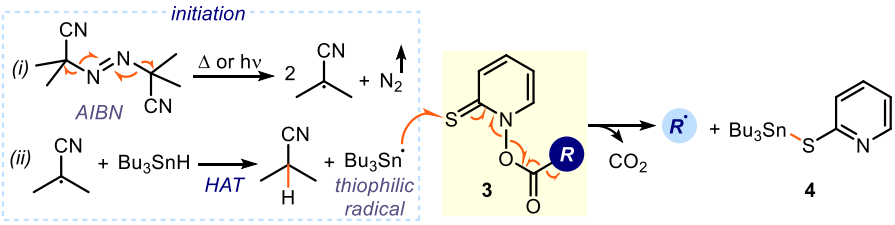

Figure 4.7. The homolytic cleavage of the weak N-O bond of Barton esters **3** can be induced through the addition of tiophilic radicals, such as $Bu_3Sn^{\cdot}$, to the C=S bond in **3**. AIBN: azobisisobutyronitrile; HAT: hydrogen atom transfer.

Overall, this radical generation strategy has enabled the design of radical-based bond forming processes using carboxylic acids or derivatives (**1**) as starting materials.

Xanthates (**7** in Figure 4.8a) and related derivatives (*e.g.* dithiocarbamates: R_2N-C(=S)-SR') are another class of thiocarbonyl-based substrates that enable the controlled production of radicals.[22] These compounds, popularized by Zard in the late 1980s,[23] are easily synthesized by displacement of a suitable leaving group in **5** with the commercially available potassium *O*-ethyl xanthate **6**.

---

[20] Bohne, C.; Boch, R.; Scaiano, J. C. Exploratory Studies of the Photochemistry of *N*-hydroxypyridine-2-thione Esters. Generation of Excited Radicals by Laser Flash Photolysis and in a Conventional Fluorescence Spectrometer. *J. Org. Chem.* **1990**, *55*, 5414–5418.

[21] (a) Barton, D. H. R.; Crich, D.; Kretzschmar, G. Formation of Carbon-Carbon Bonds with Radicals Derive From Esters of Thiohydroxamic Acids. *Tetrahedron Lett.* **1984**, *25*, 1055–1058. (b) Newcomb, M.; Deeb, T. M. *N*-Hydroxypyridine-2-thione Carbamates as Aminyl and Aminium Radical Precursors. Cyclizations for Synthesis of the Pyrrolidine Nucleus. *J. Am. Chem. Soc.* **1987**, *109*, 3163–3165. (c) Saraiva, M. F.; Couri, M. R. C.; Le Hyaric, M.; de Almeida, M. V. The Barton Ester Free-Radical Reaction: A Brief Review of Applications. *Tetrahedron* **2009**, 65, 3563–3572.

[22] (a) Zard, S. Z. Xanthates and Related Derivatives as Radical Precursors. In *Encyclopedia of Radicals in Chemistry, Biology and Materials*. John Wiley & Sons, Ltd. **2012**. (b) Zard, S. Z. On the Trail of Xanthates: Some New Chemistry from an Old Functional Group. *Angew. Chem. Int. Ed.* **1997**, *36*, 672–685. (c) Quiclet-Sire, B.; Zard, S. Z. Powerful Carbon-Carbon Bond Forming Reactions Based on a Novel Radical Exchange Process. *Chem. Eur. J.* **2006**, *12*, 6002–6016.

[23] Delduc, P.; Tailhan, C.; Zard, S. Z. A Convenient Source of Alkyl and Acyl Radicals. *J. Chem. Soc., Chem. Commun.* **1988**, 308–310.

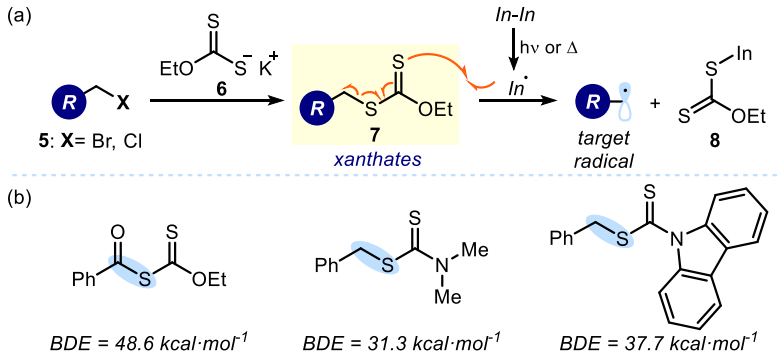

Figure 4.8. (a) Xanthates allow the generation of open-shell intermediates under mild conditions. *In-In* represents an initiator. (b) Computed bond dissociation energies (BDE) of some selected dithiocarbonyl compounds.

The radical generation process generally requires the use of initiators, such as peroxides or diazo derivatives. Specifically, the radical addition of the initiator *In*• to the sulfur of the thiocarbonyl bond in **7** triggers the homolytic cleavage of the weak C-S bond within the xanthate **7**. The BDE of some selected dithiocarbonyl compounds[24] are shown in Figure 4.8b. The presence of the radical initiator *In-In* is not always needed in stoichiometric amount.[22c] This is because xanthates **7** are usually involved in radical chain propagation processes (refer to Figure 4.9).

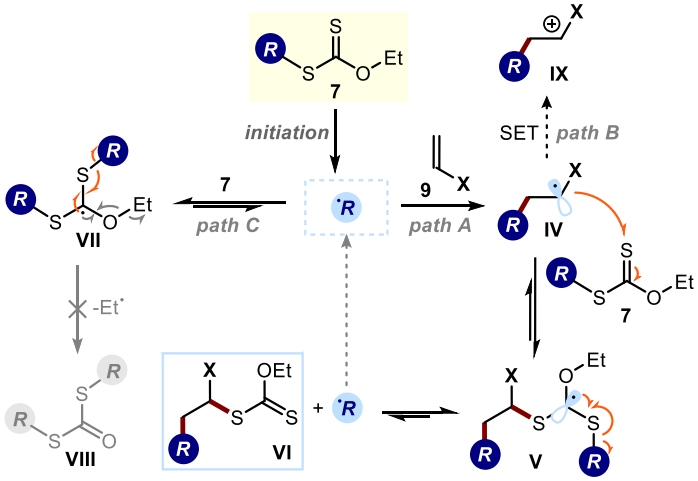

Figure 4.9. General manifold of reactions for the generation and capture of radicals from xanthates **7** (xanthate-transfer process).

[24] Lalevée, J.; Blanchard, N.; El-Roz, M.; Allonas, X.; Fouassier, J. P. New Photoiniferters: Respective Role of the Initiating and Persistent Radicals. *Macromolecules* **2008**, *41*, 2347–2352.

In this regard, the first addition of a radical species (**R·**) generated from **7** to a radical trap (*e.g* an alkene **9**, *path A* in Figure 4.9) generates the open-shell intermediate **IV**, which can be captured reversibly by another molecule of xanthate **7**, producing the intermediate **V**. Reversible collapse of this species furnishes the final group transfer adduct **VI** and another molecule of the target radical **R·** to propagate the chain. One thermodynamic requirement must be fulfilled for having an efficient group transfer propagation in xanthate chemistry: the adduct radical **IV** has to be less stable than the propagating radical **R·**. This condition ensures that radical **V** will preferentially collapse in favor of the regeneration of **R·**, thus allowing the chain to be sustained with the simultaneous formation of the group-transfer product **VI**. However, xanthates **7** are not always involved in classical radical chain processes. In some cases, the radical intermediate **IV** can be oxidized by a peroxide leading to a crossover from radical to polar manifolds (*path B* in Figure 4.9). In such reaction pathways, stoichiometric amounts of the peroxide, which behaves both as an initiator and terminal oxidant, are required. An interesting aspect of the use of xanthates **7** as radical sources is the type of *degenerative* mechanism in which the ensuing radicals are involved.[22] This is illustrated in *path C* of Figure 4.9. After the initiation step, the target radical **R·** is rapidly trapped by another molecule of the starting xanthate **7** to give adduct **VII**. This radical cannot easily undergo a β-scission of the Et-O bond, since it would lead to a high-energy ethyl radical together with the symmetrical dithiocarbonate **VIII** (fragmentation represented with grey arrows). Therefore, the cleavage of one the two C-S bonds becomes much favored, which returns the system back to **R·** and the starting xanthate **7** (equilibrium arrow in *path C*, Figure 4.9). The very fast addition-fragmentation provides a degenerate process that does not cause any macroscopic change in the system but it constantly regenerates **R·**, thus increasing its effective lifetime in the reaction medium. By using this particular manner to prolong the existence of a target radical, xanthates of type **7** have allowed radical additions to unactivated alkenes and other kinetically slow radical transformations that are not feasible using alternative radical-generating methods.[22]

The initiation step in the xanthate-transfer process (depicted in Figure 4.9) can sometimes be performed by direct photolysis of the xanthates. However, such initiation method is more convenient when the xanthate can absorb light in the near UV-vis region of the electromagnetic spectrum. For example, *S*-acyl-xanthates such as *O*-ethyl derivatives **11** (Figure 4.10) are yellow solids that can undergo homolytic cleavage through the *S*-acyl bond upon direct excitation by visible-light irradiation. [22b,25]

[25] Barton, D. H. R.; George, M. V.; Tomoeda, M. Photochemical Transformations. Part XIII. A New Method for the Production of Acyl Radicals. *J. Chem. Soc.* **1962**, 1967–1974.

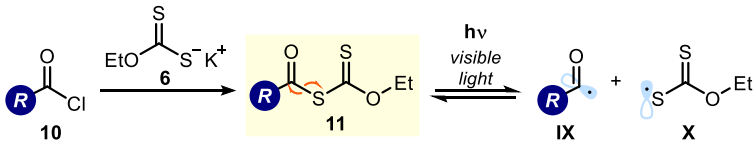

Figure 4.10. *S*-acylxanthates (**11**), formed from acyl chlorides (**10**) and potassium *O*-ethyl xanthate (**6**), undergo a photoinduced homolytic cleavage to deliver acyl (**IX**) and xanthate (**X**) radicals.

The use of Barton esters (**3**), xanthates (**7** and **11**), and related thiocarbonyl derivatives (*e.g.* dithiocarbamates) have proved to be a powerful strategy to develop new radical-based transformations.[21,22,26.]However, these methods still rely on *purposely designed stoichiometric reagents*.

4.3. A New Radical Generation Strategy: Dithiocarbamate Anion Catalysis

In the last years, our research group has exploited the ability of established organocatalytic intermediates to trigger the formation of radicals upon direct excitation by visible-light (see Chapter I, Section 1.2). So far, the excited organocatalytic intermediates have been involved in SET processes with suitable radical precursors. Along this line of research, we have recently identified a photochemical catalytic system that harnesses different physical properties of the substrates used to generate radicals. The design plan of this new catalytic method, its optimization, and its synthetic applications will be detailed in the following sections.

4.3.1. Design Plan

From a mechanistic point of view, the existing radical-generating methods (overviewed in Section 4.2) mainly rely on *atom-abstraction* or *SET processes* with substrates having *suitable BDE* or *redox potentials*, respectively. On the other hand, the methodology introduced by Barton (Section 4.2.4.) is based on the ability of photo- and thermally- sensitive compounds (represented as **R-Y** in Figure 4.11a) to afford radicals upon fragmentation induced by visible-light irradiation or heating.

---

[26] (a) Quiclet-Sire, B.; Zard, S. Z. The Xanthate Route to Amines, Anilines, and Other Nitrogen Compounds. A Brief Account. *Synlett* **2016**, *27*, 680–701. For selected examples, see: (b) Quiclet-Sire, B.; Zard, S. Z. Radical Instability in Aid of Efficiency: A Powerful Route to Highly Functional MIDA Boronates. *J. Am. Chem. Soc.* **2015**, *137*, 6762–6765. (c) Huang, Q.; Zard, S. Z. Inexpensive Radical Methylation and Related Alkylations of Heteroarenes. *Org. Lett.* **2018**, *20*, 1413–1416. (d) Revil-Baudard, V. L.; Vors, J.-P.; Zard, S. Z. Xanthate-Mediated Incorporation of Quaternary Centers into Heteroarenes. *Org. Lett*. **2018**, *20*, 3531–3535.

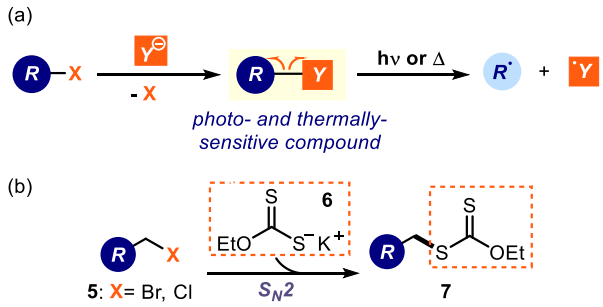

Figure 4.11. (a) The radical-generating system originally introduced by Barton relies on the previous stoichiometric synthesis of photo- and thermally- sensitive substrates (represented as **R-Y**) that deliver radicals upon excitation by UV-visible-light or upon heating. (b) The thiocarbonyl compounds **7** used in the xanthate-transfer process are accessed by a S_N2 displacement of the halide in **5** by the potassium *O*-ethyl xanthate salt **6.**

Such strategy requires the previous transformation of the radical precursor **R-X** into the photo- and thermally- active form **R-Y**. Interestingly, this procedure does not take into account the BDE or the redox properties of the precursor **R-X**. Instead, the possibility of **X** to undergo an exchange by **Y** is considered. For example, in the case of xanthate-transfer chemistry developed by Zard,[26] the required thiocarbonyl-based compounds **7** are accessed by an S_N2 reaction of alkyl halides **5** with the nucleophilic potassium *O*-ethyl xanthate salt **6** (Figure 4.11b). Therefore, the radical precursors **R-X** need to be electrophilic enough to allow the introduction of a thiocarbonyl functionality, which is provided by the nucleophilic salt **6**.

Our group wondered whether the methods based on the fragmentation of photolabile thiocarbonyl-based substrates could be performed in a *catalytic fashion*, since this would increase the overall efficiency of these radical-based processes. Moreover, a catalytic variant of this radical-generating method has not been reported to date. This research endeavor required the design of a catalytic cycle that enables the regeneration of $\mathbf{Y}^-$ after the homolytic cleavage process (*i.e.* returning $\mathbf{Y}^{\cdot}$ to $\mathbf{Y}^-$ in Figure 4.11a). In this manner, substoichiometric amounts of $\mathbf{Y}^-$ could be used. An additional goal was to induce the fragmentation of the catalytically generated intermediate **R-Y** using *low energy visible-light irradiation*, since this allows the design of radical-based transformations under mild reaction conditions. The envisioned catalytic process for the realization of this design plan is detailed in Figure 4.12.

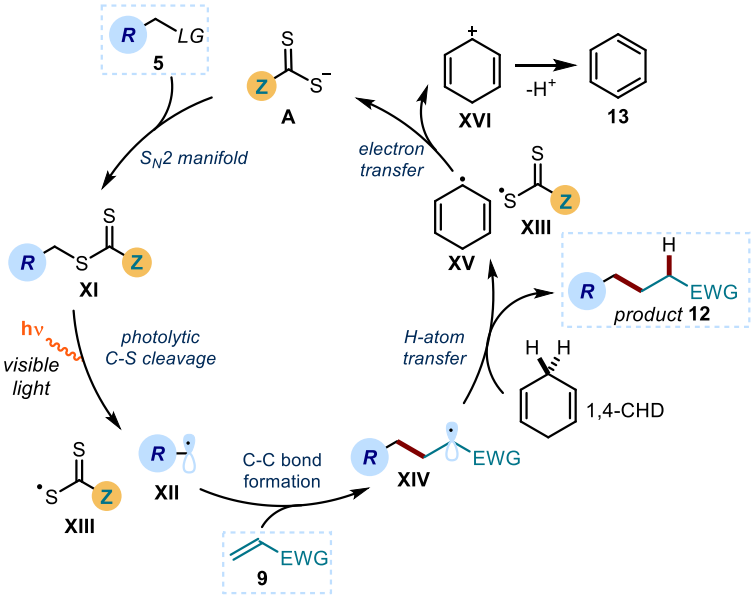

Figure 4.12. Proposed catalytic cycle using a dithiocarbamate anion catalyst **A.**

A dithiocarbonyl anion of type **A** served as an organic nucleophilic catalyst to activate alkyl electrophiles **5** upon S_N2 attack and displacement of the leaving group (LG). The resulting intermediate **XI** possesses a weak C-S bond,[24] which can be cleaved by low-energy photons to generate the target carbon radical **XII** and the dithiocarbonyl radical **XIII**. The open-shell intermediate **XII** can then participate in a radical C-C bond forming event with an electron-deficient olefin **9**, delivering radical **XIV**. This electrophilic radical (**XIV**) can in turn abstract a hydrogen atom from 1,4-cyclohexadiene (1,4-CHD), thus affording the final product **12** and the cyclohexadienyl radical **XV**. The turnover of the catalyst was achieved through an exergonic SET reduction of the dithiocarbonyl radical **XIII** from the cyclohexadienyl radical **XV** (*e.g.* the ethyl xanthogenate anion, where Z= OEt, has a reduction potential E_{red}(**XIII**/**A**)= +0.04 V vs SCE,[27] while the parent hydroxycyclohexadienyl radical has a E_{red}= -0.1 V vs SCE[28]). This mechanistic plan capitalized upon different reactivity concepts: (*i*) the high nucleophilicity[29] of dithiocarbonate and dithiocarbamate anions of type **A**; (*ii*) several studies establishing the tendency of dithiocarbonyl compounds of type **XI** to produce radicals upon

[27] Dag, Ö.; Yaman, S. Ö.; Önal, A. M.; Isci, H. Spectroelectrochemistry of Potassium Ethylxanthate, Bis(ethylxanthato)nickel(II) and Tetraethylammonium Tris(ethylxanthato)nickelate(II). *J. Chem. Soc., Dalton Trans.*, **2001**. 2819–2824.

[28] Bahtia, K.; Schuler, R. H. Oxidation of Hydroxycyclohexadienyl Radical by Metal Ions. *J. Phys. Chem.* **1974**, *78*, 2335–2338.

[29] Duan, X.-H.; Maji, B.; Mayr, H. Characterization of the Nucleophilic Reactivities of Thiocarboxylate, Dithiocarbonate and Dithiocarbamate Anions. *Org. Biomol. Chem.* **2011**, 9, 8046–8050.

photolytic cleavage,[25,30] and (*iii*) the known ability of 1,4-CHD to act as a donor of both hydrogen atoms and electrons.[31]

4.3.2. Method Optimization

The validation of the above-mentioned proposal (refer to Figure 4.12) was demonstrated in a Giese-type radical conjugate addition[32] to dimethylfumarate **9a** (Figure 4.13a), using acetonitrile (CH_3CN) as solvent and γ-terpinene as a cheaper and more stable surrogate of 1,4-CHD. Aside from providing a new catalytic system for the mild generation of radicals, our group aimed to define a strategy that enables the predictable activation of substrates that would be inert to other practical catalytic approaches, such as photoredox catalysis.

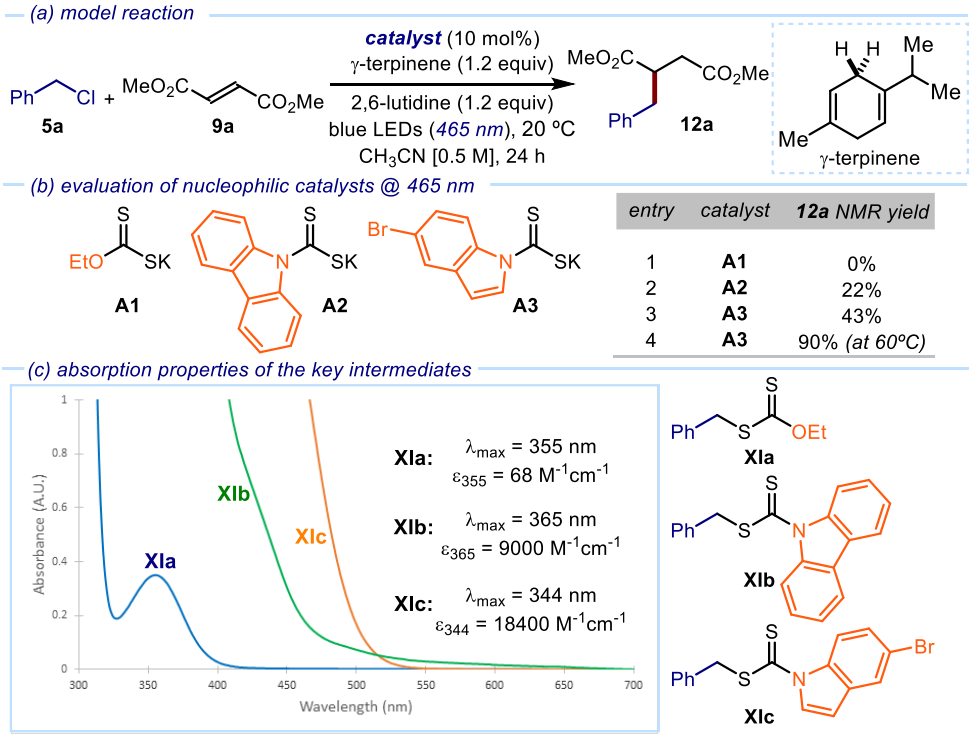

Figure 4.13. (a) Model reaction to validate the DTC-anion catalytic system; (b) nucleophilic catalysts evaluated (**A1**-**A3**); and (c) absorption of the intermediates **XIa**-**XIc**, recorded in CH3CN at [0.05 M], isolated on S_N2 reaction of the corresponding catalysts **A1**, **A2** or **A3** and benzyl chloride **5a**.

---

[30] Grainger, R. S.; Welsh, E. J. Formal Synthesis of (–)-Aphanorphine using Sequential Photomediated Radical Reactions of Dithiocarbamates. *Angew. Chem. Int. Ed.* **2007**, *46*, 5377–5380.

[31] Davies, J.; Svejstrup, T. D.; Fernandez Reina, D.; Sheikh, N. S.; Leonori, D. Visible-Light-Mediated Synthesis of Amidyl Radicals: Transition-Metal-Free Hydroamination and *N*-Arylation Reactions. *J. Am. Chem. Soc.* **2016**, *138*, 8092–8095.

[32] Giese, B. Formation of C–C Bonds by Addition of Free Radicals to Alkenes. *Angew. Chem. Int. Ed.* **1983**, *22*, 753–764.

To this end, benzyl chloride **5a** was selected as the benzyl radical precursor. This substrate has a reduction potential (E_{red} (**5a**/**5a**$^{\cdot-}$) = -2.13 vs SCE[33]) sufficiently negative to remain out of reach of most commonly used photoredox catalysts.[8,34] Therefore, SET reduction of **5a** to generate the target benzyl radical would require strong stoichiometric reductants, greatly limiting its practicality and functional group compatibility. During the optimization studies,[9] different nucleophilic catalysts (**A1**-**A3**) were evaluated (Figure 4.13b). Under the irradiation of 465 nm blue LEDs, the thiocarbamate catalysts **A2** and **A3**, both bearing chromophoric units, afforded the Giese-type addition product **12a** in 22% and 43% yield, respectively, while the commercially available potassium *O*-ethyl xanthate **A1** did not provide any formation of product **12a** (Figure 4.13b, entries 1-3). This behavior was correlated with the light-absorption properties of the key intermediates of type **XI** (Figure 4.13c). The intermediate **XIa**, emerging from a S_N2 reaction of catalyst **A1** with substrate **5a**, does not absorb at 465 nm (blue line). However, the intermediates **XIb** and **XIc** have absorption tails above 500 nm (green and orange line, respectively). Additionally, the latter species possessed a dramatically increased molar extinction coefficient (ε) with respect to **XIb**. The absorption properties of intermediates **XIb** and **XIc** translated into an enhanced catalytic activity under low-energy, blue light irradiation (λ = 465 nm). A final round of optimization established that a temperature of 60 ºC could bring the yield of the Giese-type addition product **12a** up to 90%, when using the indole-containing thiocarbamate catalyst **A3** (Figure 4.13b, entry 4).

The strategy's underlying mechanism, which is not reliant on the BDE or redox potential of the radical precursors, suggested that other benzylic substrates with leaving groups suitable for S_N2 displacement could be used in the model reaction (Figure 4.14).

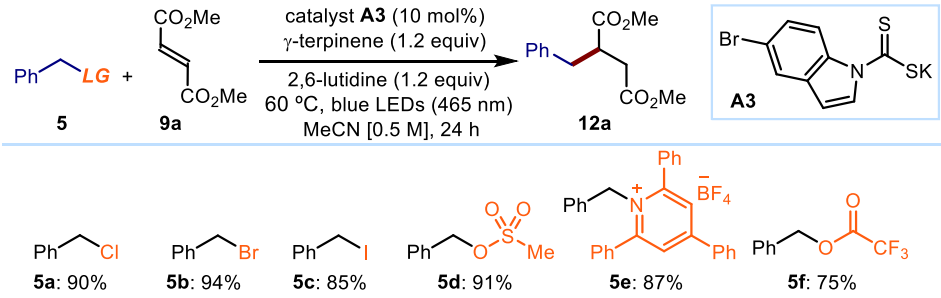

Figure 4.14. Evaluation of the leaving groups (LG) adequate for the S_N2-based benzyl radical generation strategy.

[33] Isse, A. A.; Falciola, L.; Mussini, P. R.; Gennaro, A. Relevance of Electron Transfer Mechanism in Electrocatalysis: the Reduction of Organic Halides at Silver Electrodes. *Chem. Commun*. **2006**, 344–346.

[34] Brasholz, M. "Super-reducing" Photocatalysis: Consecutive Energy and Electron Transfers with Polycyclic Aromatic Hydrocarbons. *Angew. Chem. Int. Ed.* **2017**, 56, 10280–10281.

Indeed, diverse precursors **5b-f**, including iodide, bromide, mesylate or trifluoroacetate, afforded the corresponding product **12a** in similar yields (range of 75-94% yield). Interestingly, this activation mode is not limited to halides, since amine and alcohol derivatives (**5d**-**5f**) were also adequate benzylic radical precursors.

4.3.3. Synthetic Applications

The synthetic potential of this photochemical radical generation strategy was demonstrated in the context of various C-C bond-forming transformations. On the one hand, a large variety of electrophiles **5** were successfully used as radical precursors for Giese-type additions to the electron-deficient alkene **9a** (selected examples in Figure 4.15).

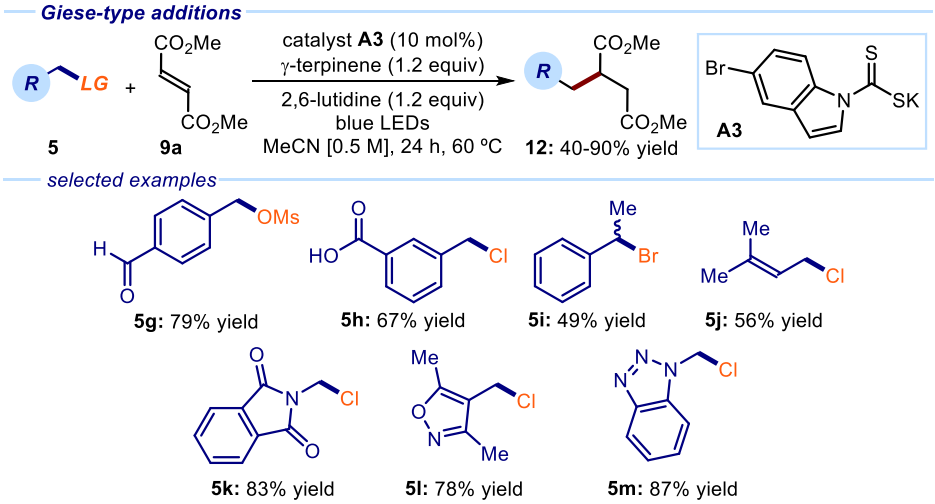

Figure 4.15. Selected examples of radical precursors (**5**) suitable for Giese-additions to the electron-deficient alkene **9a**. Yields are referred to the corresponding products (**12**).

Noteworthy, the unique mechanism of this method allowed the predictable and chemoselective activation of S_N2-prone benzylic derivatives bearing reactive functional groups, which would be incompatible with other radical generation methods or metal-based strategies. For example, substrates bearing an aldehyde (**5g**) or a free carboxylic acid (**5h**) were well tolerated and activated exclusively at the desired benzylic position. A secondary benzylic (**5i**) or an allylic substrate (**5j**) could be used as precursors of secondary and allylic radicals, respectively. Interestingly, radical α-aminomethylation processes could be performed by using readily available substrates, like *N*-(chloromethyl)phthalimide **5k**. This compound allowed the straightforward introduction of a protected primary amine within the products of type **12**. The compatibility with unprotected functional groups was also evaluated. This is an essential criterion when assessing a method's potential applicability to complex

molecule synthesis and drug discovery.[35] In this regard, the S_N2-based radical-generating system displayed a high level of tolerance towards several nitrogen-containing heterocycles (**5l-5m**).

Other type of radical-based transformations were amenable to this catalytic strategy. For example, the dithiocarbamate catalyst **A3** could promote the sequential radical addition/cyclization[36] of aromatic acrylamides **14** (Figure 4.16), affording 3,3-disubstituted 2-oxindoles **15** in moderate to excellent yields. In this case, it was hypothesized that the turnover of the catalyst could be achieved by SET reduction of the dithiocarbonyl radical **XIII** from the 1,4-CHD-type radical **XVIIa** (see Figure 4.16, below), generated after the cyclization event.

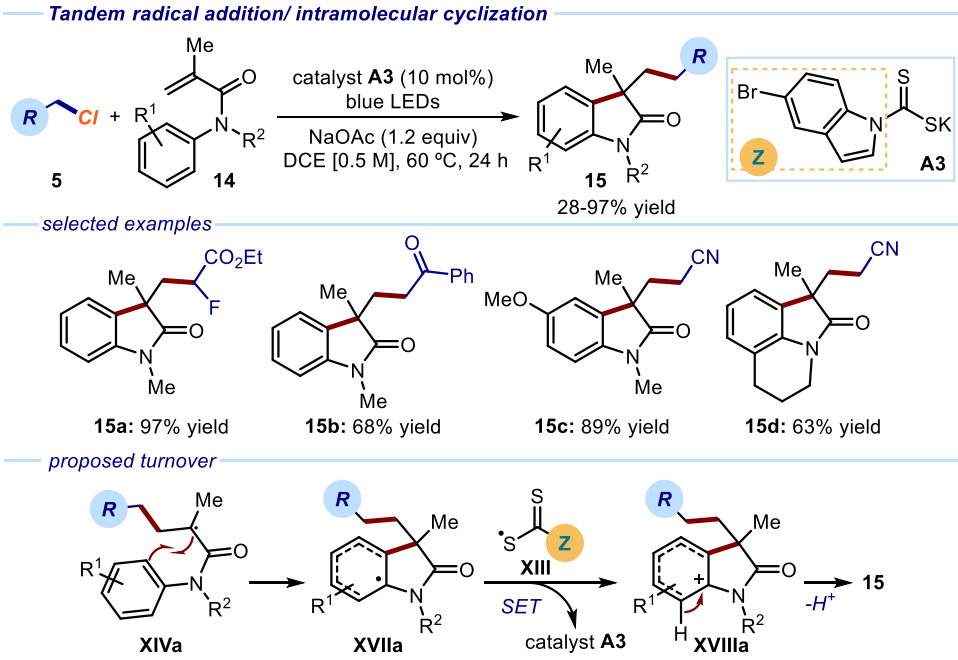

Figure 4.16. Dithiocarbamate anion-promoted tandem radical addition/cyclization of N-arylacrylamides (**14**) affording 3,3-disubstituted 2-oxindoles (**15**). Selected examples and proposed turnover of the DTC catalyst. SET: single-electron transfer.

In a similar manner, the direct radical functionalization of electron-rich (hetero)aromatics **16** could be successfully performed, using ready available alkyl chlorides **5** as radical precursors (Figure 4.17). Different reactive functional groups, such as aldehydes (**17b**), secondary

[35] Blakemore, D. C. et al. Organic Synthesis Provides Opportunities to Transform Drug Discovery. *Nat. Chem.* **2018**, *10*, 383–394.

[36] Chen, J.-R.; Yu, X.-Y.; Xiao, W.-J. Tandem Radical Cyclization of *N*-Arylacrylamides: an Emerging Platform for the Construction of 3,3-Disubstituted Oxindoles. *Synthesis* **2015**, 47, 604–629.

amides (**17c**), or free alcohols (**17d**) were well tolerated, leading to synthetically valuable substituted heteroaromatic compounds **17**.[37] Here, the turnover event was surmised to proceed through a SET reduction of **XIII** from the open-shell intermediate **XIVb** (Figure 4.17, below), which is generated after the radical addition event.

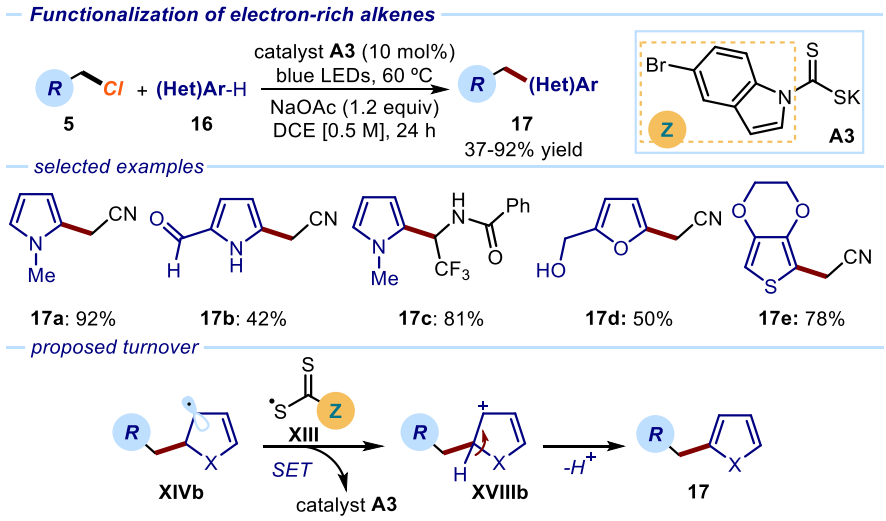

Figure 4.17. Selected examples of the dithiocarbamate anion promoted radical functionalization of electron-rich (hetero) arenes.

The utility of the dithiocarbamate-anion catalytic system was also demonstrated in the organocatalytic stereoselective intermolecular α-alkylation of aldehydes **18** (Figure 4.18).

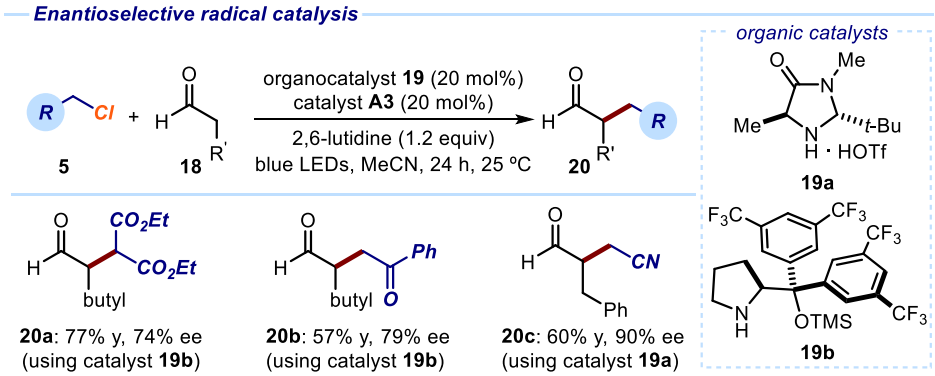

Figure 4.18. The dithiocarbamate anion catalytic strategy enables the asymmetric alkylation of aldehydes using alkyl chlorides (**5**) as precursors of carbon-centered radicals.

[37] Fujiwara, Y.; Baran, P. S. in New Horizons of Process Chemistry (eds Tomioka K., Shioiri T. & Sajiki H.) (Springer Nature, Singapore, 2017).

This transformation, originally reported by the MacMillan's group (see Chapter 1, Section 1.1.2, Figure 1.8), has served as a reference reaction to measure the efficiency of new photoredox catalysts.[38] All the procedures reported so far, since they are based on SET reductions of the radical precursors by an external photoredox catalyst, could only use alkyl bromides. The S_N2-based radical-generating methodology can extend the scope of this transformation to include alkyl chlorides **5**. The chemistry was effectively performed at ambient temperature, using the dithiocarbamate anion catalyst **A3** in combination with organocatalysts **19a** or **19b** to furnish the corresponding α-alkylation products **20a-c**.

4.4. Target of the Project

The synthetic potential of the S_N2-based radical-generating strategy has been demonstrated in different C-C bond forming reactions (Section 4.3.3). Following these studies, we aimed to seek for other transformations in which this methodology could overcome the limitations imposed by other radical generation strategies, including photoredox catalysis. Due to its importance in organic synthesis, we considered free-radical MCRs.[4,7] Although photoredox catalysis has offered mild conditions for initiating these processes,[7] the pool of radical precursors that can be used in the design of a MCR is limited by their redox properties. We aimed to design a radical cascade under the redox-neutral conditions offered by our recently developed radical-generation method. To fully exploit the synthetic opportunities provided by our method, we used difficult-to-reduce alkyl chlorides **5** as radical precursors and coupled them with readily available alkenes **9** and heteroaromatic fragments **16** (Figure 4.19).

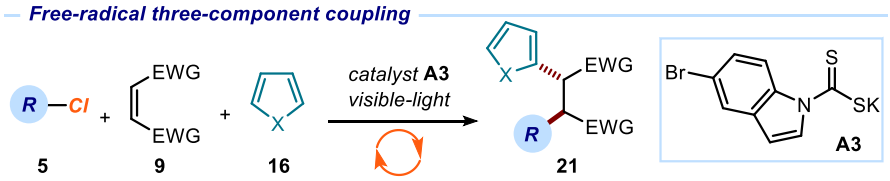

Figure 4.19. Proposed photochemical three-component radical reaction using redox-inert alkyl chlorides **5**, mediated by dithiocarbamate anion catalysis.

The mechanistic plan of our proposed photochemical radical MCR is shown in Figure 4.20. Based on our previous studies,[9] we envisioned a catalytic cycle where the dithiocarbamate anion catalyst **A3** would activate alkyl chlorides **5** upon S_N2 displacement.

[38] (a) Neumann, M.; Füldner, S; König, B.; Zeitler, K. Metal-free, Cooperative Asymmetric Organophotoredox Catalysis with Visible Light. *Angew. Chem. Int. Ed.* **2011**, *50*, 951–954. (b) Gualandi, A.; Marchini, M.; Mengozzi, L.; Natali, M.; Lucarini, M.; Ceroni, P.; Cozzi, P. G. Organocatalytic Enantioselective Alkylation of Aldehydes with $[Fe(bpy)_3]Br_2$ Catalyst and Visible Light. *ACS Catal.* **2015**, *5*, 5927–5931.

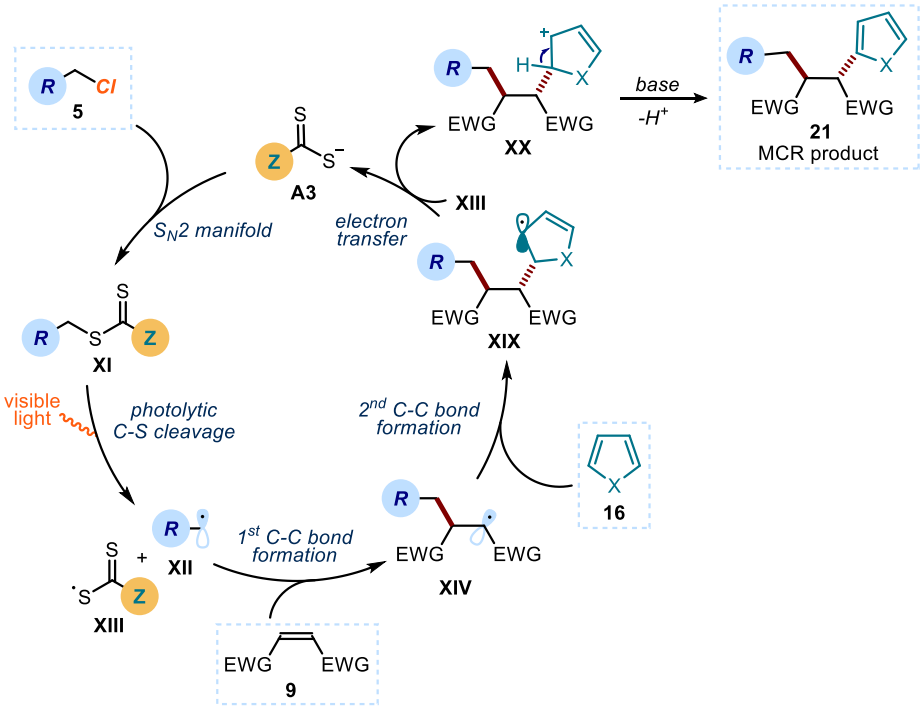

Figure 4.20. Working hypothesis for the visible-light-driven three-component radical reaction; Z: chromophore.

The weak C-S bond of the ensuing intermediate **XI** would then be cleaved by low-energy photons (blue LEDs, λ=460 nm) to generate the target carbon radical **XII** and the dithiocarbonyl radical **XIII**. The open-shell intermediate **XII** would initiate the radical cascade upon interception from the electrophilic alkene **9**, forging the first C-C bond. The emerging electrophilic radical **XIV** would then participate in a second trapping event with an electron-rich heteroaromatic compound (**16**), affording the open-shell intermediate **XIX**. We anticipated that this crucial intermediate could likely act as a reductant to turn over catalyst **A3** upon SET reduction of the dithiocarbonyl radical **XIII**. This latter hypothesis was based on the relatively low redox potential of catalyst **A3**: E_{ox} (**XIII**/**A3**) = +0.44 V[39] vs. Ag/AgCl (KCl, 3.5 M). A proton loss in **XX**, facilitated by the presence of a base, would restore the aromaticity of the hetero-aromatic fragment, delivering the functionalized cascade product **21**.

[39] The redox potential of catalyst **A3** was measured by cyclic voltammetry and reported in: Mazzarella, D.; Magagnano, G.; Schweitzer-Chaput, B.; Melchiorre, P. Photochemical Organocatalytic Borylation of Alkyl Chlorides, Bromides, and Sulfonates. *ACS Catalysis* **2019**, 9, 5876–5880.

4.5. Results and Discussions

4.5.1. Optimization Studies

We started the development of the MCR process by selecting a suitable combination of coupling partners. The knowledge accumulated during the previous investigations on dithiocarbamate anion catalysis (see Section 4.3.3) offered excellent guidelines for the initial development of this system.[40] We selected two combinations of substrates (Figure 4.21). The initial experiments were conducted at 60 ºC using blue LEDs emitting at 465 nm, 20 mol% of the DTC catalyst **A3** and a large excess of a hetero-aromatic substrate, which would serve as the terminal radical trap. 2,6-Lutidine and acetonitrile were used as base and solvent, respectively. In the first combination (combination A), we used 4-methoxybenzyl chloride **5n** as the precursor of a benzyl radical, dimethyl fumarate **9a** as the first electrophilic radical trapping agent, and *N*-methyl pyrrole **16a** as the terminal radical trap. Under the above-mentioned conditions, no formation of the desired three-component product **21a** was detected by ^{1}H NMR analysis of the crude reaction mixture. On the other hand, combination B, which coupled the chloride **5k**, maleimide **9b**, and *N*-methyl pyrrole **16a** (all of them commercially available), furnished the desired MCR product **21b** in 29% yield, with a 1.7:1 dr.

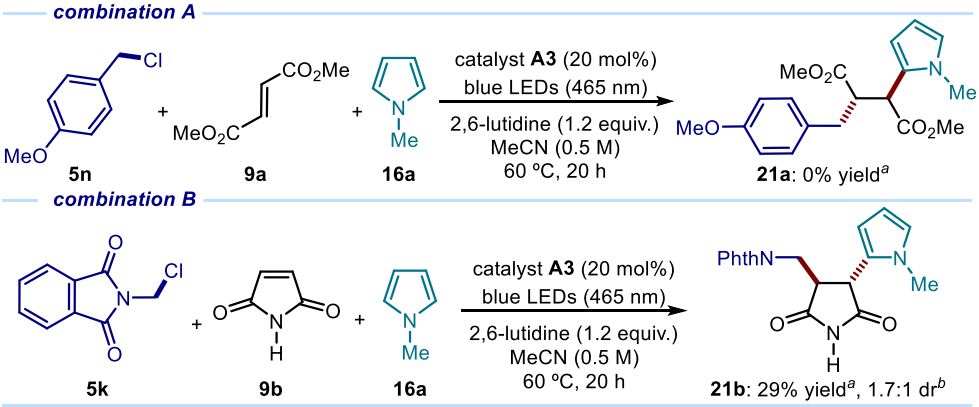

Figure 4.21. Initial hit for developing a DTC-anion mediated three-component coupling process. [a]Yield determined by ^{1}H NMR analysis of the crude mixture using trichloroethylene as the internal standard. [b]Diastereomeric ratio determined by ^{1}H NMR analysis of the crude mixture. NPhth: phthalimide.

On the basis of this promising result, we started the optimization of the three component coupling process using the substrate combination B. Firstly, we evaluated the effect of other solvents (Table 4.1). When 1,2-dichloroethane (DCE) was used, the yield of the desired MCR product **21b** increased to 77% (entry 3). However, several attempts to isolate the MCR product

[40] Preliminary investigations were carried out by Dr. Matthew A. Horwitz.

21b met with failure. Purification by flash column chromatography resulted in very poor separation from unreacted maleimide **9b** and another unidentified byproduct.

Table 4.1. Solvent screening.

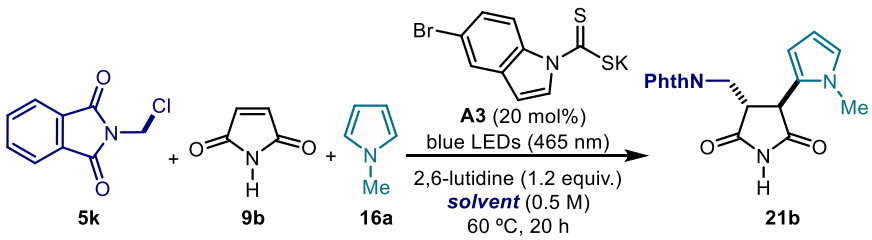

entry	solvent	yield (%)[a]	dr[b]
1	acetonitrile	29	1.7:1
2	ethyl acetate	45	2:1
3	1,2-dichloroethane	77	1.9:1
4	toluene	45	n.d

Reactions performed on a 0.1 mmol scale in a Schlenck tube, using 20 mol% of catalyst **A3**, 1.5 equiv. of **5k** and 10 equiv. of **16a**. Three cycles of freeze-pump-thaw were used to degas the reaction mixture. Blue LED strips (λ = 465 nm, 14W) were used as light source. [a]Yield of **21b** determined by ^{1}H NMR analysis of the crude mixture using trichloroethylene as the internal standard. [b] Diastereomeric ratio determined by ^{1}H NMR analysis of the crude mixture. NPhth: phthalimide.

We then moved to evaluate the effect of the maleimide-protecting group (Table 4.2). Substitution with *tert*-butyloxcarbonyl (Boc) or phenyl groups (entries 2 and 3) resulted in the formation of the corresponding product **21** in considerably lower yields (38% and 28%, respectively). In both cases, the formation of only one diastereoisomer was detected by ^{1}H-NMR analysis of the crude reaction mixture (dr >20:1).

The use of *N*-protected maleimides with different alkyl substituents (maleimides **9e**-**9h**, entries 4-7) afforded the corresponding MCR products **21** in moderate yields but preserving the excellent diastereoselective outcome (range of 62-52% yield, dr>20:1). Pleasingly, the methyl substituted maleimide **9i** furnished the product **21i** in 70% NMR yield and >20:1 dr (entry 8). In this case, the product (**21i**) could be better separated from unreacted substrates: 57% of isolated material **21i** was obtained after flash column chromatography. Crystallization from MeOH of the pure material **21i** afforded crystals suitable for X-ray diffraction analysis (data available in Section 4.7.9) which revealed a *trans* relative stereochemistry. Overall, these studies established maleimide **9i** as the model substrate to perform the last cycle of optimization.

Table 4.2. Effect of the maleimide (**9**) protecting group.

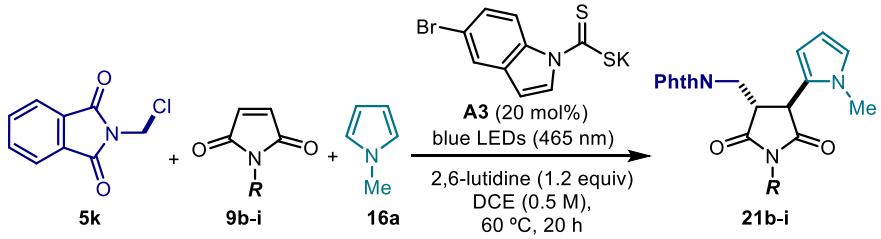

5k 9b-i 16a 21b-i

entry	maleimide (9) R =	yield (%)[a]	dr[b]
1	-H (**9b**)	77	1.9:1
2	-Boc (**9c**)	38	>20:1
3	-Ph (**9d**)	28	>20:1
4	-^{n}Pr (**9e**)	62	>20:1
5	-*t*Bu (**9f**)	60	>20:1
6	-Cy (**9g**)	59	>20:1
7	-Bn (**9h**)	52	>20:1
8	-Me (**9i**)	70 (57)	>20:1

Reactions performed on a 0.1 mmol scale in a Schlenck tube, using 20 mol% of catalyst **A3**, 1.5 equiv. of **5k** and 10 equiv. of **16a**. Three cycles of freeze-pump-thaw were used to degas the reaction mixture. Blue LED strips (λ = 465 nm, 14W) were used as light source. [a]Yield of **21** determined by ^{1}H NMR analysis of the crude mixture using trichloroethylene as the internal standard. [b]Diastereomeric ratio determined by ^{1}H NMR analysis of the crude mixture. NPhth: phthalimide. The values in parenthesis are referred to the yields of **21** after flash column chromatography purification.

We then evaluated the effect of the base in the formation of the MCR product **21i** (Table 4.3). A control experiment (entry 1) confirmed that this is an important parameter to facilitate the formation of **21i**. Considering our initial working hypothesis, the presence of the base likely triggers the re-aromatization of the pyrrole moiety (*i.e.* from **XX** to **21** in the catalytic cycle depicted in Figure 4.20). In addition, its effect also provides the basic media required to have the dithiocarbamate catalyst **A3** in its nucleophilic anionic form. We observed (Table 4.3) that other organic and inorganic bases were less effective in affording the desired product (range of 32-51% yield, entries 2-4) in comparison with 2,6-lutidine (70% yield, entry 2).

Table 4.3. Base screening.

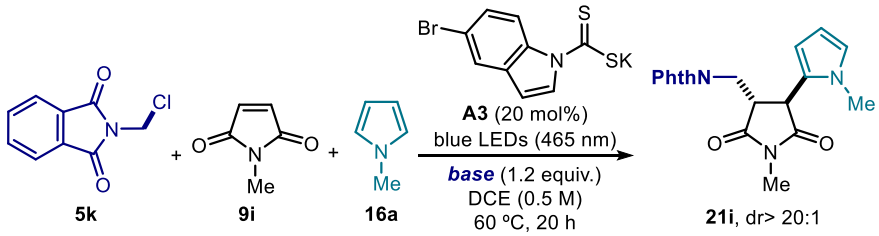

entry	base	yield (%)[a]
1	none	<10
2	2,6-lutidine	70
3	Pyridine	32
4	NaOAc	34
5	$NaHCO_3$	51

Reactions performed on a 0.1 mmol scale in a Schlenck tube, using 20 mol% of catalyst **A3**, 1.5 equiv. of **5k** and 10 equiv. of **16a**. Three cycles of freeze-pump-thaw were used to degas the reaction mixture. Blue LED strips (λ = 465 nm, 14W) were used as light source. [a]Yield of **21i** determined by ^{1}H NMR analysis of the crude mixture using trichloroethylene as the internal standard. NPhth: phthalimide.

The effect of other reaction parameters, including temperature, catalyst loading, and reaction time (Table 4.4) was finally evaluated. We found that the formation of the product **21i** after 20 hours was dramatically affected when the temperature was decreased from 60 to 40 ºC (23% yield, entry 2). A similar behavior was observed in the previous Giese-type addition studies (Figure 4.13). Due to the multistep nature of the process, the effect of the temperature could be either to accelerate the rate of both radical addition processes, or in the re-aromatization of the pyrrole. We discarded the possibility that the temperature (60 ºC) could be involved in the homolytic cleavage of the key intermediate **XI**, since a control experiment in the dark (Table 4.4, entry 8) gave no traces of the product **21i**.

Decreasing the catalyst loading from 20 to 10 mol%, or the reaction time from 20 to 10 h, also led to poorer results (Table 4.4, entries 3 and 4). Increasing the concentration from 0.5 M to 1.0 M was detrimental for the formation of the product (entry 5), while more diluted conditions (0.25 M) slightly affected the efficiency of the process (65% yield, entry 6). The radical-based MCR was very sensitive to oxygen, since no product formation was detected when the reaction mixture was not degassed via freeze-pump-thaw (entry 7). As expected, the reaction in the absence of catalyst **A3** did not give any formation of the MCR-product (entry 9), thus confirming the fundamental role of **A3** in the radical MCR process.

Table 4.4. Further optimization studies

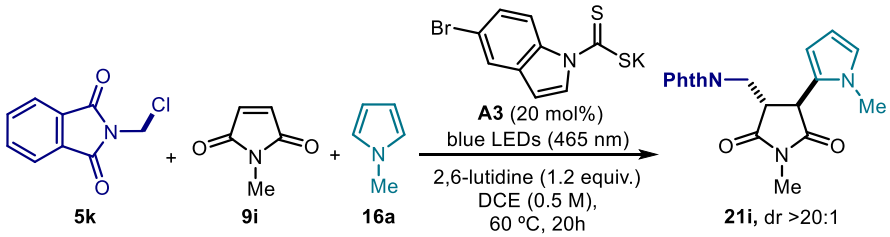

entry	deviation from standard conditions	yield (%)[a]
1	none	70 (57)
2	40ºC	23
3	10 mol% catalyst **A3**	47
4	10 h	42
5	DCE (1.0 M)	18
6	DCE (0.25 M)	65
7[b]	no freeze-pump-thaw	0
8	No light	0
9	No catalyst **A3**	0
10	*fac*-Ir(ppy)$_3$ (3 mol%), instead of **A3**	0

Reactions performed on a 0.1 mmol scale in a Schlenck tube, using 20 mol% of catalyst **A3**, 1.5 equiv. of **5k** and 10 equiv. of **16a**. Three cycles of freeze-pump-thaw were used to degas the reaction mixture. Blue LED strips (λ = 465 nm, 14W) were used as light source. [a]Yield of **21** determined by ^{1}H NMR analysis of the crude mixture using trichloroethylene as the internal standard. [b]All the reagents were added under Ar atmosphere. NPhth: phthalimide. The values in parenthesis refer to the yields of the isolated products **21**.

We then evaluated if this transformation could be promoted by a photoredox catalyst. We performed the model reaction replacing catalyst **A3** with the strongly reducing *fac*-Ir (ppy)$_3$ ($E_{1/2}$ Ir (IV)/Ir(III*) = -1.73 V vs. SCE[41]). This photoredox catalyst has a redox potential sufficiently negative to reduce the alkyl chloride **5k** (E_{red} (**5k**/**5k**$^{\bullet-}$) = -1.51 V vs. SCE, cyclic voltammogram reported in Experimental Section 4.11.7). Therefore, the reduction of **5k** by *fac*-Ir (ppy)$_3$ was expected to be thermodynamically feasible.[42] However, we observed no formation of the MCR product **21i** under photoredox conditions (Table 4.4, entry 10). This result might indicate that either a heterolytic cleavage of the C-Cl bond within the radical anion **5k**$^{\bullet-}$ does not occur (Figure 4.22, left panel), or that the oxidized photoredox catalyst cannot undergo a turnover process ($E_{1/2}$ Ir (IV)/Ir(III) = +0.77 V vs. SCE[41]).

[41] Prier, C. K.; Rankic, D. A.; MacMillan, D. W. C. Visible-Light Photoredox Catalysis with Transition Metal Complexes: Applications in Organic Synthesis. *Chem. Rev.* **2013**, *113*, 5322–5363.

[42] Romero, N. A.; Nicewicz, D. A. Organic Photoredox Catalysis. *Chem. Rev.* **2016**, *116*, 10075–10166.

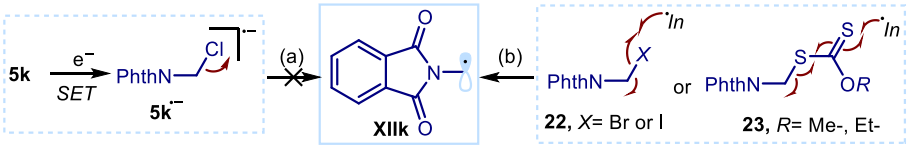

Figure 4.22. (a) The formation of the phtalimidomethyl radical **XIIk** cannot be achieved through SET reduction of the *N*-(chloromethyl)phthalimide **5k**. (b) **5k** has been previously accessed only through atom abstraction methods from compounds of type **22**, or through the use of xanthates of type **23**. NPthth: phthalimide.

Indeed, there are no precedents showing the generation of the open-shell intermediate **XIIk** through a SET mechanism from alkyl halides of type **5k**. Instead, the production of **XIIk** has been only achieved through atom abstraction mechanisms from iodo- or bromo-methyl phtalimides **22**,[43] or the use of stoichiometric xanthates of type **23**[44] (Figure 4.22, right panel). Overall, this control experiment (Table 4.4, entry 10) highlights the inability of photoredox catalysis to trigger a radical MCR process using *N*-(chloromethyl)phtalamide **5k** as a radical precursor.

4.5.2. Scope of the Reaction

Adopting the optimized conditions described in Table 4.4, entry 1, we explored the generality of the photoinduced radical cascade process (Figures 4.23 and 4.24). The method is amenable to synthetically useful purposes, since a high efficiency was maintained when running the reaction on a 5 mmol scale (Figure 4.23). This experiment did not require any modification of the standard experimental set-up (detailed in Experimental Section 4.11.3.1 of this Chapter), and it afforded product **21i** in good yield and with complete diastereoselectivity (0.91 g, 52% yield, dr > 20:1).

---

[43] (a) Receveur, J.-M.; Guiramand, J.; Récasens, M.; Roumestant, M.-L.; Viallefont, P.; Martinez, J. Synthesis and Biological Activity of Glutamic Acid Derivatives. *Bioorg. Med. Chem. Lett.* **1998**, *8*, 127–132. (b) Campbell, E. F.; Park, A. K.; Kinney, W. A.; Feng, R. W.; Liebeskind, L. S. Synthesis of 3-Hydroxy-3-Cyclobutene-1,2-dione Based Amino Acids. *J. Org. Chem.* **1995**, *60*, 1470–1472. (c) Yamada, K.; Matsumoto, Y.; Fujii, S.; Konishi, T.; Yamaoka, Y.; Takasu, K. Striking Difference Between Succinimidomethyl and Phthalimidomethyl Radicals in Conjugate Addition to Alkylidenemalonate Initiated by Dimehtylzinc. *J. Org. Chem.* **2016**, *81*, 3809–3817.

[44] (a) Quiclet-Sire, B.; Zard, S. Z. Radical Aminomethylation of Unactivated Alkenes. *Org. Lett.* **2008**, *10*, 3279–3282. (b) Postma, A.; Davis, T. P.; Li, G.; Moad, G.; O'Shea, M. RAFT Polymerization with Phthalimidomethyl Trithiocarbonates or Xanthates. On the Origin of Bimodal Molecular Weight Distributions in Living Radical Polymerization. *Macromolecules* **2006**, *39*, 5307–5318.

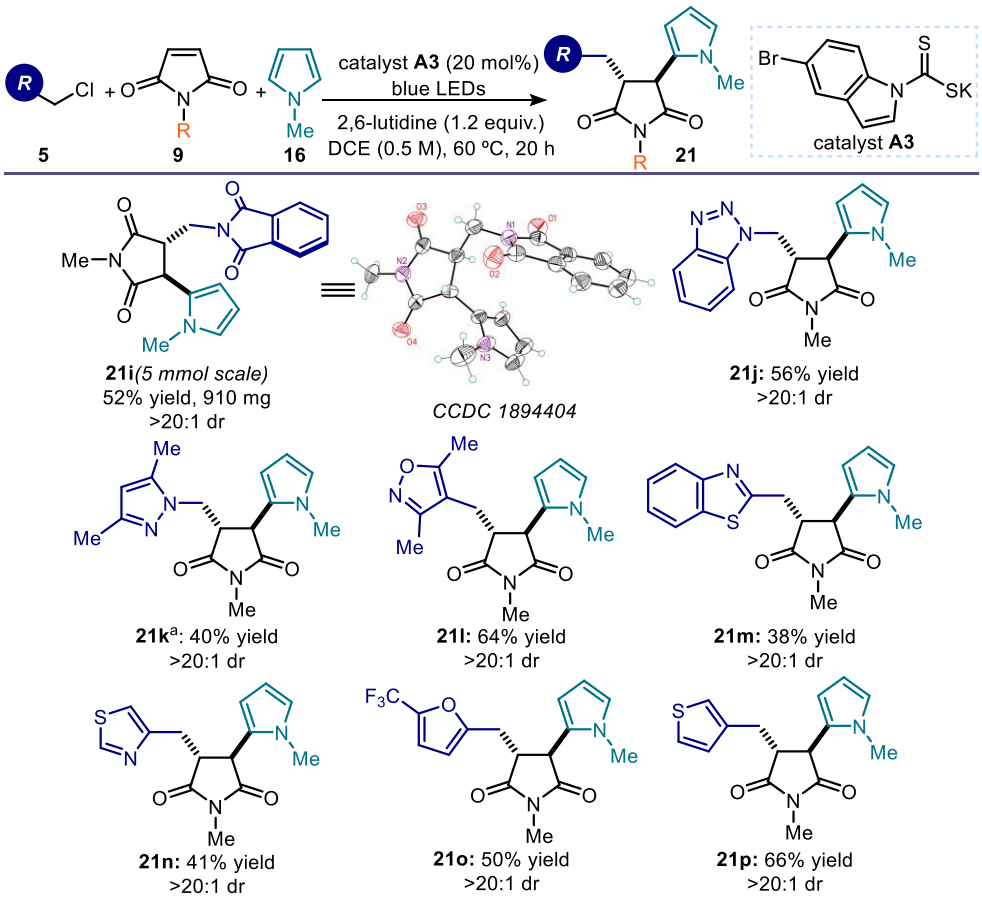

Figure 4.23. Survey of alkyl chlorides **5** that can participate in the dithiocarbamate anion-mediated three-component coupling (products **21i** – **21p**). Reaction performed on a 0.5 mmol scale using 1.5 equiv. of **5**, 10 equiv. of **16**, and 1.0 mL of 1,2-dichloroethane; yields refer to isolated product **21** after purification. [a] Yield determined by ^{1}H NMR analysis of the crude mixture using trichloroethylene as internal standard.

We then explored the scope of the radical precursors **5** that could be activated by the dithiocarbamate anion catalyst **A3**. The method displayed a high degree of tolerance towards *N*-heterocycles, as the cascade products **21** could be readily adorned with triazole (**21j**), pyrazole (**21k**), isoxazole (**21l**), benzothiazole (**21m**), and thiazole (**21n**) scaffolds. Other heterocyclic moieties, such as furan (**21o**) and thiophene (**21p**), were also tolerated. These common motifs are typically found in drug molecules. However, they generally represent a significant tolerability challenge for synthetic methods.[45] The corresponding MCR products **21** were obtained with good yields and complete diastereoselectivity. It is worth mentioning

[45] (a) Blakemore, D. C. *et al*. Organic Synthesis Provides Opportunities to Transform Drug Discovery. *Nat. Chem.* **2018**, *10*, 383–394. (b) Pitt, W. R.; Parry, D. M.; Perry, B. G.; Groom, C. R. Heteroaromatic Rings of the Future. *J. Med. Chem.* **2009**, 52, 2952–2963.

that the reduction potentials of the heterocyclic-containing substrates **5**, evaluated by cyclic voltammetry, are sufficiently negative (E_{red} < -2.0 V vs. Ag/AgCl, see Experimental Section 4.11.7 of this Chapter) to remain out of reach of most commonly used photoredox catalysts.[6,8] Therefore, SET-based reduction methods to generate the target radicals and trigger this MCR process would require the use of strong reductants, greatly limiting functional group compatibility. Benzylic radical precursors, bearing both electron-rich and electron-poor aryl substituents, were also competent substrates, affording the complex MCR products **21** in moderate to high chemical yields (Figure 4.24, products **21q**-**21aa**, 28-72% yield).

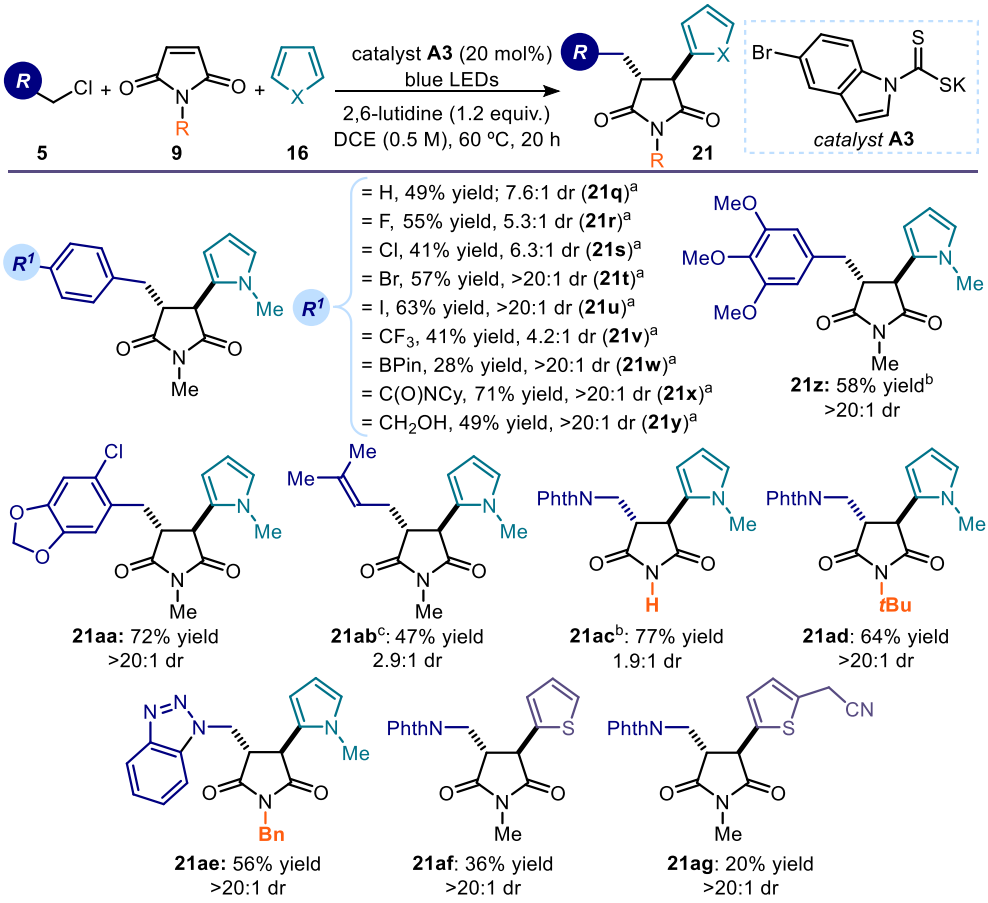

Figure 4.24. Survey of benzylic radical precursors (products **21q**-**21aa**), allylic precursors (product **21ab**), maleimides (products **21ac**-**21ae**) and terminal traps (products **21af**-**21ag**) that can participate in the reaction. Reaction performed on a 0.5 mmol scale using 1.5 equiv. of **5**, 10 equiv. of **16**, and 1.0 mL of 1,2-dichloroethane; yields refer to isolated product **21** after purification. [a]The corresponding bromides **5** were used as radical precursors. [b] Yield determined by ^{1}H NMR analysis of the crude mixture using trichloroethylene as internal standard. [c] 3 equiv. of **5**. NPhth: phthalimide.

Reactive functional groups such as aryl iodides (**21u**), boron esters (**21w**), amides (**21x**), and a free alcohol (**21y**) were all tolerated and activated exclusively at the benzylic position.

Regarding the diastereoselectivity, full control was achieved with electron-rich benzyl systems, while the presence of electron-withdrawing groups affected the relative stereocontrol (**21r-s**, **21v**). In addition, prenyl chloride, which generates an allylic radical upon dithiocarbamate-anion activation, could be successfully used in the MCR process (product **21ab**), albeit with reduced levels of diastereoselectivity (2.9:1 dr). Finally, thiophene was found to be an alternative terminal radical trap (**21af-ag**).

4.6. Chemoselectivity of the Radical Multicomponent Process

The design of MCRs requires a careful consideration of the reactivity of the substrates and the transiently generated intermediates[4c-d]. Section 4.5.1 has detailed the optimization of the MCR process that couples *N*-(chloromethyl)phthalimides **5k**, *N*-methylmaleimide **9i** and *N*-methylpyrrole **16a** (Figure 4.25).

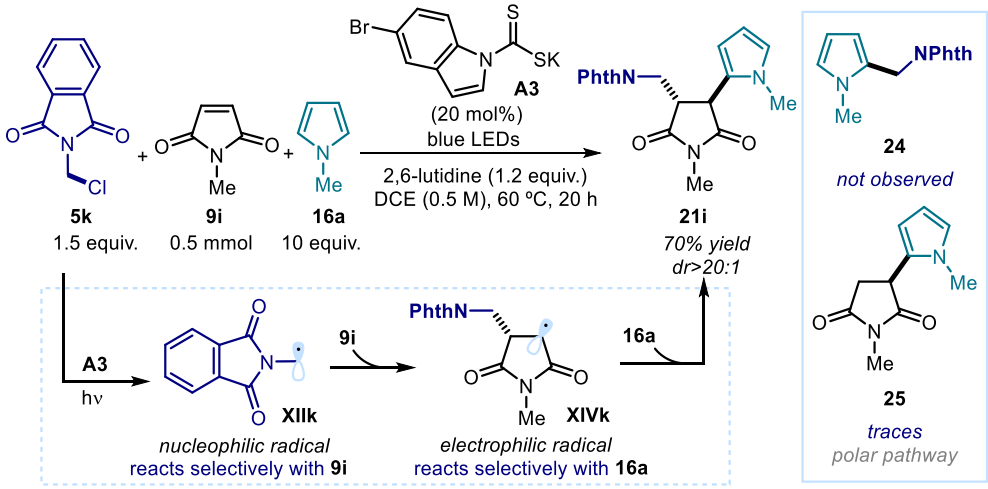

Figure 4.25. (a) Chemoselectivity aspects of the MCR reaction between *N*-(chloromethyl)phthalimide **5k**, *N*-metylmaleimide **9i** and *N*-methylpyrrole **16a.** NPhth: phthalimide.

This intermolecular cascade has been implemented by carefully matching the polarity of the different reactive species involved. In the model reaction, we have used the dithiocarbamate catalyst **A3** to activate **5k** and form a *nucleophilic* phthalimidomethyl radical **XIIk**. This radical **XIIk** can potentially be intercepted by either the electrophilic maleimide **9i** or the electron rich *N*-methylpyrrole **16a**. Polarity reasons (polarity match/mismatch) favour the chemoselective reaction of the phthalimidomethyl radical **XIIk** with the electron-poor maleimide **9i**, which largely outcompetes the trapping with the nucleophilic *N*-methylpyrrole **16a**. In consonance with this design plan, we did not observe any formation of the pyrrole radical alkylation product **24** in our model reaction under the optimised reaction conditions. Importantly, radical **XIVk**, which emerges from the previous Giese-type radical addition path,

is *electrophilic* in nature, and therefore prone to be selectively intercepted by the nucleophilic pyrrole **16a**.

We have performed further control experiments to corroborate the intrinsic low reactivity of other possible competition processes leading to **24** and **25**. On the one hand, when **5k** and **16a** were submitted to the optimal conditions of the model radical MCR process (Figure 4.26a), the C2-alkylated *N*-methylpyrrole **24** was formed in very low yields (<10% yield). This result highlights that either a radical or polar alkylation of **16a** with **5k** is not a competitive pathway in the MCR. Similarly, when *N*-methylmaleimide **9i** and *N*-methyl pyrrole **16a** were submitted to the optimal MCR conditions, only 12% of the Friedel-Craft product **25** was formed (Figure 4.26b).

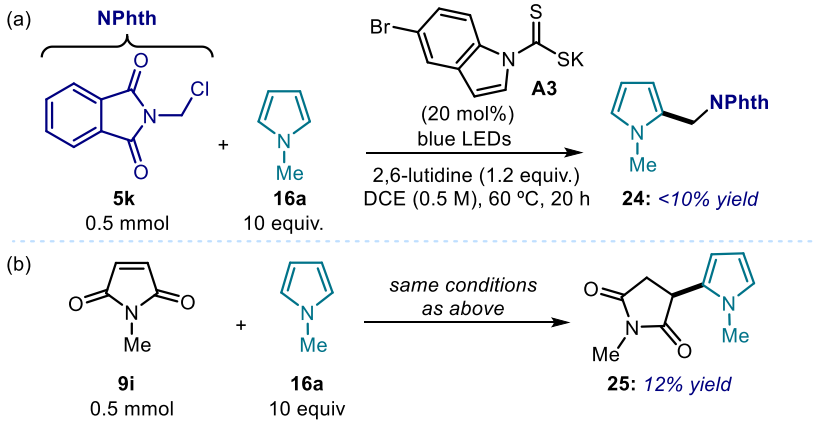

Figure 4.26. Control experiments testing the possibility of other polar or radical competition processes in the optimized conditions of the model MCR. Yields of **24** and **25** determined by ^{1}H NMR analysis of the crude mixture using trichloroethylene as the internal standard.

The latter control experiment (Figure 4.26b) also excludes the possibility to trigger the cascade process through a polar pathway. Indeed, one could envision a polar manifold leading to the formation of **21i**. This is illustrated in Figure 4.27.

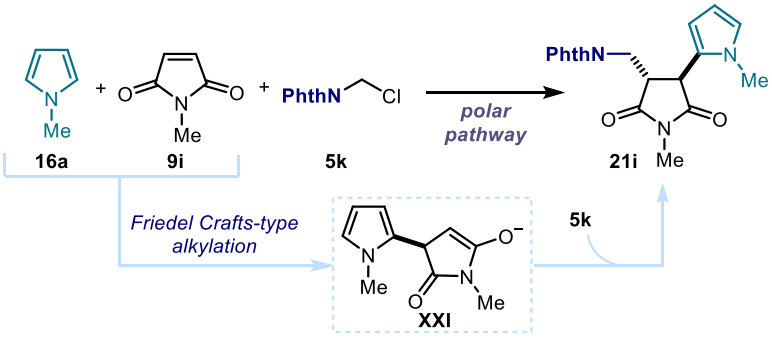

Figure 4.27. A plausible alternative polar pathway leading to the formation of the MCR product **21i**. NPhth: phthalimide.

In such hypothetic case, the MCR process would start with the Friedel-Crafts-type alkylation of **16a** with the electrophilic **9i**, followed by nucleophilic attack of the corresponding enolate **XXI** to the alkyl halide **5k**. However, on the basis of the control experiment shown in Figure 4.26b, we can discard such possibility. In addition, no trace of the product **21i** was detected during a control experiment performed in the dark, under the optimal conditions of the model MCR (refer to Table 4.4, entry 8). Hence, the coupling of the three coupling partners **5k**, **9i** and **16a** is only achievable through the radical pathway promoted by the dithiocarbamate anion catalyst **A3**.

4.7. Assembly Line Synthesis of Difunctionalized Pyrroles

Our next goal was to use the S_N2-based radical generating strategy to prepare highly functionalized pyrroles. These motifs are present in some natural products, pharmaceuticals, and materials.[46] Specifically, we envisioned an assembly line protocol that combines two sequential radical processes, governed by the dithiocarbamate anion catalyst **A3** and visible light, to achieve a 2,5-difunctionalization of a the commercial pyrrole **16a** (Figure 4.28). First, the photochemical activation of chloroacetonitrile **5ae** by **A3** generates an electrophilic radical, which is intercepted by *N*-methyl pyrrole **16a** to deliver the functionalized intermediate **17a** in 92% yield. After purification by flash column chromatography, we then submitted the pyrrole **17a** to the MCR process with **5k** and **9i,** to rapidly assemble the difunctionalized pyrrole **26** in moderate yield (32% yield) from commercially available substrates.

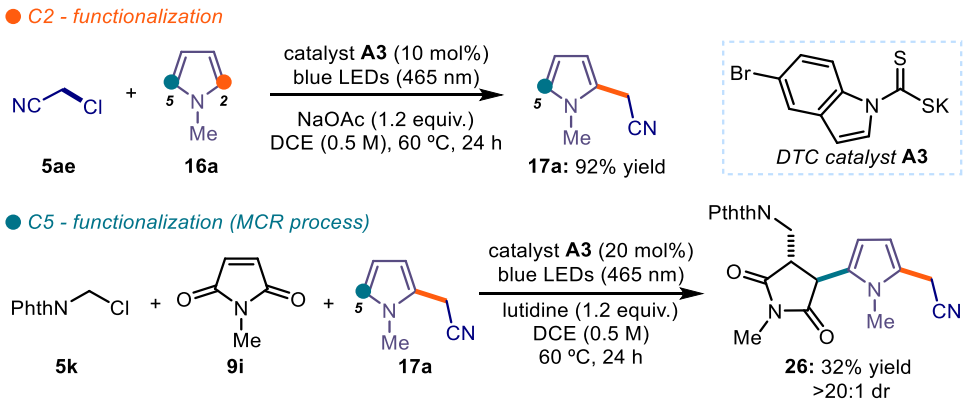

Figure 4.28. Photochemical radical assembly line synthesis of a difunctionalized pyrrole, starting from commercially available reagents. *C2-functionalization*: reaction performed on 0.5 mmol scale, using 10 mol% of catalyst **A3** and 3.5 equiv. of **16a**. *C5-functionalization:* reaction performed on 0.5 mmol scale, using 20 mol% of catalyst **A3**, 1.5 equiv. of **5k** and 10 equiv. of **17a**. NPhth: phthalimide.

[46] (a) Fürstner, A. Chemistry and Biology of Roseophilin and the Prodigioin Alkaloids: A Survey of the Last 2500 Years. *Angew. Chem. Int. Ed.* **2003**, *42*, 3582–3603. (b) Schmuck, C.; Rupprecht, D. The Synthesis of Highly Functionalized Pyrroles: A Challenge in Regioselectivity and Chemical Reactivity. *Synthesis* **2007**, 3095– 3110.

4.8. Product Manipulations

All the MCR-products **21** contain a succinimide moiety that can be reduced to access the corresponding substituted pyrrolidines.[47] Such scaffolds are synthetically and biologically relevant.[48] The feasibility of this derivatization was demonstrated with the diastereopure MCR product **21ae** (Figure 4.29). We submitted **21ae** to a reduction with $LiAlH_4$, which afforded the corresponding *trans*-3,4-disubstituted pyrrolidine **27** in 94% yield. This transformation further testifies to the potential of this MCR strategy to cover biologically relevant chemical space.

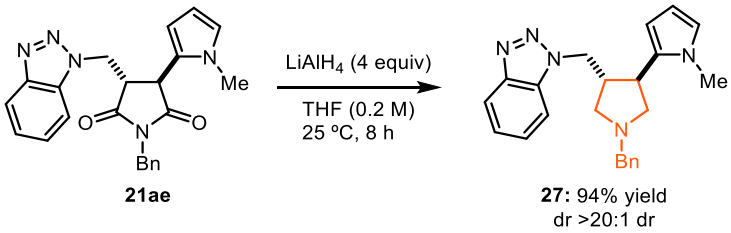

Figure 4.29. Derivatization of the MCR product **21ae** to access the diastereopure pyrrolidine **27**.

4.9. An Alternative Mechanism for Catalyst Turnover

In Section 4.4, we discussed a mechanistic hypothesis for the dithiocarbamate anion-mediated MCR. This proposed mechanism (in Figure 4.20) is likely a simplified framework of a more complex scenario. We proposed that the turnover of the catalyst **A3** is triggered by a SET between the sulfur-centered radical **XIII** and the radical **XIX** (see Figure 4.30). This proposal could be likely operative considering the relatively low redox potential of catalyst **A3**: E_{ox} (**XIII**/**A3**) = +0.44 V vs. Ag/AgCl, KCl, 3.5 M.[39]

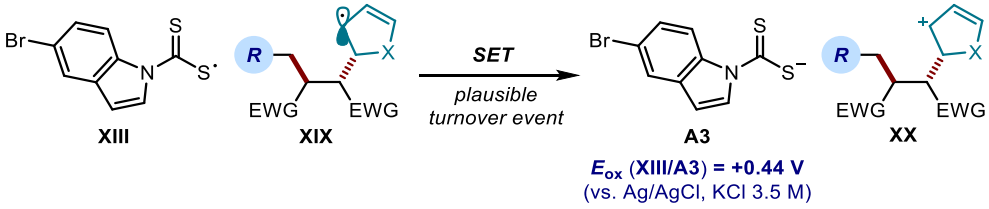

Figure 4.30. Proposed turnover event based on a SET between the open-shell intermediates **XIII** and **XIX**.

[47] Schreiber, K. C.; Fernandez, V. P. The Lithium Aluminum Hydride Reduction of Some *N*-Substituted Succinimides. *J. Org. Chem.* **1961**, *266*, 1744–1747.

[48] (a) O'Hagan, D. Pyrrole, Pyrrolidine, Pyridine, Piperidine and Tropane Alkaloids. *Nat. Prod. Rep.* **2000**, *17*, 435–446. (b) Schomaker, J. M.; Bhatacharjee, S.; Yan, J.; Borhan, B. *J. Am. Chem. Soc.* **2007**, *129*, 1996–2003.

An alternative pathway for the turnover of catalyst **A3** could be based on a group transfer mechanism, as depicted in Figure 4.31. This would require the radical **XIX** to be intercepted by the dithiocarbamate intermediate **XI**.

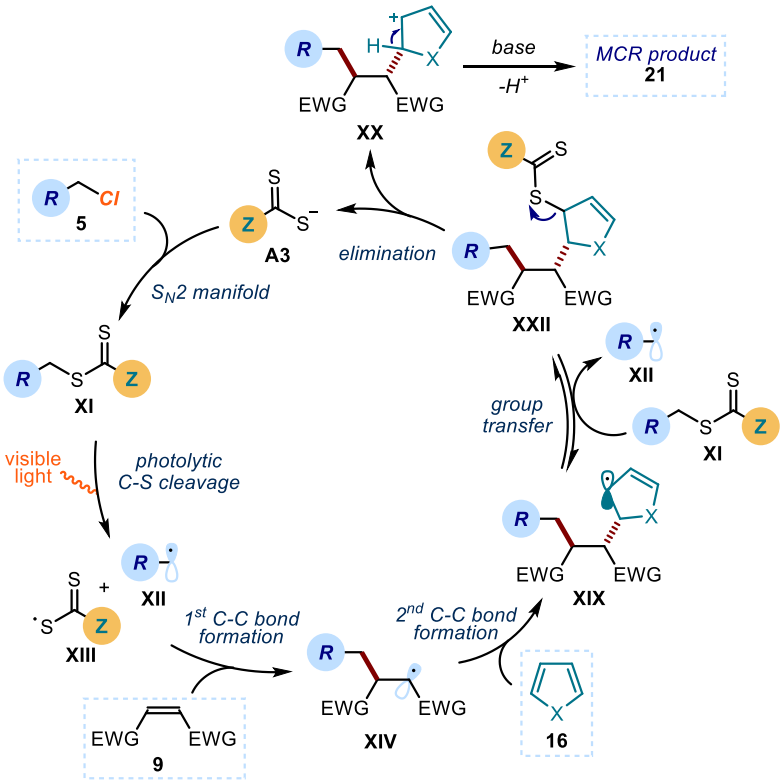

Figure 4.31. Alternative catalytic cycle wherein the turnover of catalyst **A3** is based on a group transfer/elimination process.

This group transfer manifold would provide intermediate **XXII** while regenerating the propagating radical **XII**. The turnover event would then take place via elimination from the group transfer intermediate **XXII**, which deliver the cationic intermediate **XX** and regenerates the catalyst **A3**. However, we could not design any conclusive experiment that could distinguish between these two possible operative pathways.

4.10. Conclusions

We have developed a visible light-mediated three component radical strategy, which couples readily available alkyl chlorides, maleimides, and hetereoaromatic fragments to rapidly generate complex chiral products with high diastereocontrol. The overall process is characterized by its mild and redox-neutral conditions, which make it tolerant of redox-sensitive substrates and allow the installation of multiple biologically relevant *N*-heterocycles

(*e.g.* triazole, pyrazole, thiazole, etc.) within the cascade products. Mechanistically, the MCR is founded upon a unique S_N2-based photochemical catalytic radical-generation strategy, which is not reliant on the redox properties of the radical precursors. It therefore grants access to open-shell intermediates from substrates that would be incompatible with or inert to classical radical-generating strategies. This means that this radical cascade could not be implemented with traditional methods, including photoredox catalysis. From a synthetic perspective, this study shows that difficult-to-reduce and inexpensive alkyl chlorides can be used as radical precursors and coupled with readily available maleimides and heteroaromatic fragments. Overall, the unique features of the S_N2-based radical generation strategy could inspire other applications in the design of free-radical multicomponent strategies potentially amenable to medicinal chemistry development.

4.11. Experimental Section

4.11.1. General Information

The NMR spectra were recorded at 400 MHz and 500 MHz for ^{1}H and 100 or 125 MHz for ^{13}C. The chemical shift (δ) for ^{1}H and ^{13}C are given in ppm relative to residual signals of the solvents ($CHCl_3$ @ 7.26 ppm ^{1}H NMR and 77.16 ppm ^{13}C NMR, and tetramethylsilane @ 0 ppm). Coupling constants are given in Hertz. The following abbreviations are used to indicate the multiplicity: s, singlet; d, doublet; q, quartet; m, multiplet; bs, broad signal; app, apparent.

Infrared (IR) spectra were obtained using a Bruker Alpha FT-IR spectrometer.

High resolution mass spectra (HRMS) were obtained from the ICIQ HRMS unit on MicroTOF Focus and Maxis Impact (Bruker Daltonics) with electrospray ionization. (ESI). X-ray data were obtained from the ICIQ X-Ray unit using a Brucker-Nonius diffractometer equipped with an APPEX 2 4K CCD area detector.

Yields refer to isolated materials of >95% purity, as determined by ^{1}H NMR.

General Procedures. All reactions were set up under an argon atmosphere in oven-dried glassware using standard Schlenk techniques, unless otherwise stated. Synthesis grade solvents were used as purchased; anhydrous solvents were taken from a commercial SPS solvent dispenser. Chromatographic purification of products was accomplished using forced-flow chromatography (FC) on silica gel (35-70 mesh). For thin layer chromatography (TLC) analysis throughout this work, Merck pre-coated TLC plates (silica gel 60 GF_{254}, 0.25 mm) were employed, using UV light as the visualizing agent and an acidic mixture of vanillin or basic aqueous potassium permanganate ($KMnO_4$) stain solutions, and heat as developing agents. Organic solutions were concentrated under reduced pressure on a Büchi rotatory evaporator.

Materials. Most of the starting materials used in this study are commercially available and were purchased in the highest purity available from Sigma-Aldrich, Fluka, Alfa Aesar, Fluorochem, and used as received, without further purifications.

The NMR spectra are available in the published manuscript,[1] and are not reported in the present doctoral thesis.

4.11.2. Synthesis of the Dithiocarbamate Anion Catalyst A3

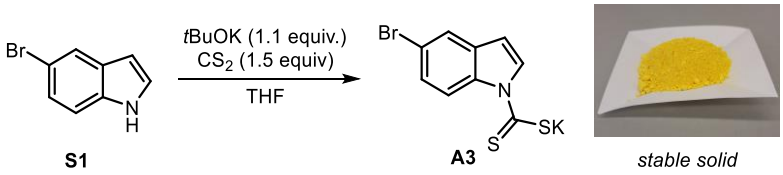

S1 **A3** *stable solid*

In an oven dried round bottom flask under an atmosphere of argon, commercially available *5*-bromoindole (1 equiv.) was dissolved in a minimal amount of THF (commercial synthesis grade; 10 $mL \cdot g^{-1}$). The flask was cooled to 0 ºC in an ice-water bath and potassium *tert*-butoxide (1.1 equiv.) was added portionwise. The mixture turned a slight yellow/orange color and was left to stir for 30 minutes. Still at 0 ºC, carbon disulfide (1.5 equiv.) was added dropwise *via* syringe addition. The mixture immediately turned a bright orange color and was left to stir for one hour at 0 ºC. After warming up to ambient temperature, THF was evaporated carefully on a rotary evaporator to a thick syrupy consistence. Toluene was added and evaporated to obtain a yellow solid residue. The residue was suspended in a 1:1 mixture of pentane and diethyl ether and stirred vigorously to obtain a fine suspension. The yellow solid was then filtered under a flow of argon, washed twice with a small amount of a 1:1 mixture of pentane and diethyl ether and further dried overnight under high vacuum to obtain the desired product as a yellow free flowing powder.

This reaction has been performed on various scales (5 to 55 mmol of starting *5*-bromoindole) with isolated yields ranging from 88 to 95%.

Note: Once isolated, **A3** is slightly hygroscopic and should therefore be protected from ambient humidity. It was typically stored in brown glass bottles in a desiccator. No degradation was detected over a 3-month period, as indicated by NMR analysis.

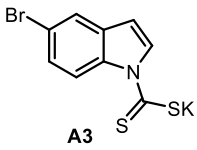

A3

Potassium 5-bromo-1*H*-indole-1-carbodithioate (A3)

^{1}H NMR (400 MHz, d^{6}-DMSO) δ 6.39 (d, *J*=3.5 Hz, 1H), 7.25 (dd, J= 9, 2.1 Hz, 1H), 7.68 (d, J=2.1 Hz, 1H), 8,69 (d, J= 3.5 Hz, 1H), 9,28 (d, J= 9 Hz, 1H). **^{13}C NMR (101 MHz, d6-DMSO)** δ 218.7 (C), 134,9 (C), 133.9 (C), 132.2 (CH), 124.9 (CH), 122.7 (CH), 120.0 (CH), 113.5 (C), 102.0 (CH).

IR (thin film) ν 1744, 1438, 1354, 1292, 1204, 1174, 1065, 1000, 829, 724 cm^{-1}.

HRMS (ESI negative): calculated for $C_9H_5{}^{79}BrNS_2$ (M): 269.9052, found 269.9044.

Using the catalog prices of the suppliers the chemicals were obtained from, a cost of 0.63 €·g^{-1} or 192 €·mol^{-1} in materials (excluding labor) was calculated.

4.11.3. Experimental Procedure

4.11.3.1. Set-up: Temperature-controlled Photoreactor and Specifications of the Light Source

The photoreactor consisted of a 12.5 cm diameter jar, fitted with 4 standard 29 sized ground glass joints arranged in a square and a central 29 sized joint. A commercial 1 meter LED strip was wrapped around the jar, followed by a layer of aluminium foil and cotton for insulation (Figure 4.32a).

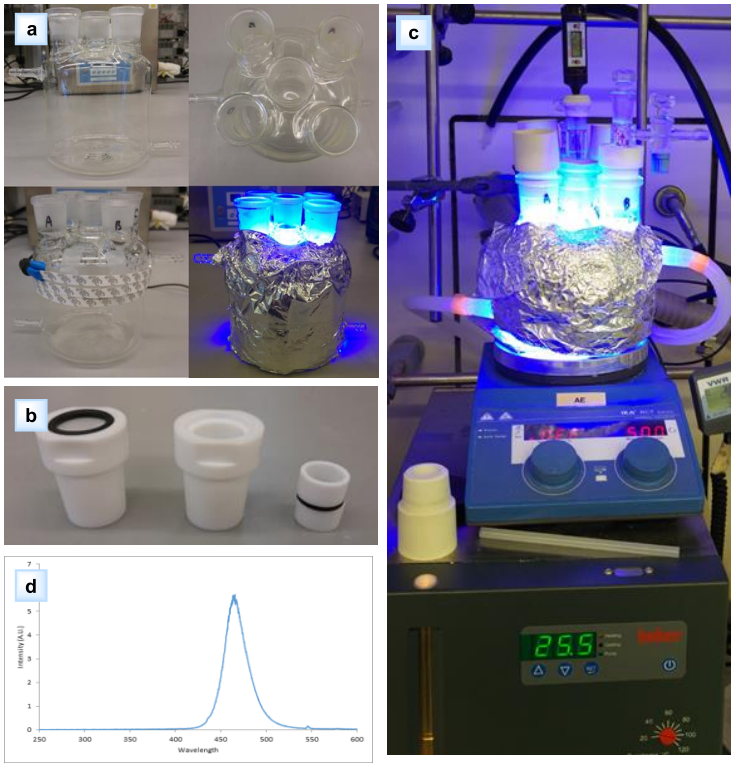

Figure 4.32. (a) Photoreactor used in this study. (b) Teflon adaptors used to accommodate Schlenk tubes in the photoreactor. (c) Fully assembled photoreactor in operation. (d) Emission spectrum of the 465 nm *blue LED strip* used in this study.

Each of the joints could be used to fit a standard 16 mm or 25 mm diameter Schlenk tube with a Teflon adaptor (Figure 4.32b). An inlet and an outlet allow the circulation of liquid from a Huber Minichiller 300 inside the jar. This setup allows to perform reactions at temperatures ranging from -20 ºC to 80 ºC with accurate control of the reaction temperature (± 1ºC) (Figure 4.32c). To maintain a consistent illumination during different experiments, only the four external positions were used to perform reactions while the central one was used to monitor the temperature inside a Schlenk tube identical to those used to perform reactions.

The light source used in this study consisted of a 1 m strip, 14.4W 'LEDXON MODULAR 9009083 LED, SINGLE 5050' purchased from Farnell, catalog number 9009083. The emission spectrum of these LEDs was recorded (Figure 4.32d).

4.11.3.2. General Procedure for the Three-Component Radical Process

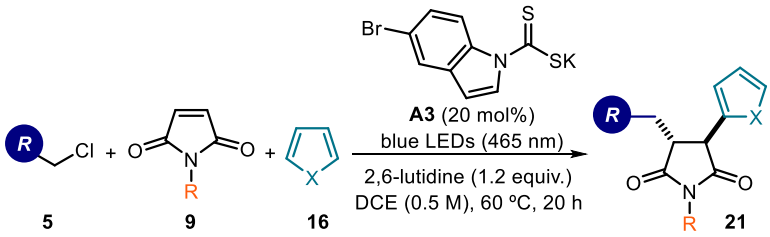

In an oven dried Schlenk tube, the DTC catalyst **A3** (31.0 mg, 0.1 mmol, 0.2 equiv.) was dissolved in dichloroethane (0.5 mL), then the alkyl chloride **5** (0.75 mmol, 1.5 equiv.) was added while stirring, followed by 2,6-lutidine (70 µL, 0.6 mmol, 1.2 equiv.), maleimide **9** (0.5 mmol, 1.0 equiv.), and pyrrole **16** (5.0 mmol, 10.0 equiv.). An additional volume of dichloroethane (0.5 mL) was added to the reaction vessel, washing the sides from residual solids. The resulting mixture was degassed via three cycles of freeze-pump-thaw. The Schlenk tube was then placed in the irradiation setup (see Section 4.7.3.1, Figure 4.31), maintained at a temperature of 60 ºC (60-61ºC measured in the central well), and the reaction was stirred for 20 hours under continuous irradiation. After cooling to ambient temperature, the solvent was evaporated and the residue purified by column chromatography to afford the corresponding product **21** in the stated yield with >95% purity according to ^{1}H NMR analysis. The exact conditions for chromatography are reported for each compound.

4.11.3.3. Characterization of the MCR Products

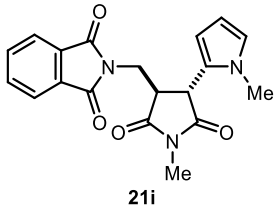

21i

2-((1-methyl-4-(1-methyl-1*H*-pyrrol-2-yl)-2,5-dioxopyrrolidin-3-yl)methyl)isoindoline-1,3-dione (21i): Synthesized according to the general procedure using *N*-(chloromethyl)phthalimide **5k** (147 mg, 0.75 mmol, 1.5 equiv.), *N*-methylmaleimide **9i** (56 mg, 0.5 mmol, 1 equiv.) and *N*-methylpyrrole **16a** (445 µL, 5 mmol, 10 equiv.). A single diastereomer was detected by ^{1}H NMR analysis of the crude reaction mixture. Product **21i** was purified by column chromatography (gradient from 20% to 35% AcOEt in hexanes as eluent): 100 mg yellow solid, 57% yield. Crystallization from MeOH afforded crystals suitable for X-ray diffraction analysis (CCDC 1894404, see Experimental Section 4.11.8), which revealed a *trans* relative stereochemistry. Product **21i** can be synthesized up to a 5 mmol scale using the same photochemical set-up (see Experimental Section 4.11.4 for details).

^{1}H NMR (500 MHz, $CDCl_3$) δ 7.73 (dd, *J* = 5.5, 3.1 Hz, 2H), 7.65 (dd, *J* = 5.4, 3.1 Hz, 2H), 6.36 (dd, *J* = 2.5, 2.0 Hz, 1H), 5.78 (dd, *J* = 3.6, 1.6 Hz, 1H), 5.72 (dd, *J* = 3.7, 2.8 Hz, 1H), 4.32 (dd, *J* = 14.0, 5.7 Hz, 1H), 4.07-4.02 (m, 2H), 3.62 (s, 3H), 3.61-3.58 (m, 1H), 2.99 (s, 3H). **^{13}C NMR (126 MHz, $CDCl_3$)** δ 175.7, 175.4, 168.5, 134.4, 131.9, 125.3, 124.0, 123.6, 107.3, 106.8, 45.2, 43.7, 38.1, 34.4, 25.5.

IR (thin film) ν 2950, 1773, 1694, 1433, 1395, 1379, 1361, 1304, 1271, 1089, 715 cm^{-1}.

HRMS: calculated for $C_{19}H_{17}N_3NaO_4^+$ ($M+Na^+$): 374.1111, found 374.1114.

TLC: 30:70 EtOAc/hexanes, R_f = 0.14.

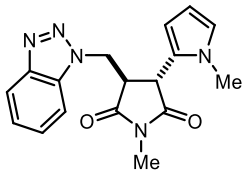

21j

3-((1*H*-benzo[*d*][1,2,3]triazol-1-yl)methyl)-1-methyl-4-(1-methyl-1*H*-pyrrol-2-yl)pyrrolidine-2,5-dione (21j): Synthesized according to the general procedure using 1-(chloromethyl)-1*H*-benzotriazole **5m** (126 mg, 0.75 mmol, 1.5 equiv.), *N*-methylmaleimide **9i** (56 mg, 0.5 mmol, 1 equiv.) and *N*-methylpyrrole **16a** (445 µL, 5 mmol, 10 equiv.). A single diastereomer was detected by ^{1}H NMR analysis of the crude reaction mixture. Product **21j** was purified by column chromatography (gradient from 20% to 35% AcOEt in hexanes as eluent): 91 mg, white foam, 56% yield.

^{1}H NMR (500 MHz, $CDCl_3$) δ 8.02-8.00 (m, 1H), 7.62-7.60 (m, 1H), 7.52-7.48 (m, 1H), 7.38-7.35 (m, 1H), 6.60 (dd, *J* = 2.5, 1.9 Hz, 1H), 6.02 (dd, *J* = 3.6, 2.8 Hz, 1H), 5.91 (dd, *J* = 3.7, 1.6 Hz, 1H), 5.21 (dd, *J* = 14.7, 4.6 Hz, 1H), 4.97 (dd, *J* = 14.8, 4.3 Hz, 1H), 4.22 (d, *J* = 6.8 Hz, 1H), 3.65 (s, 3H), 3.64-3.60 (m, 1H), 2.85 (s, 3H). **^{13}C NMR (126 MHz, $CDCl_3$)** δ 175.9, 175.2, 146.1, 133.7, 128.4, 125.6, 124.8, 124.4, 120.4, 110.0, 107.6, 106.7, 48.0, 45.5, 41.4, 34.7, 25.6.

IR (thin film) ν 2924, 1698, 1493, 1434, 1383, 1289, 1274, 1162, 1126, 724 cm^{-1}.

HRMS: calculated for $C_{17}H_{17}N_5NaO_2^+$ ($M+Na^+$): 346.1274, found 346.1282.

TLC: 30:70 EtOAc/hexanes, R_f = 0.1.

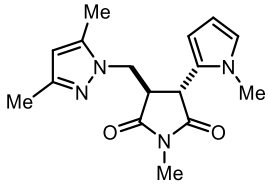

21k

3-((3,5-dimethyl-4,5-dihydro-1*H*-pyrazol-1-yl)methyl)-1-methyl-4-(1-methyl-1*H*-pyrrol-2-yl)pyrrolidine-2,5-dione (21k): Synthesized by a two-step procedure. First, the alkyl chloride **5o** was synthesized via a variation of a reported procedure:[2] in a round bottom flask, (3,5-dimethyl-1H-pyrazol-1-yl)methanol (126 mg, 1 mmol, 1 equiv.) was dissolved in dry chloroform (5 mL) and cooled at 0 ºC. Thionyl chloride (88 µL, 1.2 mmol, 1.2 equiv.) was

added dropwise and the reaction was left stirring at ambient temperature for 30 min. Solvent was removed under vacuum at 25 ºC, diethyl ether (5 mL) was added and dried (this was repeated twice) to obtain the crude 1-(chloromethyl)-3,5-dimethyl-1*H*-pyrazole hydrochloride **5o** as a white solid, which was used directly without further purification. The crude product **5o** was dissolved in 1,2-dichloroethane giving a stock solution 0.75 M. 1-(chloromethyl)-3,5-dimethyl-1*H*-pyrazole hydrochloride **5o** (0.75 M, 0.75 mmol, 1.5 equiv.) was added in an oven dried Schlenk tube, then the DTC catalyst **A3** (31.0 mg, 0.1 mmol, 0.2 equiv.) was added followed by 2,6-lutidine (70 µL, 0.6 mmol, 1.2 equiv.), *N*-methylmaleimide **9i** (57.0 mg, 0.5 mmol, 1 equiv), and *N*-methylpyrrole **16a** (445 µL, 5 mmol, 10 equiv.). The resulting yellow mixture was degassed via three cycles of freeze-pump-thaw. The Schlenk tube was then placed in the irradiation setup at a temperature of 60 ºC and irradiated for 20 hours. After cooling to ambient temperature, the solvent was evaporated. Multiple purification by column chromatography (gradient from 10% to 40% AcOEt in hexanes as eluent) resulted in poor separation from several unidentified byproducts, but an analytical amount of the pure major diastereomer was isolated for characterization. The yield (40%) of 4c and the distereomeric ration (20:1) were inferred by ^{1}H NMR analysis of the crude reaction mixture using trichloroethylene as the internal standard.

^{1}H NMR (500 MHz, $CDCl_3$) δ 6.60 (dd, *J* = 2.8, 1.7 Hz, 1H), 6.05 (dd, *J* = 3.7, 2.7 Hz, 1H), 5.90 (dd, *J* = 3.8, 1.1 Hz, 1H), 5.73 (s, 1H), 4.54 (dd, *J* = 14.4, 4.9 Hz, 1H), 4.43 (d, *J* = 5.7 Hz, 1H), 4.27 (dd, *J* = 14.4, 4.3 Hz, 1H), 3.68 (s, 3H), 3.34 (m), 2.96 (s, 3H), 2.20 (s, 3H), 2.12 (s, 3H).

^{13}C NMR (126 MHz, $CDCl_3$) δ 176.7, 176.1, 148.4, 140.0, 126.7, 123.7, 107.3, 106.2, 105.6, 48.5, 45.6, 41.1, 34.4, 25.3, 13.6, 11.0.

HRMS: calculated for $C_{16}H_{20}N_4NaO_2^+$ ($M+Na^+$): 323.1478, found 323.1472.

TLC: 40:60 EtOAc/hexanes, R_f = 0.25.

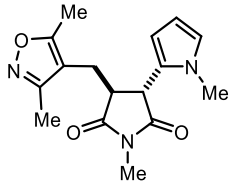

21l

3-((3,5-dimethylisoxazol-4-yl)methyl)-1-methyl-4-(1-methyl-1H-pyrrol-2-yl)pyrrolidine-2,5-dione (21l): Synthesized according to the general procedure using 4-(chloromethyl)-3,5-dimethylisoxazole **5l (**109 mg, 93 µL, 0.75 mmol, 1.5 equiv.), *N*-methylmaleimide **9i** (56 mg, 0.5 mmol, 1 equiv.) and *N*-methylpyrrole **16a** (445 µL, 5 mmol, 10 equiv.). A single diastereomer was detected by ^{1}H NMR analysis of the crude reaction mixture. Product **21l** was purified by column chromatography (gradient from 10% to 30% AcOEt in hexanes as eluent): 96.3 mg pale yellow solid, 64% yield.

^{1}H NMR (500 MHz, $CDCl_3$) δ 6.61 (dd, *J* = 2.8, 1.7 Hz, 1H), 6.04 (dd, *J* = 3.7, 2.8 Hz, 1H), 5.90 (dd, *J* = 3.8, 1.8, 0.7 Hz, 1H), 3.59 (s, 3H), 3.58 (d, *J* = 6.3 Hz, 1H), 3.26 (app q, *J* = 6.4

Hz, 1H), 2.96 (s, 3H), 2.86 (d, *J* = 6.3 Hz, 2H), 2.23 (s, 3H), 2.08 (s, 3H). **^{13}C NMR (126 MHz, $CDCl_3$)** δ 177.5, 175.3, 166.6, 159.6, 125.3, 124.2, 109.5, 107.4, 106.6, 46.5, 43.2, 34.3, 25.2, 21.9, 11.2, 10.2.

IR (thin film) ν 2924, 1779, 1701, 1429, 1377, 1268, 1110, 980, 698 cm^{-1}.

HRMS: calculated for $C_{16}H_{20}N_3O_3^+$ (M^+): 302.1496, found 302.1499

TLC: 30:70 EtOAc/hexanes, R_f = 0.27.

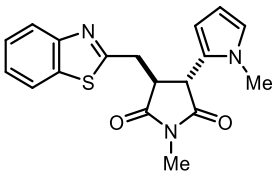

21m

3-(benzo[d]thiazol-2-ylmethyl)-1-methyl-4-(1-methyl-1H-pyrrol-2-yl)pyrrolidine-2,5-dione (21m): Synthesized according to the general procedure using 2-(chloromethyl)-1,3-benzothiazole **5p** (138 mg, 0.75 mmol, 1.5 equiv.), *N*-methylmaleimide **9i** (56 mg, 0.5 mmol, 1 equiv.) and *N*-methylpyrrole **16a** (445 µL, 5 mmol, 10 equiv.). A single diastereomer was detected by ^{1}H NMR analysis of the crude reaction mixture. Product **21m** was purified by column chromatography (gradient from 10% to 30% EtOAc in hexanes as eluent, two consecutive purifications): 75.9 mg of a pink oil. The isolated material consisted of a mixture containing **21m** an inseparable byproduct in a proportion 6.3:1 (see Figure S2 below), arising from a polar Friedel-Crafts type alkylation of pyrrole with maleimide. Corrected yield of product **21m**: 38%.

^{1}H NMR (500 MHz, $CDCl_3$) δ 7.90 (d, *J* = 8.1 Hz, 1H), 7.83 (d, *J* = 7.9 Hz, 1H), 7.45 (ddd, *J* = 8.3, 7.2, 1.3 Hz, 1H), 7.37 (ddd, *J* = 8.2, 7.3, 1.2 Hz, 1H), 6.60 (dd, *J* = 2.7, 1.8 Hz, 1H), 6.06 (dd, *J* = 3.7, 2.7 Hz, 1H), 5.98 (dd, *J* = 3.8, 1.7 Hz, 1H), 4.33 (d, *J* = 5.9 Hz, 1H), 3.78 (dd, *J* = 15.9, 5.5 Hz, 1H), 3.66 (s, 3H), 3.56 (dd, *J* = 16.0, 4.6 Hz, 1H), 3.51 (app q, *J* = 5.3 Hz, 1H), 3.04 (s, 3H). **^{13}C NMR (126 MHz, $CDCl_3$)** δ 177.4, 176.1, 166.2, 153.1, 135.4, 126.6, 126.3, 125.4, 123.9, 123.1, 121.7, 107.4, 106.5, 46.6, 42.8, 34.5, 32.4, 25.4.

IR (thin film) ν 2924, 1776, 1695, 1491, 1432, 1381, 1279, 1108, 760, 709 cm^{-1}.

HRMS: calculated for $C_{18}H_{18}N_3O_2S^+$ (M^+): 340.1114, found 340.1113.

TLC: 30:70 EtOAc/hexanes R_f = 0.23.

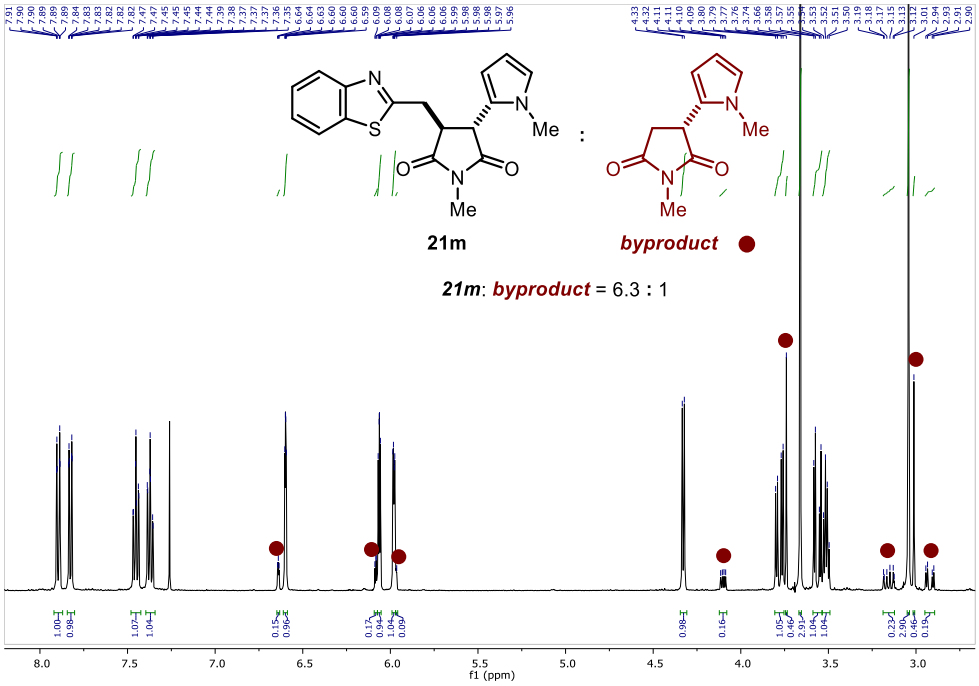

Figure 4.32. ^{1}H NMR spectrum of the mixture of product **21m** and byproduct (red dots) arising from a polar Friedel-Crafts type alkylation path.

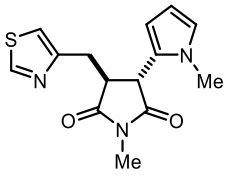

21n

1-methyl-3-(1-methyl-1H-pyrrol-2-yl)-4-(thiazol-4-ylmethyl)pyrrolidine-2,5-dione (21n): Synthesized according to a modification of the general procedure: in an oven dried Schlenk tube, 4-(chloromethyl)thiazole hydrochloride **5q** (128 mg, 0.75 mmol, 1.5 equiv.) was dissolved in 1,2-dichloroethane (1 mL, 0.5 M). Then 2,6-lutidine (157 µL, 1.35 mmol, 2.7 equiv.) was added followed by the DTC catalyst **A3** (31 mg, 0.2 equiv., 20 mol%), *N*-methylmaleimide **9i** (56 mg, 0.5 mmol, 1 equiv) and *N*-methylpyrrole **16a** (445 µL, 5 mmol, 10 equiv.). The resulting yellow mixture was degassed via three cycles of freeze-pump-thaw. The Schlenk tube was then placed in the irradiation setup set at a temperature of 60 ºC and irradiated for 20 hours. After cooling to ambient temperature, the solvent was evaporated. A single diastereomer was detected by ^{1}H NMR analysis of the crude reaction mixture. Product **21n** was purified by column chromatography (gradient from 20% to 30% AcOEt in hexanes as eluent): 58.6 mg of a pale yellow solid, 41% yield.

^{1}H NMR (500 MHz, $CDCl_3$) δ 8.69 (d, *J* = 2.0 Hz, 1H), 7.05 (d, *J* = 1.5 Hz, 1H), 6.59 (t, *J* = 2.2 Hz, 1H), 6.05 (dd, *J* = 3.7, 2.8 Hz, 1H), 5.92 (dd, *J* = 3.9, 1.7 Hz, 1H), 4.13 (d, *J* = 5.4 Hz, 1H), 3.64 (s, 3H), 3.47 – 3.39 (m, 2H), 3.36 – 3.27 (m, 1H), 2.95 (s, 3H). **^{13}C NMR (126**

MHz, $CDCl_3$) δ 178.0, 176.3, 153.0, 152.9, 127.0, 123.6, 115.8, 107.3, 106.4, 47.4, 42.6, 34.4, 30.0, 25.2.

IR (thin film) ν 3078, 2921, 1691, 1433, 1290, 1067, 993, 731 cm^{-1}.

HRMS: calculated for $C_{14}H_{15}N_3NaO_2S^+$ ($M+Na^+$): 312.0777, found 312.0773.

TLC: 30:70 EtOAc/hexanes, R_f = 0.13.

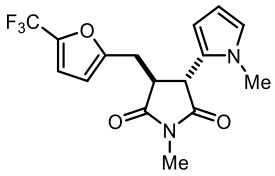

21o

1-methyl-3-(1-methyl-1H-pyrrol-2-yl)-4-((5-(trifluoromethyl)furan-2-yl)methyl)pyrrolidine-2,5-dione (21o): Synthesized according to the general procedure using 2-(bromomethyl)-5-(trifluoromethyl)furan **10l** (172 mg, 0.75 mmol, 1.5 equiv.), *N*-methylmaleimide **5r** (56 mg, 0.5 mmol, 1 equiv.) and *N*-methylpyrrole **16a** (445 µL, 5 mmol, 10 equiv.). A single diastereomer was detected by ^{1}H NMR analysis of the crude reaction mixture. Product **21o** was purified by column chromatography (gradient from 0% to 2% acetone in toluene as eluent; two consecutive purifications): 85.0 mg of a brown oil, 50% yield.

^{1}H NMR (500 MHz, $CDCl_3$) δ 6.66 (dd, J = 3.3, 1.4 Hz, 1H), 6.61 (dd, *J* = 2.7, 1.7 Hz, 1H), 6.15 (d, *J* = 3.2 Hz, 1H), 6.05 (dd, *J* = 3.7, 2.8 Hz, 1H), 5.91 (dd, *J* = 3.8, 1.7 Hz, 1H), 3.81 (d, *J* = 5.9 Hz, 1H), 3.64 (s, 3H), 3.36 (app q, *J* = 5.9 Hz, 1H), 3.24 (d, *J* = 5.9 Hz, 2H), 2.99 (s, 3H). **^{13}C NMR** (100 MHz, $CDCl_3$) δ 177.0, 175.4, 154.3 (d, J = 1.5 Hz), 141.4 (q, J = 42.8 Hz), 125.9, 124.0, 119.0 (q, J = 266.8 Hz), 112.6 (q, J = 2.9 Hz), 109.0, 107.3, 106.4, 46.4, 43.2, 34.2, 27.9, 25.2.

IR (thin film) ν 2950, 1779, 1698, 1616, 1560, 1434, 1382, 1321, 1173, 1122, 1103, 712 cm^{-1}.

HRMS: calculated for $C_{16}H_{16}F_3N_2O_3^+$ (M^+): 341.1108, found 341.1105.

TLC: 2:98 acetone/toluene, R_f = 0.35.

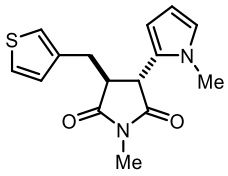

21p

1-methyl-3-(1-methyl-1H-pyrrol-2-yl)-4-(thiophen-3-ylmethyl)pyrrolidine-2,5-dione (21p): Synthesized by a two-step procedure. First, the alkyl chloride was synthesized: in an oven dried Schlenk tube, 3-thiophenemethanol (115 mg, 0.75 mmol, 1.5 equiv.) was dissolved in dry dichloromethane (5 mL) and cooled at 0 ºC. Thionyl chloride (88 µL, 1.2 mmol, 1.2 equiv.) was added dropwise and the reaction was left stirring at ambient temperature for 30 min. Solvent was removed under vacuum at 25 ºC, diethyl ether (5 mL) was added and dried (this was repeated twice) to obtain the crude 3-(chloromethyl)thiophene **5s** as a colorless oil in quantitative yield, which was used without further purification. The crude adduct **5s** was dissolved in 1,2-

dichloroethane giving a stock solution 0.75 M. 3-(chloromethyl)thiophene **5s** (0.75 M, 0.75 mmol, 1.5 equiv.) was added in an oven dried Schlenk tube, then the DTC catalyst **A3** (31 mg, 0.2 equiv.) was added followed by 2,6-lutidine (157 µL, 1.35 mmol, 2.7 equiv.), *N*-methylmaleimide **9i** (56 mg, 0.5 mmol, 1 equiv.) and *N*-methylpyrrole **16a** (445 µL, 5 mmol, 10 equiv.). The resulting yellow mixture was degassed via three cycles of freeze-pump-thaw. The Schlenk tube was then placed in the irradiation setup at a temperature of 60 ºC and irradiated for 20 hours. After cooling to ambient temperature, the solvent was evaporated and the residue purified by column chromatography (two consecutive purifications; first purification: gradient from 10% to 20% AcOEt in hexanes as eluent; second purification: gradient from 0% to 2% acetone in toluene as eluent): 100.3 mg of **21p** isolated as a brown oil, 66% yield. A single diastereomer was detected by ^{1}H NMR analysis of the crude reaction mixture.

^{1}H NMR (500 MHz, $CDCl_3$) δ 7.27 – 7.25 (m, 1H), 6.98 – 6.96 (m, 1H), 6.86 (dd, *J* = 5.0, 1.3 Hz, 1H), 6.60 (dd, *J* = 2.7, 1.8 Hz, 1H), 6.07 (dd, *J* = 3.7, 2.7 Hz, 1H), 5.95 (ddd, *J* = 3.7, 1.8, 0.6 Hz, 1H), 3.71 (d, *J* = 5.5 Hz, 1H), 3.54 (s, 3H), 3.37 – 3.33 (m, 1H), 3.29 (ddd, *J* = 14.5, 6.3, 0.8 Hz, 1H), 3.12 (dd, *J* = 14.5, 5.1 Hz, 1H), 2.96 (s, 3H). **^{13}C NMR (100 MHz, $CDCl_3$)** δ 178.1, 176.0, 136.8, 128.4, 126.6, 126.5, 123.7, 123.0, 107.3, 106.5, 47.9, 42.5, 34.2, 29.5, 25.1.

IR (thin film) ν 2925, 1776, 1695, 1491, 1432, 1380, 1286, 1119, 1090, 752, 711 cm^{-1}.

HRMS: calculated for $C_{15}H_{17}N_2O_2S^+$ ($M+H^+$):289.1005, found 289.1016

TLC: 30:70 EtOAc/hexanes, R_f = 0.38.

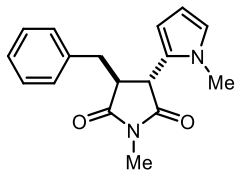

21q

3-benzyl-1-methyl-4-(1-methyl-1*H*-pyrrol-2-yl)pyrrolidine-2,5-dione (21q): Synthesized according to the general procedure using benzyl bromide **5b** (89 µL, 0.75 mmol, 1.5 equiv.), *N*-methylmaleimide **9i** (56 mg, 0.5 mmol, 1 equiv.) and *N*-methylpyrrole **16a** (445 µL, 5 mmol, 10 equiv.). The diastereomeric ratio (7.6:1) was determined by ^{1}H NMR spectroscopic analysis of the crude reaction mixture by comparison of the resonances at δ 5.95 (minor diastereomer) and δ 5.87 (major diastereomer). Product **21q** purified by column chromatography (gradient from 15% to 25% AcOEt in hexanes as eluent): 69 mg of a brown oil, 49% yield.

^{1}H NMR (500 MHz, $CDCl_3$) δ 7.29-7.20 (m, 3H), 7.14-7.11 (m, 2H), 6.55 (dd, *J* = 2.6, 1.8 Hz, 1H), 6.04 (dd, *J* = 3.6, 2.9 Hz, 1H), 5.91 (dd, *J* = 3.6, 1.6 Hz, 1H), 3.70 (d, *J* = 5.5 Hz, 1H), 3.47 (s, 3H), 3.37 (app q, *J* = 5.7 Hz, 1H), 3.22 (dd, *J* = 14.1, 6.5 Hz, 1H), 3.10 (dd, *J* = 14.1, 5.5 Hz, 1H), 2.94 (s, 3H). **^{13}C NMR (126 MHz, $CDCl_3$)** δ 178.2, 176.0, 136.7, 129.5, 128.9, 127.3, 126.6, 123.6, 107.3, 106.5, 48.4, 42.3, 35.1, 34.2, 25.1.

IR (thin film) ν 2926, 1776, 1695, 1494, 1432, 1382, 1287, 1122, 992, 703 cm^{-1}.

HRMS: calculated for $C_{17}H_{19}N_2O_2^+$ ($M+H^+$): 283.1441, found 283.1437.

TLC: 20:80 EtOAc/hexanes, R_f = 0.19.

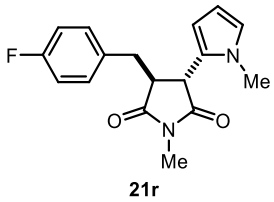

21r

3-(4-fluorobenzyl)-1-methyl-4-(1-methyl-1H-pyrrol-2-yl)pyrrolidine-2,5-dione (21r): Synthesized according to the general procedure using 4-fluorobenzyl bromide **5t** (142 mg, 0.75 mmol, 1.5 equiv.), *N*-methylmaleimide **9i** (56 mg, 0.5 mmol, 1 equiv.) and *N*-methylpyrrole **16a** (445 µL, 5 mmol, 10 equiv.). The diastereomeric ratio (5.3:1) was determined by ^{1}H NMR spectroscopic analysis of the crude reaction mixture by comparison of the resonances at δ 5.92 (major diastereomer) and δ 5.95 (minor diastereomer). Product **21r** purified by column chromatography (gradient from 10% to 20% AcOEt in hexanes as eluent): 82.2 mg of a brown oil, 55% yield.

^{1}H NMR (500 MHz, $CDCl_3$) δ 7.13 – 7.08 (m, 2H), 7.00 – 6.94 (m, 2H), 6.59 (dd, *J* = 2.8, 1.7 Hz, 1H), 6.06 (dd, *J* = 3.7, 2.7 Hz, 1H), 5.93 (dd, *J* = 3.7, 1.6 Hz, 1H), 3.68 (d, *J* = 5.7 Hz, 1H), 3.52 (s, 3H), 3.37 (app q, *J* = 5.8 Hz, 1H), 3.21 (dd, *J* = 14.3, 6.3 Hz, 1H), 3.08 (dd, *J* = 14.3, 5.5 Hz, 1H), 2.96 (s, 3H). **^{13}C NMR (126 MHz, $CDCl_3$)** δ 178.0, 175.8, 162.1 (d, *J* = 246.0 Hz), 132.4 (d, *J* = 3.3 Hz), 131.0 (d, *J* = 8.0 Hz), 126.3, 123.9, 115.8 (d, *J* = 21.3 Hz), 107.3, 106.7, 48.3, 42.4, 34.3, 34.2, 25.2. **^{19}F NMR decoupled ^{1}H (471 MHz, $CDCl_3$)** δ: -115.32

IR (thin film) ν 2925, 1696, 1508, 1432, 1381, 1286, 1221, 1120, 711 cm^{-1}.

HRMS: calculated for $C_{17}H_{18}FN_2O_2^+$ (M^+): 301.1347, found 301.1359.

TLC: 20:80 EtOAc/hexanes, R_f = 0.15.

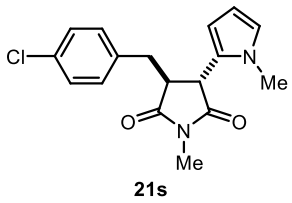

21s

(3*S*,4*R*)-3-(4-chlorobenzyl)-1-methyl-4-(1-methyl-1*H*-pyrrol-2-yl)pyrrolidine-2,5-dione (21s): Synthesized according to the general procedure using 4-chlorobenzyl bromide **5u** (154 mg, 0.75 mmol, 1.5 equiv.), *N*-methylmaleimide **9i** (56 mg, 0.5 mmol, 1 equiv.) and *N*-methylpyrrole **16a** (445 µL, 5 mmol, 10 equiv.). The diastereomeric ratio (6.3:1) was determined by ^{1}H NMR spectroscopic analysis of the crude reaction mixture by comparison of the resonances at δ 5.82 (major diastereomer) and δ 5.77 (minor diastereomer). Product **21s** was purified by column chromatography (gradient from 15% to 25% AcOEt in hexanes as eluent): 65 mg of a brown oil, 41% yield. DMSO-d_6 was used as a co-solvent in the ^{13}C NMR spectra to prevent overlap of aliphatic peaks.

^{1}H NMR (500 MHz, $CDCl_3$) δ 7.23 (d, *J* = 8.5 Hz, 2H), 7.06 (d, *J* = 8.4 Hz, 2H), 6.58 (dd, *J* = 2.6, 1.8 Hz, 1H), 6.04 (d, *J* = 3.6, 2.9 Hz, 1H), 5.91 (dd, *J* = 3.6, 1.6 Hz, 1H), 3.65 (d, *J* =

5.8 Hz, 1H), 3.51 (s, 3H), 3.36 (app q, *J* = 5.9 Hz, 1H), 3.20 (dd, *J* = 14.3, 6.4 Hz, 1H), 3.05 (dd, *J* = 14.2, 5.6 Hz, 1H), 2.94 (s, 3H). **^{13}C NMR** (126 MHz, $CDCl_3$ + DMSO-d_6) δ 177.0, 175.2, 135.7, 131.5, 130.4, 128.0, 126.1, 122.7, 106.4, 106.1, 47.4, 42.2, 33.8, 33.4, 24.4.

IR (thin film) ν 2945, 1776, 1697, 1491, 1433, 1382, 1286, 1092, 1015, 716 cm^{-1}.

HRMS: calculated for $C_{17}H_{18}ClN_2O_2^+$ (M^+): 317.1051, found 317.1054.

TLC: 25:75 EtOAc/hexanes, R_f = 0.26.

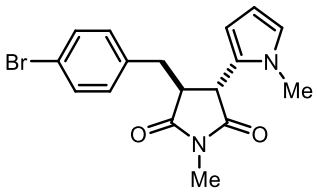

21t

(3*S*,4*R*)-3-(4-bromobenzyl)-1-methyl-4-(1-methyl-1*H*-pyrrol-2-yl)pyrrolidine-2,5-dione (21t): Synthesized according to the general procedure using 4-bromobenzyl bromide **15v** (187 mg, 0.75 mmol, 1.5 equiv.), *N*-methylmaleimide **9i** (56 mg, 0.5 mmol, 1 equiv.) and *N*-methylpyrrole **16a** (445 µL, 5 mmol, 10 equiv.). Product **21t** was purified by column chromatography (gradient from 15% to 25% AcOEt in hexanes as eluent): 104 mg browm oil, 57% yield. A single diastereomer was detected by ^{1}H NMR analysis of the crude reaction mixture.

^{1}H NMR (500 MHz, $CDCl_3$) δ 7.40 (d, *J* = 8.4 Hz, 2H), 7.02 (d, *J* = 8.4 Hz, 2H), 6.59 (dd, *J* = 2.5, 1.9 Hz, 1H), 6.06 (dd, *J* = 3.6, 2.9 Hz, 1H), 5.93 (dd, *J* = 3.6, 1.6 Hz, 1H), 3.66 (d, *J* = 5.9 Hz, 1H), 3.53 (s, 3H), 3.37 (app q, *J* = 5.9 Hz, 1H), 3.20 (dd, *J* = 14.3, 6.3 Hz, 1H), 3.05 (dd, *J* = 14.3, 5.6 Hz, 1H), 2.95 (s, 3H). **^{13}C NMR (126 MHz, $CDCl_3$)** δ 177.7, 175.6, 135.7, 131.9, 131.1, 126.1, 123.8, 121.2, 107.3, 106.6, 47.9, 42.3, 34.3, 34.2. 25.1.

IR (thin film) ν 2945, 1776, 1694, 1488, 1431, 1381, 1284, 1121, 1090, 714 cm^{-1}.

HRMS: calculated for $C_{17}H_{17}BrN_2NaO_2^+$ ($M+Na^+$): 383.0366, found 383.0360.

TLC: 25:75 EtOAc/hexanes, R_f = 0.26.

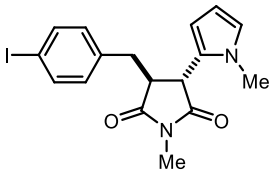

21u

3-(4-iodobenzyl)-1-methyl-4-(1-methyl-1H-pyrrol-2-yl)pyrrolidine-2,5-dione (**21u**): Synthesized according to the general procedure using 4-iodobenzyl bromide **5w** (223 mg, 0.75 mmol, 1.5 equiv.), N-methyl maleimide **9i** (56 mg, 0.5 mmol, 1 equiv) and N-methylpyrrole **16a** (445 µL, 5 mmol, 10 equiv.). Product **21u** was purified by column chromatography (gradient from 15% to 25% AcOEt in hexanes as eluent): 128 mg of a pale yellow sticky oil, 63% yield. A single diastereomer was detected by ^{1}H NMR analysis of the crude reaction mixture.

^{1}H NMR (500 MHz, $CDCl_3$) δ 7.60-7.55 (m, 2H), 6.89-6.84 (m, 2H), 6.87 (dd, *J* = 2.5, 1.8 Hz, 1H), 6.04 (dd, *J* = 3.6, 2.5 Hz, 1H), 5.9 (dd, *J* = 3.6, 1.8 Hz; 1H), 3.64 (d, *J* = 5.8 Hz; 1H), 3.51 (s, 3H), 3.35 (d, *J* = 5.9 Hz; 1H), 3.17 (dd, *J* = 14.7, 6.2 Hz; 1H), 3.01 (dd, *J* = 14.7, 5.5

Hz; 1H), 2.93 (s, 3H). **^{13}C NMR** (125 MHz, $CDCl_3$) δ 178.0, 175.9, 138.2 (x2), 136.6, 131.7 (x2), 126.3, 124.2, 107.6, 106.9, 93.0, 48.2, 42.6, 34.6, 34.6, 25.4.

IR (thin film) ν 2924, 1775, 1694, 1484, 1430, 1380, 1285, 1120, 1089, 1006, 711 cm^{-1}.

HRMS: calculated for $C_{17}H_{17}IN_2O_2^+$ ($M+H^+$): 409.0708, found 409.0387

TLC: 20:80 EtOAc/hexanes, *Rf* = 0.2.

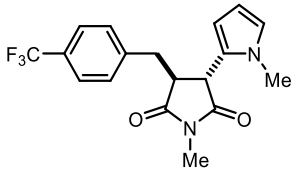

21v

1-methyl-3-(1-methyl-1H-pyrrol-2-yl)-4-(4-(trifluoromethyl)benzyl)pyrrolidine-2,5-dione (21v): Synthesized according to the general procedure using 4-(trifluoromethyl)benzyl bromide **5x** (180 mg, 0.75 mmol, 1.5 equiv.), *N*-methylmaleimide **9i** (56 mg, 0.5 mmol, 1 equiv.) and *N*-methylpyrrole **16a** (445 µL, 5 mmol, 10 equiv.). The diastereomeric ratio (4.2:1) was determined by ^{1}H NMR spectroscopic analysis of the crude reaction mixture by comparison of the resonances at δ 5.92 (major diastereomer) and δ 5.95 (minor diastereomer). Product **21v** was purified by column chromatography (gradient from 10% to 20% AcOEt in hexanes as eluent): 72.4 mg of a brown oil, 41% yield.

^{1}H NMR (500 MHz, $CDCl_3$) δ 7.53 (d, *J* = 8.0 Hz, 2H), 7.26 (d, *J* = 7.8 Hz, 2H), 6.58 (dd, *J* = 2.7, 1.8 Hz, 1H), 6.04 (dd, *J* = 3.7, 2.7 Hz, 1H), 5.92 (dd, *J* = 3.9, 1.7 Hz, 1H), 3.64 (d, *J* = 5.9 Hz, 1H), 3.51 (s, 3H), 3.42 (app q, *J* = 6.0 Hz, 1H), 3.26 (dd, *J* = 14.2, 6.4 Hz, 1H), 3.17 (dd, *J* = 14.2, 5.7 Hz, 1H), 2.95 (s, 3H). **^{13}C NMR (126 MHz, $CDCl_3$)** δ 177.6, 175.5, 141.0, 129.9, 129.7 (q, J = 32.5 Hz), 125.9, 125.8 (q, J = 3.8 Hz), 124.1 (q, J = 272.0 Hz), 124.0, 107.4, 106.8, 47.9, 42.6, 34.8, 34.3, 25.2. **^{19}F NMR decoupled ^{1}H (471 MHz, $CDCl_3$)** δ: -62.67

IR (thin film) ν 2925, 1778, 1698, 1433, 1382, 1322, 1287, 1162, 1110, 1066, 712 cm^{-1}.

HRMS: calculated for $C_{18}H_{17}F_3N_2NaO_2^+$ ($M+Na^+$): 373.1134, found 373.1119.

TLC: 20:80 EtOAc/hexanes, R_f = 0.23.

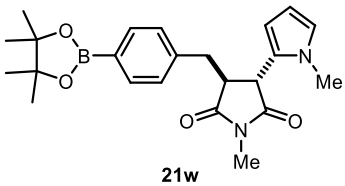

21w

1-methyl-3-(1-methyl-1H-pyrrol-2-yl)-4-(4-(4,4,5,5-tetramethyl-1,3,2-dioxaborolan-2-yl)benzyl)pyrrolidine-2,5-dione (21w): Synthesized according to the general procedure using 4-(4,4,5,5-tetramethyl-1,3,2-dioxaborolan-2-yl)benzyl bromide **5y** (223 mg, 0.75 mmol, 1.5 equiv.), *N*-methylmaleimide **9i** (56 mg, 0.5 mmol, 1 equiv.) and *N*-methylpyrrole **16a** (445 µL, 5 mmol, 10 equiv.). Product **21w** was purified by column chromatography (gradient from 10% to 30% AcOEt in hexanes as eluent): 39.3 mg pale brown

oil, 28% yield. A single diastereomer was detected by ^{1}H NMR analysis of the crude reaction mixture.

^{1}H NMR (500 MHz, $CDCl_3$) δ 7.72 (d, *J* = 8.0 Hz, 2H), 7.14 (d, *J* = 8.0 Hz, 2H), 6.58 (dd, *J* = 2.8, 1.8 Hz, 1H), 6.06 (dd, *J* = 3.7, 2.7 Hz, 1H), 5.94 (dd, *J* = 3.6, 1.6 Hz, 1H), 3.68 (d, *J* = 5.5 Hz, 1H), 3.50 (s, 3H), 3.40 (app q, *J* = 5.7 Hz, 1H), 3.30 (dd, *J* = 14.0, 6.0 Hz, 1H), 3.07 (dd, *J* = 14.1, 5.4 Hz, 1H), 2.94 (s, 3H), 1.34 (s, 12H). **^{13}C NMR (126 MHz, $CDCl_3$)** δ 178.1, 176.0, 139.8, 135.4, 129.0, 126.5, 123.8, 107.3, 106.5, 84.0, 48.2, 42.1, 35.0, 34.3, 25.2, 25.0. **^{11}B NMR (160 MHz, $CDCl_3$)** δ 30.76.

IR (thin film) ν 3399, 2978, 1696, 1612, 1433, 1359, 1289, 1142, 1090, 1022, 658 cm^{-1}.

HRMS: calculated for $C_{23}H_{29}N_2NaO_4{}^{11}B^+$ (M+Na$^+$): 431.2113, found 431.2122.

TLC: 20:80 EtOAc/hexanes, R_f = 0.31.

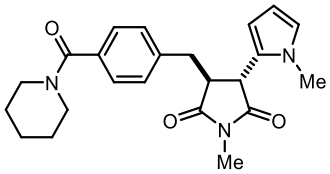

21x

2-(5-(4-((1,3-dioxoisoindolin-2-yl)methyl)-1-methyl-2,5-dioxopyrrolidin-3-yl)thiophen-2-yl)acetonitrile (**21x**): Synthesized according to the general procedure using (4-(bromomethyl)phenyl)(piperidin-1-yl)methanone **5z** (212 mg, 0.75 mmol, 1.5 equiv.), *N*-methylmaleimide **9i** (56 mg, 0.5 mmol, 1 equiv.) and *N*-methylpyrrole **16a** (445 µL, 5 mmol, 10 equiv.). Product **21x** was purified by column chromatography (two consecutive purifications. First purification: gradient from 40% to 60% AcOEt in hexanes as eluent. Second purification: 90:10 tol:acetone): 140.3 mg of a pale yellow solid, 71% yield. A single diastereomer was detected by ^{1}H NMR analysis of the crude reaction mixture.

^{1}H NMR (500 MHz, $CDCl_3$) δ 7.34 – 7.29 (m, 2H), 7.19 – 7.15 (m, 2H), 6.56 (dd, J = 2.8, 1.7 Hz, 1H), 6.03 (dd, J = 3.7, 2.7 Hz, 1H), 5.91 (ddd, J = 3.8, 1.8, 0.6 Hz, 1H), 3.69 (d+bs, J = 6.0 Hz, 1H+2H), 3.52 (s, 3H), 3.41 (app q, J = 5.9 Hz, 1H), 3.28 (s, 2H), 3.24 (dd, J = 14.2, 6.5 Hz, 1H), 3.14 (dd, J = 14.2, 5.4 Hz, 1H), 2.96 (s, 3H), 1.67 (bs, 4H), 1.50 (bs, 2H). **^{13}C NMR (126 MHz, $CDCl_3$)** δ 177.7, 175.5, 169.8, 138.0, 135.4, 129.4 (x2), 127.3 (x2), 125.9, 123.7, 107.1, 106.5, 48.8 (broad), 47.1, 43.2 (broad), 42.3, 34.5, 34.2, 26. (broad), 25.5 (broad), 25.0, 24.5.

IR (thin film) ν 2932, 2854, 1776, 1696, 1619, 1430, 1274, 1109, 706 cm^{-1}.

TLC: 60:40 EtOAc/hexanes, *Rf* = 0.16.

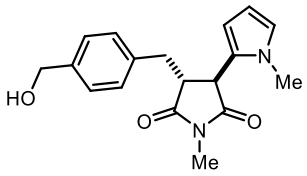

21y

3-(4-(hydroxymethyl)benzyl)-1-methyl-4-(1-methyl-1H-pyrrol-2-yl)pyrrolidine-2,5-dione (**21y**): Synthesized according to the general procedure using 4-hydroxymethylbenzyl bromide **5aa** (150 mg, 0.75 mmol, 1.5 equiv.), *N*-methyl maleimide **9i** (56 mg, 0.5 mmol, 1 equiv) and *N*-methylpyrrole **16a** (445 µL, 5 mmol, 10 equiv.). Product **21y** was purified by column chromatography (gradient from 40% to 60% AcOEt in hexanes as eluent): 77 mg of a yellowish sticky oil, 49% yield. A single diastereomer was detected by ^{1}H NMR analysis of the crude reaction mixture.

^{1}H NMR (500 MHz, $CDCl_3$) δ 7.27-7.23 (m, 2H), 7.12-7.08 (m, 2H), 6.56 (dd, *J* = 2.6, 1.9 Hz, 1H), 6.03 (dd, *J* = 3.4, 2.6 Hz, 1H), 5.9 (dd, *J* = 3.4, 1.9 Hz; 1H), 4.62 (br s, 2H); 3.68 (d, *J* = 5.5 Hz; 1H), 3.49 (s, 3H), 3.36 (q, *J* = 5.7 Hz; 1H), 3.23 (dd, *J* = 14.1, 6.1 Hz; 1H), 3.05 (dd, *J* = 14.1, 5.4 Hz; 1H), 2.92 (s, 3H); 1.89 (br s, 1H). **^{13}C NMR (125 MHz, $CDCl_3$)** δ 178.4; 176.2; 140.2; 136.2; 129.9 (x2); 127.7 (x2); 126.6;.124.0; 107.5; 106.8; 65.2; 48.5; 42.5; 34.8; 34.5; 25.4.

IR (thin film) ν 3455, 2924, 1693, 1434, 1382, 1288, 1122, 717cm^{-1}.

HRMS: calculated for $C_{18}H_{20}N_2NaO_3^+$ ($M+Na^+$): 335.1366, found 335.1365.

TLC: 50:50 EtOAc/hexanes, *Rf* = 0.25.

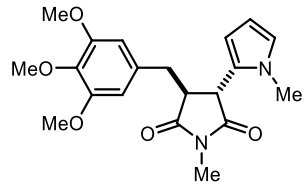

21z

1-methyl-3-(1-methyl-1*H*-pyrrol-2-yl)-4-(3,4,5-trimethoxybenzyl)pyrrolidine-2,5-dione (21z): Synthesized according to the general procedure using 5-(chloromethyl)-1,2,3-trimethoxybenzene **5ab** (162 mg, 0.75 mmol, 1.5 equiv.), *N*-methylmaleimide **9i** (56 mg, 0.5 mmol, 1 equiv.) and *N*-methylpyrrole **16a** (445 µL, 5 mmol, 10 equiv.). A single diastereomer was detected by ^{1}H NMR analysis of the crude reaction mixture. Purification by column chromatography (gradient from 20% to 35% AcOEt in hexanes as eluent) resulted in poor separation, but a clean amount (50 mg) of pure **21z** was isolated for characterization (50 mg). 58% NMR-yield, determined using trichloroethylene as the internal standard.

^{1}H NMR (500 MHz, $CDCl_3$) δ 6.57 (dd, *J* = 2.6, 1.9 Hz, 1H), 6.32 (s, 2H), 6.06 (dd, *J* = 3.5, 2.9 Hz, 1H), 5.94 (dd, *J* = 3.6, 1.7 Hz, 1H), 3.80 (s, 3H), 3.74 (s, 6H), 3.71 (d, *J* = 5.7 Hz, 1H), 3.50 (s, 3H), 3.40 (app q, *J* = 5.8 Hz, 1H), 3.15 (dd, *J* = 14.5, 6.8 Hz, 1H), 3.08 (dd, *J* = 14.4, 5.5 Hz, 1H), 2.97 (s, 3H). **^{13}C NMR (126 MHz, $CDCl_3$)** δ 178.5, 176.3, 153.7, 137.3, 132.7, 126.9, 124.0, 107.7, 106.8, 106.5, 61.2, 56.4, 48.4, 42.8, 35.6, 34.5, 25.5.

IR (thin film) ν 2939, 2839, 1697, 1589, 1507, 1458, 1431, 1382,1123, 1006 cm^{-1}.

HRMS: calculated for $C_{20}H_{24}N_2NaO_5^+$ ($M+Na^+$): 395.1577, found 395.1581.

TLC: 30:70 EtOAc/hexanes, R_f = 0.11.

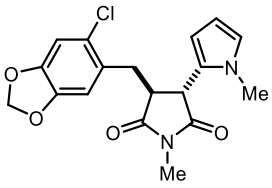

21aa

3-((6-chlorobenzo[d][1,3]dioxol-5-yl)methyl)-1-methyl-4-(1-methyl-1H-pyrrol-2-yl)pyrrolidine-2,5-dione (21aa): Synthesized according to the general procedure 6-chloropiperonyl chloride **5ac** (154 mg, 0.75 mmol, 1.5 equiv.), *N*-methylmaleimide **9i** (56 mg, 0.5 mmol, 1 equiv.) and *N*-methylpyrrole **16a** (445 µL, 5 mmol, 10 equiv.). A single diastereomer was detected by ^{1}H NMR analysis of the crude reaction mixture. Product **21aa** was purified by column chromatography (gradient from 10% to 30% AcOEt in hexanes as eluent): 133 mg of a white foam, 72% yield.

^{1}H NMR (500 MHz, $CDCl_3$) δ 6.8 (s, 1H), 6.7 (s, 1H), 6.6 (dd, *J* = 2.7, 1.7 Hz, 1H), 6.0 (dd, *J* = 3.7, 2.7 Hz, 1H), 5.9 (s, 2H), 5.9 (dd, *J* = 3.6, 1.5 Hz, 1H), 3.8 (d, *J* = 5.4 Hz, 1H), 3.6 (s, 3H), 3.4 (m, 1H), 3.3 (dd, *J* = 14.1, 5.7 Hz, 1H), 3.1 (dd, *J* = 14.2, 7.1 Hz, 1H), 3.0 (s, 3H). **^{13}C NMR (126 MHz, $CDCl_3$)** δ 178.0, 175.9, 147.5, 147.1, 127.7, 126.4, 126.0, 123.7, 110.4, 109.9, 107.1, 106.2, 101.9, 47.5, 42.6, 34.2, 32.7, 25.2

IR (thin film) ν 2900, 1776, 1696, 1478, 1433, 1381, 1286, 1232, 1118, 1035, 749, 712 cm^{-1}.

HRMS: calculated for $C_{18}H_{17}ClN_2NaO_4^+$ ($M+Na^+$): 383.0769, found 383.0770.

TLC: 30:70 EtOAc/hexanes, R_f = 0.33

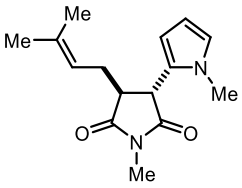

21ab

1-methyl-3-(1-methyl-1*H*-pyrrol-2-yl)-4-(3-methylbut-2-en-1-yl)pyrrolidine-2,5-dione (21ab): Synthesized according to the general procedure using 1-chloro-3-methylbut-2-ene chloride **5ad** (170 µL, 1.50 mmol, 3.0 equiv.), *N*-methylmaleimide **9i** (56 mg, 0.5 mmol, 1 equiv.) and *N*-methylpyrrole **16a** (445 µL, 5 mmol, 10 equiv.). The diastereomeric ratio (2.9:1) was determined by ^{1}H NMR spectroscopic analysis of the crude reaction mixture by comparison of the resonances at δ 5.10 (minor diastereomer) and δ 4.87 (major diastereomer). Product **21ab** was purified by column chromatography (gradient from 15% to 20% AcOEt in hexanes as eluent): 62 mg of a brown oil, 47% yield.

^{1}H NMR (400 MHz, $CDCl_3$) δ 6.62 (dd, *J* = 2.6, 1.9 Hz, 1H), 6.07 (dd, *J* = 3.6, 2.9 Hz, 1H), 5.93 (dd, *J* = 3.6, 1.6 Hz, 1H), 5.05-5.00 (m, 1H), 3.73 (d, *J* = 5.3 Hz, 1H), 3.67 (s, 3H), 3.11 (app q, *J* = 5.5 Hz, 1H), 2.99 (s, 3H), 2.57-2.52 (m, 2H), 1.69 (d, *J* = 0.9 Hz, 1H), 1.62 (s, 3H). **^{13}C NMR (101 MHz, $CDCl_3$)** δ 178.5, 176.4, 136.6, 126.9, 123.8, 118.5, 107.3, 106.7, 47.2, 43.0, 34.4, 28.2, 26.0, 25.1, 18.1.

IR (thin film) ν 2918, 1776, 1696, 1492, 1432, 1380, 1285, 1095, 995, 713 cm^{-1}.

HRMS: calculated for $C_{15}H_{20}N_2NaO_2^+$ ($M+Na^+$): 283.1417, found 283.1415.

TLC: 20:80 EtOAc/hexanes, R_f = 0.28.

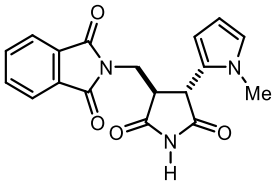

21ac

2-((4-(1-methyl-1*H*-pyrrol-2-yl)-2,5-dioxopyrrolidin-3-yl)methyl)isoindoline-1,3-dione (21ac): Synthesized according to the general procedure using *N*-(chloromethyl)phthalimide chloride **5k** (147 mg, 0.75 mmol, 1.5 equiv.), unprotected maleimide **9b** (48 mg, 0.5 mmol, 1 equiv.) and *N*-methylpyrrole **16a** (445 µL, 5 mmol, 10 equiv.). The diastereomeric ratio (1.9:1) was determined by ^{1}H NMR spectroscopic analysis of the crude reaction mixture by comparison of the resonances at δ 5.96 (minor diastereomer) and δ 5.72 (major diastereomer). Purification by column chromatography (gradient from 40% to 55% AcOEt in hexanes as eluent) resulted in very poor separation, but an analytical amount of the major diastereomer was isolated for characterization. NMR yield of the mixture of diastereoisomers (1.9:1) is 77%. DMSO-d_6 was used either as a solvent or co-solvent in the NMR spectra to promote solubility; in the case of ^{13}C NMR, chloroform was required in order to prevent overlap of aromatic peaks.

^{1}H NMR (500 MHz, DMSO-d_6) δ 11.30 (s, 1H), 7.77 (s, 4H), 6.48 (app t, *J* = 2.1 Hz, 1H), 5.76 (dd, *J* = 3.5, 1.8 Hz, 1H), 5.60 (dd, *J* = 3.5, 2.8 Hz, 1H), 4.22 (d, *J* = 7.3 Hz, 1H), 4.09 (dd, *J* = 14.0, 6.0 Hz, 1H), 4.02 (dd, *J* = 14.1, 9.0 Hz, 1H), 3.53 (s, 3H), 3.52-3.48 (m, 1H).
^{13}C NMR (126 MHz, $CDCl_3$ + DMSO-d_6) δ 176.2, 175.9, 168.4, 134.3, 131.9, 125.4, 123.8, 123.5, 107.2, 106.8, 46.2, 45.0, 38.0, 34.3.

IR (thin film) ν 3415, 2924, 2255, 1715, 1399, 1364, 1024, 1003, 823, 722 cm^{-1}.

HRMS: calculated for $C_{18}H_{15}N_3NaO_4^+$ ($M+Na^+$): 360.0955, found 360.0958.

TLC: 50:50 EtOAc/hexanes, R_f = 0.31.

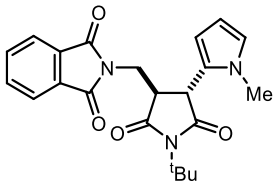

21ad

2-((1-(*tert*-butyl)-4-(1-methyl-1*H*-pyrrol-2-yl)-2,5-dioxopyrrolidin-3-yl)methyl)isoindoline-1,3-dione (21ad): Synthesized according to the general procedure using *N*-(chloromethyl)phthalimide chloride **5k**(147 mg, 0.75 mmol, 1.5 equiv.), *N*-*tert*-butylmaleimide **9f** (76 mg, 0.5 mmol, 1 equiv.) and *N*-methylpyrrole **16a** (445 µL, 5 mmol, 10 equiv.). A single diastereomer was detected by ^{1}H NMR analysis of the crude reaction mixture. Product **21ad** was purified by column chromatography (gradient from 15% to 25% AcOEt in hexanes as eluent): 127 mg of an orange foam, 64% yield.

^{1}H NMR (500 MHz, $CDCl_3$) δ 7.73-7.69 (m, 2H), 7.65-7.62 (m, 2H), 6.32 (dd, *J* = 2.5, 1.9 Hz, 1H), 5.74 (dd, *J* = 3.6, 1.6 Hz, 1H), 5.68 (dd, *J* = 3.6, 2.8 Hz, 1H), 4.26 (dd, *J* = 14.0, 5.7

Hz, 1H), 3.99 (dd, *J* = 14.0, 9.6 Hz, 1H), 3.88 (d, *J* = 7.3 Hz, 1H), 3.59 (s, 3H), 3.47-3.42 (m, 1H), 1.55 (s, 9H). **^{13}C NMR (126 MHz, CDCl$_3$)** δ 176.7, 176.2, 168.5, 134.3, 132.0, 126.1, 123.8, 123.5, 107.3, 106.4, 59.2, 45.0, 43.9, 38.4, 34.3, 28.7.

IR (thin film) ν 2976, 1774, 1697, 1436, 1396, 1330, 1263, 1158, 1106, 714 cm^{-1}.

HRMS: calculated for $C_{22}H_{24}N_3O_4^+$ ($M+H^+$): 394.1761, found 394.1765.

TLC: 20:80 EtOAc/hexanes, R_f = 0.14.

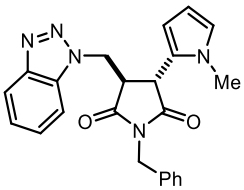

21ae

3-((1H-benzo[d][1,2,3]triazol-1-yl)methyl)-1-benzyl-4-(1-methyl-1H-pyrrol-2-yl)pyrrolidine-2,5-dione (21ae): Synthesized according to the general procedure using 1-(chloromethyl)-1*H*-benzotriazole **5m** (126 mg, 0.75 mmol, 1.5 equiv.), *N*-benzylmaleimide **9h** (94 mg, 0.5 mmol, 1 equiv.) and *N*-methylpyrrole **16a** (445 µL, 5 mmol, 10 equiv.). A single diastereomer was detected by ^{1}H NMR analysis of the crude reaction mixture. Product **21ae** was purified by column chromatography (gradient from 10% to 30% AcOEt in hexanes as eluent): 112.1 mg of a white foam, 56% yield.

^{1}H NMR (400 MHz, CDCl$_3$) δ 8.02 (dt, *J* = 8.4, 0.9 Hz, 1H), 7.61 (dt, *J* = 8.4, 0.9 Hz, 1H), 7.49 – 7.45 (m, 1H), 7.37 (ddd, *J* = 8.1, 6.9, 1.0 Hz, 1H), 7.20 – 7.15 (m, 1H), 7.14 – 7.09 (m, 2H), 7.03 – 6.98 (m, 2H), 6.62 (dd, *J* = 2.7, 1.7 Hz, 1H), 6.05 (dd, *J* = 3.7, 2.7 Hz, 1H), 5.92 (dd, *J* = 3.5, 1.6 Hz, 1H), 5.24 (dd, *J* = 14.7, 4.3 Hz, 1H), 5.00 (dd, *J* = 14.8, 4.1 Hz, 1H), 4.57 (d, *J* = 14.3 Hz, 1H), 4.48 (d, *J* = 14.3 Hz, 1H), 4.32 (d, *J* = 6.7 Hz, 1H), 3.67 (s, 3H), 3.62 (dt, *J* = 6.7, 4.2 Hz, 1H). **^{13}C NMR (100 MHz, CDCl$_3$)** δ 175.4, 174.5, 145.9, 135.0, 133.4, 128.7 (2C), 128.2, 128.1 (2C), 128.0, 125.4, 124.5, 124.2, 120.1, 109.9, 107.4, 106.6, 47.9, 45.3, 42.9, 41.1, 34.6.

HRMS: calculated for $C_{23}H_{22}N_5O_2^+$ ($M+H^+$): 400.1778, found 400.1768.

TLC: 30:70 EtOAc/hexanes, R_f = 0.13.

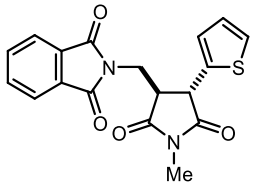

21af

2-((1-methyl-2,5-dioxo-4-(thiophen-2-yl)pyrrolidin-3-yl)methyl)isoindoline-1,3-dione (21af): Synthesized according to the general procedure using *N*-(chloromethyl)phthalimide chloride **5k** (147 mg, 0.75 mmol, 1.5 equiv.), *N*-methylmaleimide **9i** (56 mg, 0.5 mmol, 1 equiv.) and thiophene **16b** (400 µL, 5 mmol, 10 equiv.). A single diastereomer was detected by ^{1}H NMR analysis of the crude reaction mixture. Product **21af** was purified by column chromatography (gradient from 10% to 30% AcOEt in hexanes as eluent): 64.6 mg pale brown solid, 36% yield.

^{1}H NMR (500 MHz, $CDCl_3$) δ 7.81 (dd, *J* = 5.5, 3.0 Hz, 2H), 7.73 – 7.69 (m, 2H), 7.08 (dd, *J* = 5.1, 1.2 Hz, 1H), 6.89 (dd, *J* = 3.6, 1.1 Hz, 1H), 6.78 (dd, *J* = 5.2, 3.5 Hz, 1H), 4.32 (dd, *J* = 14.1, 6.2 Hz, 1H), 4.21 (d, *J* = 6.3 Hz, 1H), 4.09 (dd, *J* = 14.1, 9.2 Hz, 1H), 3.66 – 3.56 (m, 1H), 3.07 (s, 3H). **^{13}C NMR (126 MHz, $CDCl_3$)** δ 175.0, 175.0, 168.2, 136.9, 134.4, 131.8, 127.1, 126.3, 125.7, 123.6, 47.7, 46.3, 37.9, 25.6.

IR (thin film) ν 2924, 1766, 1693, 1435, 1401, 1365, 1298, 1190, 1107, 1067, 692 cm^{-1}.

HRMS: calculated for $C_{18}H_{14}N_2NaO_4S^+$ ($M+Na^+$): 377.0566, found 377.0558

TLC: 30:70 EtOAc/hexanes, R_f = 0.22.

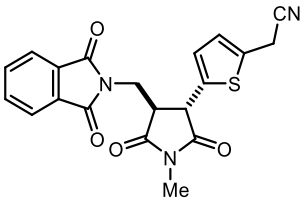

21ag

2-(5-(4-((1,3-dioxoisoindolin-2-yl)methyl)-1-methyl-2,5-dioxopyrrolidin-3-yl)thiophen-2-yl)acetonitrile (**21ag**): Synthesized according to the general procedure using *N*-(chloromethyl)phthalimide **5k** (147 mg, 0.75 mmol, 1.5 equiv.), *N*-methylmaleimide **9i** (56 mg, 0.5 mmol, 1 equiv.) and thiophene-2-acetonitrile **16c** (615 µL, 5 mmol, 10 equiv.). Product **21ag** was purified by column chromatography (gradient from 10% to 30% AcOEt in hexanes as eluent): 40 mg of a pale yellow solid, 20% yield. A single diastereomer was detected by ^{1}H NMR analysis of the crude reaction mixture.

^{1}H NMR (400 MHz, DMSO-d_6) δ 7.83 – 7.80 (m, 4H), 6.82 (dd, *J* = 3.6, 0.9 Hz, 1H), 6.75 (dt, *J* = 3.6, 1.1 Hz, 1H), 4.27 (d, *J* = 6.9 Hz, 1H), 4.14 (dd, *J* = 14.1, 6.4 Hz, 1H), 4.10 (d, *J* = 1.0 Hz, 2H), 4.04 (dd, *J* = 14.1, 8.3 Hz, 1H), 3.54 (dt, *J* = 8.2, 6.6 Hz, 1H), 2.85 (s, 3H). **^{13}C NMR (125 MHz, $CDCl_3$)** δ 175.2, 175.0, 167.8 (x2), 137.7, 134.5 (x2), 132.0, 131.3, 126.7, 125.9, 123.1 (CN), 123.1(x2), 118.2, 46.2, 45.6, 36.9, 24.9, 17.4.

IR (thin film) ν 2913, 1767, 1693, 1440, 1399, 1363, 1299, 1019, 724 cm^{-1}.

HRMS: calculated for $C_{20}H_{15}N_3NaO_4S^+$ (M+Na+): 416.0675, found 416.0669.

TLC: 50:50 EtOAc/hexanes, *Rf* = 0.43.

4.11.4. Procedure for the 5 mmol Scale Reaction

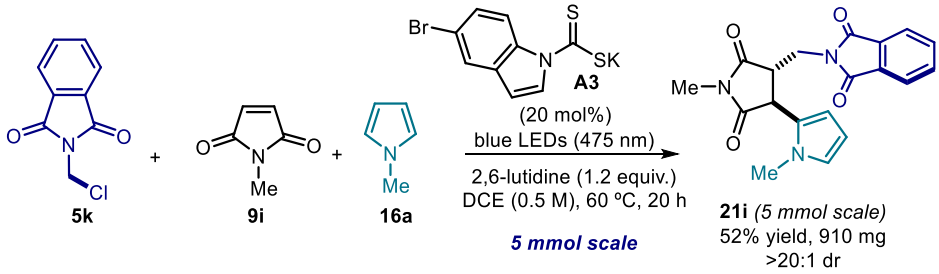

The model photoinduced multicomponent reaction can be scaled-up up to 5 mmol scale by using the same experimental set-up described in Figure 4.31. In an oven dried Schlenk tube (length x diameter = 22 x 2 cm), the DTC catalyst **A3** (310 mg, 1 mmol, 0.2 equiv.) was dissolved in dichloroethane (5 mL), then the *N*-(chloromethyl)phthalimide **5k** (1.5 g, 7.5 mmol, 1.5 equiv.) was added, with stirring, followed by 2,6-lutidine (700 µL, 6 mmol, 1.2 equiv.), *N*-methylmaleimide **9i** (556 mg, 5 mmol, 1.0 equiv.), and *N*-methylpyrrole **16a** (4.4 mL, 50 mmol, 10.0 equiv.). An additional volume of dichloroethane (5 mL) was added to the reaction tube, washing the sides from residual solids. The resulting mixture was degassed via three cycles of freeze-pump-thaw. The Schlenk tube was then placed in the irradiation setup, maintained at a temperature of 60 ºC (60-61ºC measured in the central well), and the reaction was stirred for 30 hours under continuous irradiation.

After cooling to ambient temperature, the solvent was evaporated and the residue purified by column chromatography (gradient from 10% to 30% AcOEt in hexanes as eluent). Product **21i** was isolated as a mixture containing about 14% of an inseparable byproduct, arising from a polar Friedel-Crafts type alkylation of pyrrole **16a** with maleimide **9i**: 1.05 g (containing 14% of byproduct). Corrected yield of product **21i**: 52% (910 mg). The NMR yield of the observed single diastereomer was measured as 62%, using 1,1,2-trichloroethene as the internal standard.

4.11.5. Product Modifications

4.11.5.1. Assembly Line Synthesis of Difunctionalized Pyrroles

C2 - functionalization

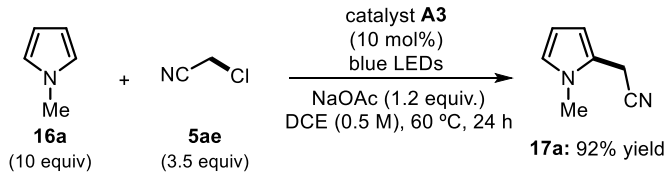

C5 - functionalization

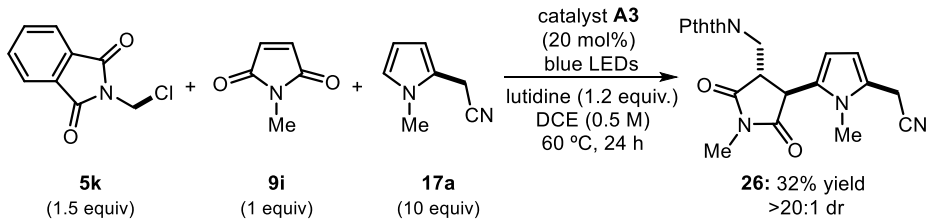

C2-functionalization. In an oven dried Schlenk tube, the DTC catalyst **A3** (15.5 mg, 0.05 mmol, 0.1 equiv.) and sodium acetate (49 mg, 0.6 mmol, 1.2 equiv.) were suspended in 1,2-dichloroethane (1 mL), then chloroacetonitrile **5ae** (32 µL, 0.5 mmol, 1 equiv.) was added followed by *N*-methylpyrrole **16a** (444 µL, 5 mmol, 10 equiv.). The resulting yellow mixture was degassed via three cycles of freeze-pump-thaw. The Schlenk tube was then placed in the irradiation setup (see Figure 4.32) set at a temperature of 60 ºC (60-61ºC measured in the central well) and irradiated for 24 hours. After cooling to ambient temperature, the volatiles were evaporated and the residue purified by column chromatography on silica gel (toluene as eluent): 55 mg, 92% yield; spectral data matched those reported in the literature.[9]

C5-functionalization. Substrate **26** was synthesized according to the general procedure for the radial MCR reaction using *N*-(chloromethyl)phthalimide **5k** (147 mg, 0.75 mmol, 1.5 equiv.), maleimide **9i** (56 mg, 0.5 mmol, 1.0 equiv.) and the C2-functionalized pyrrole **17a** (600 mg, 5.0 mmol, 10.0 equiv.). Irradiation time: 24 hours. A single diastereomer was detected by ^{1}H NMR analysis of the crude reaction mixture. Product **26** was purified by column chromatography (gradient from 10% to 40% AcOEt in hexanes as eluent): 61.8 mg of a pale brown solid, 32% yield.

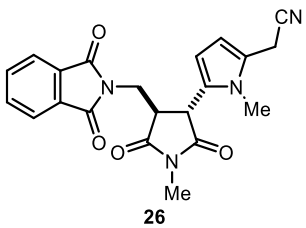

4-((1,3-dioxoisoindolin-2-yl)methyl)-1-methyl-2,5-dioxopyrrolidin-3-yl)-1-methyl-1H-pyrrol-2-yl)acetonitrile (26). ^{1}H NMR (500 MHz, $CDCl_3$) δ 7.75 (dd, *J* = 5.5, 3.0 Hz, 2H), 7.68 (dd, *J* = 5.5, 3.0 Hz, 2H), 5.74 (d, *J* = 3.8 Hz, 1H), 5.68 (d, *J* = 3.8 Hz, 1H), 4.38 (dd, *J* = 14.0, 5.3 Hz, 1H), 4.12 – 4.01 (m, 2H), 3.61 (ddd, *J* = 10.2, 7.3, 5.2 Hz,

1H), 3.57 (s, 3H), 3.49 (dd, *J* = 5.6, 0.8 Hz, 2H), 3.02 (s, 3H). **^{13}C NMR (126 MHz, $CDCl_3$)** δ 175.0, 174.7, 168.3, 134.4, 131.5, 126.9, 123.5, 121.6, 116.2, 108.3, 106.0, 44.7, 43.9, 37.8, 31.0, 25.3, 16.4.

IR (thin film) ν 2936, 1778, 1765, 1697, 1498, 1400, 1274, 1094, 725 cm^{-1}.

HRMS: calculated for $C_{21}H_{18}N_4NaO_4^+$ ($M+Na^+$): 413.1220, found 413.1215.

TLC: 40:60 EtOAc/hexanes, R_f = 0.23.

4.11.5.2. Synthesis of Pyrrolidine 27

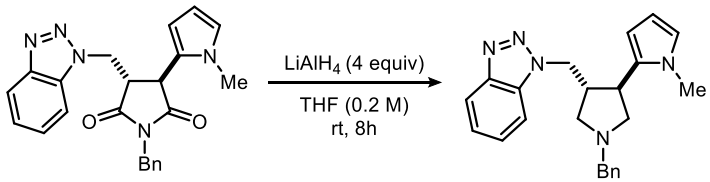

MCR product (**21ae**) **27**

A solution of the MCR adduct **21ae** (80 mg, 0.2 mmol, 1 equiv.) in dry THF (0.5 mL) was added dropwise to a cooled suspension of $LiAlH_4$ (31 mg, 0.8 mmol, 4 equiv.) in dry THF (0.5 mL) at 0 °C. After completion of the addition, the reaction was stirred at room temperature for 6 h. Complete conversion of **21ae** was observed after 6 h, as judged by TLC analysis of the reaction mixture. The reaction mixture was then diluted with Et_2O (1 mL), and quenched successively with water (1 mL) and NaOH (1M, 0.5 mL). The aqueous phase was extracted three times with Et_2O, and the collected organic phase was washed successively with brine, water and dried over magnesium sulfate. Further evaporation under reduced pressure afforded **27** in 94% yield. No further purification was required.

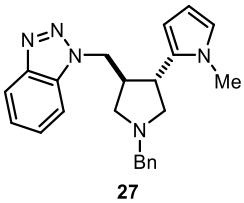

27

1-(((3R,4R)-1-benzyl-4-(1-methyl-1H-pyrrol-2-yl)pyrrolidin-3-yl)methyl)-1H-benzo[d][1,2,3]triazole (27)

^{1}H NMR (500 MHz, $CDCl_3$) δ 8.00 (dt, *J* = 8.3, 1.0 Hz, 1H), 7.38 (ddd, *J* = 8.4, 6.7, 1.0 Hz, 1H), 7.34 – 7.19 (m, 8H), 6.47 (dd, *J* = 2.7, 1.8 Hz, 1H), 6.01 (dd, *J* = 3.6, 2.7 Hz, 1H), 5.98 (dd, *J* = 3.6, 1.8 Hz, 1H), 4.71 (s, 1H), 4.70 (d, *J* = 1.7 Hz, 1H), 3.64 (d, *J* = 12.9 Hz, 1H), 3.55 (d, *J* = 12.9 Hz, 1H), 3.24 – 3.13 (m, 2H), 3.06 – 2.96 (m, 1H), 2.76 (dd, *J* = 9.7, 4.7 Hz, 1H), 2.63 (dd, *J* = 9.7, 7.5 Hz, 1H), 2.41 (td, *J* = 7.1, 1.4 Hz, 1H). **^{13}C NMR (125 MHz, $CDCl_3$)** δ 146.0, 138.8, 133.7, 133.3, 128.8 (x2C), 128.4 (x2C), 127.4, 127.2, 123.9, 122.3, 120.1, 109.3, 107.0, 105.0, 61.0, 60.1, 56.9, 51.1, 45.1, 39.2, 33.9.

TLC: 2:98 MeOH/DCM, R_f = 0.15.

4.11.6. Unsuccesful Substrate Combinations

The optimized conditions of the model reaction were evaluated with a variety of substrates. Those shown in Figures 4.33, 4.34 and 4.35 failed to deliver yields higher than the catalyst loading or any product at all.

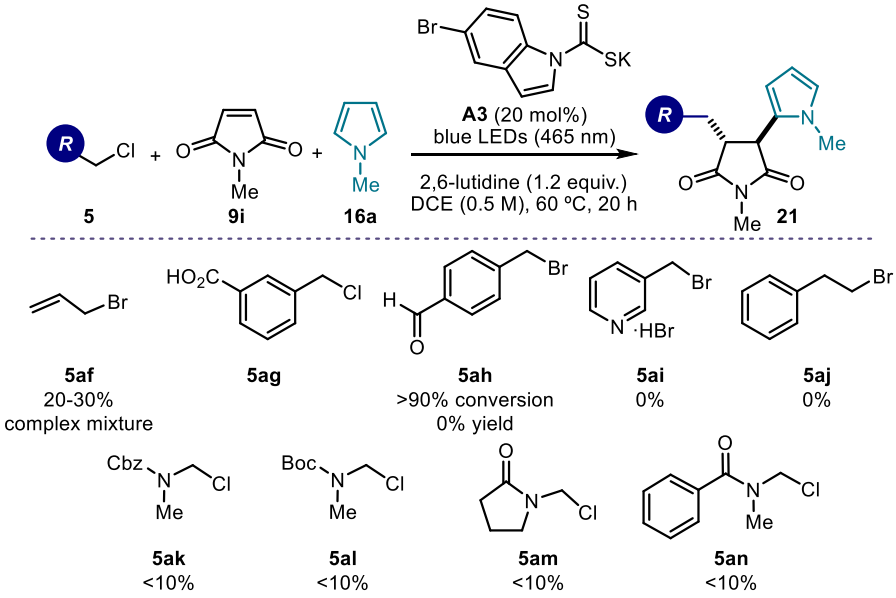

Figure 4.33. Alkyl halides that failed to give useful yields of MCR products. Unless otherwise noted, yields determined by ^{1}H NMR analysis of the crude mixture using trichloroethylene as the internal standard.

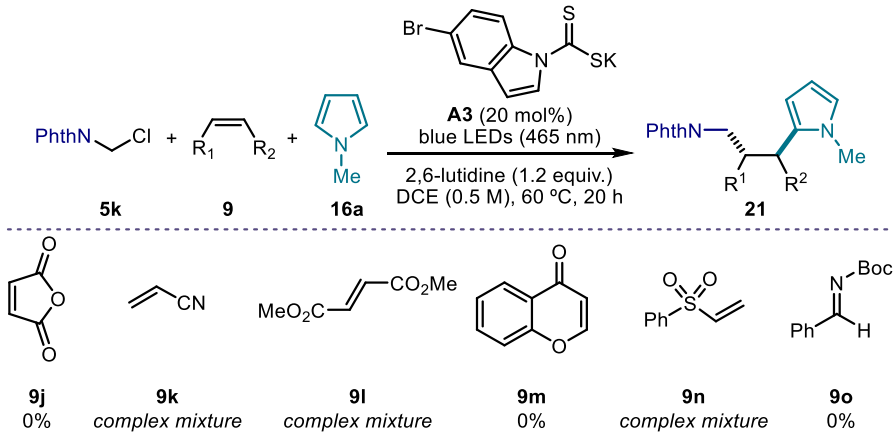

Figure 4.34. Radical traps that failed to give useful yields of MCR products. Unless otherwise noted, yields determined by ^{1}H NMR analysis of the crude mixture using trichloroethylene as the internal standard.

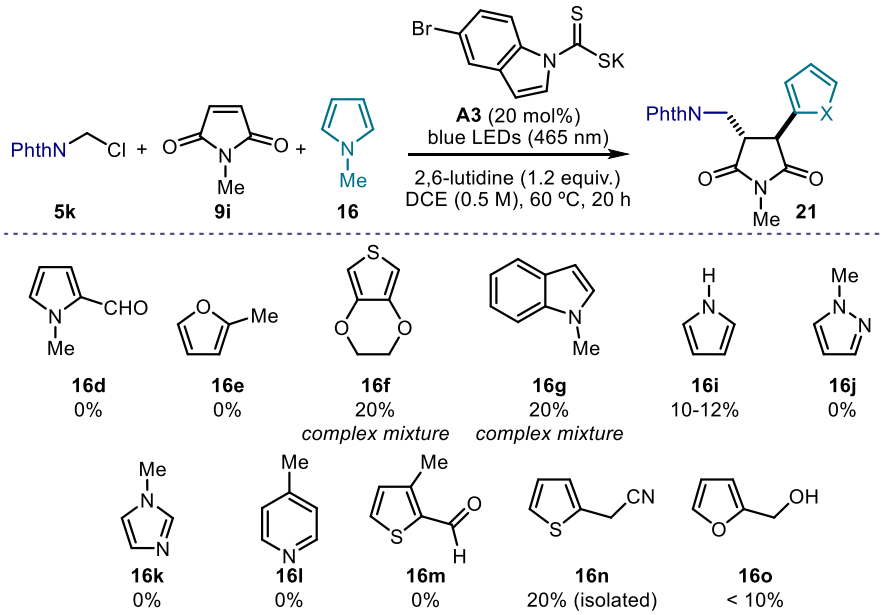

Figure 4.35. Terminal heteroaromatic traps that failed to give useful yields of MCR products. Unless otherwise noted, yields determined by ^{1}H NMR analysis of the crude mixture using trichloroethylene as the internal standard.

4.11.7. Cyclic Voltammetry Measurements

Substrates **5k**, **5l**, **5m**, **5p**, **5q**, **5r**, **5u**, **5x**, **5y**, **5ab** and **5ac** were electrochemically characterized. The measured reduction potential values are compiled in Figure 4.36. The cyclic voltammograms are shown in Figures 4.37-4.47.

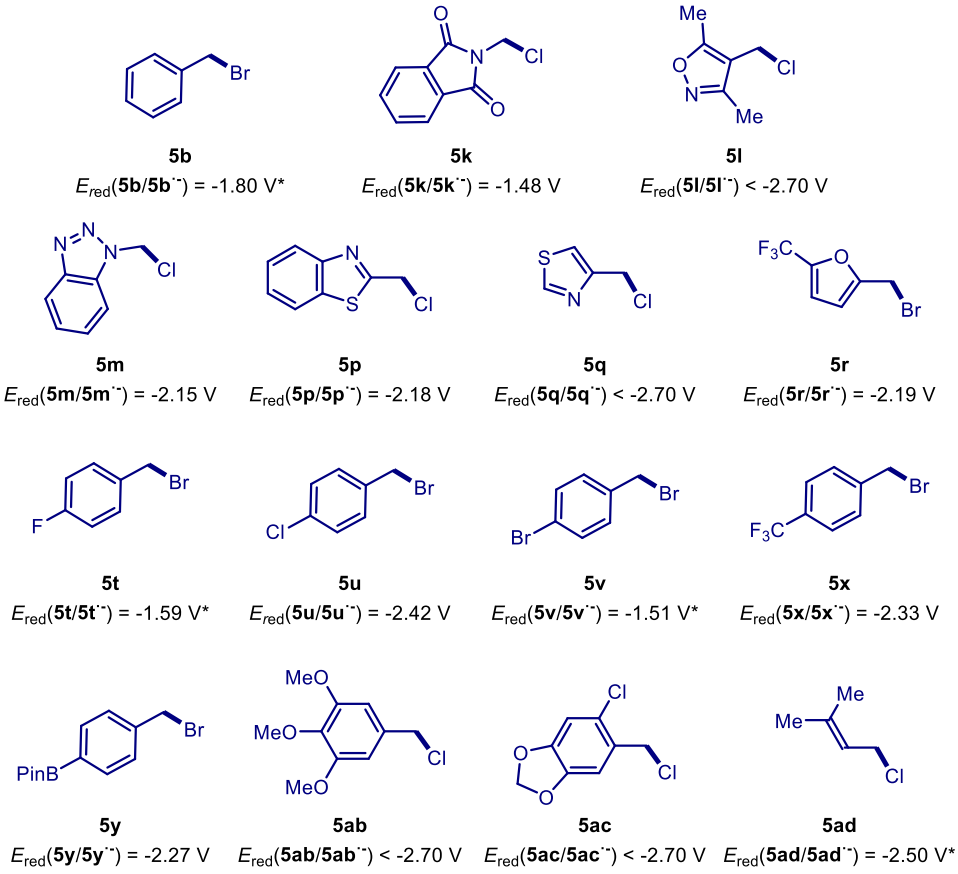

Figure 4.36. Reduction potentials (E_{red}) measured vs. Ag/AgCl (KCl, 3.5 M). *Reported in literature and referenced to Ag/AgCl (KCl saturated), according to reference 49.

[49] (a) Pavlishchuk, V. V.; Addison, A. W. Conversion Constants for Redox Potentials Measured Versus Different Reference Electrodes in Acetonitrile Solutions at 25°C. *Inorganica Chim. Acta* **2000**, *298*, 97–102. (b) L Meites, ed. *Handbook of Analytical Chemistry*. McGraw Hill, NY, 1963.

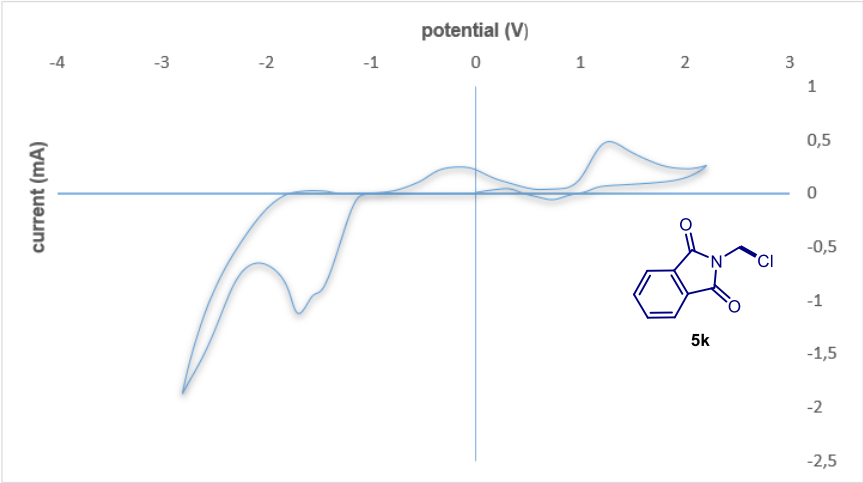

Figure 4.37. Cyclic voltammogram for *N*-(chloromethyl)phtalamide chloride **5k** [0.02M] in [0.1 M] $TBAPF_6$ in CH_3CN. Sweep rate: 100 mV/s. Pt electrode working electrode, Ag/AgCl (KCl 3.5 M) reference electrode, Pt wire auxiliary electrode. Irreversible reduction, $E_p^C = E_{red}$(**5k**/**5k**$^{\cdot-}$) = -1.48 V, E_p^C refers to the cathodic peak potential, while the E_{red} value describes the electrochemical properties of **5k**.

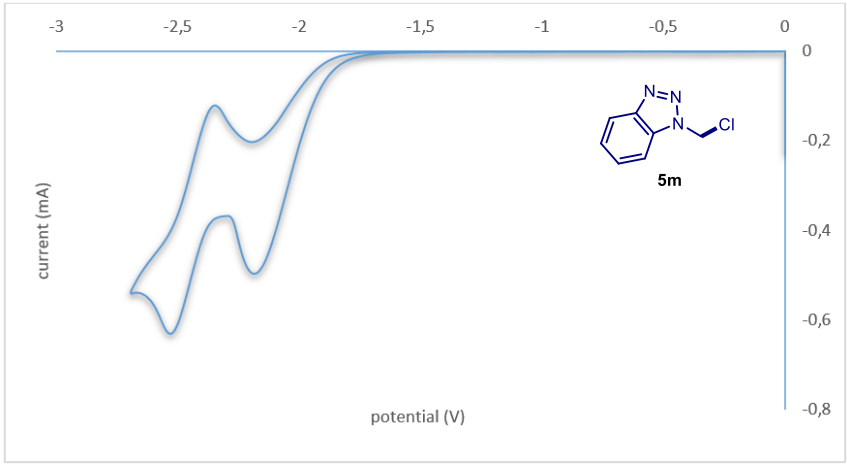

Figure 4.38. Cyclic voltammogram for 1-(chloromethyl)-1H-benzotriazole **5m** [0.02M] in [0.1 M] $TBAPF_6$ in CH_3CN. Sweep rate: 100 mV/s. Pt electrode working electrode, Ag/AgCl (KCl 3.5 M) reference electrode, Pt wire auxiliary electrode. First irreversible reduction, $E_p^C = E_{red}$(**5m**/**5m**$^{\cdot-}$) = -2.15 V, E_p^C refers to the cathodic peak potential, while the E_{red} value describes the electrochemical properties of **5m**.

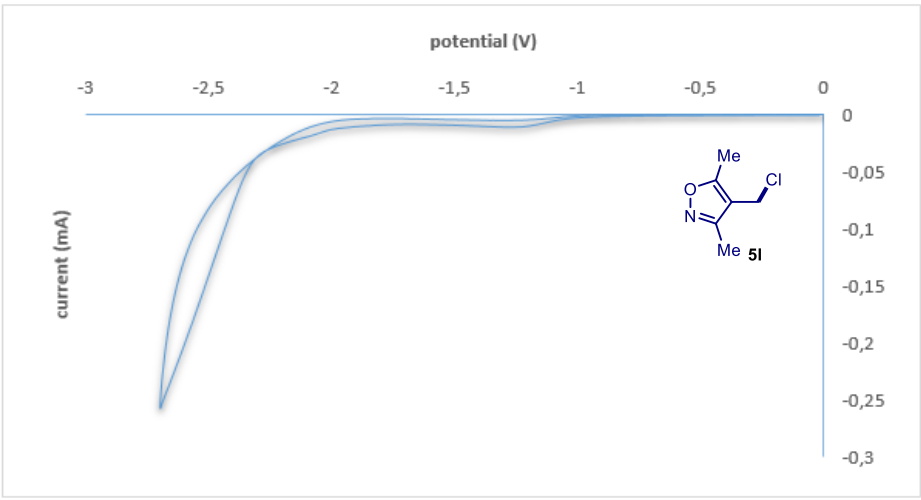

Figure 4.39. Cyclic voltammogram for 4-(chloromethyl)3,5-dimehtylisoxazole chloride **5l** [0.02M] in [0.1 M] $TBAPF_6$ in CH_3CN. Sweep rate: 50 mV/s. Glassy carbon electrode working electrode, Ag/AgCl (KCl 3.5 M) reference electrode, Pt wire auxiliary electrode. Reduction of substrate **5l** was not observed in the registered potential window (from 0 to -2.70 V).

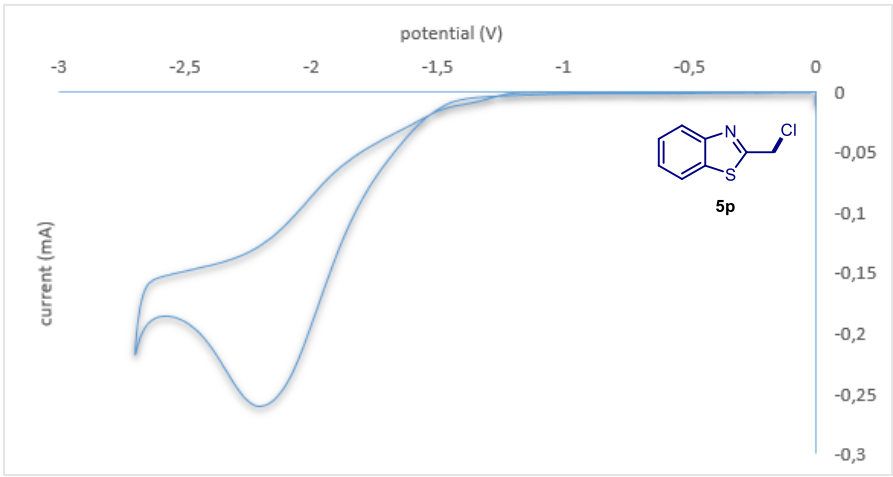

Figure 4.40. Cyclic voltammogram for 2-(chloromethyl)-1,3-benzothiazole chloride **5p** [0.02M] in [0.1 M] $TBAPF_6$ in CH_3CN. Sweep rate: 50 mV/s. Glassy carbon electrode working electrode, Ag/AgCl (KCl 3.5 M) reference electrode, Pt wire auxiliary electrode. Irreversible reduction, $E_p^C = E_{red}$(**5p**/**5p**$^{\bullet-}$) = -2.18 V, E_p^C refers to the cathodic peak potential, while the E_{red} value describes the electrochemical properties of **5p**.

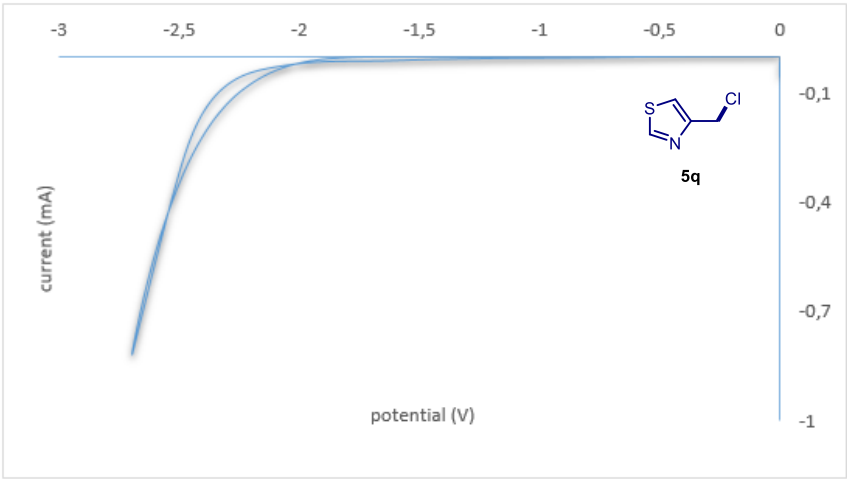

Figure 4.41. Cyclic voltammogram for 4-(chloromethyl)thiazole **5q** [0.02M] in [0.1 M] $TBAPF_6$ in CH_3CN. Sweep rate: 500 mV/s. Pt electrode working electrode, Ag/AgCl (KCl 3.5 M) reference electrode, Pt wire auxiliary electrode. Reduction of substrate **5q** was not observed in the registered potential window (from 0 to -2.70 V).

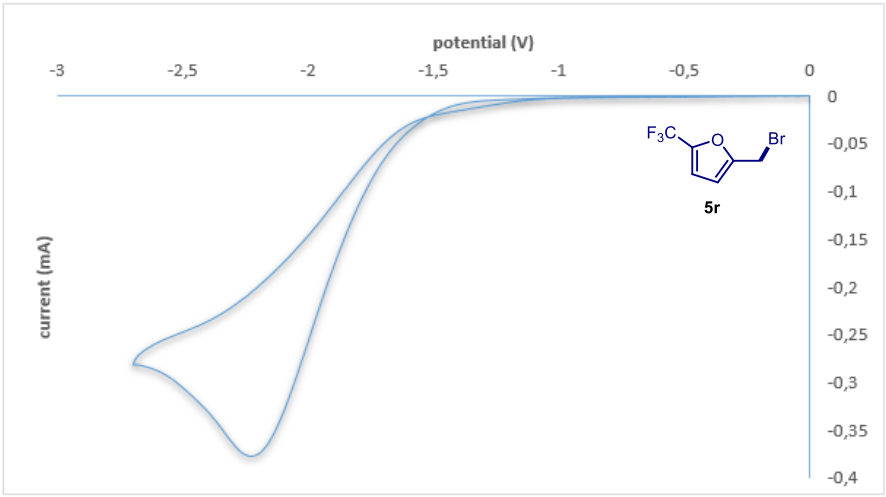

Figure 4.42. Cyclic voltammogram for 2-(bromomethyl)-5-(trifluoromethyl)furan bromide **5r** [0.02M] in [0.1 M] $TBAPF_6$ in CH_3CN. Sweep rate: 50 mV/s. Glassy carbon electrode working electrode, Ag/AgCl (KCl 3.5 M) reference electrode, Pt wire auxiliary electrode. Irreversible reduction, $E_p^C = E_{red}$(**5r**/**5r**$^{\bullet-}$) = -2.19 V, E_p^C refers to the cathodic peak potential, while the E_{red} value describes the electrochemical properties of **5r**.

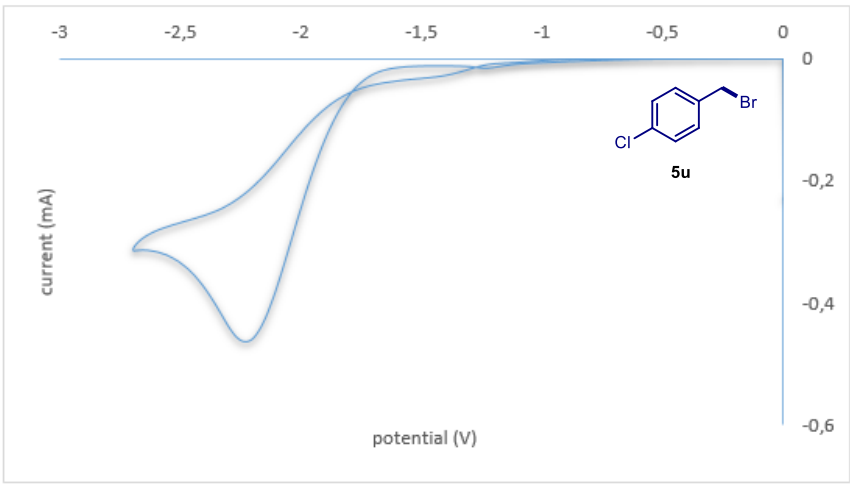

Figure 4.43. Cyclic voltammogram for 4-chlorobenzyl bromide **5u** [0.02M] in [0.1 M] $TBAPF_6$ in CH_3CN. Sweep rate: 500 mV/s. Pt electrode working electrode, Ag/AgCl (KCl 3.5 M) reference electrode, Pt wire auxiliary electrode. Irreversible reduction, $E_p^C = E_{red}$(**5u**/**5u**$^{\bullet-}$) = -2.42 V, E_p^C refers to the cathodic peak potential, while the E_{red} value describes the electrochemical properties of **5u**.

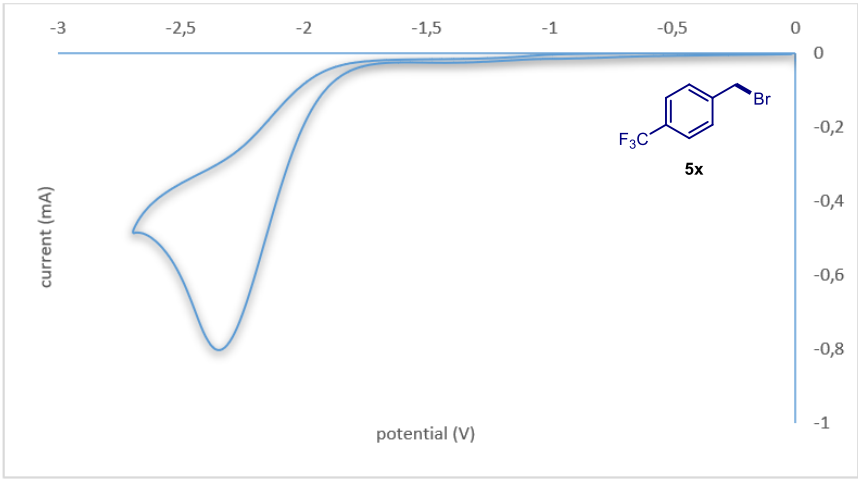

Figure 4.44. Cyclic voltammogram for 4-(trifluoromethyl)benzyl bromide **5x** [0.02M] in [0.1 M] $TBAPF_6$ in CH_3CN. Sweep rate: 500 mV/s. Pt electrode working electrode, Ag/AgCl (KCl 3.5 M) reference electrode, Pt wire auxiliary electrode. Irreversible reduction, $E_p^C = E_{red}$(**5x**/**5x**$^{\bullet-}$) = -2.33 V, E_p^C refers to the cathodic peak potential, while the E_{red} value describes the electrochemical properties of **5x**.

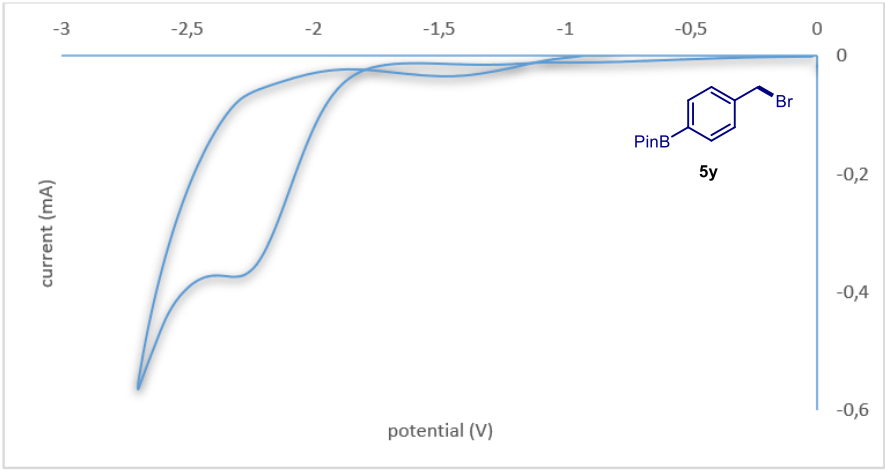

Figure 4.45. Cyclic voltammogram for 4-(4,4,5,5-tetramethyl-1,3,2-dioxaborolan-2-yl)benzyl bromide **5y** [0.02M] in [0.1 M] $TBAPF_6$ in CH_3CN. Sweep rate: 500 mV/s. Pt electrode working electrode, Ag/AgCl (KCl 3.5 M) reference electrode, Pt wire auxiliary electrode. Irreversible reduction, $E_p^C = E_{red}$(**5y**/**5y**$^{\cdot-}$) = -2.27 V, E_p^C refers to the cathodic peak potential, while the E_{red} value describes the electrochemical properties of **5y.**

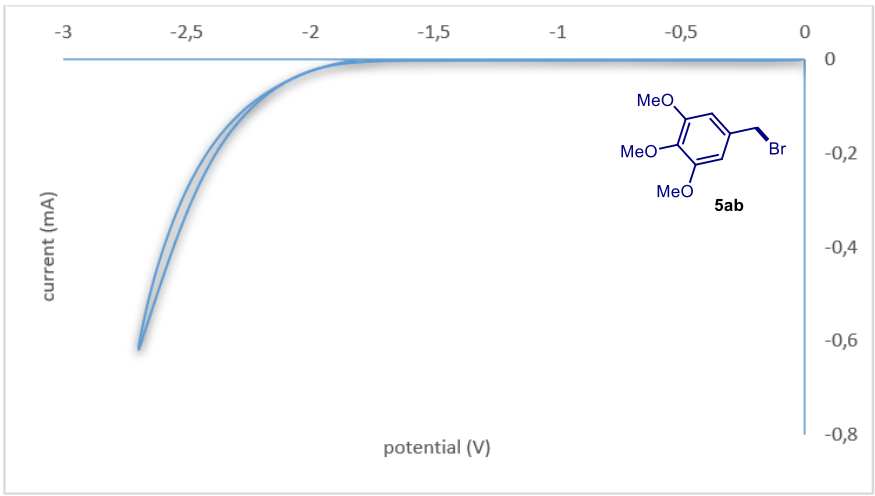

Figure 4.46. Cyclic voltammogram for 5-(chloromethyl)-1,2,3-trimethoxybenzene **5ab** [0.02M] in [0.1 M] $TBAPF_6$ in CH_3CN. Sweep rate: 100 mV/s. Pt electrode working electrode, Ag/AgCl (KCl 3.5 M) reference electrode, Pt wire auxiliary electrode. Reduction of substrate **5ab** was not observed in the registered potential window (from 0 to -2.70 V).

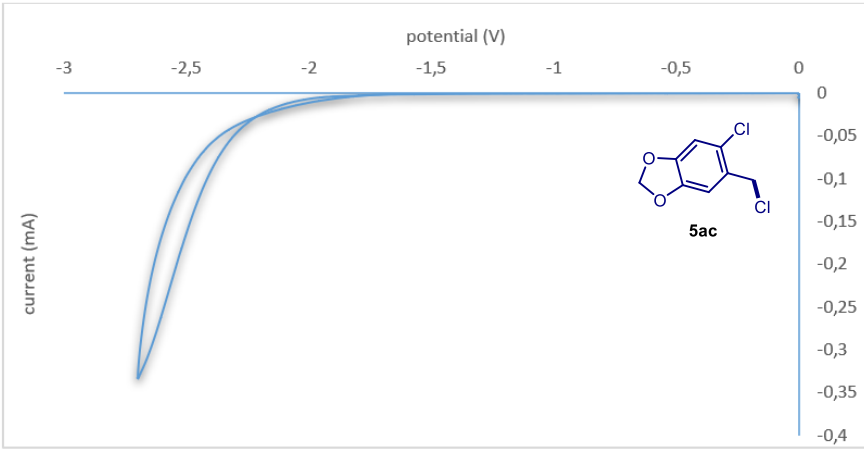

Figure 4.47. Cyclic voltammogram for 6-chloropiperonyl chloride **5ac** [0.02M] in [0.1 M] $TBAPF_6$ in CH_3CN. Sweep rate: 50 mV/s. Glassy carbon electrode working electrode, Ag/AgCl (KCl 3.5 M) reference electrode, Pt wire auxiliary electrode. Reduction of substrate **5ac** was not observed in the registered potential window (from 0 to -2.70 V).

The reduction potential of substrates **5b**, **5t**, **5v**, **5ad** are reported in literature.[50] The literature values were referenced to Ag/AgCl. KCl saturated,[49] and are the following:

E_{red}(**5b**/**5b**$^{\bullet-}$) = -1.80 V (vs. Ag/AgCl, KCl saturated)

E_{red}(**5t**/**5t**$^{\bullet-}$) = -1.59 V (vs. Ag/AgCl, KCl saturated)

E_{red}(**5v**/**5v**$^{\bullet-}$) = -1.51 V (vs. Ag/AgCl, KCl saturated)

E_{red}(**5ad**/**5ad**$^{\bullet-}$) = -2.50 V (vs. Ag/AgCl, KCl saturated)

[50] (a) Shih, H.-W.; Vander Wal, M. N.; Grange, R. L.; MacMillan, D. W. C. Enantioselective α-Benzylation of Aldehydes via Photoredox Organocatalysis. *J. Am. Chem. Soc.* **2010**, *132*, 13600–13603. (b) Zhang, X.-M. Homolytic Bond Dissociation Energies of the Carbon-Halogen Bonds in the Benzyl Halide Radical Anion Intermediates Formed in Radical Nucleophilic Substitution Reactions. *J. Chem. Soc., Perkin Trans.* 2, **1993**, 2275–2279. (c) Amemiya, F.; Fuse, K.; Fuchigami, T.; Atobe, M. Chemoselective Reaction System Using a Two Inlet Micro-Flow Reactor: Application to Carbonyl Allylation. *Chem. Commun.* **2010**, *46*, 2730–2732.

4.11.8. X-Ray Crystallographic Data

Single Crystal X-ray Diffraction Data for Compound 21i

Crystals of the compound **21i** were obtained by slow evaporation of a methanol solution.

Data Collection. Measurements were made on a Bruker-Nonius diffractometer equipped with an APPEX 2 4K CCD area detector, a FR591 rotating anode with $Mo_{K\alpha}$ radiation, Montel mirrors and a Cryostream Plus low temperature device (T = 100K). Full-sphere data collection was used with ω and φ scans.

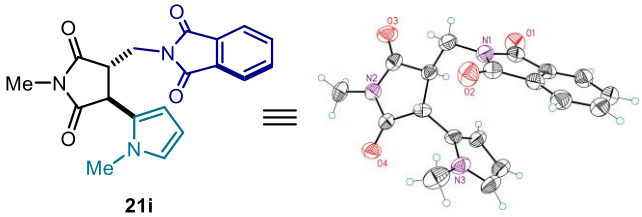

Table 4.5. Crystal data and structure refinement for **21i**. ***CCDC 1894404***

Empirical formula	C19 H17 N3 O4
Formula weight	351.35
Temperature	100(2) K
Wavelength	0.71073 Å
Crystal system	Orthorhombic
Space group	Pbca
Unit cell dimensions	a = 10.5086(4)Å; α= 90°.
b = 12.0160(4)Å	β = 90°.
c = 27.2839(11)Å	γ = 90°.
Volume	3445.2(2) $Å^3$
Z	8
Density (calculated)	1.355 Mg/m^3
Absorption coefficient	0.097 mm^{-1}
F(000)	1472
Crystal size	0.20 x 0.10 x 0.10 mm^3
Theta range for data collection	2.446 to 27.116°.
Index ranges	-8<=h<=13,-15<=k<=13,-35<=l<=35
Reflections collected	27430
Independent reflections	3774[R(int) = 0.0358]
Completeness to theta =27.116°	99.0%
Absorption correction	Multi-scan
Max. and min. transmission	0.990 and 0.898
Refinement method	Full-matrix least-squares on F^2
Data / restraints / parameters	3774/ 461/ 365
Goodness-of-fit on F^2	1.078
Final R indices [I>2sigma(I)]	R1 = 0.0422, wR2 = 0.1126
R indices (all data)	R1 = 0.0564, wR2 = 0.1208
Largest diff. peak and hole	0.179 and -0.205 $e.Å^{-3}$

Chapter V
General Conclusions

This dissertation has shown how the potential of some well-established photochemical processes can be further enhanced upon combination with organocatalysis. In Chapter II, we demonstrated that the photoenolization/Diels-Alder (PEDA) sequence can be performed with high stereoselectivity by using a cinchona alkaloid-based thiourea catalyst. The fleeting nature of the key reactive intermediate (photoenol) and the difficulty of controlling racemic background reactions have previously hampered the development of a catalytic enantioselective variant of this historical photochemical process. Our mechanistic investigations have shown that the cinchona alkaloid-based thiourea controls both the photochemical pathway and the stereoselectivity-defining event. Specifically, the tertiary amino moiety of the chiral organocatalyst lowers the amount of reactive photoenol, thereby decreasing the possibility that an undesired background racemic reaction will take place; in the meantime, the thiourea moiety activates the dienophile upon H-bonding activation, channeling the Diels-Alder trapping toward an enantioselective pattern.

In a related follow-up investigation, we used the highly reactive photoenols in a desymmetric aldol-type process with symmetric 2-fluoro-2-alkyl cyclopentane-1,3-diones (Chapter III). This enantioselective photoenolization/aldol-type trapping was performed with high stereoselectivity using a chiral amido-thiourea catalyst, which directed the aldol addition process selectively on one of the two enantiotopic groups of the symmetric fluorinated 1,3-diketone. Aside from demonstrating that photoenols can participate in stereoselective aldol-type processes, this transformation provided a strategy for the stereoselective construction of valuable fluorine-containing quaternary stereocenters.

Finally, in Chapter IV, we reported the use of a dithiocarbamate anion catalyst that promotes a photoinduced radical-based three-component process that could not be implemented with traditional radical-generating methods, including photoredox catalysis. Specifically, difficult-to-reduce alkyl chlorides were used as radical precursors, and they were coupled with readily available maleimides and heteroaromatic fragments. Mechanistically, the multicomponent radical reaction is founded upon a unique S_N2-based photochemical catalytic radical-generation strategy, which is not reliant on the redox properties of the radical precursors. The overall transformation proceeds under redox-neutral conditions, thus allowing the use of coupling partners bearing redox-sensitive functionalities.